Experimental Investigation of Chevron Special Concentrically Braced Frames with a Yielding Beam Plastic Mechanism

Sara M. Ibarra

A thesis
in partial fulfillment of the
requirements for the degree of

Master of Science in Civil Engineering

University of Washington
2018

Committee
Jeffrey W. Berman, Chair
Dawn E. Lehman
Charles W. Roeder

Program Authorized to Offer Degree:
Civil and Environmental Engineering

University of Washington

Abstract

Experimental Investigation of Chevron Special Concentrically Braced Frames with a Yielding Beam Plastic Mechanism

Sara M. Ibarra
Chair of the Supervisory Committee:
Professor Jeffrey W. Berman
Civil and Environmental Engineering

Chevron-braced frames are preferred structural systems by architects and contractors in low to mid-rise buildings for seismic design because they accommodate architectural elements while providing the necessary lateral stiffness and resistance. This system was more common prior to the advent of Special Concentrically Braced Frame (SCBF) seismic provisions based on capacity design in the late 1980's, which require that the beam develop the idealized expected unbalanced capacities of full yielding of the tension brace and degraded capacity of the compression brace. This results in large and costly beams, which deter their use in construction.

Previous experimental tests of chevron SCBFs with beam strengths that do not satisfy the theoretical unbalanced force prescribed by AISC SCBF Seismic Provisions result in a yielding beam plastic mechanism. These tests suggest that the current beam strength requirement is not necessary for assuring life safety and collapse prevention. Three single-story chevron SCBFs were tested at the University of Washington to further evaluate the beam yielding mechanism. One of the tested specimens had a beam weaker than any previously tested to establish a lower bound for comparison of seismic performance. A second specimen had A500 Gr. C braces to determine the impact of brace steel type on seismic performance. The third single-story specimen used a deeper beam to determine the effect of beam stiffness on frame resistance and ductility. Finally, a capstone 3-story chevron SCBF was tested at the National Center for Research on Earthquake Engineering in Taiwan to evaluate the system's performance with a yielding beam. Results show that the beam yielding mechanism improved the deformability of the SCBF and the weaker beam did not compromise the capacity of the system if the beam was not excessively weak.

Table of Contents

List of Figures

List of Tables

Acknowledgements

I would like to acknowledge my advisors, Professors Jeffrey Berman, Dawn Lehman, and Charles Roeder for bringing me onto this project and providing funding for the research. I would like to thank them for their guidance, support, and encouragement in the design and construction of the specimens and writing of this thesis. They spent many hours reading this thesis and offered invaluable feedback and recommendations for its improvement.

I would also like to extend my gratitude to Professor Keh-Chyuan Tsai of the National Taiwan University (NTU) and the National Center for research on Earthquake Engineering (NCREE), for facilitating experimental testing of a specimen extending incredible hospitality during my visit to Taiwan. This test would not have been possible without the incredible hard work of Ching-Yi Tsai and An-Chien Wu who coordinated construction and instrumentation of the specimen at NCREE. Thank you also to, Professor Tsai's students at NTU, and the staff at NCREE for their support during the test and their hospitality during my visit.

Thank you to Clare, who I've worked with since my days at Northwestern, for starting this project, building the huge test rig, and for getting me started in the lab and providing guidance all throughout the construction of my first specimen. Andy Sen was an invaluable resource, being one of the few people who knew how to run the actuator, and never complained during the 12-hour long tests. He also played a significant role in final test in Taiwan and always promptly answered my questions despite the 16 hour time difference.

Thank you to Ian McWhirter, lab assistant extraordinaire. Despite his issues with overtightening bolts, he provided invaluable moral support and help with the heavy lifting so we never missed a deadline. Michael Hanek, Nicholas Weiss, John Hastings, and Ross were also of great assistance in the lab during specimen construction and testing. I would also like to acknowledge Vince C., our lab technician at UW. Thank you for the help during the year I was working in the lab, and for getting a reusable coffee mug. I will miss our talks and lunches. Thank you also to Doug Lindblad for welding.

Thank you to my great friends and classmates Cassie Gills, Ingimar Johannsson, and Alex Shegay for their awesome advice and encouragement. Even though they left UW (me) right before I started writing my thesis, they continued to support me from afar. Sarah Wichman, Leikune Aragaw, Tom Lin, and many other graduate students made this experience more enjoyable and one I'll never forget.

Thank you to the American Institute of Steel Construction for providing funding and advice for this research.

Most importantly, thank you to my family, without whom I would be lost. Their unconditional love, support, and endless encouragement got me through this program.

CHAPTER 1
Introduction

1.1 Background

Chevron-concentrically braced frames (CBFs) are preferred structural systems by architects and contractors in low to mid-rise buildings for seismic design because they accommodate architectural elements such as doors and windows while providing the necessary lateral stiffness and resistance. SCBFs are expected to withstand large inelastic deformations under strong ground motions. The majority of the resistance in these frames is provided by the diagonal braces which are intended to yield in tension and buckle in compression during major seismic events. The braces dissipate energy and provide inelastic deformation capacity to the system. The brace buckling capacity deteriorates due to large post-buckling deformation, and this post-buckling deterioration causes a significant difference between the resistances of tensile and compressive braces. The difference in tensile yield and post-buckling compressive capacity typically require them to be used in pairs to achieve symmetric response in both directions. Other configurations of paired braces in SCBFs are shown in Figure 1.1.

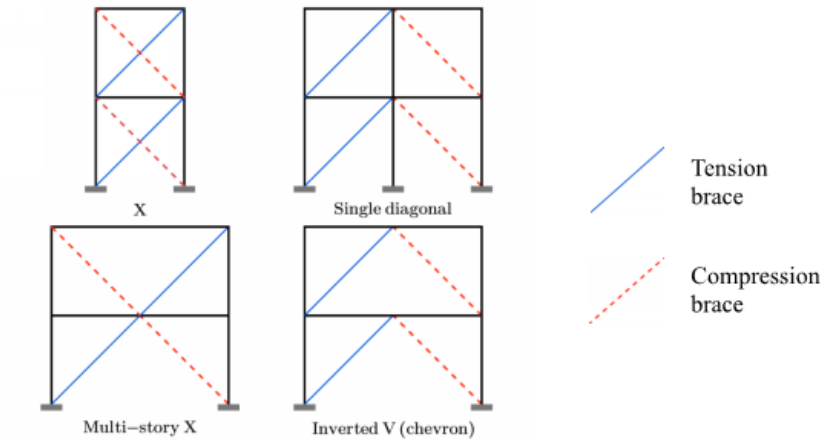

Figure 1.1 Concentrically braced frame configurations (Terpstra 2017)

This system was more common prior to the advent of new seismic provisions which adopted capacity based design philosophies. Capacity based design requirements significantly impacted chevron braced frames resulting in less prevalent use of chevron bracing today, due to the stringent requirements of the beam connected to the chevron bracing. Seismic Provisions (AISC 2016a) place special restrictions on connection details, brace configuration, and global and local slenderness of the brace. These requirements have been studied and optimized to improve ductility and inelastic deformation capacity of the system and accommodate brace end rotations. However, there is little research to validate the current chevron beam strength requirement, which requires that beams support the vertical component of idealized unbalanced capacities of full yielding of the tension and degraded capacity of the compression brace. This requirement results in large and costly beams, and as a consequence, chevron SCBFs are now rarely designed. Instead, alternatives such as buckling restrained braced frames, diagonal bracing or reinforced concrete shear walls are used.

1.2 Project Overview

This research is a study into the effect of yielding of beams in chevron CBFs during earthquake loading, rather than brace yielding in tensions. This was done to better understand how chevron beam yielding changes system behavior and improves system performance. The proposed mechanism is shown in Figure 1.2(a) The experimental program was conducted in three phases. Phase I consisted of Terpstra's (2017) tests at the University of Washington in which three frames, one meeting current Seismic Provision requirements (Chevron 1), and two with beams that did not meet the requirement and resulted in yielding beam plastic mechanisms (Chevrons 2 and 3). This phase of testing provided promising results regarding the extent to which the beam strength of a chevron frame could be reduced and still achieve design strength and prompted Phases II and III of the experimental program.

Phase II continued to study the impact of the relative strength of the beam and demand of the braces. Based on Phase I results it was postulated that the brace unbalanced force after brace buckling was different from the Seismic Provision required forces shown in Figure 1.2 since the weaker beam could not develop the AISC idealized brace loads. This phase, performed by the author, consisted of experimental testing of single story chevron frames with a weaker beam than Chevron 3 in Terpstra's tests (Chevron 4), a frame with A500 braces to evaluate performance

relative to A1085 braces (Chevron 5), and a frame with a previously tested strength but stiffer beam (Chevron 6). All of which had simple bolted shear tab beam-to-column connections and were tested at the University of Washington.

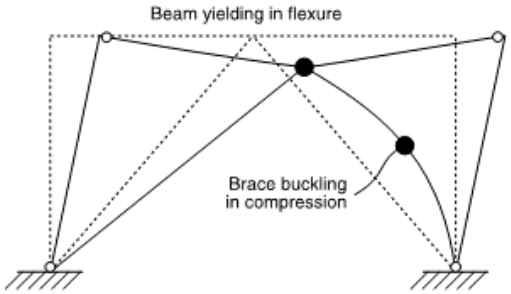

(a) Proposed beam yielding meachanism

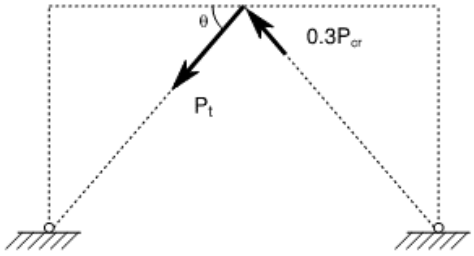

(b) Idealized postbuckling brace loads

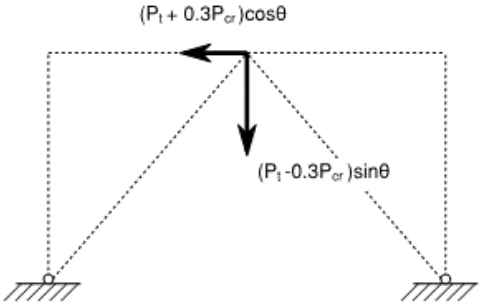

(c) Resultant horizontal and vertical demands on the beam

Figure 1.2 Beam yielding schematic and demands (Sen et al.)

Phase III of the research studied the response a 3-story chevron braced frame with beam yielding. Design of the 3-story frame was aided by the use of a high-resolution finite-element analyses (FEA) in ABAQUS performed by Andrew Sen and Ruyue Liu. The FEA results are not presented

in this thesis, but they showed that the beam-to-column connection and relative resistance of the beam were critically important to the frame behavior. Analyses also showed that the gusset plate above the beam at the beam-to-column connection provided rigidity to the connection so that a plastic hinge occurred in the beam adjacent to the corner gusset plates. To study this effect experimentally, the three-story, full-scale chevron SCBF was tested in collaboration with the National Center for Research on Earthquake Engineering (NCREE) at their laboratories in Taipei, Taiwan.

1.3 Research Objectives

The research objectives for the work presented in this thesis are as follows:

- Experimentally evaluate the effect of beam strength on the lateral resistance and seismic performance of chevron SCBFs.
- Determine the effect of beam stiffness , brace ductility, and connection .
- Compare the performance of all single-story chevron SCBFs tested at UW.
- Correlate the inelastic behavior or single story and multi-story chevron SCBF.
- Propose an improved design method for SCBFs that results in a less costly beam section yet achieves the design strength and good seismic behavior.

1.4 Document Overview

To address the stated objectives this report is divided into six additional chapters. Chapter 2 provides a review of previous research work that provided motivation for this research. Chapter 3 describes the design of the single-story experimental specimens. It also includes a description of the existing experimental setup at the University of Washington Structural Research Lab. Chapter 4 documents observations from the three single-story chevron frames tested at UW. This chapter also uses observations from Phase I of the experimental program to make comparisons of all the single-story frames tested at various drift levels. Chapter 5 describes data collection methods and processing of raw data. It proceeds with detailed analysis of the measured response of the three specimens locally and globally. It then compares the response of the six specimens from Phases I and II. Chapter 6 documents the 3-story experiment. It provides the motivation, design methodology, test setup at NCREE, experimental observations, and a limited analysis of the

measured response. Finally, Chapter 7 summarizes the experimental research, draws conclusions from the entire experimental program, and provides suggestions for future work.

Appendices to the work include: Appendix A, which includes sample design calculations of the single and multi-story frames. Appendix B includes the construction and instrumentation drawings for the four tested specimens, as well as detailed drawings for the two experimental setups. Appendix C includes experimental data processing explanations and data verification studies. Appendix D contains supplemental data analysis and response plots.

CHAPTER 2
Project Background

2.1 Introduction

This chapter provides impetus and justification for the research program presented in this thesis through the presentation of past research on the topic of SCBFs with braces in a chevron configuration. Relatively little comparative research has been done specifically on the topic of chevrons with beams weaker than required to develop the unbalanced forces of the braces in a post-buckling condition. First, the evolution U.S. of seismic design code requirements for chevron CBFs is reviewed. Then experimental programs from around the world focused on chevron CBFs are described. Finally, the previous University of Washington research that is the precursor to the research in this thesis is reviewed.

2.2 Evolution of Chevron CBF Seismic Design Code Provisions

Considerable modifications have been made to CBF design requirements since the late 1980's based on extensive research studying the performance of steel buildings. The 1985 UBC restrictions on chevron braced frames focused on assuring that the beam could support gravity loads after buckling of the brace. In this revision of the UBC all frame members, braces, and connections were required to be sized for the same reduced seismic forces. This made braced frames susceptible to unexpected failure due to the braces having larger tensile capacity than compressive capacity, which governed the brace design. With braces sized for a compressive capacity that is much lower than the tensile capacity, the forces attracted by the braces in tension could be much larger than the design seismic forces and the design strength of the frame. In general, braced frame design in the 1985 UBC aimed at avoiding brace buckling and providing nearly elastic behavior.

The introduction of capacity design philosophies for braced frames for the first time came with the adoption of the 1988 Uniform Building Code, laying the foundation for modern SCBF design. The capacity design procedures used for modern SCBF design limit inelastic action to one ductile mechanism, brace buckling and yielding, by requiring the capacity of all other mechanism within the system to exceed that of the ductile mechanism. Additionally, brace compactness and slenderness criteria, which prolong the onset of local buckling effects, have contributed to the ductility of the system.

In the past decade, a wealth of research has been carried out to maximize the seismic performance of braced frames and has resulted in improved connection design procedures such as the balanced designed procedure (BDP), proposed by Roeder et al. (2011) and a brace rotational elliptical clearance (Lehman et al. 2008). The BDP has been shown to improve the deformation capacity of SCBFs by Johnson (2005), Kotulka (2007) and Lumpkin (2008). The BDP considers ductile limit states in addition to that of the braces, and taking advantage of them to promote desirable yielding mechanisms and evade undesirable failure modes such as weld fracture. Clearance for brace end rotation is required due to the high strain demands on the connection from brace buckling. Traditionally a 2_{tp} linear clearance model had been recommended, where tp is the gusset plate thickness, but the elliptical clearance model results in thinner and more compact gusset plates.

The 1997 Seismic Provisions (AISC 1997) also introduced the consideration of unbalanced load applied to the beam in V and inverted V (Chevron) configurations resulting from the degraded compressive capacity of the buckled brace after large buckling deformations. Prior to buckling, the braces develop opposing axial forces equal in magnitude. After buckling, the compressive strength degrades, while the tensile strength remains stable, resulting in a net downward vertical force at the beam mid-span. This resultant force causes a large bending moment in the beam and 2016 Seismic Provisions (AISC 2016a) require the beam develop the unbalanced load from the tensile brace at its expected yield strength and the compressive brace with a compressive capacity degraded to 30% of the expected critical buckling load. Table 2.1, developed by Terpstra(2017) , summarizes major CBF design criteria changes.

The ramifications of these design provisions are that beams in chevron frames are required to be uneconomically large, resulting in few uses of the system today. However, as shown below, there is very little evidence that chevron frames have poor seismic performance when the beams yield under unbalanced forces. This gap in understanding is the motivation for this research

Table 2.1 Pre-1988 and present day CBF design criteria (Terpstra 2017)

Component	Pre-1988 Requirement	Modern (SCBF) Requirement
Brace Slenderness	No limit	$KL/r < 100$
Brace Compactness	No limit	Compactness ratio $< \lambda_{hd}$
Framing Member Compactness	No limit	Compactness ratio $< \lambda_{md}$
Brace End Rotational Clearance	No limit	$2t_p$ linear or $8t_p$ elliptical for corner gusset plates, 6tp for mid-span gusset plates
Connection Design	Design for brace force from seismic loads	Design for expected brace capacity
Framing Member Design	Design for brace force from seismic loads	Design for expected brace capacity
Chevron Beam Design	Design for brace force from seismic loads	1) Design for brace unbalanced load ($P_y + 0.3P_{cr}$)
		2)Beams must be continuous
		3)Provide minimum lateral bracing

2.3 US/Japan Research: Six-Story Steel Building

A Full scale six story steel building was built and tested in in the Large Size Structures laboratory of the building Research Institute (BRI) operated by Ministry of Construction in Tsukuba, Japan in 1981 as part of the U.S.- Japan Joint Research Program. The test and results are discussed in Foutch et al. (1987) and Roeder (1989). The test program consisted of four phases. Phase I of the program involved braced frame testing and is the only phase of interest here. The goal of the test was to reach large enough displacements to understand the strength, ductility, and failure mechanism and determine relationships between full scale, small scale, component tests, and analytical studies.

The dimensioned tested structure is shown in Figure 2.1. The braces were rectangular HSS tubes in a chevron configuration, and the beam-to-column connections were FR (fully-welded) connections. This test did not use gusset plates, the braces were welded directly to the beams. Every beam had a composite concrete slab. The member sizes and DCR at each story are reported in Table 2.2, created by Sen (2014) where the beam DCR is computed for the unbalanced load from the expected brace tensile strength and 0.3 of the expected brace compressive strength. The erection of the frame used a variation of the Japanese Christmas tree erection procedure. Beam stubs of one half the beam length were welded to the column at ground level, the columns were stood up and the webs of the beam stubs were bolted together on erection. After erection, the flanges and webs of beam stubs were welded with CJP welds, and a composite slab was placed. The bolted-welded beam splice occurred right over the center of the chevron brace-to-beam connections. Loading was conducted using a pseudodynamic test system to simulate seismic excitations at a slow test rate and used the Miyagi-ken-Oki acceleration record. The frame was tested under three separate earthquake simulations (small, moderate and large).

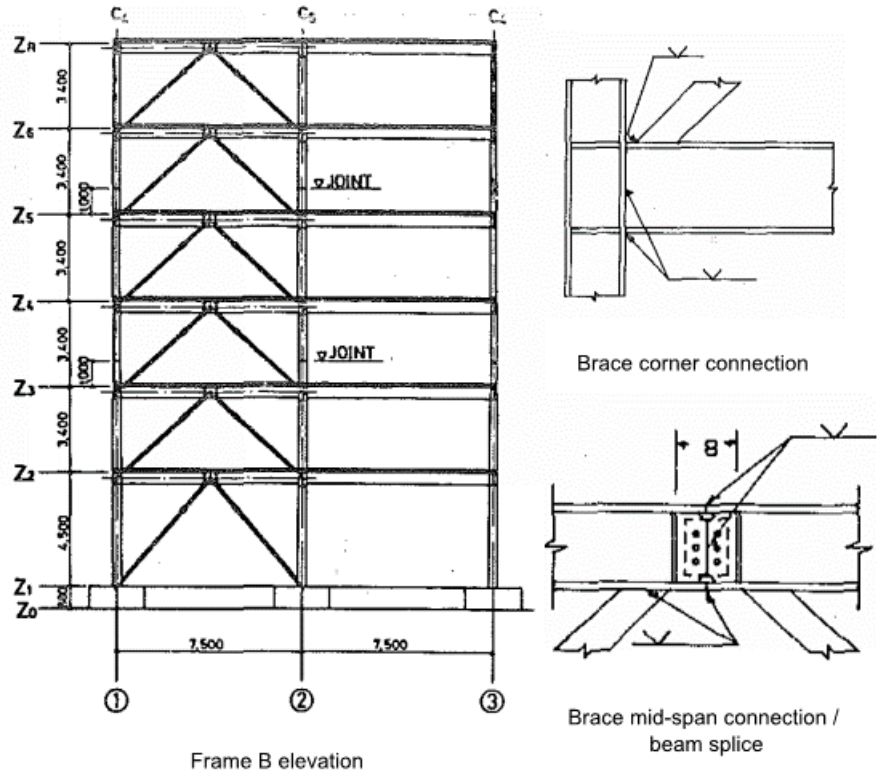

Figure 2.1 Elevation and connection details in six-story US/Japan specimen (Foutch et al. 1987)

Table 2.2 Members, geometry, and beam interaction DCRs in US/Japan specimen (Sen 2014)

Story	Story Height (mm)	Beam Shape	Brace Shape	Beam Interaction DCR
1	4500	W18x40	ST6x6x1/2	3.77
2	3400	W18x40	ST6x6x1/4	1.83
3	3400	W18x40	ST6x6x1/4	1.83
4	3400	W18x35	ST5x5x1/4	1.81
5	3400	W18x35	ST4x4x3/16	1.11
6	3400	W16x31	ST4x4x3/16	1.43*

* P_{cr} estimated using K = 0.82, L = centerline length

2.3.1 Findings

- The small earthquake test resulted in fairly linear behavior. The moderate test resulted in more significant inelastic behavior with some limited brace buckling. It was noted that the bolted-welded splices had some permanent shear deformation, because the region had acted as a short eccentric shear link. After the moderate earthquake, significant damage was found including some tearing at one splice location.
- During the large earthquake test there was much more brace buckling, deflections were three times larger than for the moderate test. Buckling occurred mostly in-plane but some out-of-plane buckling. The third story brace had a large b/t ratio and the brace fractured about two thirds of the way through the test.
- Initially, the braces carried 80% of total shear and the moment frames 20% and later the moment frames carried 60% of the total shear once the braces were severely buckled.
- Composite action of the beam and concrete slab may have increased early stiffness by 10-15% and strength by 5-10% based on linear elastic and inelastic calculations. However, the strength and stiffness were lost later in test due to the deterioration in composite action and brace post buckling behavior.
- Soft story effects at the second and third stories concentrated deformation at these locations and reduced the stiffness and resistance significantly, which could have caused serious stability issues had the test continued.

2.3.2 Commentary

Because this test was designed prior to the adoption of capacity design procedures, the beams were not required to develop the unbalanced force from the post buckled brace behavior and resulted in relatively small beams with DCRs above one. However, the splice at the center of the beam was very different from modern SCBF's where the beam is required to be continuous. This makes the failure of the connection at the mid beam splice during the moderate test irrelevant to the study of frames with weak beams, although it does show the importance of connection detailing and justifies current seismic provisions. Further, this test shows the importance of the redundancy inherent in most braced frames. The moment resisting beam-to-column connections provided reserve strength and stiffness, enabling the building to survive large seismic shaking after significant brace damage and deterioration.

2.4 US/Japan Research: Half-Scale Three-Story Steel Building

The research presented here was part of the U.S.-Japan Cooperative Earthquake Research Program Utilizing Large-Scale Testing Facilities and was motivated by the limited understanding of dual seismic load resisting systems with chevron frames and moment resisting frame. The research and results are presented in Fukuta et al. (1987). Six half-scale three-story steel frames were tested under static loading at the building Research Institute, Ministry of construction, Japanese Government. Vertical and horizontal forces were imposed on these frames to simulate the expected stress conditions of the prototype buildings. All tested frames were had the same bay width and height and were of the general form shown in Figure 2.2 and moment-resisting connections at the beam-to-column joints. Five of the frames had inverted-V braces and one did not have any braces. All the frames had brace sizes, and degree of composite action. Table 2.3 developed by Sen (2014) presents the member sections used, story heights, and unfactored axial-flexural DCRs of each story for the five tested braced frames. The axial-flexural interaction demand to capacity ratios (iDCRs) were determined using the expected idealized unbalanced brace loads based on material properties and an effective length factor of 0.82 as observed in the related full-scale six-story tests (Roeder 1989). The expressions used for this calculation are discussed in detail in Chapter 3. The iDCR of the first and second story beams was greater than one for all first and second story beams based on current seismic provisions.

The results from this test were used to verify a hysteretic model predicting the lateral resistance of chevron braced frames. The model accounts for the post-buckling resistance of the braced frame, the ductility and resistance of the moment frame, and the brace-beam interaction using plastic analysis. The shear force of the brace in tension, Q_{bt}, in Eq. 2.1 is limited by the shear force of the compression brace, Q_{bc}, and the beam strength, Q_g as defined in Eq. 2.2. Where P_y is the yield axial force of the brace, h is the story height, and Mg is the full plastic moment of the beam. Thus, the maximum contribution from the beam strength is the lateral resistance of the moment frame in a sway mechanism with plastic hinging in the beam.

$$Q_{bt}(x) = -Q_{bc}(X) - Q_g(X) \leq P_y cos\theta \qquad \text{Eq. 2.1}$$

Where

$$Q_g(X) \leq Q_{gmax} = \frac{2M_{gp}}{h} \qquad \text{Eq. 2.2}$$

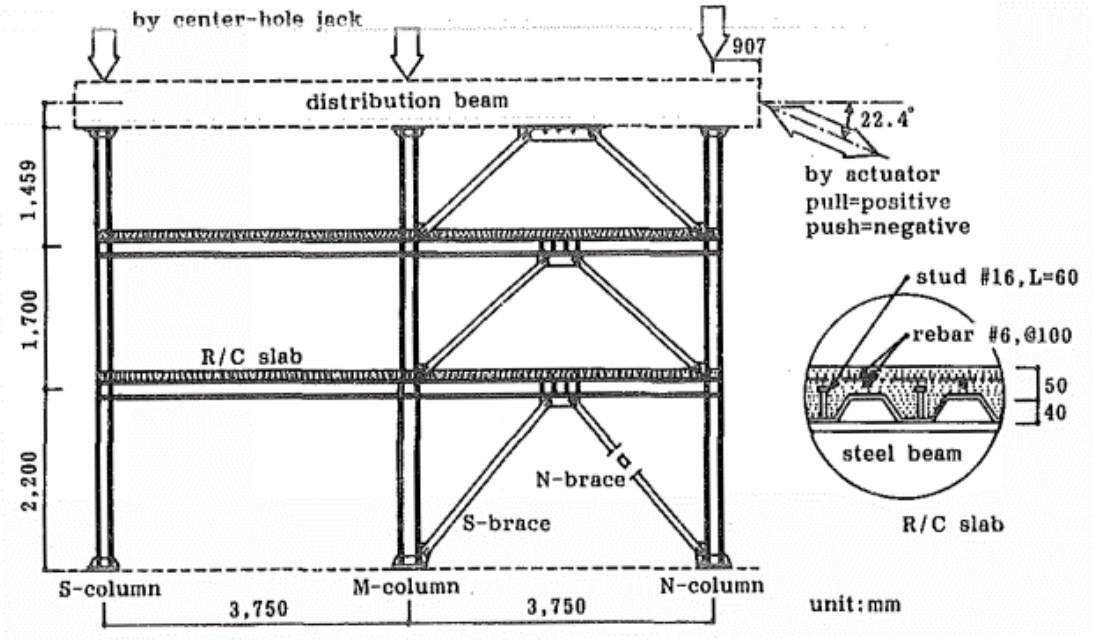

Figure 2.2 Elevation and loading details in three-story US/Japan tests (Fukuta et al. 1989)

Table 2.3 Members, geometry, and beam interaction values in three-story US/Japan test (Sen 2014)

Story	Frame No.	Story height (mm)	Beam	Brace (d×b×t)	Interaction (DCR)[a]
3F		1459	Rigid	□−105×45×4.5	$\ll 1$
2F	1,2,3	1700	W8×10	□−105×45×4.5	1.82
1F		2200	W8×13	□−110×55×4.5	1.92
3F		1459	Rigid	□−70×35×6.0	$\ll 1$
2F	4	1700	W8×10	□−70×35×6.0	2.31
1F		2200	W8×13	□−70×40×9.0	2.80
3F		1459	Rigid	□−105×45×4.5	$\ll 1$
2F	5	1700	W8×13	□−105×45×4.5	1.60
1F		2200	W10×17	□−110×55×4.5	1.17

[a] P_{cr} estimated using $K = 0.58$, L = centerline length

2.4.1 Findings

- In the elastic range, the braces contributed 80% of the lateral resistance of the system and in the post-buckling range, they contributed 50% of the resistance.
- Composite action and the resulting increase in flexural beam strength did not have an effect on the lateral resistance before brace buckling. However, the beam strength did have an impact on the maximum shear force carried by the braces. Beam stiffness permits more elongation of the braces in frame development of larger tensile forces, increasing the lateral resistance in post-buckling behavior.
- The braces in most of the frames formed three plastic hinges, one at each end and at the brace midpoint. None of the braces elongated enough to yield in tension, and most of the damage occurred in compression due to local buckling at the plastic hinge.
- The proposed hysteretic model agrees well with results from the tested frames.

2.4.2 Commentary

This series of half-scale test provides much of the existing experimental data on braced frames with beams that are not strong enough to develop the unbalanced brace forces after brace buckling as predicted by AISC Seismic Provisions. Despite the weak beams, frame behavior showed good ductility and energy dissipation. However, the frames were not cycled to failure so definitive conclusions cannot be made about the beam-brace interaction and its effect on the seismic resisting

system. Additionally, the proposed hysteretic model seems to overpredict lateral resistance at higher drifts, which could mean it does not accurately capture brace cyclic strength degradation at larger drifts.

2.5 Chevron concentrically braced frames with yielding beams

The research presented here was part of an experimental program that tested four two-story chevron braced frames at the National Center for Earthquake Engineering (NCREE) between 2013 and early 2014 as part of University of Washington –National Taiwan University collaborative research. The test and results are described in detail in Sen et al. (2016). Seismic provisions for SCB design promote a yielding brace mechanism. Evaluation of existing infrastructure in the US using 2010 Seismic Provisions (AISC 2010) showed that the beams of existing chevron NCBFs predating the implementation of capacity design principles in the building code in the 1980's consistently fail to meet requirement for axial-flexural resistance. This results in a beam plastic yielding mechanism instead of a yielding brace mechanism, which were believed to make the system seismically vulnerable. These two yielding mechanisms are demonstrated in Figure 2.3

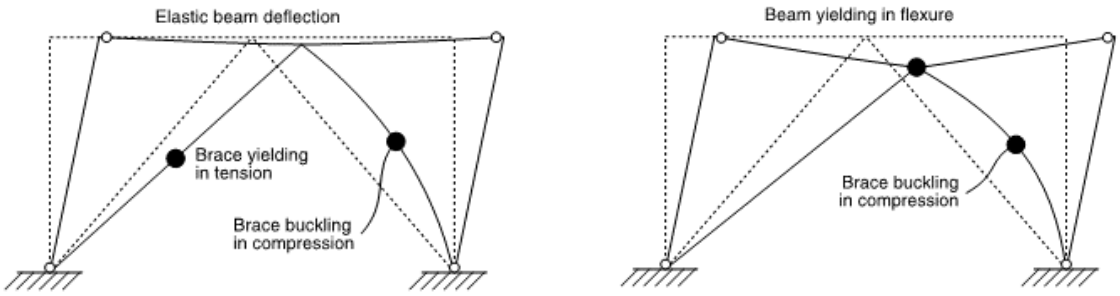

(a) yielding-brace mechanism (b) yielding-beam mechanism

Figure 2.3 Plastic mechanisms for chevron CBFs (Sen et al. 2016)

The four frames tested by Sen et al. 2016 had the same bay width and story heights of 6286mm and 3297mm respectively. The two stories were of the same height. The differences among the frames are highlighted in Figure 2.4 and involve connection details and brace size and compactness. The beam sizes were consistent for all the frames and are specified along with brace size and beam iDCR in Table 2.4. The specimens were loaded with three 1000kN actuators at the second story

under a quasi-static displacement control loading protocol. In order to transfer the lateral load from actuators the second floor beam was designed as a strong beam so damage was expected to concentrate at the first story with the yielding beams.

The first specimen (NCBF-INV-1) was designed to simulate a non-ductile concentrically braced frame (NCBF) with a chevron configuration with a beam unable to develop the unbalanced force from the braces in a post-buckling condition elastically, as specified by Seismic Provisions and hence here forth considered as a yielding beam. The specimen also had non-compact braces, and connections representative of the frames being investigated. The second and third specimens investigated repair strategies for the first specimen by replacing the braces and gusset plates of the first story. These two specimens retained the seismically deficient beam and beam-to-column connections of NCBFs, and had repaired welds from previous tests' damage. The second specimen (NCBF-INV-2) had seismically compact braces with knife plate brace end connections to achieve in plane brace buckling. The third specimen (NCBF-INV-3) had seismically compact wide flange braces and gusset plates designed using the BDP. The fourth and final specimen (NCBF-INV-4) was designed to be compliant with Seismic Provisions (AISC 2010) for SCBFs except for the yielding-beam and had gusset plates designed using the BDP.

Table 2.4 Geometry, members, and beam interaction iDCRs (Sen 2014)

Test Number	Specimen Name	Story	Story Height (mm)	Beam Shape	Brace Shape	Beam Interaction DCR
1	TNCBF1-N-HSS	1	3297	W16x45	HSS7x7x1/4	2.52
		2	3297	W24x94	HSS7x7x1/4	0.42
2	TNCBF1-R-HSS	1	3297	W16x45	HSS5x5x3/8k	2.66
		2	3297	W24x94	HSS7x7x1/4	0.42
3	TNCBF1-R-WF	1	3297	W16x45	H175x175x7.5x11	2.55
		2	3297	W24x94	HSS7x7x1/4	0.42
4	TNCBF2-D-HSS	1	3297	W16x45	HSS5x5x3/8	1.43
		2	3297	W24x94	HSS5x5x3/8	0.44

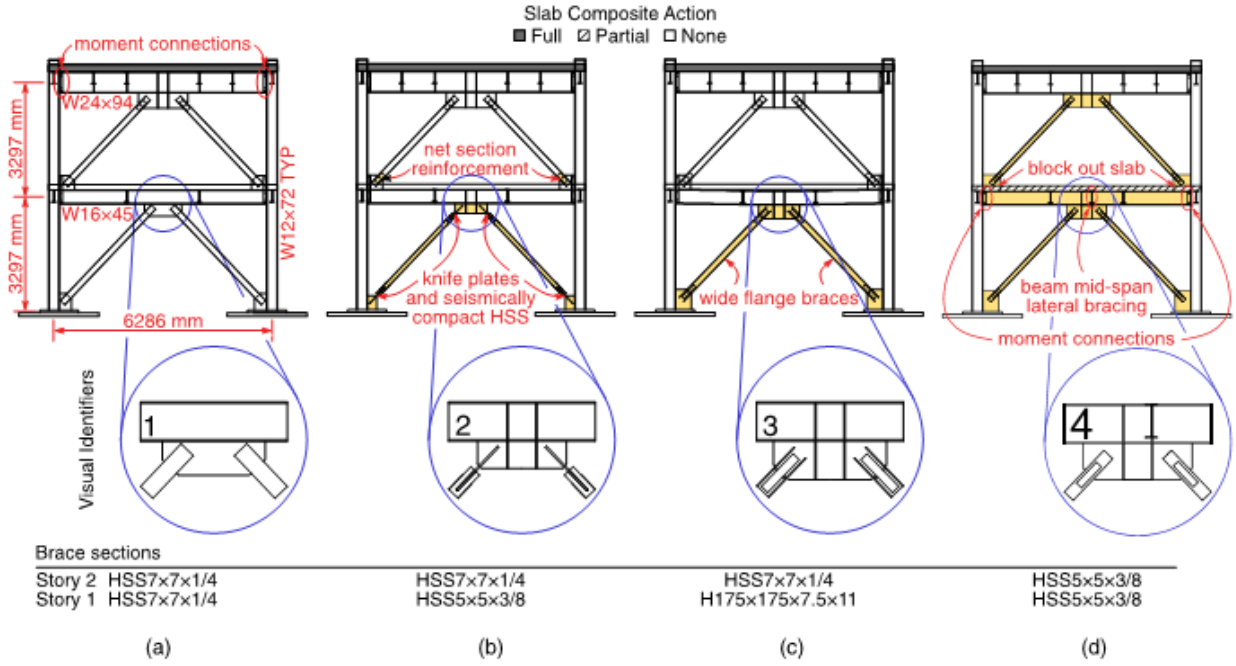

Figure 2.4 Specimen elevations and visual identifiers: (a) Specimen1; typical sections and geometry; (b) Specimen 2; (c) Specimen 3; (d) Specimen 4 (Sen et al. 2016)

2.5.1 Findings

- HSS braces with compactness noncompliant with SCBF criteria have very low ductility and fracture very quickly after buckling.
- Large inelastic deformation demands from the beam deflection and frame action of beam-yielding frames result in large beam-to-column connection rotation and significant weld damage.
- The welds of NCBF gusset plates originally designed for the reduced seismic demand forces and not for the expected tensile demand of the brace are deficient and susceptible to early fracture.
- The yielding beam mechanism of chevron frames with DCR up to 2.5 and compliant connections had minimal impact on the frame resistance and deformation
- Frames with non-compact braces should take priority for seismic retrofit schemes, followed by frames with weld deficient connections. The frames with weak beams and axial-flexural interaction DCR less than 2.5 rank lowest for retrofitting priority.

2.5.2 Commentary

The results from these test provided valuable insight into the behavior of CBFs with a yielding beam mechanism. The weak beam did not result in considerably lower lateral resistance or impact frame ductility. Early failures of tests 1 and 3 were due to connection and retrofit deficiencies unrelated to the beam strength and Specimens 2 and 4 achieved drift ranges comparable to current SCBFs. The increased beam end rotation due to the larger beam deflection of weak beams requires attention and a connection design that will tolerate the rotation demand. It is difficult to make definitive conclusions about chevron frames with yielding beams based on these results because there were different variables between the specimens affecting frame performance. However the results in particular from Specimen 4 provides motivation for the development of a test program that more specifically studies the impact of the weak beams on seismic performance of modern SCBFs.

2.6 Okasaki Weak Beam SCBF research

The research presented here involves large-scale shake table tests of a 70% scale single bay, single story chevron braced frame conducted at E-Defense, Japan to study the dynamic response of steel CBFs. The tests and results are described by Okasaki et al. (2013). The frame of dimensions shown in Figure 2.5 was representative of a 3 to 5 story building in Japan. It had HSS braces slightly violating Seismic Provision compactness criteria and gusset plates designed with the elliptical clearance model and BDP but also meeting 2005 AISC specification requirements. The beam of the frame specimen was part of a rigid frame and had fully restrained beam-to-column connections. The beam was designed to meet 2005 AISC Seismic Provision requirements, and thus had an axial-flexural interaction DCR below one for the brace unbalanced force. However, coupon tests showed brace yield strengths 56% larger than nominal strength, and thus the beam actually had a DCR higher than 1. The single-story frame was subjected to the JR Takatori motions, which consists of a motion record from the 1995 Kobe earthquake. This motion was introduced 7 times with amplification factors increasing from 0.10 to 0.70.

2.6.1 Findings

- The frame behaved essentially elastically during all ground motion amplifications until the 42% motion where limited buckling occured.

- During the 70% motion, the final excitation, both of the braces buckled and eventually fractured. The frame reached a drift range of 2.5% which is lower than expected from SCBFs. The low drift is attributed to the failure to meet the brace compactness limit and deviation from all suggested reduction factors of the BDP in the gusset plate design.
- The braces in both the 42% and 70% scaled ground motions shortened more than they elongated and never developed the tensile yielding capacity. This behavior was attributed to a beam downward deflection of 15mm resulting from the pull-down by the braces' unbalanced load. The deflection prevented brace elongation and promoted shortening.

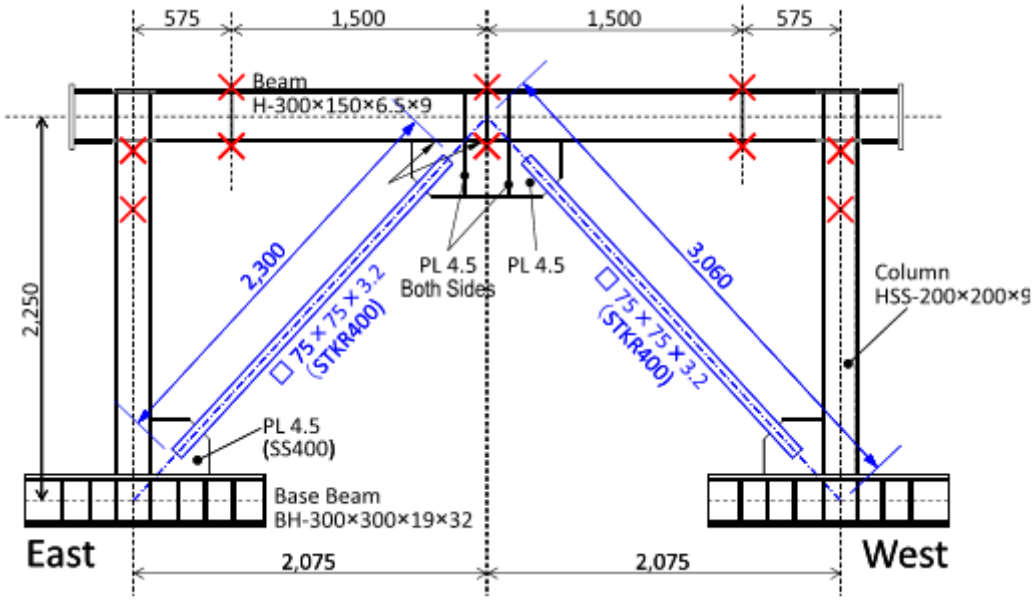

Figure 2.5 Test Specimen and out of plane bracing points (Okasaki et al. 2013)

2.6.2 Commentary

This is one of a few large scale CBFs tested dynamically. Several design deficiencies prevent the frame from qualifying as an SCBF but the results of the experiment are consistent with the behavior of other tested frames with DCRs greater than one, such as the failure of the brace to develop its tensile strength due to deformation of the beam.

2.7 Impact of Beam Strength on Seismic Performance of Chevron CBFs

The experimental research presented here was conducted at the University of Washington Structural Research Lab between October 2016 and February 2017. The experiment and results are reported in Terpstra (2017). Followings Sen's tests at NCREE there was an impetus to continue studying the effects of beam strength on chevron SCBF performance and a new experimental program was designed for the Structural Research Laboratory at the University of Washington to test a series of single story chevron SCBFs. The study was developed to test single-story single-bay chevron braced frames and examine the impact of beam yielding under the unbalanced load occurring after deterioration of compressive resistance during post-buckling brace behavior. The test setup was designed to allow this effect to be studied under conditions as close as possible to what would be found in an actual building frame.

The only variable in these tests was the beam section. Three specimens had the same connection details, bay widths, column heights, and brace sizes and lengths of the dimensions shown in Figure 2.6. The specimen dimensions, brace size, and column size were based on experimental setup restrictions. The chevron beam and the connections were designed using AISC 360-10 LRFD and the seismic capacity design methods of AISC 341-10. The frame strengths were quantified by comparing the demand of idealized unbalanced vertical load to the plastic capacity of a one-story system assuming beam yielding on either side of the mid-beam gusset plate. The gusset plates were designed using the BDP. Final connection and member sizes for all the specimens are summarized in Table 2.5.

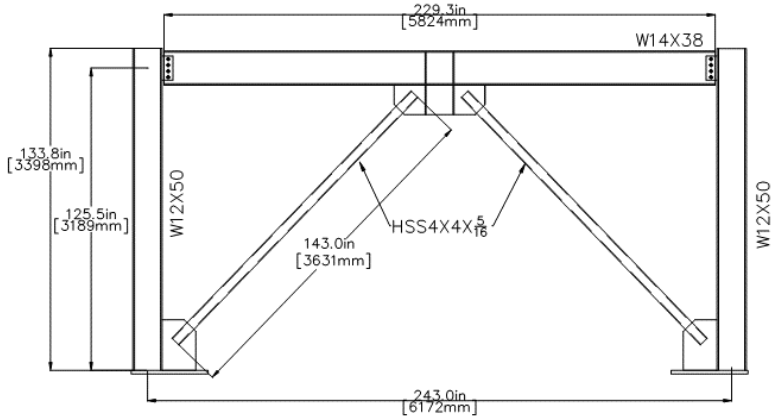

Figure 2.6 Typical test specimen in Terpstra (2017)

Table 2.5 Material Specification and Dimensions

Component	Material	Size	Dimensions
Beam	A992 Gr. 50	W14x120 (Chevron 1) W14x61 (Chevron 2) W14x38 (Chevron 3)	19’ 1-5/16” long
Columns	A992 Gr. 50	W12x50	11’ 1-13/16” long
Braces	A1085 (Chevron 1-4 & 6) A500 Gr. 50 (Chevron 5)	HSS4x4x5/16	11’ 11” long
Gusset Plates	A572 Gr. 50	3/8” thick	37-13/16”x12-5/16” (mid-span) 14”x21” (corner) 7-1/8”x12-5/16” (stiffeners)
Shear Tab	A572 Gr. 50	5/8” thick	10”x4-1/2”
Base Plate	A572 Gr. 50	1-1/2” thick	32”x10”
Cap Plate	A572 Gr. 50	3/4” thick	19”x22”
Doubler Plate	A572 Gr. 50	½” thick (column) ¼” thick (beam)	10”x16” (column) 11”x6” (beam)

Table 2.6 summarizes the final design of the test specimens. The first specimen (Chevron 1) was designed to satisfy all current code provisions, in particular that the beam was able to resist the unbalanced load that results from the difference between the post-buckling and tensile yield strength of the braces in a chevron frame. The second and third specimens were designed with beams that provide a reduced resistance for this unbalanced load. The second specimen (Chevron 2) was designed to have a beam demand-to-capacity ratio (iDCR) for the combined axial and flexural demands of the unbalanced load of approximately 2, while the third specimen (Chevron 3) was designed to have a beam iDCR of approximately 3.

Table 2.6 Specimen Design Summary

Specimen Name		Chevron 1	Chevron 2	Chevron 3
	Beam Size	W14x120	W14x61	W14x38
	Brace Size	HSS4x4x5/16	HSS4x4x5/16	HSS4x4x5/16
	Column Size	W12x50	W12x50	W12x50
	Brace ASTM Designation	A1085	A1085	A1085
Beam iDCR	**Axial DCR**	0.07	0.14	0.25
	Flexural DCR	0.84	1.74	2.9
	Interaction DCR	0.87	1.81	2.83

The specimens were tested with a quasi-static cyclic displacement protocol to large drift demands. Two full cycles were run at each target displacement in order to capture cyclic strength degradation. After fracture of both braces, post-fracture cycles were run to determine the residual lateral resistance of the frame after both braces had fractured. Strains, deflections, loads and deformations were continuously monitored during the entire test through the post fracture cycles.

The following sections summarize test results. It should be noted that the design strength used for the calculation of the brace buckling strength in Terpstra's original text used an incorrect brace cross sectional area and therefore underestimated the design strength. The corrected value was used for reproduction of the figures shown.

2.7.1 Chevron 1 Summary

The Chevron 1 force response hysteresis in Figure 2.7 notes the expected lateral resistance at $2P_{cr}Cos\theta$. Chevron 2 exceeded this resistance by approximately 40%. The beam didn't yield and the maximum elastic deformation at the midspan was 1.1 inches, and there was minimal plastic deformation of approximately ¼". The frame exhibited high ductility with a maximum drift range of 6.3% story drift. The braces developed 92% of their tensile capacity and did not yield through the cross section. The maximum shear load developed in the beam from the vertical component of the unbalanced brace forces was 93% of the design load required by Seismic Provisions (AISC 2016a). Severe local deformation in the braces resulting from a large out of plane deformation ultimately caused brace fracture, and after brace fracture the columns were able to resist 38% of the lateral load achieved by the braced frame.

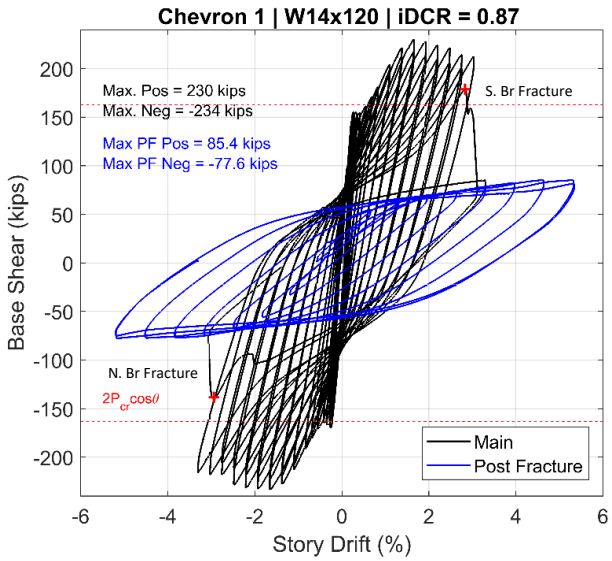

Figure 2.7 Measured Response of Chevron 1

Table 2.7 Chevron 1 results summary

Yielding Hierarchy		Drift (%)
1	Brace	0.28%
2	Gusset Plate	0.55%
3	Shear Tab	1.10%
4	Columns	1.38%
Failure mode		Brace Fracture
Drift Range		6.3%
Max. beam deflection		1.1 in

(a) Chevron 1 beam

(b) Chevron 1 north column

Figure 2.8 Frame damage at 2.5% story drift

2.7.2 Chevron 2 Summary

The Chevron 2 force response hysteresis in Figure 2.9 notes the expected lateral resistance at $2P_{cr}Cos\theta$. Chevron 2 exceeded this resistance by approximately 30%. As summarized in Table 2.8, the beam started to yield at 1.4% story drift and the maximum elastic deformation at the midspan was 1.8 inches. The beam sustained plastic deformation of about ½" by the end of the test. The frame exhibited high ductility with a maximum drift range of 6.3% story drift. The braces developed only 73% of their tensile capacity and did not yield through the cross section. The maximum shear load developed in the beam from the vertical component of the unbalanced brace forces was 65% of the design load required by Seismic Provisions (AISC 2016a). Severe local deformation in the braces resulting from a large out of plane deformation ultimately caused brace fracture, and after brace fracture the columns were able to resist 40% of the lateral load achieved by the braced frame.

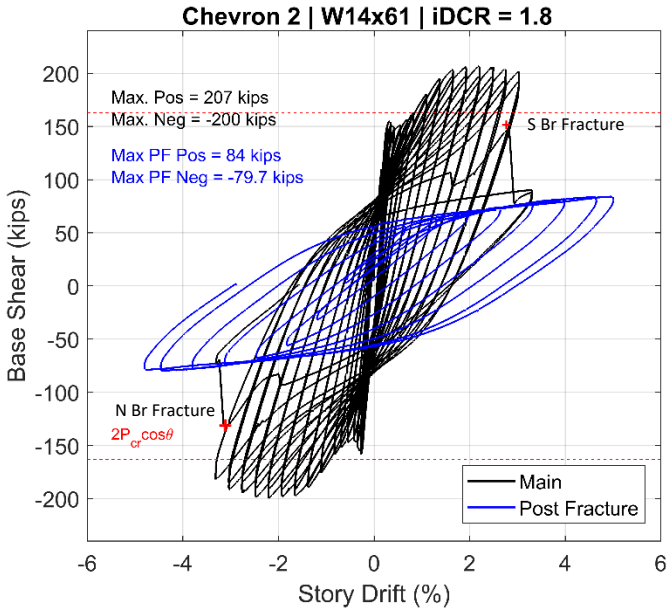

Figure 2.9 Measured Response of Chevron 2

Table 2.8 Chevron 2 results summary

Yielding Hierarchy		Drift (%)
1	Brace	0.28%
2	Gusset Plate	0.41%
3	Shear Tab	0.41%
4	Beam	1.38%
5	Columns	1.38%
Failure mode		Brace Fracture
Drift Range		6.3%
Max. beam deflection		1.8 in

(a) Chevron 2 beam yielding

(b) Chevron 2 north column yielding

Figure 2.10 Frame damage at 2.5% story drift

2.7.3 Chevron 3 Summary

The Chevron 3 force response hysteresis in Figure 2.11 notes the expected lateral resistance at $2P_{cr}Cos\theta$. Chevron 3 exceeded this resistance by approximately 8%. As summarized in Table 2.9, the beam started to yield at 0.41% story drift and the maximum elastic deformation at the midspan was 3.0 inches. The beam sustained plastic deformation of about 1.8 inches by the end of the test. The frame exhibited high ductility with a maximum drift range of 6.6% story drift. The braces developed 48% of their tensile capacity, or 112% of their expected compressive capacity. The maximum shear load developed in the beam from the vertical component of the unbalanced brace forces was 30% of the design load required by Seismic Provisions (AISC 2016a). Severe local deformation resulted in brace fracture, and after brace fracture the columns were able to resist 42% of the lateral load achieved by the braced frame.

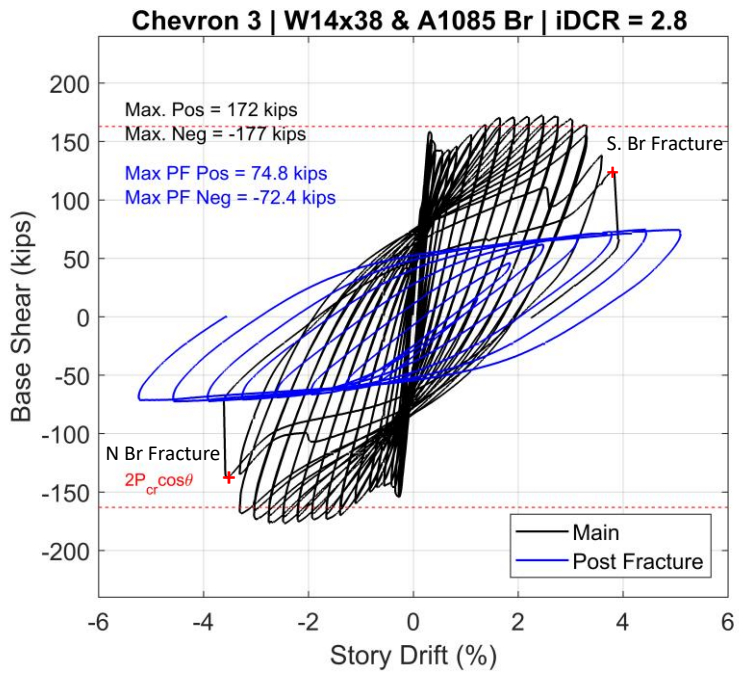

Figure 2.11 Measured Response of Chevron 3

Table 2.9 Chevron 3 results summary

Yielding Hierarchy		Drift (%)
1	Brace	0.28%
2	Gusset Plate	0.34%
3	Shear Tab	0.41%
4	Beam	0.41%
5	Columns	1.38%
Failure mode		Brace Fracture
Drift Range		7.2%
Max. beam deflection		3.0 in

(a) Chevron 3 beam yielding

(b) Chevron 3 north column yielding

Figure 2.12 Frame damage at 2.5% story drift

2.7.4 Commentary

The experimental results from these tests show that the inelastic story drift achieved prior to brace fracture was larger for chevron-braced frames with beam yielding than for chevron braced frames without the beam yielding. The drift capacity was also larger with increasing amounts of beam yielding. The lateral resistance of the frame decreases with beam yielding, but the decrease is smaller than the reduction in beam resistance. That is a 40% reduction in beam strength does not result in a 40% decrease in strength. As expected, vertical deflections of the beam increase with decreased beam strength, but the deflections were consistently smaller than would be expected given the reduction in beam resistance. The vertical unbalanced load developed by the braces appears to decrease proportionally to the reduction in beam strength. Further investigation of frames with beams of lower strength and stiffness could provide a limit at which the beam is too weak to achieve adequate strength and ductility of the frame. The specimens tested all used W14 beam sections, but deeper beams with larger stiffness are often used in practice. They also all used A1085 braces, but A500 are more commonly used. Additionally, there are unstudied questions about the effect of changing boundary conditions such as connection ridgidity on the yielding mechanism of the beam, the composite action contribution from a concrete slab, and the potential concentration of damage in multi-story chevron frames. These outstanding unaddressed factors were the motivation for continuation of research on the behavior of chevron CBFs with yielding beams.

CHAPTER 3
Single-Story Frame Experimental Setup and Specimen Design

3.1 Introduction

This chapter discusses the rationale for the design of the experimental specimens. A discussion of the AISC Seismic Provisions (AISC 2016a), which provide motivation for the experimental program precedes explanation of the test objectives and specimen design. Finally, the experimental setup and testing procedure is presented.

The experimental program was composed of seven specimens and was conducted in three phases. Phase I of the program involved three full-scale single-story chevron SCBFs, Chevrons 1 through 3, tested by Terpstra (2017), as summarized in Section 2.5. Phase II of the experimental program, which will be the focus of this chapter, tested three additional single-story chevron SCBFs, Chevrons 4 through 6. These had the same boundary conditions as those in Part I as shown in Figure 3.1. Phase III of the program tested one 3-story chevron SCBF frame, Chevron 7, and is discussed further in Chapter 6.

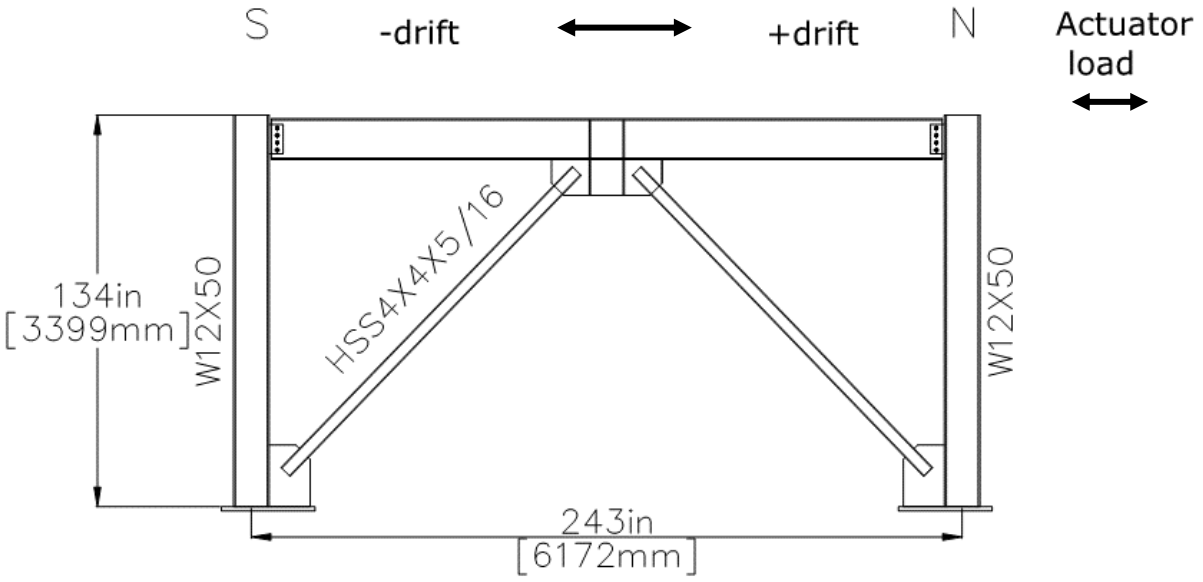

(a) Typical single story chevron frame dimensions

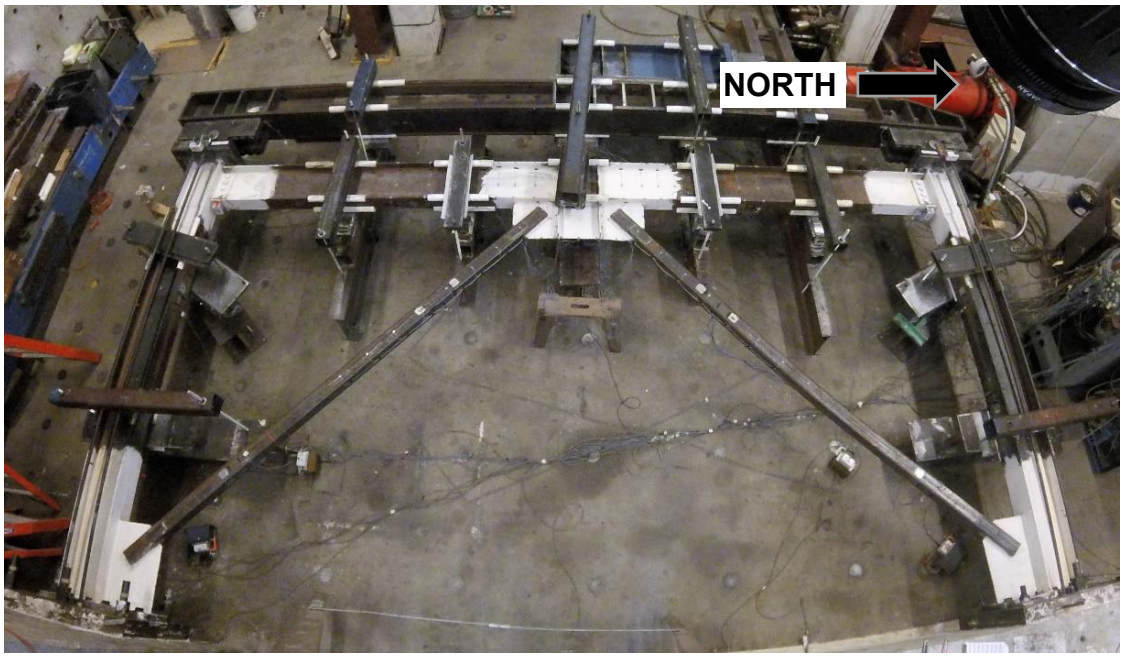

(b) Single story chevron picture

Figure 3.1 Test frame overview

The overall test program was designed to investigate the system response of chevron braced frames with beam strengths that do not satisfy the theoretical unbalanced force prescribed by Seismic Provisions (AISC 2016a). Phase 1 investigated the axial-flexural demand-capacity ratio with the demand based on the idealized unbalanced load (iDCR). Phase 2 furthered this study by investigating the impact of stiffness and brace type. All specimens in Phase II of the series were built and tested in the University of Washington (UW) Structural Research Lab (SRL).

3.2 Overview of Single-Story Chevron Specimens

In chevron SCBFs, the demand considering the post-buckling capacity of one brace with the expected tensile capacity of the other brace normally controls the beam design. The fact that the compressive brace provides less resistance than the tensile brace results in a net downward force at the center of the beam. Beam flexural demands are greatest when the compressive brace strength degrades after buckling while the tensile brace reaches yield, as illustrated in Figure 3.2, where θ is the brace angle relative to horizontal.

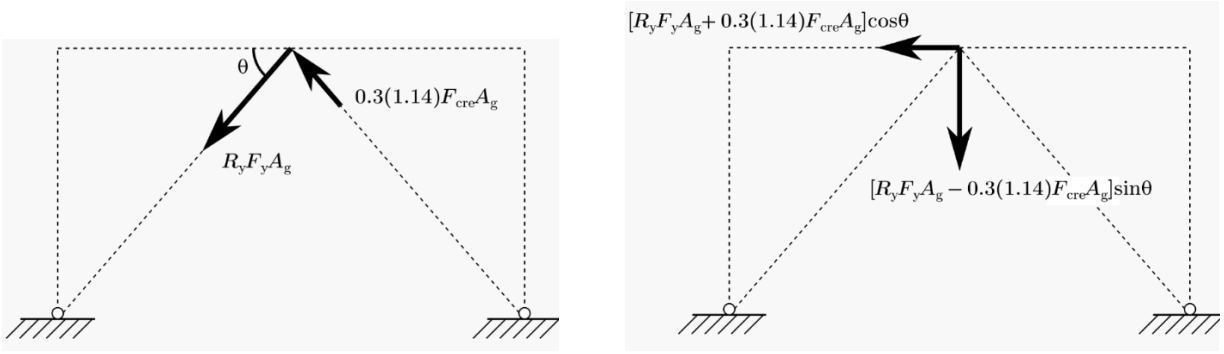

Figure 3.2 AISC 341-16 required unbalanced brace forces on beams in chevron (Sen et al. 2016)

To achieve the research objectives, the frames had varying degrees of beam stiffness and resistance to isolate the effect of beam size on chevron frame performance, all other braced frame details remained identical for all specimens. Thus, the frame geometry, column section, brace section, and connection details were identical in each of the specimens. The test specimens were designed within the constraints imposed by the UW Structural Research Lab equipment and test setup. To maintain the same geometry for each tests, it was necessary to use beams of similar depth for all specimens since the constraints of the test setup required the brace length and angle to change with

changing beam depth. Any change in geometry makes it difficult to compare test results. In the initial stages of Phase I, W14 beams were chosen for all the specimens to accommodate all expected beam iDCRs, a beam any deeper in the frame geometry would not result in the higher iDCRs desired. The objective of Chevron 6 was modified after the experimental program was in progress and the experimental setup built. Therefore, Chevron 6 used a deeper beam section (W21) and, as such, the geometry of this specimen was different from the prior specimens. Specifically it had slightly smaller brace angles, shorter braces, and a longer beam mid-span gusset plate. Table 3.1 shows the resulting braces, beams, and column sizes of all the specimens in Phases I and II of the experimental series. Detailed drawings for the three specimens can be found in Appendix B.

- Chevron 4 was designed to have a beam iDCR of approximately four. This was the chevron with the highest iDCR tested and was intended to be used as the lower bound for the comparison of Chevrons 1 through 4.
- Chevron 5 was designed to be identical to Chevron 3 from Phase I of the test program, but had A500 Gr.C braces, resulting in an iDCR of 3.0 instead of 2.8. This was done to determine the difference in brace and frame ductility and strength with braces of these two different commonly used HSS steel grades. Based on the results from Part I, it was postulated that A1085 braces might have improved ductility relative to A500 braces.
- Chevron 6 was designed to have the same strength as Chevron 2 from Phase I of the program, but with a stiffer beam, resulting in iDCR or 1.77. The stiffer beam, a W21x44, represents a beam section more commonly used in practice for braced frame beams. The objective here was to determine the effect of beam stiffness on frame stiffness, resistance, and ductility.

Table 3.1 Specimen Design Summary

		Phase I Specimens (Terpstra 2017)			Phase II Specimens (This thesis)		
Specimen Name		**Chevron 1**	**Chevron 2**	**Chevron 3**	**Chevron 4**	**Chevron 5**	**Chevron 6**
Beam Size		W14x120	W14x61	W14x38	**W14x26**	W14x38	**W21x44**
Beam Moment of Inertia (in4)		1380	640	385	245	385	**843**
Brace ASTM Designation		A1085	A1085	A1085	A1085	**A500 Gr. 50**	A1085
Beam iDCRs	**Axial**	0.07	0.14	0.25	0.37	0.26	0.23
	Flexural	0.84	1.74	2.9	4.44	3.1	1.73
	Interaction	0.87	1.81	2.83	4.32	3.02	1.77

3.3 Member Slenderness Requirements for SCBFs

The following is a summary of AISC Seismic Provisions (AISC 2016a) and Specifications (AISC 2016b) used for SCBF design and consequently the design of the test specimens described in this chapter.

Capacity design limits inelastic behavior to a specified ductile element in order to avoid undesirable failure modes. The braces are the ductile elements in SCBFs, and all other components of the frame were designed to develop the strength and deformation capacity of the braces from the limit states of tensile yielding and compressive buckling. The beams, columns, and connections in SCBFs were all designed for the larger of the forces determined from two scenarios. The first, where the braces were assumed to resist forces corresponding to their expected strength in tension or compression. The second, where the brace in tension is assumed to resist its expected strength while the braces in compression is assumed to have a degraded compressive strength due to repeated buckling

The Seismic Provisions (AISC 2016a) have stringent local slenderness limits to avoid local buckling of member sections and delay strength deterioration and increase deformation capacity under cyclic loading. Columns, braces, and beams of SCBFs must meet compactness criteria, in Table D1.1 (AISC 2016a) and summarized below, for “highly ductile members”. In the previous

edition of the Seismic Provisions (AISC 2010a) the requirement was more relaxed and specified that beams SCBFs satisfy the requirements for moderately ductile members. Therefore, the beams designed for the experiments satisfied the moderately ductile, but not the highly ductile requirements.

For HSS sections, the highly ductile criterion is defined by the width-to-thickness ratio of the walls of the tube:

$$b/t \leq 0.65\sqrt{E/R_y F_y}$$

For W shapes in bending or combined bending and axial load, these ductility criteria are defined by the width-to-thickness ratio of compression elements. The flanges, unstiffened elements, of W shapes are limited to:

$$b/t \leq 0.32\sqrt{E/R_y F_y} \quad \text{for moderately ductile members.}$$

$$b/t \leq 0.40\sqrt{E/R_y F_y} \quad \text{for highly ductile members.}$$

For the webs, stiffened elements, of W shapes, the local slenderness limit is dependent on the axial demand-to-capacity ratio, $C_a = P_u/\phi_c P_y$. In members with low axial demand ($C_a \leq 0.114$), the ratio is limited to:

$$\frac{h}{t_w} \leq 2.57\sqrt{E/R_y F_y}\,(1\text{-}1.04C_a) \text{ for moderately ductile members.}$$

$$\frac{h}{t_w} \leq 3.96\sqrt{E/R_y F_y}\,(1\text{-}3.04C_a) \text{ for highly ductile members.}$$

For webs of W-shapes with relatively high axial demand, ($C_a > 0.114$), the ratio is limited to:

$$\frac{h}{t_w} \leq 0.88\sqrt{E/R_y F_y}\,(2.68\text{-}C_a) \quad \text{for moderately ductile members.}$$

$$\frac{h}{t_w} \leq 1.29\sqrt{E/R_y F_y}\,(2.12\text{-}C_a) \text{ for highly ductile members.}$$

All specimens were designed to meet the highly ductile member requirements in the 2016 AISC Seismic Provisions and Specifications (AISC 2016b) except for the beam, which meets the moderately ductile member slenderness requirement. All equations presented in this section are from the AISC Seismic Provisions unless otherwise noted.

3.4 Design of Single-Story Chevron Specimens

3.4.1 Beam and iDCR calculation

AISC Seismic Provisions (AISC 2016a) stipulate for the unbalanced load in the braces of the Chevron frame to be calculated using 30 percent of the expected critical buckling strength in compression and the expected yield strength in tension. The horizontal resultants of both the elastic (unbuckled case) and post buckling brace cases per AISC 2016a are given by Eq. 3. 1 and Eq. 3. 3 respectively, and the vertical resultants are given by Eq. 3. 2 and Eq. 3. 4, where P_{cre} and P_{te}.are the expected brace strengths in tension and compression. Thus, it is evident that the vertical component is much larger in the post-buckling case, which ultimately controls the design, but the net axial load on the beam is lower in the post-buckling configuration than when both braces are at their expected capacity.

In the elastic case before braces buckle (case 1)

$$H_{br,d,e} = [P_{te} + P_{cre}]cos\theta \quad \textbf{Eq. 3. 1}$$

$$V_{br,d,e} = [P_{cre} - P_{te}]sin\theta \quad \textbf{Eq. 3. 2}$$

Post buckling case (case 2)

$$H_{br,d,post} = [P_{te} + 0.3P_{cre}]cos\theta \quad \textbf{Eq. 3. 3}$$

$$V_{br,d,post} = [0.3P_{cre} - P_{te}]sin\theta \quad \textbf{Eq. 3. 4}$$

The iDCR (idealized demand-to-capacity ratio) of the beam was computed as the value of the AISC axial-flexure interaction equation for the beam, Equation H1-1 in the AISC Specifications (AISC 2016b), and given in Eq. 3. 5 and Eq. 3. 6.

$$if \frac{P_r}{\phi_c P_n} < 0.2$$

$$iDCR = \frac{M_r}{M_c} + \frac{P_r}{2P_c} \quad \textbf{Eq. 3. 5}$$

$$if \frac{P_r}{\phi_c P_n} > 0.2$$

$$iDCR = \frac{8}{9}\frac{M_r}{M_c} + \frac{P_r}{P_c} \quad \textbf{Eq. 3. 6}$$

Where, P_r and M_r are the axial and flexural components of the demands on the beam, respectively. P_r was assumed to be distributed evenly on both sides of the beam, therefore half of the horizontal unbalanced load was allocated to the portion of the beam that was in tension, and half was allocated to the portion of the beam that was in compression as shown in the free body diagram in **Figure 3.3**. M_r was calculated assuming simply supported beam end conditions per Eq. 3. 8 from the braces unbalanced vertical load as shown in the moment diagram in **Figure 3.3**.

$$H_u = H_{br,d}$$
$$P_r = H_u/2 \quad \textbf{Eq. 3. 7}$$
$$V_u = V_{br,d}$$
$$M_r = \frac{V_u L_g}{2} \quad \textbf{Eq. 3. 8}$$

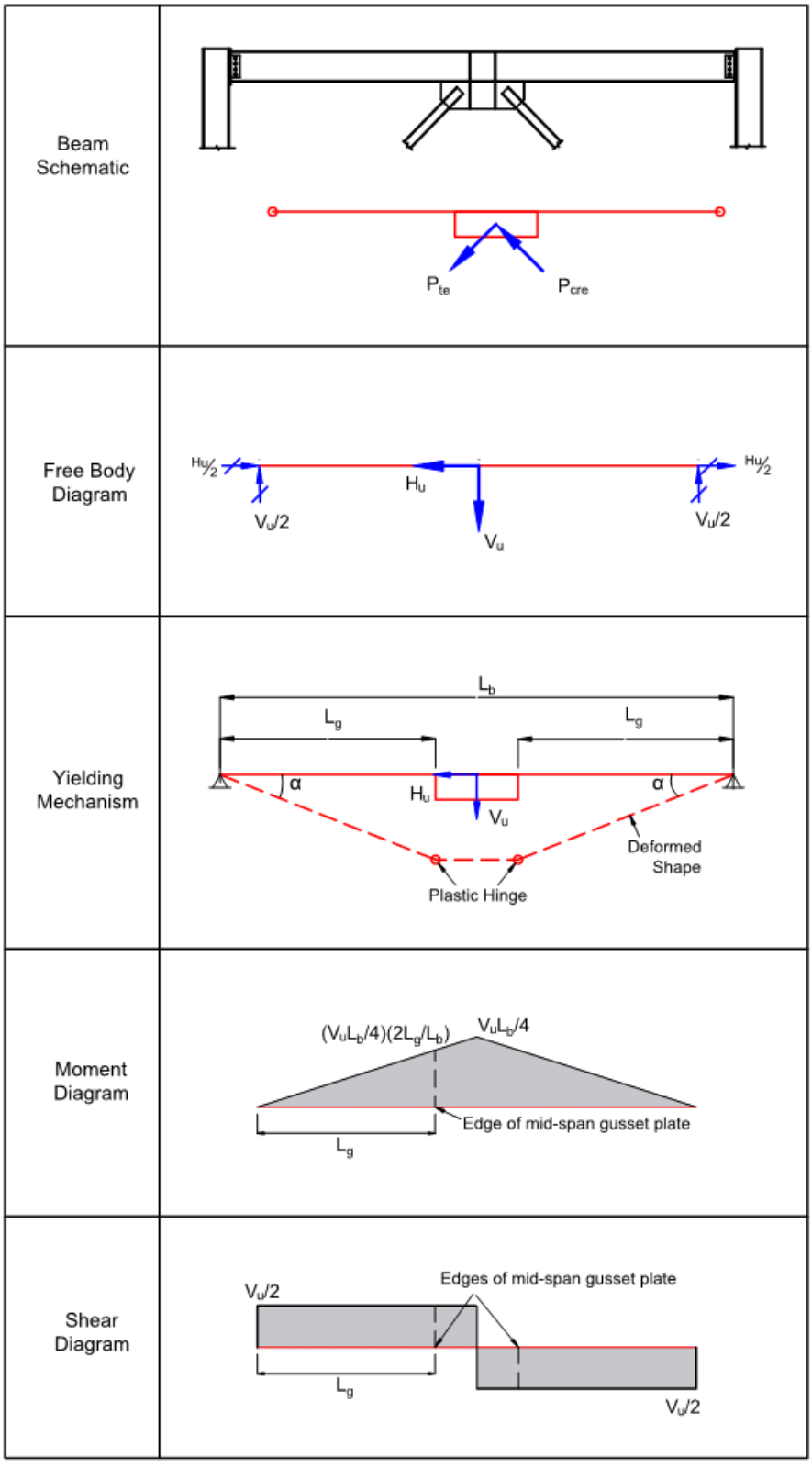

Figure 3.3 Mechanism and free-body diagram used to determine beam iDCR

P_c and M_c are the factored available axial and flexural strength of the beam, respectively, calculated according to the AISC Specification (AISC 2016b). By design, the flexural strength of the beams in the tested specimens are lower than the required flexural strength as defined above, resulting in the assumed yielding mechanism shown in Figure 3.3. The maximum moment demand in the beam occurs at the midpoint. However, when the mid-span gusset plate and stiffeners are welded to the beam, the new combined section is much deeper than the beam itself, which increases the moment of inertia and plastic moment capacity significantly. Therefore, yielding will typically occur at the edges of the mid-span gusset plate where the moment of inertia abruptly changes rather than the center of the beam where the moment demand and capacity are the highest. It follows that M_r is the moment at the edge of the gusset plate and the beam length (L_g) for use in a yielding mechanism analysis is the distance from the center of the beam-to-column connection to the edge of the gusset plate as is illustrated in Figure 3.3.

It is noted that in weaker beams the axial capacity plays a more significant role in the design of the beam and contribution to beam yielding due to P-M interaction effects. For calculation of the beam's axial capacity, P_c, the strong axis unbraced length was L_g and the weak axis unbraced length (L_y) was the distance between the beam out-of-plane supports as will be described with the experimental setup in Section 3.6.1.4. This resulted in weak axis buckling controlling the axial capacity of the beam using an effective length factor of K=1 per the simply supported beam end conditions. A sample calculation of the iDCR for the tested single-story specimens is included in Appendix A.

Furthermore, the beams met slenderness requirements for moderately ductile members and lateral bracing was provided to resist flexural and lateral-torsional buckling, so the beams were expected to be able to develop their full plastic capacity in flexure.

3.4.2 Braces

The length and angle of the braces was finalized after the frame setup was completed and square sections, as commonly used in practice for SCBF, were chosen. In a typical building, braces are designed to resist the lateral forces as determined from analysis. For the experimental program, the braces were sized based on the actuator capacity and the final frame geometry as constrained

by available space in the SRL as described in Terpstra (2017). The braces were designed so their expected lateral capacity plus a 30% frame strength contribution from the columns would not exceed 75% of the actuator capacity. The final brace size used in all single-story specimens, except Chevron 5, was an HSS4x4x5/16 of A1085 with slenderness ratio of 9.8, which met criteria for highly ductile members limited by a b/t of 14. Chevron 5 with A500 Gr.C braces had a b/t of 10.7. The length L of the braces was the end-to-end length of the element and K=1 assuming pinned-pinned ends was used for calculations.

3.4.3 Columns

Terpstra (2017) sized the columns for gravity loads typical of a 2 or 3-story office building, capacity to develop the expected strength of the braces, and with a b/2t of 6.31< 9.2 limit and h/t of 26.8 < 54 limit, meet criteria for highly ductile members as defined in the Seismic Provisions (AISC 2016a) . The resulting column section used in all tests was a W12x50 of A992 steel.

3.4.4 Connections

3.4.4.1 Gusset Plate Connections

Connections are important to achieve ductile system behavior and good SCBF performance. To avoid sudden and brittle SCBF failure modes the connections were designed using the balanced design procedure [denoted the BDP] (Roeder et al. 2011). The BDP, based on capacity design principles, promotes gusset plate yielding and allows sufficient brace end rotation. The gusset plates are designed to develop the brace capacity in tension and compression with the maximum strength limited to develop yielding of the gusset plate following brace yielding. To accommodate brace end rotation it employs an elliptical clearance for corner gusset plates and a $6t_p$ vertical clearance for mid-span gussets, which results in thinner, more compact gusset plates relative to a linear clearance, as is used in alternative gusset plate design procedures. The BDP uses a 30-60-90 triangle to calculate the Whitmore width and it encourages yielding of the gusset plate by using a resistance factor of 1.0 for yielding on the Whitmore section. In addition, it uses block-shear resistance factor of 0.85. The AISC block shear requirement has been shown to be conservative for concentrically applied loads (Huns et al. 2002).

Prior to the BDP gusset plates were designed using a linear clearance model and the Uniform Force Method (UFM) to determine forces for interface welds between the gusset plate and the beam or column. The UFM is an equilibrium method that does not account for additional strain on the welds due to inelastic deformation of the gusset plate. The BDP requires the interface plate welds to develop the yield capacity of the gusset plate because of the additional demands on the weld due to inelastic action caused by gusset plate rotation from brace end rotation. The BDP approach was used here.

Figure 3.5 and Figure 3.4 show the final design of the mid-span and corner gusset plates, respectively. The corner gusset plate connections are identical in each of the three specimens since the brace size is the same for all specimens and the geometry is very similar. Stiffeners were added to the center of the mid-span gusset and beam to stabilize the plate and beam against excess deformation while keeping the gusset plate thin to encourage tensile yielding (Lumpkin, 2009). The stiffeners are the same thickness as the gusset plate and are spaced at 12 inches to mimic column flange spacing.

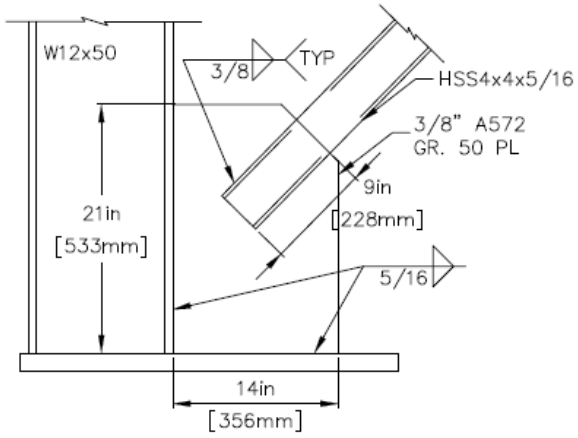

Figure 3.4 Corner gusset plate detail (All specimens)

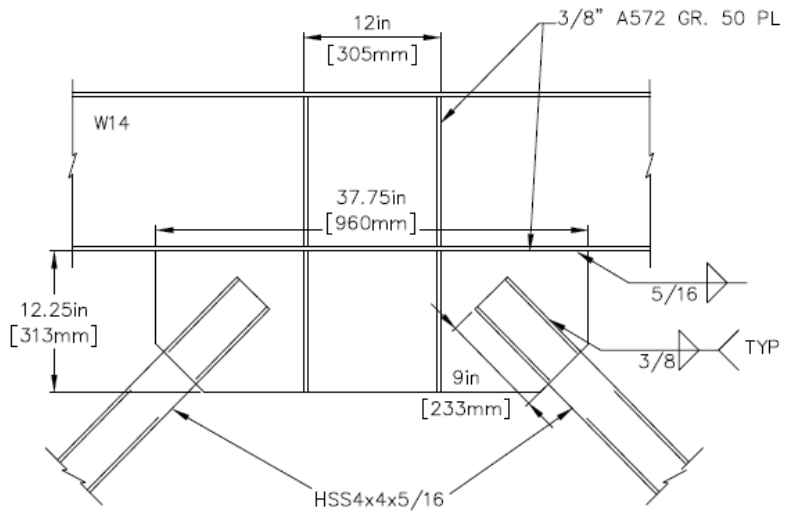

(a) Chevron 4 and Chevron 5

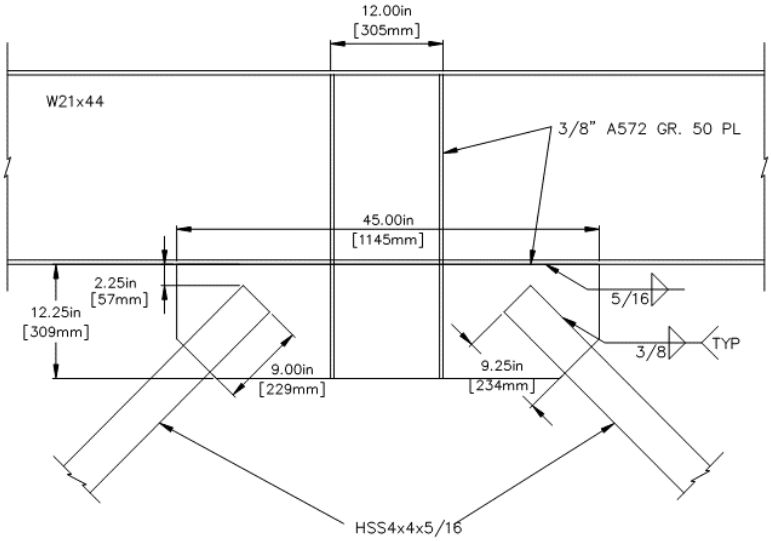

(b) Chevron 6

Figure 3.5 Beam midspan gusset plate

3.4.4.2 Beam-to-Column Connections

In each specimen the beam is connected to the columns via shear plate connections as shown in Figure 3.6. The shear plates were designed for the plastic shear and axial forces from the two analysis scenarios described in Section 3.2.2. The capacity is calculated according to the equations in Chapter J of the AISC Specification (AISC 2016b).

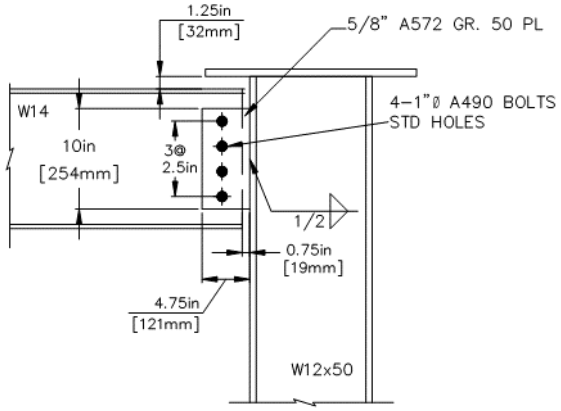

(a) W14 beam-to-column shear tab

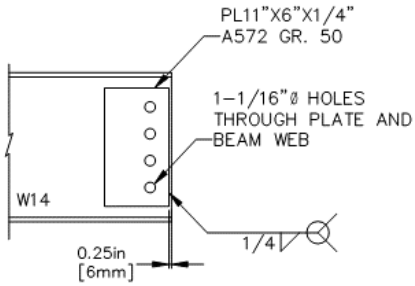

(b) W14 beam doubler

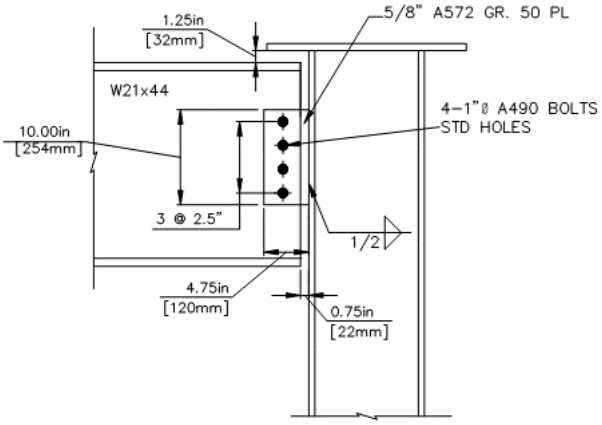

(c) W21 beam-to-column shear tab

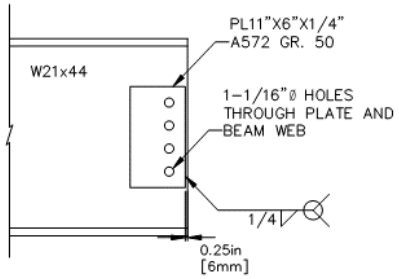

(d) W14 beam doubler

Figure 3.6 Shear Tab and beam web doubler plate

3.4.4.3 Column Web Doubler and Cap Plate

There was a ¾ inch cap plate welded to the top of each column and bolted to the bottom plate of each clevis (see the test setup description in Section 3.6.1) to provide force transfer between the clevises and the tops of the columns, as shown in Figure 3.7. This allowed replacement of the specimen and reuse of the clevises in each test. The cap plate connection was designed to resist half of the maximum actuator capacity in order to ensure that there would be no damage to this critical connection.

The webs of the W12x50 column required a ½-inch doubler plate as shown in Figure 3.7 because they did not have sufficient shear strength to ensure full transfer the force from the spreader beam through the clevis at the top of the columns to the test frame beam at the beam-to-column shear tab connection.

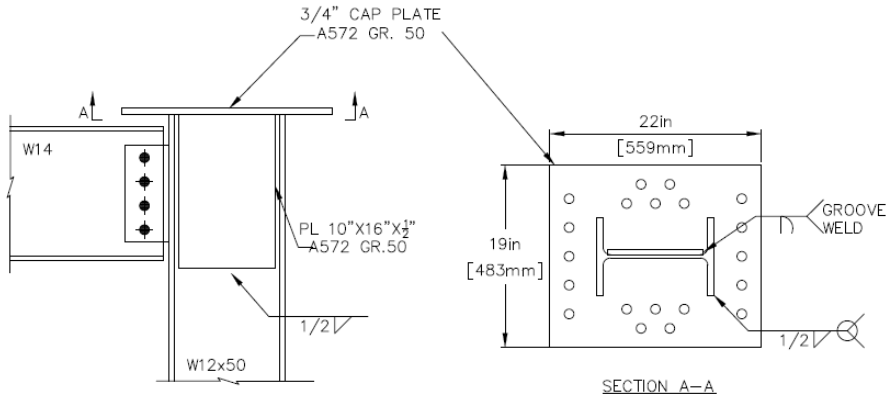

Figure 3.7 Column web doubler (left) and cap plate (right)

3.5 Materials

The material specifications of the structural sections and plates used in the test series are given in Table 3.2 below. The yield and ultimate tensile strengths, F_y and F_u, measured from on-site tensile coupon tests per ASTM E8/E8M (ASTM Standards) are provided along with overstrength factors, i.e., the ratio of measured to nominal strengths.

Table 3.2 Measured material properties

Chevron	Section	Material	F_y		F_u		F_y/F_{ynom}	F_u/F_{unom}
			(MPa)	(ksi)	(MPa)	(ksi)		
1	W14x120	A992	391	56.7	483	70.1	1.13	1.08
2	W14x61	A992	403	58.5	512	74.3	1.17	1.14
3,5	W14x38	A992	366	53.1	474	68.7	1.06	1.06
4	W14x26	A992	359	52.1	419	60.8	1.04	0.94
6	W21x44	A992	400	58	500	72.5	1.16	1.12
1 thru 6	W12x50	A992	361	52.4	454	65.9	1.05	1.01
1,2,3,4,6	HSS4x4x5/16	A1085	431	62.5	516	74.8	1.25	1.15
5	HSS4x4x5/16	A500 Gr.C	467	67.7	572	82.9	1.35	1.34
1 thru 6	3/8 in plate	A572 Gr. 50	519	75.3	586	85	1.51	1.31

3.6 Single-Story Experimental Setup

3.6.1 Existing Experimental Setup

The tests of Chevrons 4 through 6 conducted at the UW SRL for Phase II of the test series utilized the pre-existing experimental setup designed by Terpstra (2017) for Phase I. This setup was designed to test the frames in a horizontal configuration, where the plane of the frame was parallel to the strong floor. This section provides an overview of the test setup; more detailed description of the design of the setup is documented in Terpstra (2017) and the detailed drawings are repeated in Appendix B. A photograph in Figure 3.8 show the features of this setup.

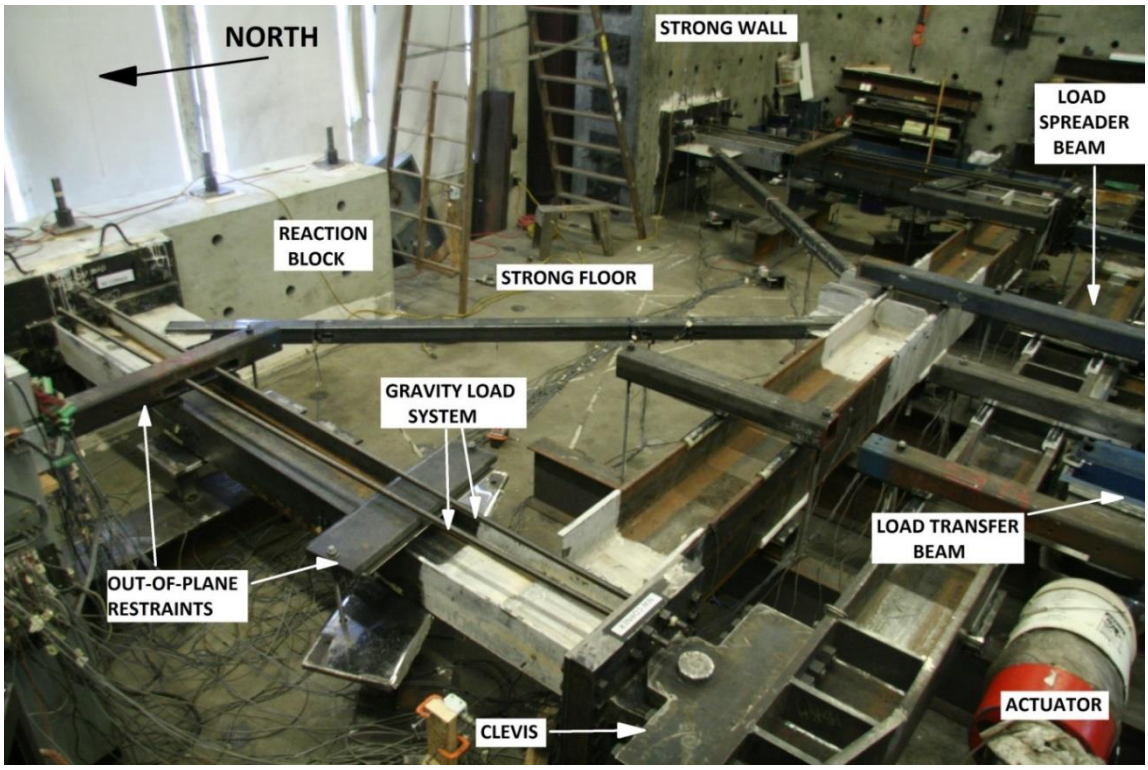

(a) Photo of setup (view from northwest corner)

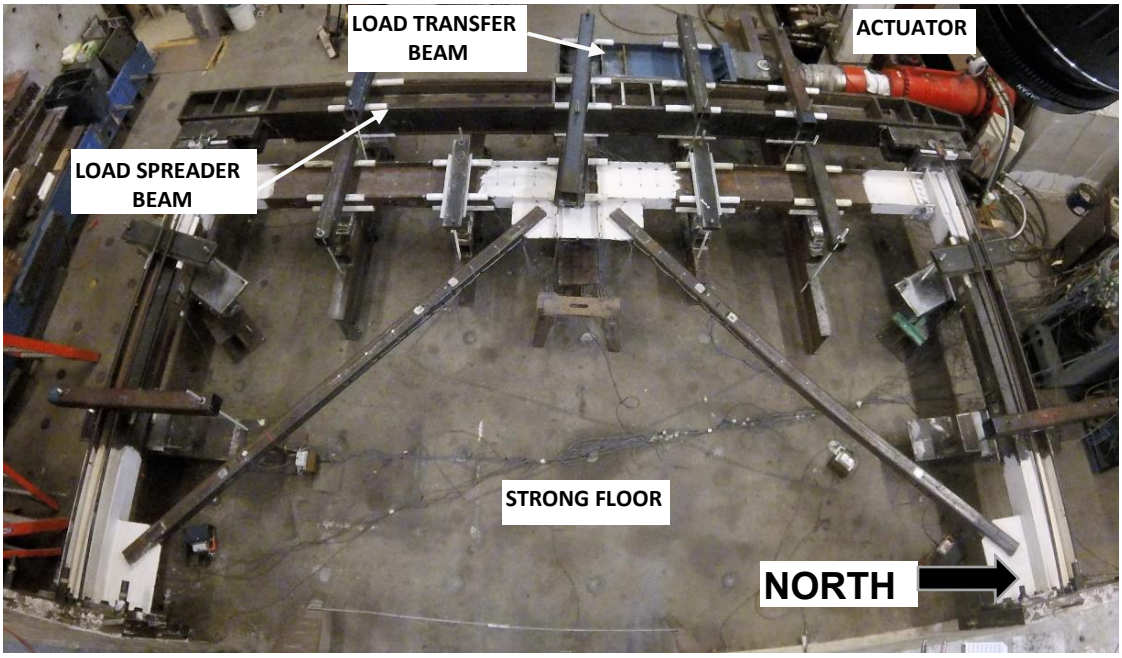

(b) Photo of setup (view from ceiling)

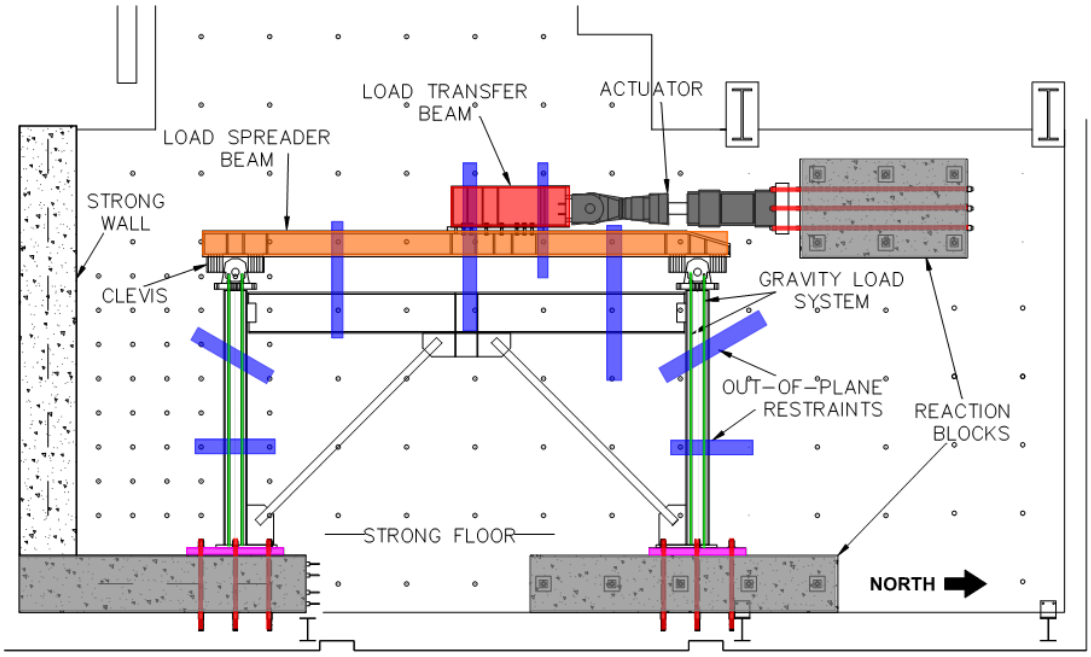

(c) Original experimental setup drawing

Figure 3.8 Picture of experimental setup

3.6.1.1 Lateral Loading

A hydraulic actuator, shown in Figure 3.9 was used to apply the lateral force and displacement history to the specimens. The actuator had a range of $\pm$10 inches and a capacity of 450 kips in tension and 550 kips in compression. Because the focus of this experimental research program is to study the performance of a yielding chevron beam, the actuator was not attached directly to the chevron beam, because the deflections would complicate force transfer.

An existing load transfer beam, shown in Figure 3.9, was employed to transfer the lateral load from the actuator to a beam. The transfer beam was designed by Johnson (2005) for a series of braced frame tests in a different configuration. The load was spread approximately evenly through the tops of the frame columns with the load spreader beam to ensure approximately symmetric distribution of load to the frame. A pair of existing clevises designed by Winkley (2009) for another research project were utilized to achieve the transfer of lateral load from the spreader beam to the top of the columns while ensuring no moment transfer at the connection.

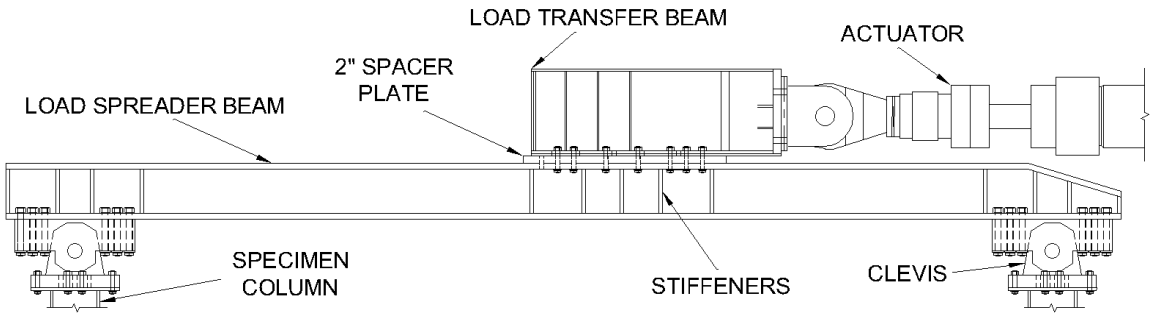

Figure 3.9 Lateral load system (Terpstra 2017)

3.6.1.2 Column Base

An anchorage system was used to connect the columns to the reaction block and strong wall to simulate boundary conditions for the lower story of a braced frame. The system consisted of an interface plate permanently affixed to the strong wall or concrete reaction block shown in Figure 3.10 and a base plate welded to the column. The two plates were connected by 12 bolts tensioned to 70 kips.The interface plates were reused but the columns and base plates were replaced for each test. The base plates, shown in Figure 3.11, were designed to develop the full plastic flexural capacity of the column plus additional axial forces from overturning of the frame.

Figure 3.10 Interface plate attached to strong wall (Terpstra 2017)

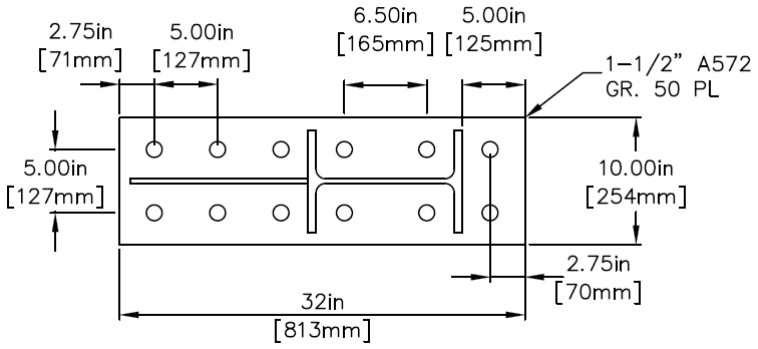

Figure 3.11 Column base plate detail

3.6.1.3 Gravity Load

A gravity load was applied to each column using 4-post tensioned rods that were positioned in pairs above and below the columns. The gravity load system utilized 1-inch threaded rods that extended from the bottom plate of the clevis to the interface plate, as shown in **Figure 3.12**. A representative load of 160 kips simulated the gravity load on columns of a single story frame. To achieve this force, each of the four rods was tensioned to 40 kips. This resulted in a compressive stress in the column of approximately 11 ksi or approximately $0.2F_y$.

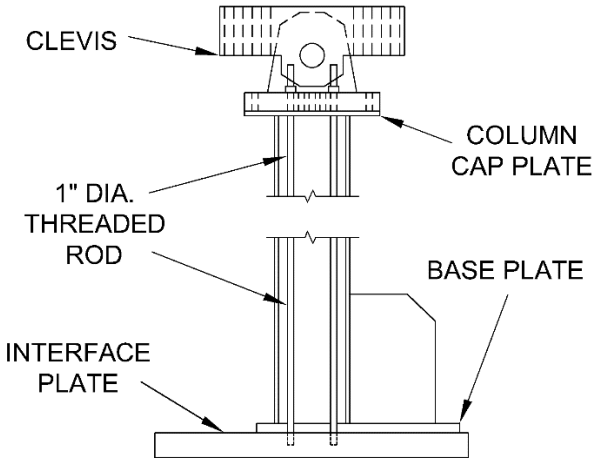

Figure 3.12 Column and gravity load system (Terpstra 2017)

3.6.1.4 Lateral Support

The out of plane restraints were used to ensure the beam and column stability. The OOP restraint locations for the beam were determined to simulate the restraint typically provided by transverse beams. In addition, the columns, load transfer beam, and load spreader beam were restrained from moving out-of-plane at selected locations (Figure 3.8) to control out-of-plane lateral torsional buckling, to facilitate delivery of load to the frame, and to prevent damage to the hydraulic actuator. The bracing also provided support to the frame during erection. Out-of-plane restraint of the beam was provided at spacing no greater than L_p for the beam sections used. The beam was braced at the locations shown in Figure 3.8.

The out-of-plane restraint was provided by steel section that were placed on the top and bottom of the elements, which were then anchored to the strong floor with long threaded rods as shown in Figure 3.13. The lateral supports did not impede in-plane movement of the frame. Teflon "sleeves" were placed on the flanges of the members, which bore on stainless steel sheets which were welded to the out-of-plane restraint and covered with a layer of lubricant to ensure frictionless sliding.

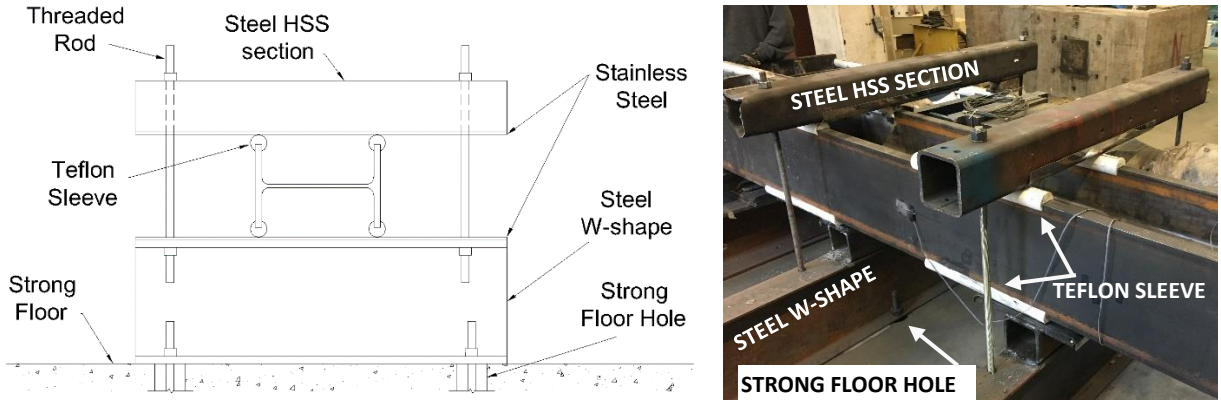

Figure 3.13 OOP restraint (Terpstra 2017)

3.6.2 Modified Experimental Setup

For Part II of the experimental series, the test setup was modified with the addition of two out-of-plane restraints. This was done to decrease the unbraced length of the beam and inhibit beam out of plane rotation as the beam required closer spacing to comply with L_p. In order to count on the

nominal flexural strength the beams of Chevrons 4 and 6 this shorter unbraced length was required. The added OOP restraints are shown in Figure 3.14. Some of the existing OOP restraints also had to be lengthened from the original configuration shown in Figure 3.8(c) in order to provide enough bearing surface for the deeper beam (W21x44) used in Chevron 6.

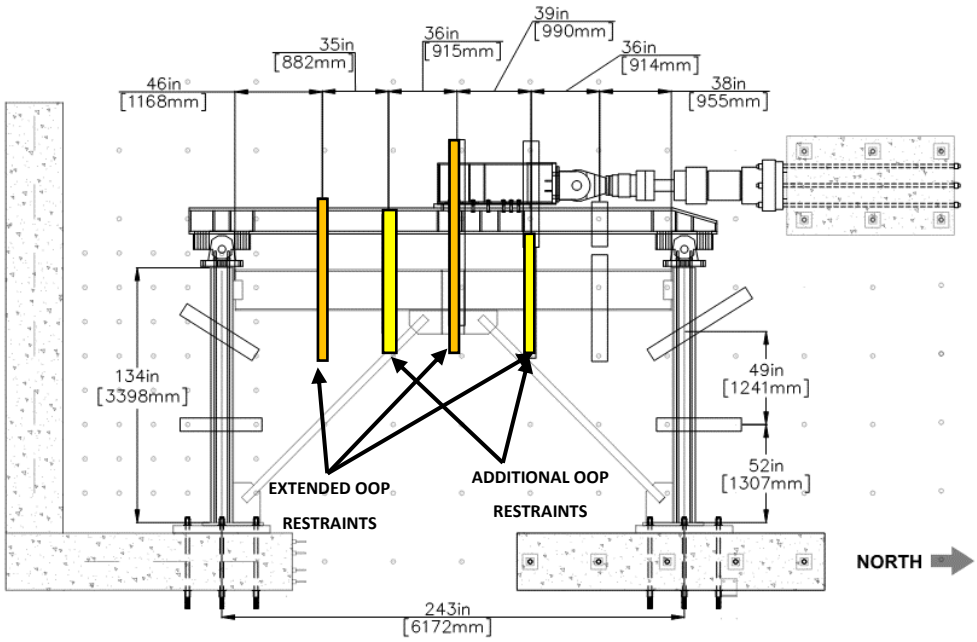

(a) Location and modifications of OOP restraints

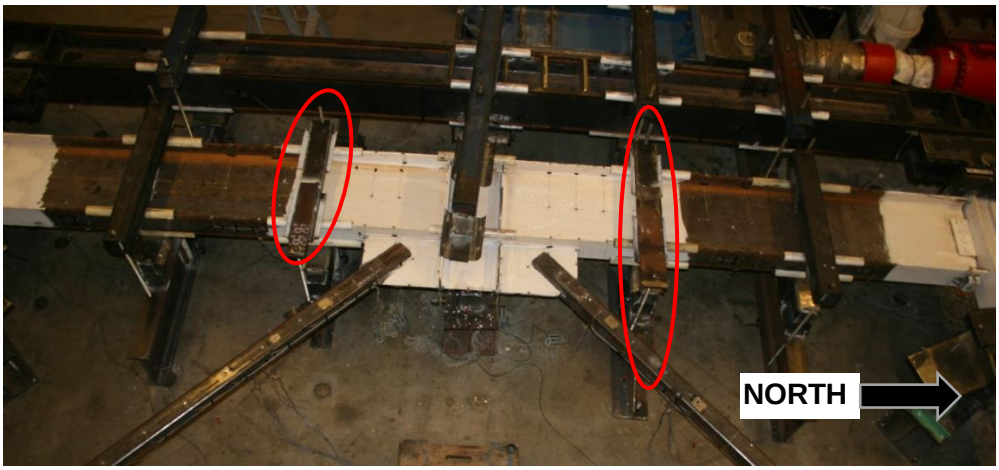

(b) Photograph of beam midspan with additional OOP restraints

Figure 3.14 Modified experimental setup

3.7 Loading Protocol

The lateral loading protocol was divided into two components: (1) prior to brace fracture (main cycles), and (2) post-fracture cycles. The cyclic loading protocol for the main cycles was conducted using displacement control of the test frame. The actuator displacement was measured during testing using the load cell within the actuator which included lateral movement of the test rig. Therefore, string pots at each end of the beam were used to verify the average movement of the frame to the target displacement. The frame was pushed to increasingly larger displacements until failure, first to the positive target displacement (North brace in compression) and then the same target displacement in the negative direction (South brace in compression) The loading protocol was based on a yield drift, Δ_y, of 8.9 mm determined from preliminary analyses and Part I tests. As shown in Table 3.3, the frame was subjected to two full cycles were run at each target displacement to capture cyclic strength degradation. The target displacements were set as multiples of the yield displacement, i.e. $0.25\Delta_y$, Δ_y, $2\Delta_y$, $3\Delta_y$, $4\Delta_y$ and so on. The larger downward displacement of the beam restricted brace elongation in the higher iDCR frames of Chevrons 3 and 4, therefore, once the brace initially tore, the actuator was pushed to result in complete brace fracture (through the cross section).

Table 3.3 Loading protocol values

Cycle	Ductility Δ/Δy	Story Disp Δ (mm)	% Story Drift	Main Cycle End Points
1,2	± -0.25	± 2.22	±-0.07	
3,4	± 0.5	± 4.45	±0.14	
5,6	± 0.75	± 6.67	±0.21	
7,8	± 1	± 8.89	±0.28	
9,10	±1.25	±11.1	±0.34	
11,12	±1.5	±13.3	±0.41	
13,14	±2	±17.8	±0.55	
15,16	±2.5	±22.2	±0.69	
17,18	±3	±26.7	±0.83	
19,20	±4	±35.6	±1.1	
21,22	±5	±44.5	±1.38	
23,24	±6	±53.3	±1.65	
25,26	±7	±62.2	±1.93	
27,28	±8	±71.1	±2.2	
29,30	±8	±80	±2.48	
31,32	±9	±88.9	±2.76	
33,34	±11	±97.8	±3.03	
35,36	±12	±106.7	±3.31	Chevrons 1,2,6
37,38	±13	±115.6	±3.58	Chevrons 3,5
37,38	±16	±142.2	±4.41	Chevron 4

After fracture of both braces, post-fracture cycles were run to determine the residual lateral resistance of the frame after both braces had fractured. The goal was to determine the lateral resistance provided by frame action. The loading consisted of actuator displacement at one-inch increments with one cycle at each displacement, as presented in Table 3.4.

Table 3.4 Post fracture loading protocol values

Cycle	Actuator Disp (mm)	Target Story Drift%
1	±25.4	0.79
2	±50.8	1.57
3	±76.2	2.36
4	±101.6	3.15
5	±127	3.94
6	±152.4	4.72
7	±177.8	5.51
8	±203.2	6.30

3.8 Instrumentation

Physical and optical sensors were installed to monitor global and local movements. Instruments used and their purpose are outlined in Table 3.5 below. The instrumentation plan was very similar to that used for Part I of the program as carefully described in Terpstra (2017).

Slight modifications were made to the Optotrak LED configuration due to conflicting locations with the addition of the out of plane restraints. Additional strain gauges were added to the beam of Chevron 6 for redundancy but the potentiometer location plan was not modified. Fully detailed instrumentation plans for all the specimens are included in Appendix B.

3.8.1 Whitewash

Regions of expected yielding were painted with a thin layer of whitewash, a lime and water mixture. When hot-rolled steel yields, mill scale on the surface of the member flakes off. The whitewash layer flakes off with the mill scale, permitting observation of initial and progression of yielding as shown in Figure 3.15.

a. Specimen before yielding b. Yielded specimen

Figure 3.15 Example of whitewash on specimen

Table 3.5 Overview of instrument description and uses

Sensor	Photo	Locations	Derived quantity
Uniaxial strain gauge	N/A	Braces …… Beams …… Columns ……	Axial force Axial and shear force, moment Axial and shear force, moment
String potentiometer		Beam …… Column …… Braces…… Gusset plates …….	Lateral and midspan displacement Elongation and shortening OOP displacement, elongation and shortening OOP rotation
Duncan potentiometer		Beams …… Anchor/Base plates	In-plane rotation Slip, uplift
Internal load cell (MTS)	N/A	Actuator …….	Applied lateral force
NDI Optotrak LED marker		*Beams* …… *Braces* …… *Mid Gusset plates*..	3D displacement and rotation OOP displacement OOP rotation

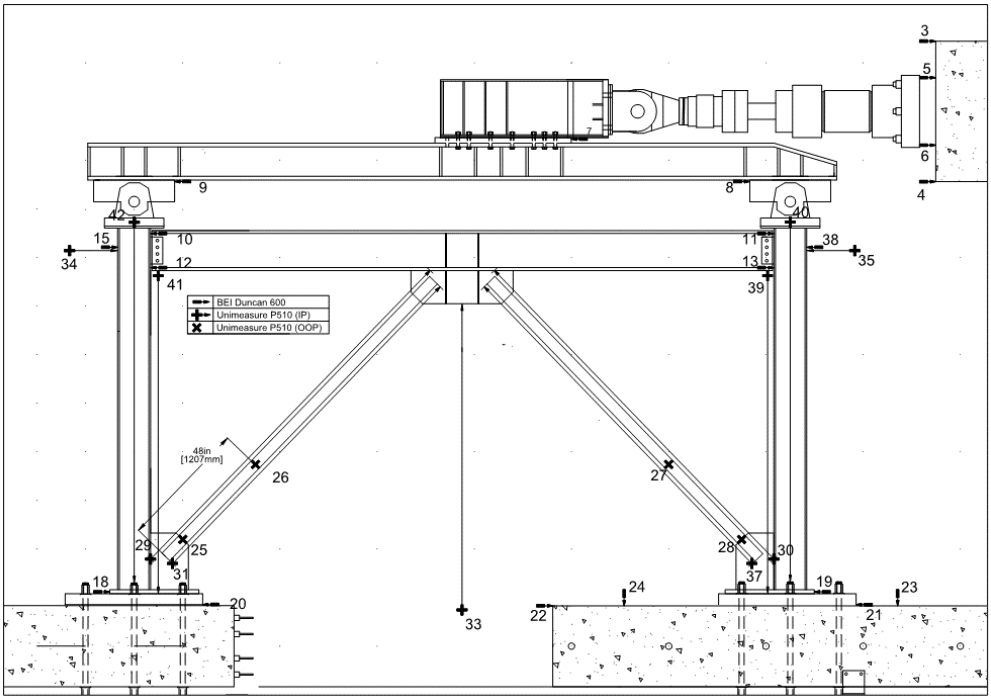

Figure 3.16 Typical potentiometer layout plan

3.8.2 Frame

The internal load cells in the actuators was used to determine the base shear forces. String potentiometers were mounted on reference stands at the north and south ends of the frame (string pots 35 and 35 in Figure 3.16) to monitor the frame displacement at each story. This measurement was used to control the actuator displacement and ensure the target story drifts were reached. The absolute actuator internal displacement was not equal to the frame displacement because of uncontrollable slip in the elements between the actuator and frame, which included the loading beam, the spreader beam, and the column clevises. The string potentiometers were mounted on reference columns at the north and south ends of the frame to monitor the frame displacement at each story.

3.8.3 Braces

The brace movement and local strains were measured at several locations as summarized in Table 3.5 to analyze elongation, out of plane movement and axial force. The out of plane deflection of each brace was measured with Optotrak LED sensors spaced every 230 mm from the beam-end of the brace to the center of each brace as illustrated in Figure 3.17(a) for the south brace. As the test

progressed and the brace deflected, the sensors near the inflection point moved out of range of the Optotrak cameras. The brace deflection in the final loading cycles was extrapolated assuming a linear relationship in the brace position along its length, in the manner illustrated in Figure 3.18. This assumption was only appropriate after the brace had formed a plastic hinge and the deflected shape was truly linear.

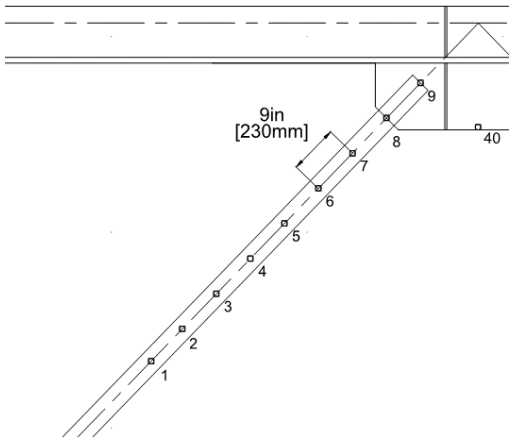

Brace Optotrak sensors

Figure 3.17 Brace instrumentation

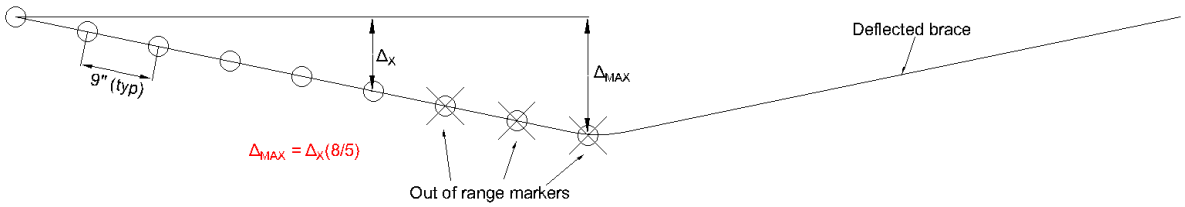

Figure 3.18 Extrapolation of brace deflected shape after plastic hinge formation (Terpstra 2017)

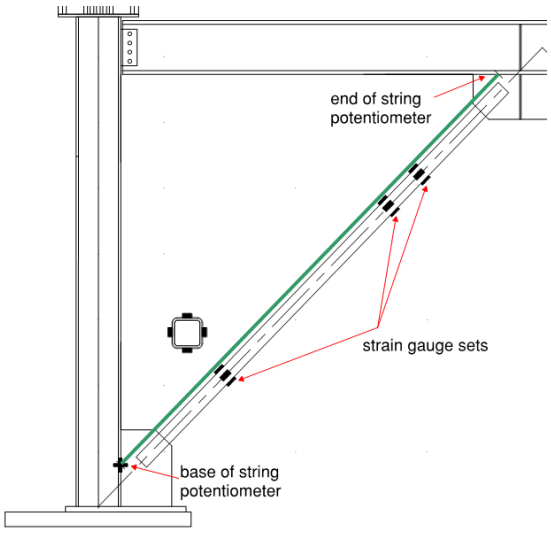

Figure 3.19 Typical Brace strain gauges and string pot

The end to end elongation of the brace was directly measured with string potentiometers anchored to the beam and column flanges, parallel to the brace. This is configuration is shown for the South brace by the green line in Figure 3.19.

The brace forces were calculated from strain measurements. A cyclic constitutive model was required to find stresses beyond yield, and then the area of the brace was used to find the force. Strain gauges at three locations on the brace as shown in Figure 3.19 were used. The sets consisted of one gauge centered on each face of the square brace at each location for a total of 12 strain gauges on each brace. The four measurements at a particular cross section were averaged to obtain the axial force at that cross section along the length of the brace, and then the three axial forces were averaged for the final reported brace axial force.

3.8.4 Beams

The beam movement and local strains were measured at several locations as summarized in Table 3.5 to analyze midspan vertical deflection, axial force, shear force, and moments.

The absolute beam vertical deflection was measured with string pot #33 and corrected for shortening of the columns and beam end movement using string pots #39 to 42. These measurements were verified with Optotrack measurements from LED #40.

Four pairs of strain gauges along the length of the beam were used to compute the axial, shear, and moment demands on the beam. Unlike in the braces, yielding did not occur at the beam gauged locations, thus the stress in the beam was directly calculated using measured strains and section properties. The beam schematic showing the strain gauges, which were attached to the center of the top and bottom flanges of the beam are shown in Figure 3.20. This figure also shows the assumed shear and moment diagrams. The expressions used to calculate these forces are given by Eq. 3. 9 and Eq. 3. 10 (dimensions used are detailed in the full instrumentation drawings in Appendix B). P and M are the axial force and bending moment at the strain gauge pair respectively, σ is the stress at each strain gauge location, and S_x is the elastic section modulus of the beam section. The stresses used for force derivation were obtained by multiplying the strain recorded from each strain gauge by the elastic modulus.

$$P = A\left(\frac{\sigma_i + \sigma_j}{2}\right) \quad \textbf{Eq. 3. 9}$$

$$M = S_x\left(\frac{\sigma_i - \sigma_j}{2}\right) \quad \textbf{Eq. 3. 10}$$

$$V_N = \frac{M_{bm,NC} - M_{bm,N}}{L_{bm,sg}} \quad \textbf{Eq. 3. 11}$$

$$V_S = \frac{M_{bm,SC} - M_{bm,S}}{L_{bm,sg}} \quad \textbf{Eq. 3. 12}$$

$$M_{bm,gN} = M_{bm,NC} + V_{bm,N} * L_{bm,gus} \quad \textbf{Eq. 3. 13}$$

$$M_{bm,gS} = M_{bm,SC} + V_{bm,S} * L_{bm,gus} \quad \textbf{Eq. 3. 14}$$

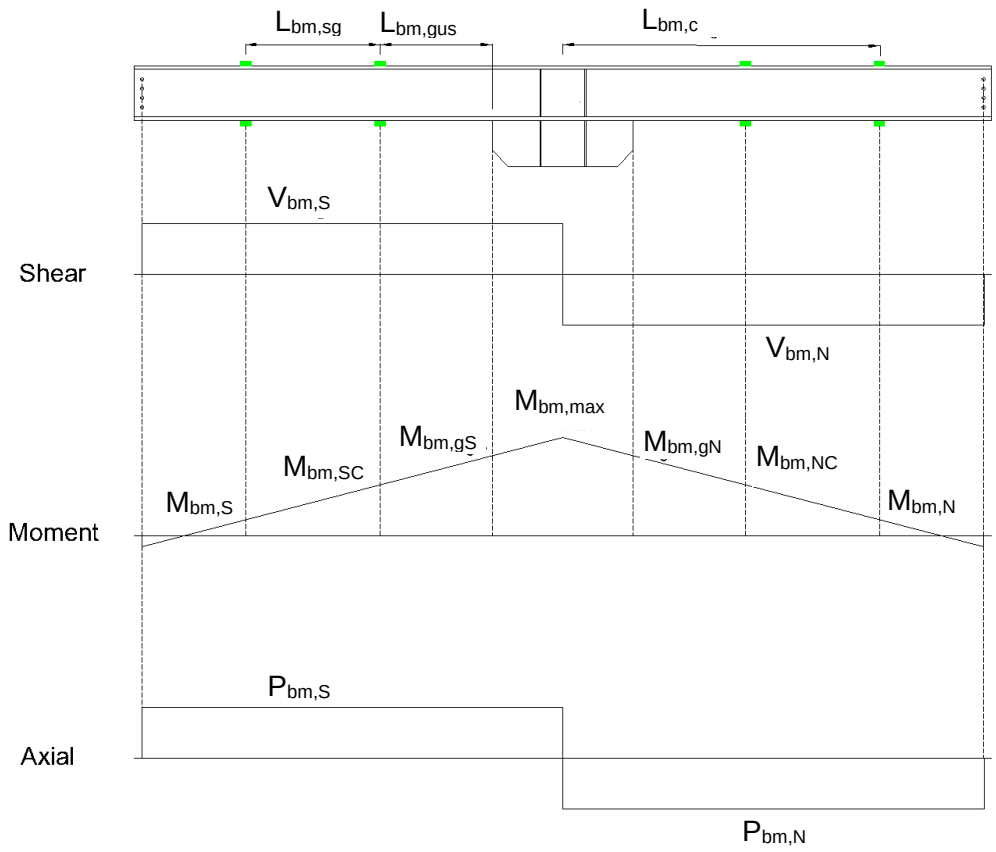

Figure 3.20 Beam shear, moment, and axial force determination

3.8.5 Columns

The column movement and local strains were measured at several locations as summarized in Table 3.5 to analyze column shortening, axial force, shear force and moments. Pairs of strain gauges on the flanges at two locations along each column were used to compute the axial, shear, and moment demands on the column. The strain gauge layout, the assumed shear and moment diagrams, and the expressions used to calculate these forces are shown in Figure 3.21 (dimensions used are detailed in the full instrumentation drawings in Appendix B) . The axial force and moment at each gauge pair was determined in the same way as for the beam.

$$V_{col} = \frac{M_{col,bot} - M_{col,top}}{L_{col,sg}}$$ **Eq. 3. 15**

$$M_{col,gus} = M_{col,bot} + V_{col} * L_{col,sg}$$ **Eq. 3. 16**

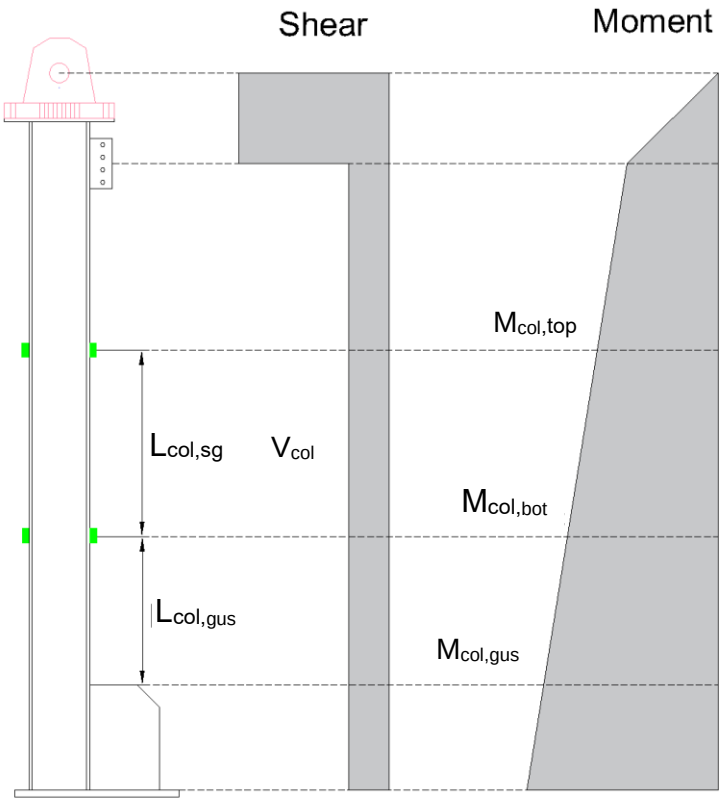

Figure 3.21 Column shear and moment determination

CHAPTER 4
Single Story Frame Test Observations

4.1 Introduction

In this chapter, the observed performance of the three chevron SCBF specimens tested at the University of Washington Structural Research Lab is described in detail. For consistency and comparison, the performance states used to describe the specimens are specifically defined in the following sections. For each specimen an overview is given of the test objective and parameters, and is followed by load - drift and beam midspan vertical deflection–drift hystereses, and tabulated documentation of each component's performance throughout the test. After this, a detailed review of the damage and cyclic response of the specimen is provided at the stages of low, moderate, and high drift. Finally, observations made the six single-story chevron SCBF specimens tested in Phases I (see Section 2.7 and (Terpstra 2017)) and II of the experimental program are compared.

The story drift δ is the ratio of lateral displacement to the height of the relevant location. In the following sections, story drifts will be presented and were calculated as shown in Eq. 4. 1 where *h* is the frame height measured from the mid-depth of the baseplate to the mid-depth of the beam, and Δ is the lateral displacement at each step, as shown in Figure 4.1. The lateral displacement Δ was calculated from the reading of two string potentiometers on opposite sides of the frame attached at the top outer flange of the north and south columns. The base shear was determined from the actuator load cell measurement recording

$$\delta_{Story} = \frac{\Delta}{h}\ x\ 100\% \qquad \text{Eq. 4. 1}$$

For Chevrons 1 through 5

h = 127 in [3226 mm]

For Chevron 6

h = 123 in [3124 mm]

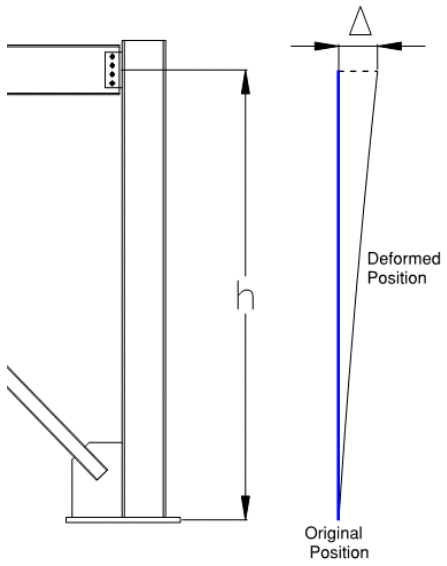

Figure 4.1 Frame parameters for drift calculation

4.2 Performance State Descriptions

Overall frame performance depends on component damage progression as evidenced by yielding, buckling, and connection damage. The performance is supported through test observations at the locations of interested shaded in Figure 4.2. Terpstra (2017) developed specific nomenclature to differentiate the performance states that consist of letter and number combinations. The abbreviations are provided in Table 4.1 where the letters describe the type of damage and the numbers describe the severity of the damage: 1-initial, 2-moderate, 3-severe, and 4-failure. Table 4.2 through Table 4.6 in the following sections provide specific descriptions of the performance states for each component of the specimen. In addition to the numerical code, the damage severity

is signified by shading damage progressively darker in the summary tables that precede detailed description of each test specimen.

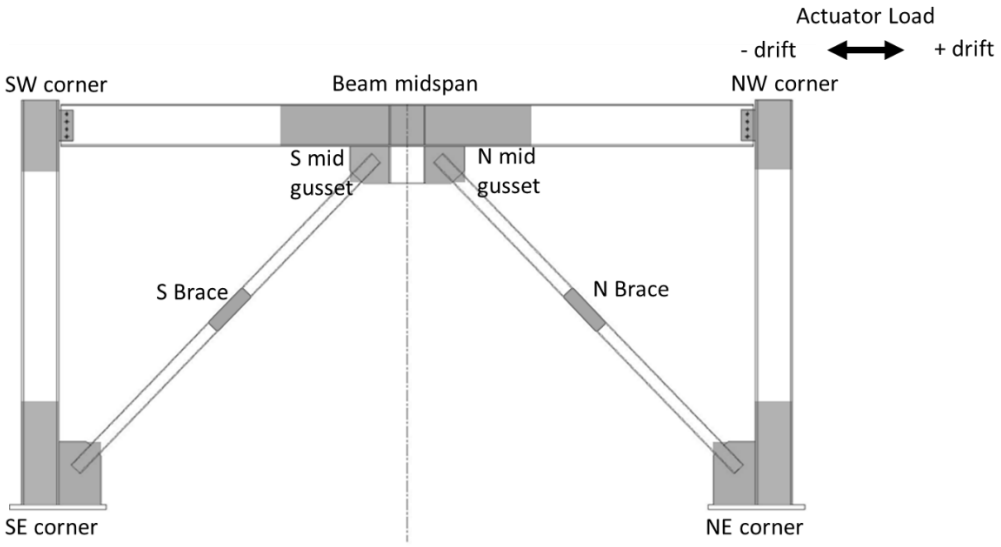

Figure 4.2 Frame notation

Table 4.1 Observed Yield Mechanisms and Failure Modes (Terpstra 2017)

Brace Performance States	**Connection Performance States**	**Frame Performance States**
Brace Buckling (B1,B2)	Weld Tearing (WT1,WT2,WT3)	Frame Yielding (Y1,Y2,Y3)
Brace Plastic Hinging (B3-PC)	Plate Yielding (Y1,Y2,Y3)	Frame Local Buckling (LB1,LB2,LB3)
Brace Tearing (B3-BT)	Plate Cracking (PC1) (PC2)	
Brace Fracture (B4-BF)		

4.2.1 Brace Performance States

Brace performance involves the progression from buckling to plastic hinge formation, tearing, and ultimately fracture of the cross section. Initial brace buckling was not visibly distinguishable but was identified in the data at the point of reduced brace compressive capacity. Further buckling continues in an approximate half sine wave until plastic hinge formation, which was evident in cupping at the brace midpoint. As local buckling continues initial tears or striation lines begin to

form in the compression face of the plastic hinge, which is where the most severe strain accumulation occurs. Increased tearing eventually leads to complete rupture of the cross section in tension. Table 4.2 further distinguishes brace performance states.

Table 4.2 Brace Performance States (Terpstra 2017)

Abb.	Performance State	Description
B1	Initial Global Buckling	Brace mid-span deflection is visible but less than twice the brace depth.
B2	Moderate Global Buckling	Brace mid-span deflection exceeds twice the brace depth.
B3 – BC	Brace Local Cupping Deformation	Visible cupping at brace midpoint.
B3 – BT	Brace Tearing	Striation lines begin to separate in plastic hinge region of the brace.
B4-BF	Brace Fracture	Brace factures through entire section.

4.2.2 Frame Performance States

In this context, the framing members are the beam and the columns. Performance of these members throughout each test for all specimens involved yielding and local buckling of the web and flanges. Yielding in these members was identified by the flaking of the steel's mill scale, which was made more apparent by the application of the whitewash. Yielding occurred at the inner and outer flanges of the beam and column in the plastic hinge region, which extended as outlined in Figure 4.3 and Figure 4.4.

Table **4.3** further distinguishes the performance states of the framing members.

Table 4.3 Frame Performance States

Abb.	Performance State	Description
Y1	Initial Yielding	First visible yield lines in specified location.
Y2	Moderate Yielding	Whitewash is flaked off on 50% of the specified location.
Y3	Severe Yielding	Whitewash is flaked off on >80% of the specified location.
LB1	Initial Local Buckling	OOP local deformation observed in flange or web.
LB2	Moderate Local Buckling	OOP local deformation exceeds element thickness.
LB3	Severe Local Buckling	OOP local deformation exceeds two times the element thickness.

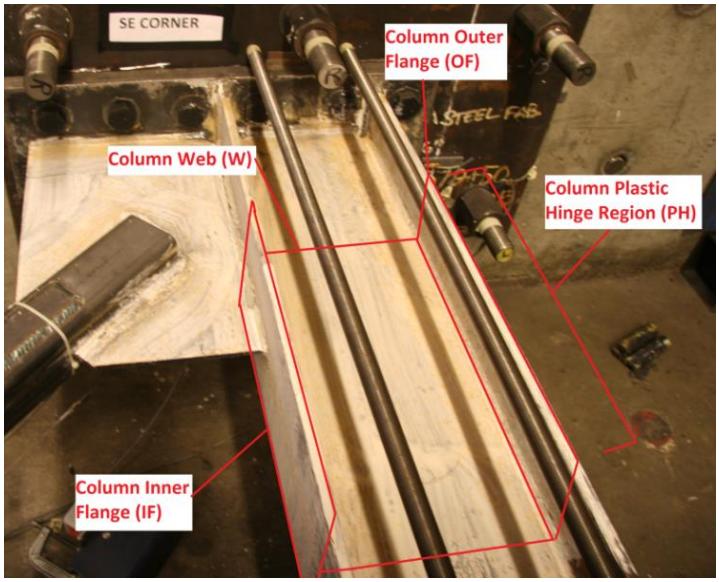

Figure 4.3 Nomenclature for column damage locations (Terpstra 2017)

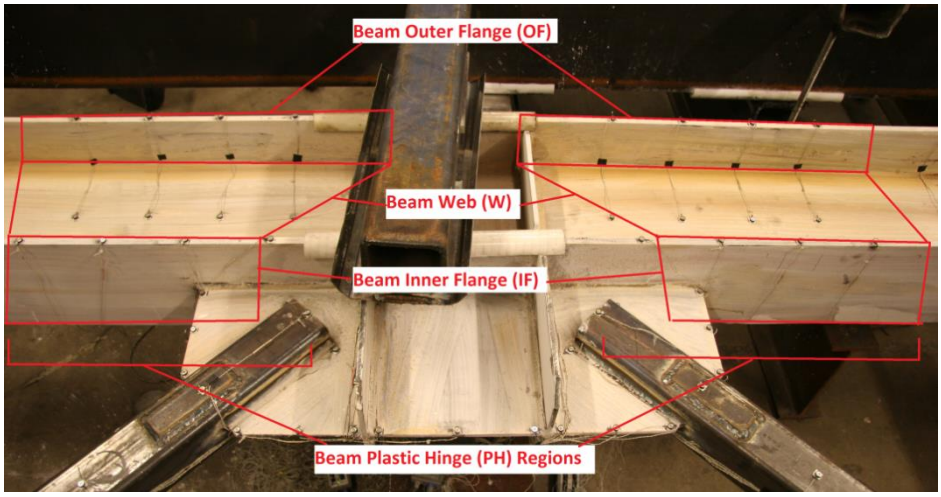

Figure 4.4 Nomenclature for beam damage locations (Terpstra 2017)

4.2.3 Connection Performance States

The connection performance states include plate yielding, plate cracking, and weld tearing. The gusset plate connections experienced plate yielding, plate cracking, and weld tearing. The shear plate connections only experienced plate yielding and to a much lesser extent than the gusset plates. There was also some bolt-hole elongation in the beam web, which was observed after a series of post fracture load cycles at the end of the test and is documented at the end of the main narrative of each test. No damage was observed in the base plate or cap plate connections for any of the specimens.

4.2.3.1 Plate Yielding

As in the framing members, plate yielding performance states are distinguished by the percentage of whitewash that flaked off of the component. The initial (Y1), moderate (Y2), and severe (Y3) plate yielding performance states are defined in Table 4.4 and differ from the frame yielding performance states.

4.2.3.2 Plate Cracking

Observed plate cracking, due to rotation demands, was very limited in the three tests described here. Plate cracking occurred near the welds but is differentiated from weld tearing, defined in the next section, where a crack initiates past the toe of the weld. Cracking was observed in the gusset plates at the toe of the mid-span gusset-to-stiffener welds as shown in Figure 4.5. Definitions for

initial (PC1) and moderate (PC2) performance states are defined and differentiated from weld tearing, but only initial cracking was observed on one of the tests. The additional abbreviation is shown in Table 4.5 comparison purposes with Phase I chevrons. In the performance state tables for each specimen, plate cracking is described alongside the weld at which it occurred rather than the element that cracked in order to clearly differentiate multiple crack locations at the mid-span gusset plate.

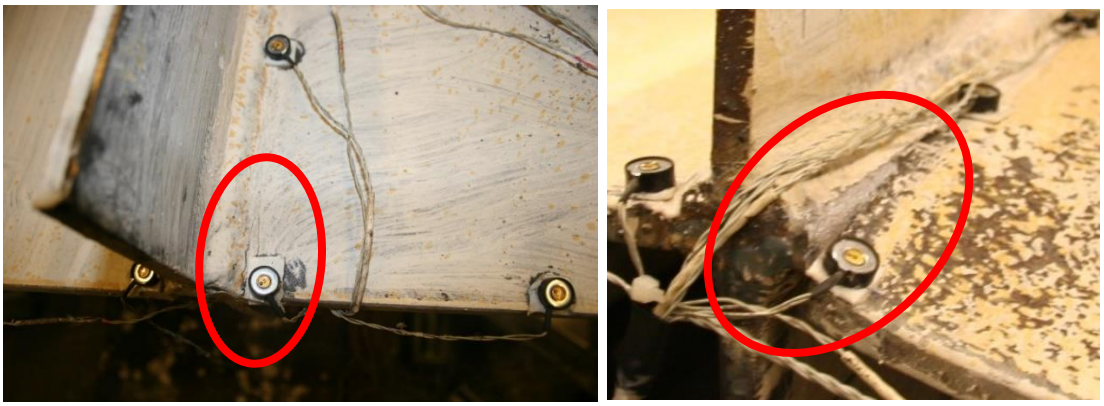

Figure 4.5 Location of observed plate cracking (gusset plate and stiffener)

4.2.3.3 Weld Tearing

Weld damage occurred due to large OOP rotation of the gusset plate connections. The weld performance states shown in Table 4.6 are distinguished by the percentage of the weld length that has torn. At the midbeam gusset plate, the beam to gusset weld length was defined from the edge of the stiffener to the edge of the gusset plate. The weld performance states reflect fracture mechanics concepts of crack initiation (WT1), stable crack growth (WT2), and unstable crack growth (WT3). As described in Table 4.6 each of the performance states was differentiated by the crack length that defines each performance state. A clear example of the observed weld damage is shown in Figure 4.6.

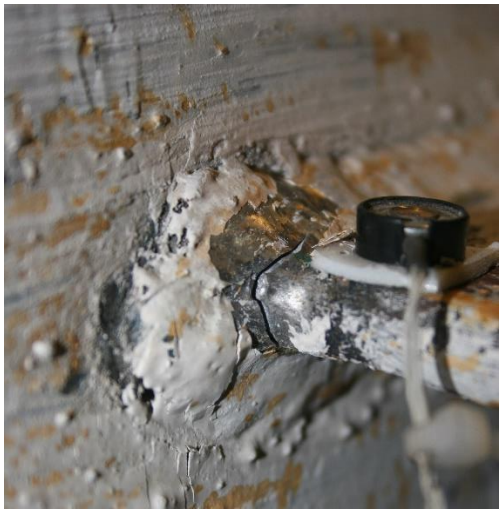

Figure 4.6 Weld crack in gusset plate–to-beam interface weld

Table 4.4 Plate Yielding Performance States

Abb.	Performance State	Description
Y1	Initial Yielding	First visible yield lines in specified location.
Y2	Moderate Yielding	Whitewash is flaked off on 20-50% of the plate area.
Y3	Severe Yielding	Whitewash is flaked off on >50% of the plate area.

Table 4.5 Plate Cracking Performance States

Abb.	Performance State	Description
PC1	Initial Cracking	First visible cracks appear in plate.
PC2	Moderate Cracking	Plate cracks through entire thickness.
PC3	Severe Cracking	Plate crack exceeds 30% of plate dimension.

Table 4.6 Weld Tearing Performance States

Abb.	Performance State	Description
WT1	Initial Weld Tearing	First visible weld cracks appear.
WT2	Moderate Weld Tearing	Weld tear exceeds 10% of weld length.
WT3	Severe Weld Tearing	Weld tear exceeds 30% of weld length.

4.3 Chevron 4 Observations

Chevron 4, built as the elevation in Figure 4.7, was tested on July 27, 2017. The purpose of this test was to investigate the effect of a weak beam on the cyclic behavior of chevron SCBFs. Chevron 4 had identical frame geometry, column size, brace size, and connection details as Chevron 1 (Terpstra 2017) but utilized a W14x26 beam instead of a 14x120 beam. The W14x26 beam had an iDCR of 4.32 for the AISC requirement to develop the unbalanced load from the braces. The gusset plates were designed using the BDP and all other components and welds met seismic code requirements (AISC 2010b).

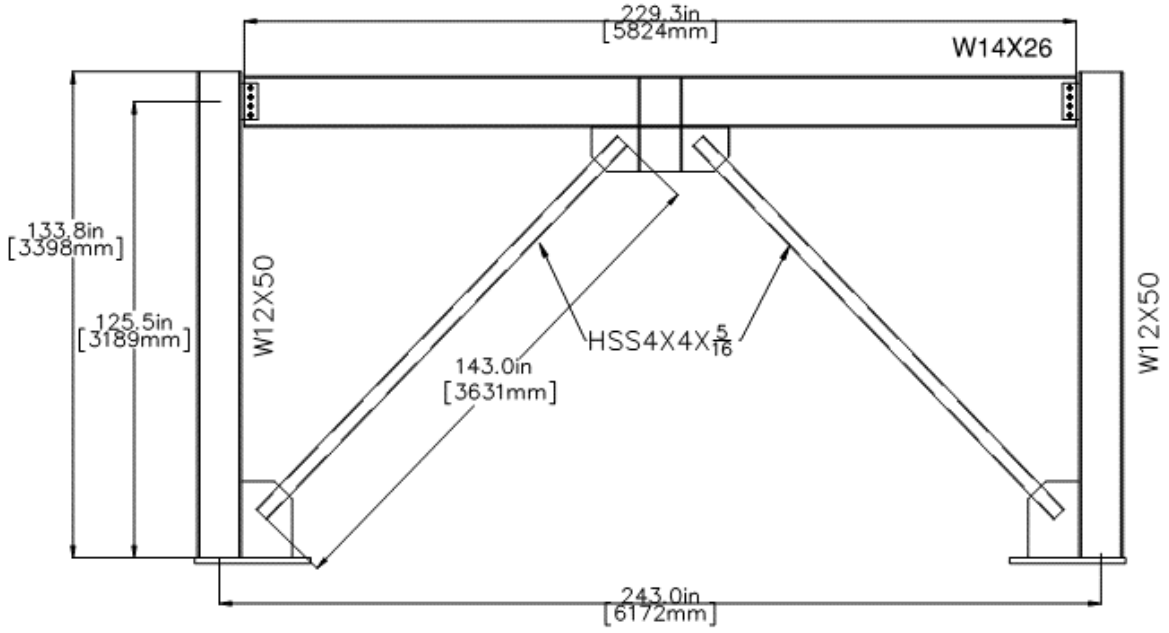

Figure 4.7 Chevron 4 elevation drawing

4.3.1 Overview of Performance

Chevron 4 achieved a drift range of 9.1% until the second brace fracture and had a maximum lateral resistance of 162 kips. The hysteretic base shear vs. story drift relationship is shown in Figure 4.8 shows the expected lateral resistance of the braces, $2P_{cr}\cos\theta$. The beam experienced initial yielding at 0.34% drift and had a maximum midspan deflection of 3.8 inches as shown in the hysteretic deflection plot in Figure 4.9. The residual deflection at the end of cyclic loading was 3.2 inches. The failure mode was brace fracture; the south brace fractured first at the first +4.4% drift cycle, and the north brace fractured at -4.7% drift. The braces began to buckle OOP at ±0.28% drift, and sustained progressively larger OOP buckling deformations each cycle, leading to plastic hinge formation in the center of the braces. The braces began to deform locally at mid-span as a result of plastic hinge formation, eventually leading to tearing and fracture of the braces. The maximum deflection of the two braces was approximately 20.5 inches. Connection damage included plate yielding, weld tearing, and gusset plate deflection of up to 2.8 inches downward. The columns sustained yielding and local buckling in the plastic hinge region.

After both braces had fractured, post-fracture cycles were run to determine the residual lateral resistance from frame action. The frame was cycled to ±5.0% drift; the force-drift response is shown in Figure 4.8. With a maximum resistance in post buckling of 86 kips, the columns resisted 53% of the frame's maximum lateral resistance The columns sustained more severe yielding and local bucking at high drift ranges, but no other damage was observed.

4.3.2 Result Summary

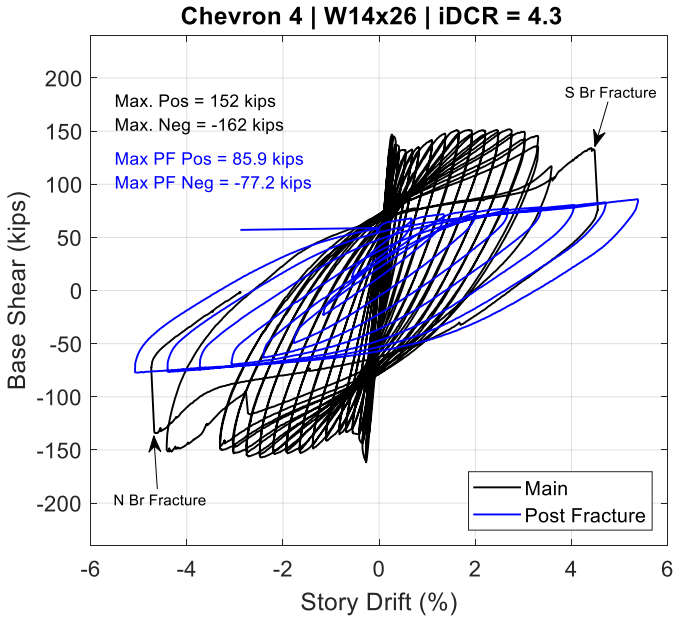

Figure 4.8 Chevron 4 Hysteresis

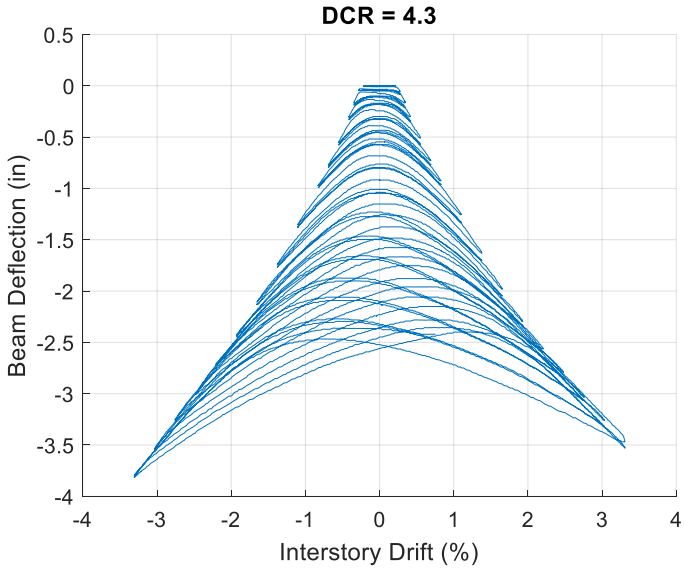

Figure 4.9 Chevron 4 Beam Deflection

Table 4.7 Chevron 4 Performance States

		Low Drift									Moderate Drift				High Drift						
	Cycle	1-2	3-4	5-6	7-8	9-10	11-12	13-14	15-16	17-18	19-20	21-22	23-24	25-26	27-28	29-30	31-32	33-34	35-36	37	38
	Drift (+/-)(%)	0.088	0.14	0.21	0.28	0.34	0.41	0.55	0.7	0.83	1.1	1.4	1.7	1.9	2.2	2.5	2.8	3.0	3.3	-4.4	4.6
	Drift Range (%)	0.18	0.28	0.41	0.55	0.69	0.83	1.1	1.38	1.65	2.2	2.76	3.31	3.86	4.41	4.96	5.51	6.06	6.61	8.02	9.28
	South Brace				B1				B2							B3-BC			B3-BT		B4-BF
	North Brace				B1				B2							B3-BC				B3-BT	B4-BF
SE Corner	South Column										Y1				Y2	Y3		LB1	LB2		
SE Corner	GP-Column Weld												WT1	WT2				WT3			
SE Corner	Gusset Plate			Y1								Y2					Y3				
NE Corner	North Column										Y1				Y2	Y3					
NE Corner	GP-Column Weld														WT1	WT2			WT3		
NE Corner	Gusset Plate			Y1								Y2					Y3				
Mid-Span Gusset	GP-Beam Weld (N)												WT1	WT2				WT3			
Mid-Span Gusset	GP-Beam Weld (S)												WT1	WT2					WT3		
Mid-Span Gusset	GP-Stiffener Weld (N)																				
Mid-Span Gusset	GP-Stiffener Weld (S)																				
Mid-Span Gusset	Gusset Plate (N)			Y1					Y2							Y3					
Mid-Span Gusset	Gusset Plate (S)			Y1					Y2							Y3					
Mid-Span Gusset	Beam					Y1							Y2								
	North Shear Tab				Y1												Y2				
	South Shear Tab				Y1										Y2						

4.3.3 Low Drift (Story drift < 1%)

Significant events during the low drift cycles included:

- The corner gusset plates began to yield (Y1) at ±0.208% drift (Figure 4.10 andFigure 4.11).
- The North brace began to buckle (B1) on the first cycle of 0.28% drift.
- The South brace began to buckle (B1) on the first cycle of -0.28% drift.
- The mid-span gusset and shear plates began to yield (Y1) at ±0.28% drift.
- The mid-span gusset plate experience moderate yielding (Y2) at ±0.70% drift
- The beam began to yield (Y1) at the outer and inner flange near the stiffeners at ±0.70% drift (Figure 4.13).
- At ±0.7% story drift, the braces buckled out of plane more than twice the depth of the brace (B2)

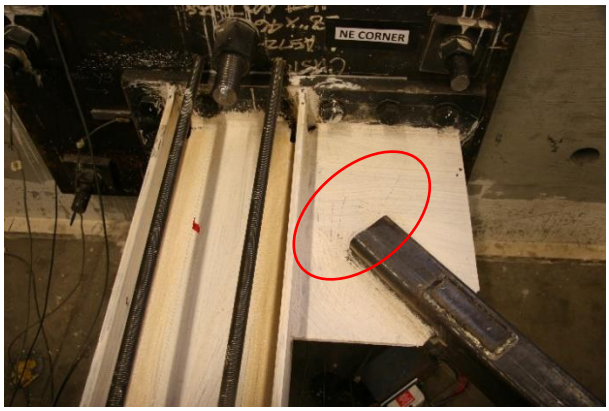

Figure 4.10 NE Corner Gusset yielding @ -0.21%

Figure 4.11 NE gusset @ -0.28% drift

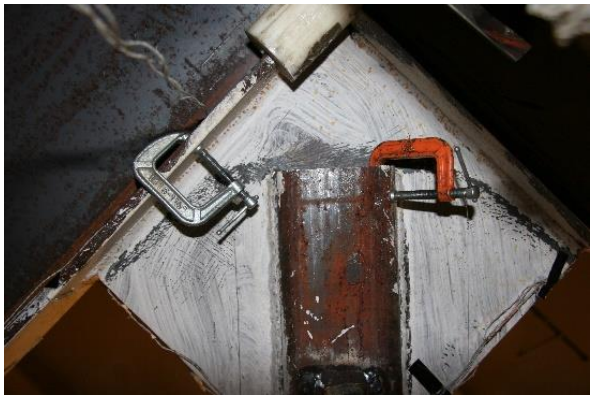

Figure 4.12 Elliptical yielding @ S mid gusset @ -0.55%

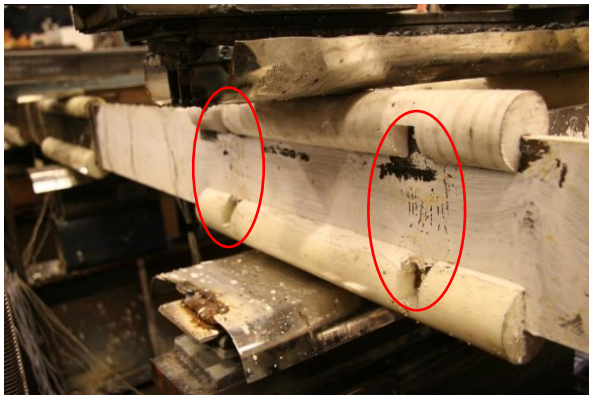

Figure 4.13 Beam yielding @ +0.7% drift

4.3.4 Moderate Drift (1% < Story drift < 2%)

Significant events during the moderate drift cycles included:

- At ±1.1% story drift, the inside beam flange began to yield (Y1) (Figure 4.15).
- At ±1.1% story drift the columns began to yield (Y1)
- At -1.4% story drift, tearing initiated at the toes of the south brace-to-mid-span gusset plate welds (WT1) (Figure 4.17)
- At ±1.4% story drift the corner gusset plates experienced moderate yielding (Y2)
- At -1.7% story drift, beam began to twist out of plane slightly at midspan
- At ±1.7% story drift the beam experienced moderate yielding (Y2) in the plastic hinge region (Figure 4.19)
- At +1.7% story drift, crack initiated at the NE corner gusset weld (WT1)
- At ±1.9% story drift moderate buckling of corner gusset plate was observed (Figure 4.21)

Figure 4.14 SE corner gusset @ +1.1%

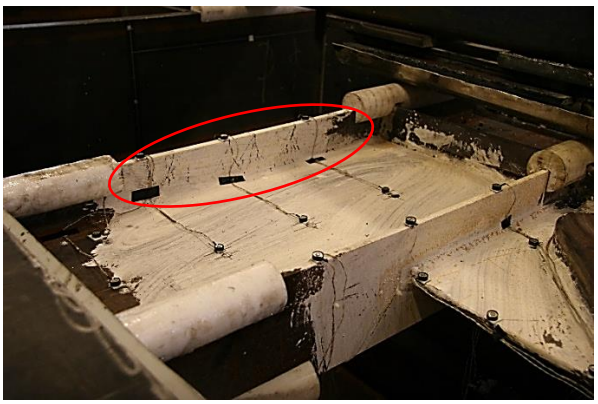

Figure 4.15 Beam yielding @ +1.1%

Figure 4.16 S column yielding @ -1.4% drift

Figure 4.17 N mid gusset @ -1.4% drift

Figure 4.18 N Column @ -1.7 %

Figure 4.19 Beam yielding @ -1.7%

Figure 4.20 Beam end torsion @-1.9% drift

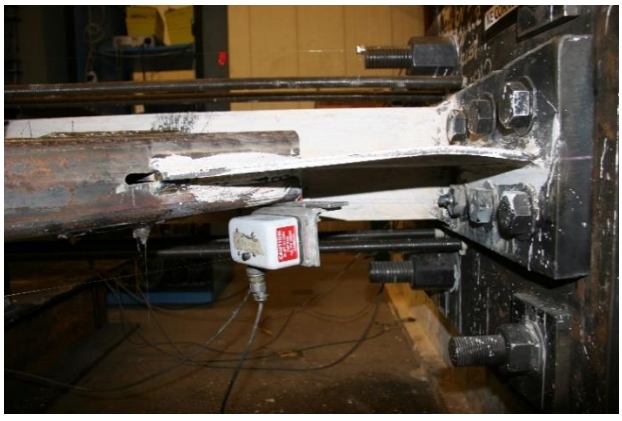

Figure 4.21 Buckling @ NE corner gusset @ +1.9%

4.3.5 High Drift (Story drift > 2%)

At high story drifts there was tearing at the edge of all gusset-to-column and gusset-to-beam welds. Table 4.8 shows the progression of damage to these welds throughout the higher drift cycles. Weld cracks were consistently longer on the top than bottom side of the gusset weld due to downward rotation of the gusset plates. The reported weld crack lengths in this chapter are the longer measurements recorded, on the top side unless noted otherwise. In addition to weld tearing, the following significant events occurred:

- At ±2.2% story drift the beam experienced moderate yielding (Y2) in the plastic hinge region
- At ±2.5% story drift, the braces experienced slight cupping (B3-BC)
- At ±2.5% drift, the columns underwent initial local buckling (LB1) of the flanges in the plastic hinge region
- At ±2.5% drift, the columns experienced severe yielding (Y3) in the plastic hinge region
- At ±3.31% drift, striation lines (B3-BT) appeared in the center of each brace
- At the second cycle of +3.31% drift S brace tore slightly (B3-BT) (Figure 4.29)
- At +3.58 story drift, the S brace tore 3/4 through the cross-section (B3-BT), leaving only the bottom face of the brace intact (Figure 4.30)
- At the second cycle of -3.58% drift N brace didn't fracture so actuator was pushed to -4.4% drift to incite N brace tearing halfway through cross section (B3-BT)
- At -4.55% drift, the columns experienced moderate local buckling (LB2) of the flanges in the plastic hinge region
- Frame pushed to +4.4% drift to incite complete S brace fracture (B4-BF)
- Frame pushed to -4.7% drift to incite complete N brace fracture (B4-BF)

Table 4.8 Chevron 4 Weld Crack Propagation

Drift (%)	N mid-span gusset-to-beam	S mid-span gusset-to-beam	NE gusset-to-column	SE gusset-to-column
1.7	1-1/8”	3/8”	1-1/8”	
1.9	2”	1-3/8”	2-5/8”	
2.2	2-5/8”	2-1/8”	3-3/4”	1-3/8”
2.5	3-1/8” (top) 2” (bot)	2-7/8”	4-3/4” (top) 3.25” (bot)	2-3/4” (top) 1-1/2” (bot)
2.8	3-3/4”	3-1/2”	5-7/8”	4-1/4”
3.0	4/1/4”	3-5/8”	6-3/4”	4-5/8”
3.3	4-5/8”	4-5/8”	7-1/4”	6-1/2”
3.5		4-3/4”		7-1/4”
4.5	5-1/4” (top) 4-1/2” (bot)	5” (top) 4-1/2” (bot)	9-3/8”(top) 9-1/2” (bot)	9-7/8” (top) 9-3/8” (bot)

Figure 4.22 SW Shear plate @ +2.2%

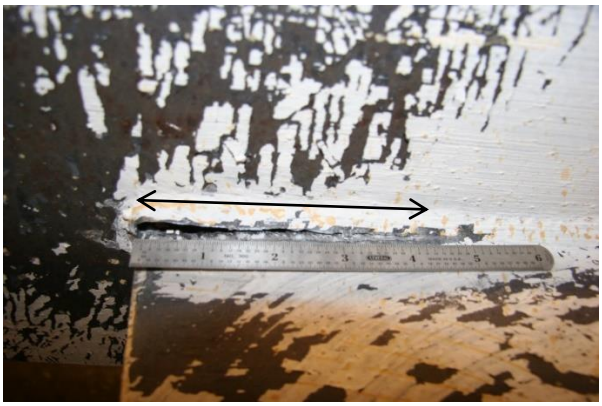

Figure 4.23 NE gusset weld crack @ +2.5%

Figure 4.24 N mid gusset weld crack @ 2.8% drift

Figure 4.25 N Brace plastic deformation @ -2.8%

Figure 4.26 Beam end torsion @ 3.0% drift

Figure 4.27 Beam yielding @ -3.0 % drift

Figure 4.28 N col yielding and buckling @ +3.3%

Figure 4.29 S brace @ 3.3% drift

Figure 4.30 S Brace @ +3.6% drift

4.3.6 Post-Fracture Cycles

The frame was cycled to ±5% drift after both braces had fractured. The columns continued sustain yielding and local buckling, reaching the performance state of severe local buckling. After the test the frame was disassembled and it was noted that slight bolt-hole elongation had occurred in the top and bottom holes in the beam web, as shown in Figure 4.31 and Figure 4.32.

Figure 4.31 S Beam web bolt hole elongation

Figure 4.32 N Beam web bolt hole elongation

4.4 Chevron 5 Observations

Chevron 5, was built with the same dimensions as Chevron 4 shown in Figure 4.7 and was tested on May 31, 2017. The purpose of this test was to investigate the difference in ductility between A500 and A1085 braces. Chevron 5 had identical frame geometry, column size, brace size, and connection details as Chevron 3 from Phase I, but utilized an A500 Gr.C brace instead of an A1085 brace. With the different braces, the W14x38 beam had an iDCR of 3.0 for the AISC requirement to develop the unbalanced load from the braces, which is just slightly larger than the iDCR of 2.8 for Chevron 3. The gusset plates were designed using the BDP and all other components and welds met seismic code requirements (AISC 2010b).

4.4.1 Overview of Performance

Chevron achieved a drift range of 6.5% until second brace fracture and had a maximum lateral resistance of 175 kips as shown in Figure 4.33. Yielding in the beam initiated at the bottom flanges in the plastic hinge region at 0.7% drift and had a maximum midspan deflection of 2.5 inches as shown the beam deflection hysteresis in Figure 4.34. The residual deflection at the end of cyclic loading was 1.5 inches. The failure mode was brace fracture; the north brace fractured first at -3.0% drift , and the south brace fractured at +3.5% drift. The braces began to buckle OOP at ±0.28% drift, and sustained progressively larger OOP buckling deformations each cycle, leading to plastic hinge formation in the center of the braces. The braces began to deform locally at mid-span as a result of plastic hinge formation, eventually leading to tearing and fracture of the braces. The average maximum deflection of the two braces was 17.6 inches. Connection damage included plate yielding, plate cracking, weld tearing, and average gusset plate deflection of 2.3 inches. The columns sustained yielding and local buckling in the plastic hinge region.

After both braces had fractured, post-fracture cycles were run to determine the residual lateral resistance from frame action. The frame was cycled to ±5.0% drift as shown in Figure 4.33. With a maximum resistance in post buckling of 83 kips, the columns resisted 45% of the frame's maximum lateral resistance The columns sustained more severe yielding and local bucking at high drift ranges, but no other damage was observed.

4.4.2 Result Summary

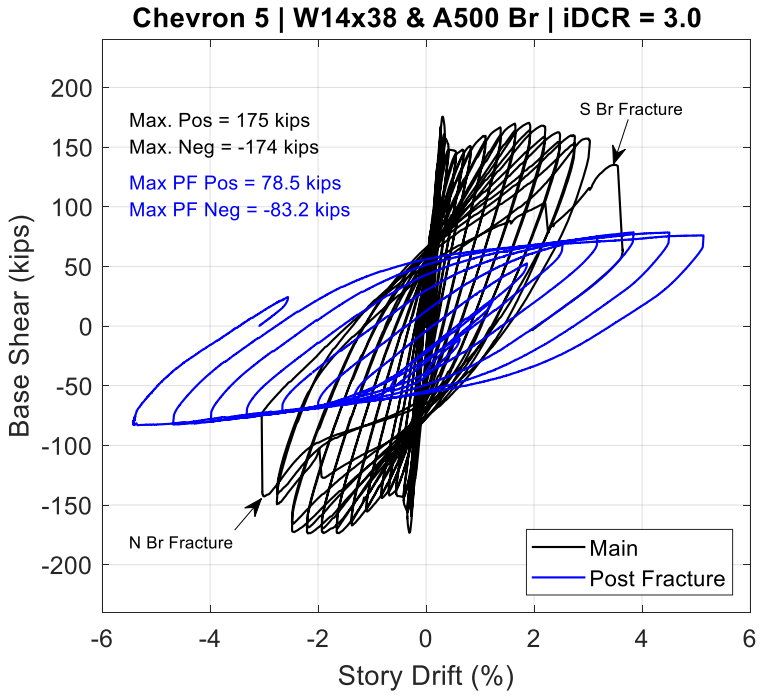

Figure 4.33 Chevron 5 Hysteresis

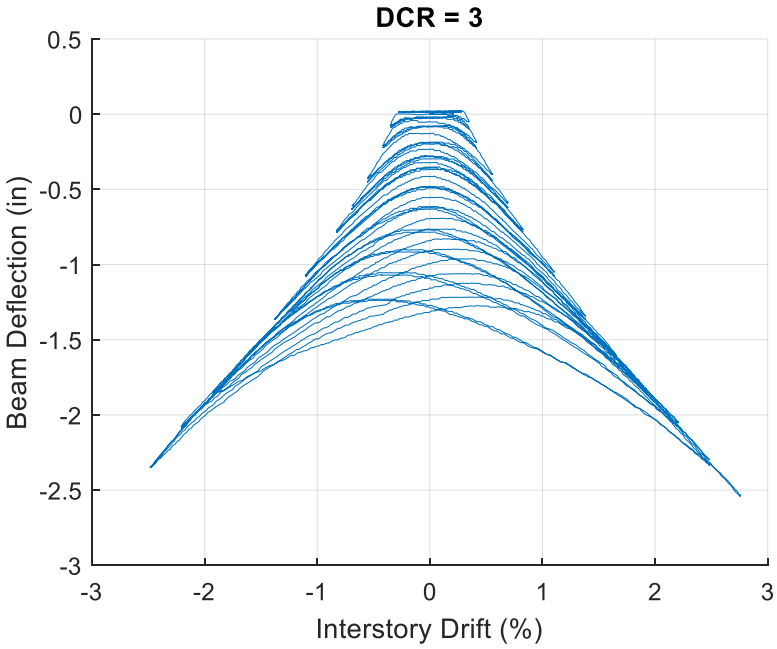

Figure 4.34 Chevron 5 Beam Deflection

Table 4.9 Chevron 5 Performance States

		Low Drift									Moderate Drift				High Drift					
	Cycle	1-2	3-4	5-6	7-8	9-10	11-12	13-14	15-16	17-18	19-20	21-22	23-24	25-26	27-28	29-30	31-32	33-34	35-36	37-38
	Drift (+/-)(%)	0.088	0.138	0.207	0.276	0.344	0.413	0.551	0.689	0.827	1.10	1.38	1.65	1.93	2.21	2.48	2.76	3.03	3.31	3.65
	Drift Range (%)	0.18	0.28	0.41	0.55	0.69	0.83	1.1	1.38	1.65	2.2	2.76	3.31	3.86	4.41	4.96	5.51	6.06	6.61	7.17
	South Brace				B1					B2					B3-BC		B3-BT			B4-BF
	Noth Brace				B1					B2					B3-BC	B3-BT		B4-BF		
SE Corner	South Column										Y1			Y2		LB1	Y3/LB2			
SE Corner	GP-Column Weld															WT1			WT2	
SE Corner	Gusset Plate							Y1					Y2							
NE Corner	North Column										Y1			Y2		LB1	Y3/LB2			
NE Corner	GP-Column Weld															WT1			WT2	
NE Corner	Gusset Plate							Y1					Y2							
Mid-Span Gusset	GP-Beam Weld (N)													WT1			WT2			
Mid-Span Gusset	GP-Beam Weld (S)															WT1				
Mid-Span Gusset	GP-Stiffener Weld (N)								PC1											
Mid-Span Gusset	GP-Stiffener Weld (S)																			
Mid-Span Gusset	Gusset Plate (N)						Y1					Y2								
Mid-Span Gusset	Gusset Plate (S)						Y1					Y2								
Mid-Span Gusset	Beam						Y1		Y1-IF									Y2		
	North Shear Tab					Y1												Y2		
	South Shear Tab					Y1												Y2		

4.4.3 Low Drift (Story drift < 1%)

Significant events during the low drift cycles included:

- The North brace began to buckle (B1) on the first cycle of 0.28% drift.
- The South brace began to buckle (B1) on the first cycle of -0.28% drift.
- Initial shear plate yielding (Y1) at ±0.34% drift.
- Initial yielding of the beam (Y1) at beam mid span bottom flange near gusset (N) at 0.41% story drift
- The middle gusset plates began to yield (Y1) at ±0.41% drift.
- The corner gusset plates began to yield (Y1) at ±0.55% drift.
- Initial plate cracking (PC1) of the beam mid span gusset (N) plate at the toe of stiffener at 0.7% story drift (Figure 4.36)
- Initial yielding of the column base (S) web at 0.7% story drift
- At ±0.83% story drift, the braces buckled out of plane more than twice the depth of the brace (B2)

Figure 4.35 South Brace Buckling @ 0.7% drift

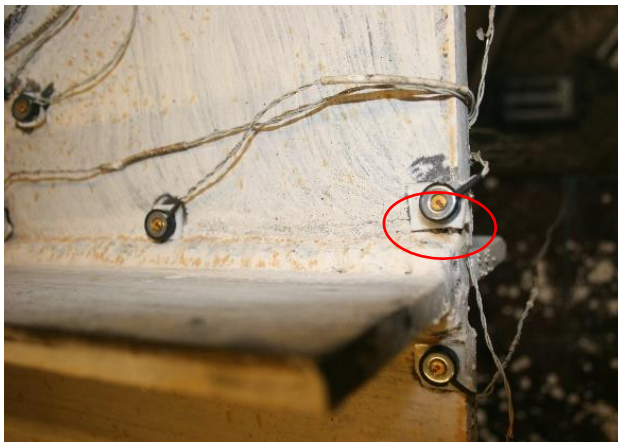

Figure 4.36 Beam Midspan Gusset Crack at Toe of Stiffener (N) 0.7%

Figure 4.37 Beam Top Flange Yielding at Stiffeners 0.7% Drift

Figure 4.38 Beam Midspan Gusset Elliptical Yielding (SW) 0.83% drift

4.4.4 Moderate Drift (1% < Story drift < 2%)

Significant events during the moderate drift cycles included:

- At ±1.1% story drift, the column flanges experienced initial yielding (Y1)
- At ±1.4% story drift, the midspan gusset plates experienced moderate yielding (Y2)
- At ±1.4% story drift there was slight out of plane twisting of the beam at the midspan
- At ±1.7% story drift the columns experience moderate yielding (Y2) in the plastic hinge region
- At ±1.7% story drift, the corner gusset plates experienced moderate yielding (Y2)
- At ±1.9% story drift weld crack initiated (WT1) on the toe of beam mid span gusset at gusset to beam interface (N)

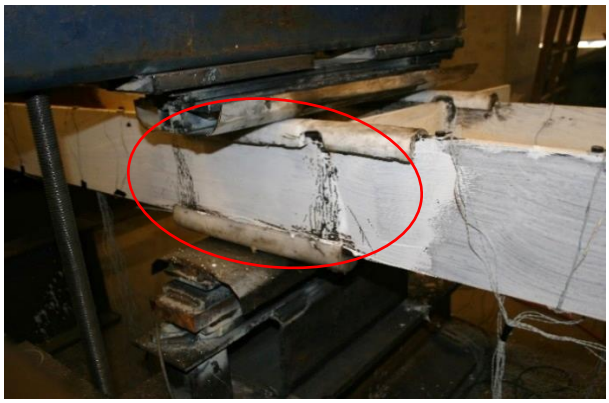

Figure 4.39 Beam top flange yielding at midspan 1.4% drift

Figure 4.40 Outer Flange Yielding at Column Base (NE) 1.4% drift

Figure 4.41 SW Shear Tab @ 1.4% drift

Figure 4.42 NW Shear Tab @ 1.4% drift

Figure 4.43 Beam Yielding Extending from Stiffeners @ 1.9%

Table 4.10 Chevron 5 Weld Crack Propagation

Drift (%)	N mid-span gusset-to-beam	S mid-span gusset-to-beam	NE gusset-to-column	SE gusset-to-column
2.5	~1-1/2"	~1/4"	1-13/16"	2-15/16"
2.8		2-1/2"	3-3/4"	4-1/8"
3.0	3"		4-1/4"	

4.4.5 High Drift (Story drift > 2%)

At high story drifts there was tearing at the edge of all gusset-to-column and gusset-to-beam welds. Table 4.10 shows the progression of damage to these welds throughout the higher drift cycles. Weld cracks were consistently longer on the top than bottom side of the gusset weld due to downward rotation of the gusset plates. The reported weld crack lengths in this chapter are the longer measurements recorded, on the top side unless noted otherwise. In addition to weld tearing, the following significant events occurred:

- At ±2.2% story drift, the braces experienced cupping (B3-BC)
- At ±2.2% crack initiates (WT1) in the NE corner gusset plate weld
- At -2.5% drift, striation lines appeared (B3-BT) in the center of North brace (Figure 4.44)
- At ±2.5% drift, the columns underwent initial local buckling (LB1) of the flanges in the plastic hinge region
- At ±2.5% drift, crack initiated (WT1) at beam mid gusset stiffener weld toe
- At ±2.8% drift, the columns experienced moderate local buckling (LB2) of the flanges in the plastic hinge region
- At -2.8% story drift, the north brace tore partially (B3-BT) (Figure 4.46)
- At +2.8% drift, striation lines appeared (B3-BT) in the center of South brace (Figure 4.45)
- At -3.0% drift, the N brace fractured through the cross section (B4-BF) on the first cycle peak
- At +3.0% story drift, the south brace tore partially (B3-BT)
- The frame was pushed to +3.5% drift to incite complete S brace fracture (B4-BF)

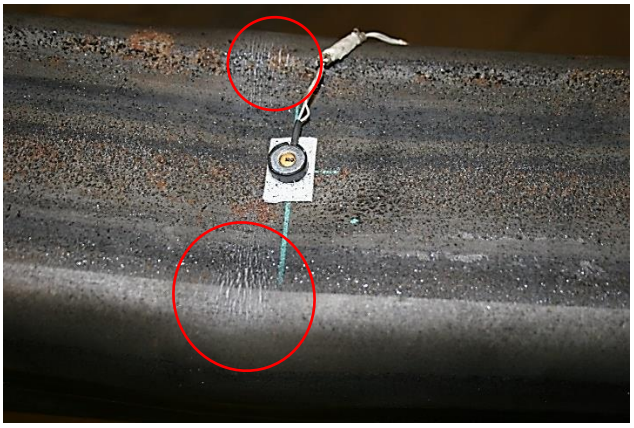

Figure 4.44 Striations in N Brace @ -2.5%

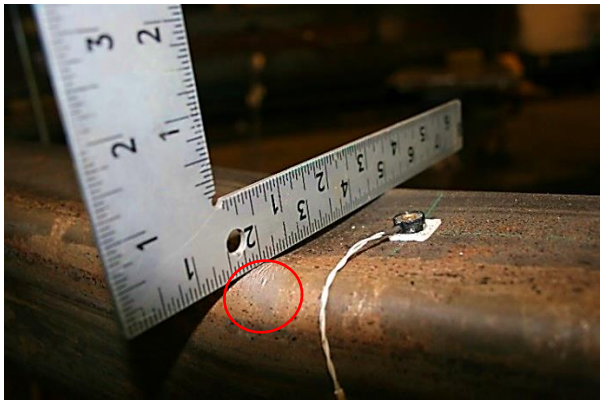

Figure 4.45 South Brace @ 2.75%

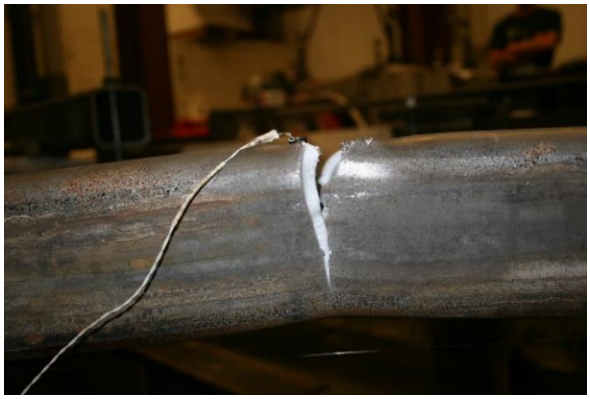

Figure 4.46 North Brace @ -2.75%

Figure 4.47 Beam @ 3.0% drift

Figure 4.48 N mid gusset 3.0%

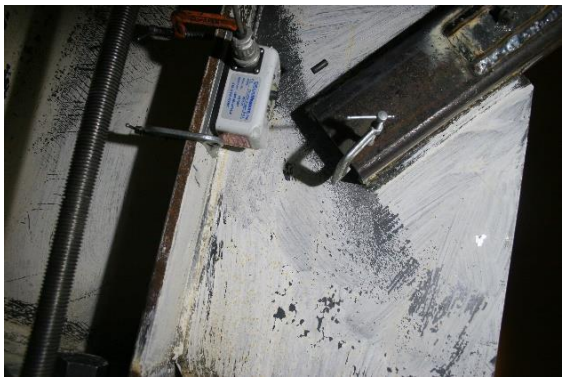

Figure 4.49 SE corner @ 3.65%

Figure 4.50 Local yielding/buckling at S Column base 3.65%

4.4.6 Post-Fracture Cycles

The frame was cycled to ±5% drift after both braces had fractured. The columns continued sustain yielding and local buckling, reaching the performance state of severe local buckling. After the test the frame was disassembled and it was noted that slight bolt hole elongation had occurred in the top and bottom holes in the beam web to accommodate large rotation demands due to the large beam deflections, as shown in Figure 4.51 and Figure 4.52.

Figure 4.51 Final Condition South Beam Web and Shear Tab

Figure 4.52 Final Condition North Beam Web and Shear Tab

4.5 Chevron 6 Observations

Chevron 6, as shown in Figure 4.53, was tested on September 8, 2017. The purpose of this test was to investigate the effect of a stiffer beam on the behavior of chevron SCBFs. Chevron 6 had similar frame geometry, column size, brace size, and connection details as Chevron 2 but utilized a W21x44 beam instead of a W14x61. The moment of inertia of the W21 beam was 30% larger than that of the W14x61. Just like the beam in Chevron 2, the W21x44 beam had an iDCR of 1.8 for the AISC requirement to develop the unbalanced load from the braces. The gusset plates were designed using the BDP and all other components and welds met seismic code requirements (AISC 2010b).

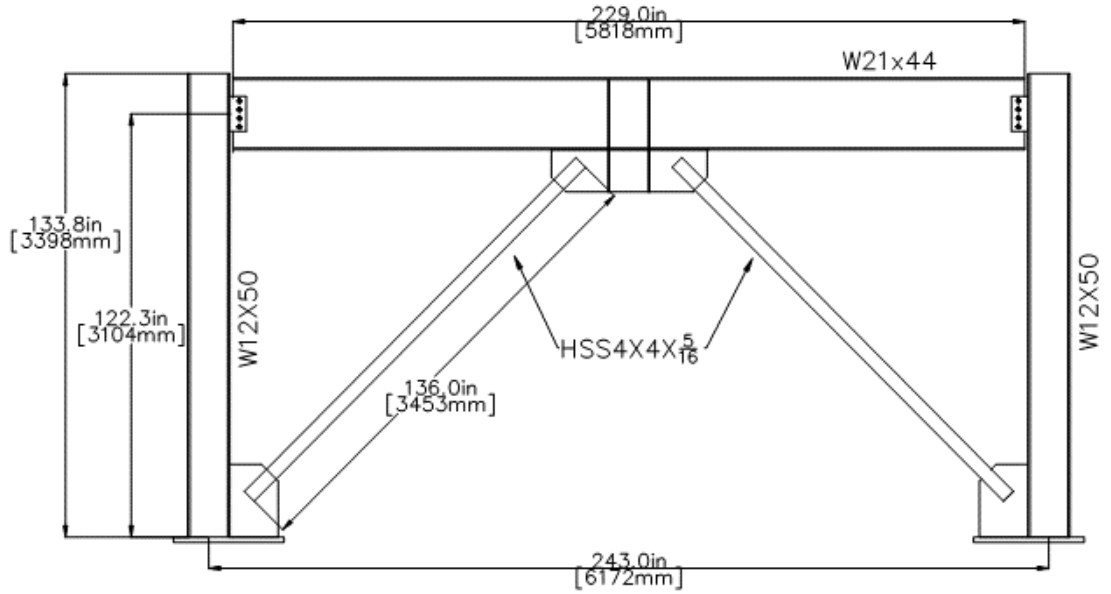

Figure 4.53 Chevron 6 elevation drawing

4.5.1 Overview of Performance

Chevron achieved a drift range of 6% until the second brace fracture and had a maximum lateral resistance of 205 kips as shown in Figure 4.54. The beam began to yield at 1.4% drift and had a maximum midspan deflection of 1.4 inches as shown in Figure 4.55. The residual deflection at the end of cyclic loading was 0.41 inches. The failure mode was brace fracture; the south brace fractured first at the second +3.0% drift cycle, and then the north brace fractured at -3.0% drift. The braces began to buckle OOP at ±0.28% drift, and sustained progressively larger OOP buckling deformations each cycle, leading to plastic hinge formation in the center of the braces. The braces

began to deform locally at mid-span as a result of plastic hinge formation, eventually leading to tearing and fracture of the braces. The average maximum deflection of the two braces was 18.8 inches. Connection damage included plate yielding, weld tearing, and an average of 2.4 inches of downward deflection of the gusset plates. The columns sustained yielding and local buckling in the plastic hinge region.

After both braces had fractured, post-fracture cycles were run to determine the residual lateral resistance from frame action. The frame was cycled to ±5.0% drift as shown in Figure 4.54. With a maximum resistance in post buckling of 85 kips, the columns resisted 41% of the frame's maximum lateral resistance The columns sustained more severe yielding and local bucking at high drift ranges, but no other damage was observed.

4.5.2 Result Summary

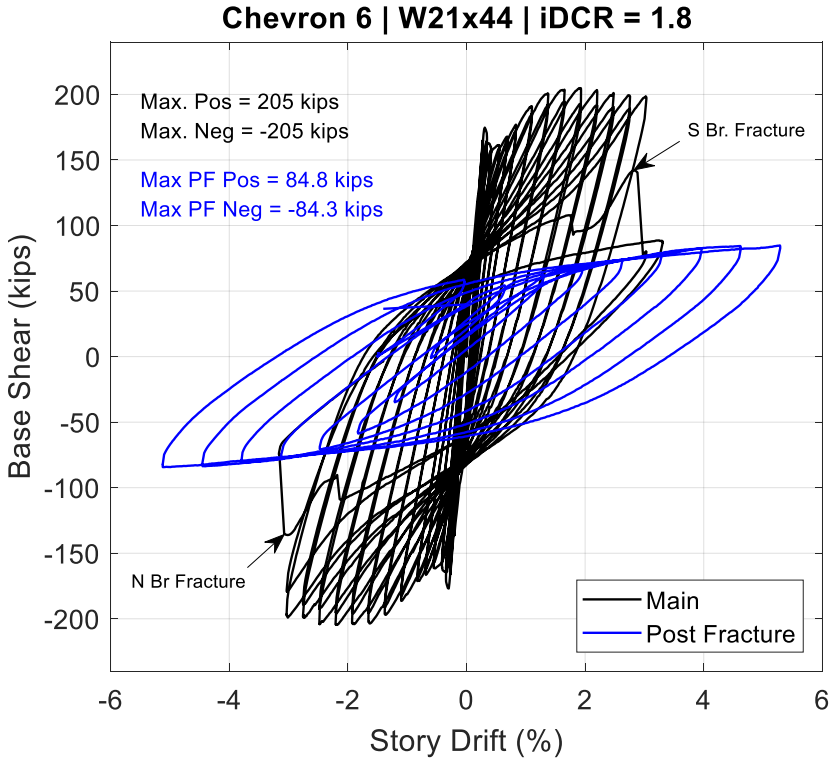

Figure 4.54 Chevron 6 Hysteresis

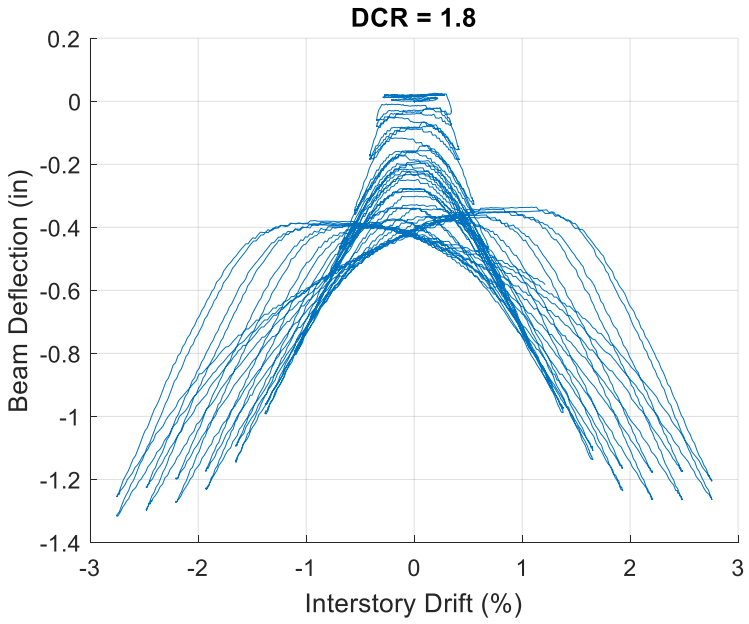

Figure 4.55 Chevron 6 Beam Deflection

Table 4.11 Chevron 6 Performance States

		Low Drift									Moderate Drift				High Drift				
	Full Cycle #	1-2	3-4	5-6	7-8	9-10	11-12	13-14	15-16	17-18	19-20	21-22	23-24	25-26	27-28	29-30	31-32	33-34	35-36
	Drift (+/-)(%)	0.088	0.138	0.207	0.276	0.344	0.413	0.551	0.689	0.827	1.102	1.378	1.654	1.929	2.205	2.48	2.756	3.031	3.307
	Drift Range (%)	0.18	0.28	0.41	0.55	0.69	0.83	1.1	1.38	1.65	2.2	2.76	3.31	3.86	4.41	4.96	5.51	6.06	6.61
	South Brace				B1						B2				B3-BC			B3-BT/B4-BF	
	Noth Brace				B1						B2				B3-BC			B3-BT	B4-BF
SE Corner	South Column											Y1		Y2	LB1		Y3		
SE Corner	GP-Column Weld														WT1		WT2		
SE Corner	Gusset Plate							Y1					Y2						
NE Corner	North Column											Y1		Y2	LB1		Y3		
NE Corner	GP-Column Weld															WT1			
NE Corner	Gusset Plate							Y1					Y2						
Mid-Span Gusset	GP-Beam Weld (N)															WT1			
Mid-Span Gusset	GP-Beam Weld (S)															WT1			
Mid-Span Gusset	GP-Stiffener Weld (N)																		
Mid-Span Gusset	GP-Stiffener Weld (S)																		
Mid-Span Gusset	Gusset Plate (N)						Y1					Y2							
Mid-Span Gusset	Gusset Plate (S)						Y1					Y2							
Mid-Span Gusset	Beam											Y1-OF		Y1-IF					
	North Shear Tab						Y1												
	South Shear Tab						Y1												

4.5.3 Low Drift (Story drift < 1%)

Significant events during the low drift cycles included:

- The North brace began to buckle (B1) on the first cycle at 0.28% drift.
- The South brace began to buckle (B1) on the first cycle at -0.28% drift.
- Initial midbeam gusset plate yielding (Y1) at ±0.28% drift.
- Initial shear plate yielding (Y1) at ±0.28% drift.
- Initial corner gusset plate yielding (Y1) at ±0.34% drift.
- Initial yielding (Y1) of the beam at 0.7% story driftFigure 4.57

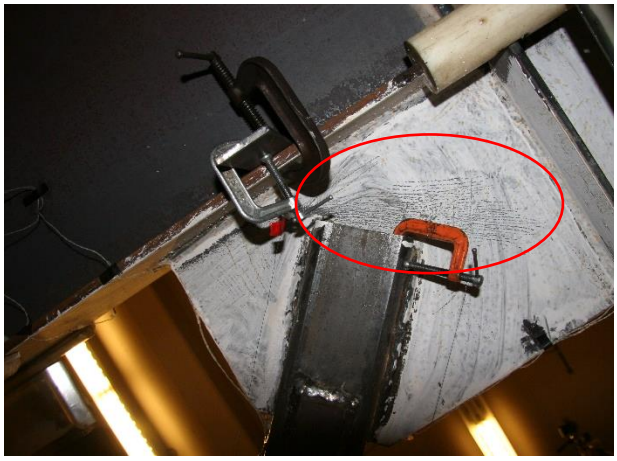

Figure 4.56 N. Beam mid gusset yielding@ 0.41% drift

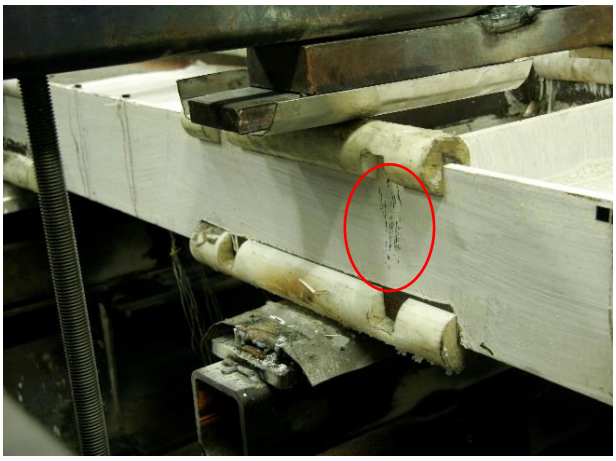

Figure 4.57 Beam yielding @ 0.7% drift

4.5.4 Moderate Drift (1% < Story drift < 2%)

Significant events during the moderate drift cycles included:

- At ±1.1% story drift, the braces buckled out of plane more than twice the depth of the brace (B2)
- At ±1.1% story drift, the outside column flanges started to yield (Y1)
- At ±1.1% story drift, the inner flange at the beam midspan began to yield (Y1-IF)
- At ±1.9% story drift the columns experienced moderate (Y2) yielding in the plastic hinge region

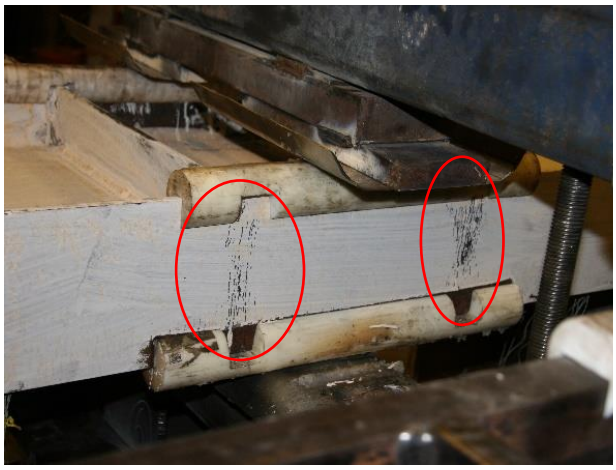

Figure 4.58 Beam OF yielding @1.1% drift

Figure 4.59 South column yielding @ 1.4% drift

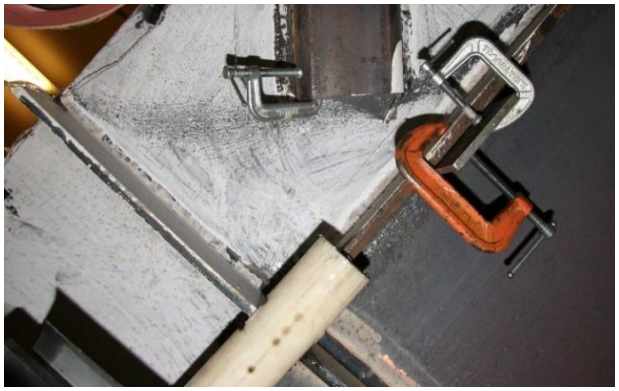

Figure 4.60 S mid gusset yielding @ 1.4% drift

Figure 4.61 S brace buckling @ 1.7%

4.5.5 High Drift (Story drift > 2%)

At high story drifts there was tearing at the edge of some of the gusset-to-column and gusset-to-beam welds. Table 4.12 shows the progression of damage to these welds throughout the higher drift cycles. Weld cracks were consistently longer on the top than bottom side of the gusset weld due to downward rotation of the gusset plates. The reported weld crack lengths in this chapter are the longer measurements recorded, on the top side. In addition to weld tearing, the following significant events occurred:

- At ±2.5% story drift, the braces experienced initial cupping (B3-BC) Figure 4.62
- At ±2.5% story drift, a crack initiated in NE corner gusset plate weld (WT1)
- At ±2.5% drift, the columns experienced moderate yielding (Y2) at the plastic hinge region Figure 4.63

- At ±2.5% drift, the columns underwent initial local buckling (LB1) of the flanges in the plastic hinge region
- At ±3.0% drift, striation lines (B3-BT) appeared in the center of braces Figure 4.65
- At second cycle peak of +3.0% story drift, the south brace fractured (B4-BT)
- In the next deformation step the north brace fractured (B4-BT) at -3.0% story drift.

Table 4.12 Chevron 6 Weld Crack Propagation

Drift (%)	N mid-span gusset-to-beam	S mid-span gusset-to-beam	NE gusset-to-column	SE gusset-to-column
2.2				<1/4”
2.5	<1/4”	<1/4”	<1/4”	1”
2.8	<1/4”	3/8”	1/2”	2-3/8”
3.0	<1/4”	1-1/4”	1/2"	3-3/4”

Figure 4.62 Cupping in N brace @+2.5% drift

Figure 4.63 S column yielding @-2.5% drift

Figure 4.64 North Shear tab @ 2.8% drift

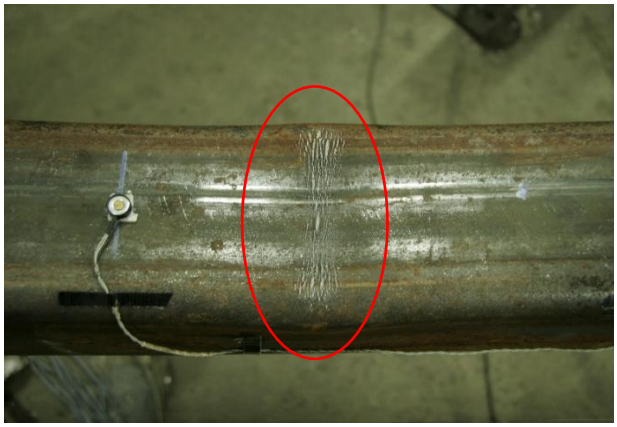

Figure 4.65 S brace @ first cycle 3.0% drift

Figure 4.66 S brace @ first cycle -3.0% drift

Figure 4.67 S Column @ -3.2% drift

Figure 4.68 Beam yielding @ -3.2% Drift

4.5.6 Post-Fracture Cycles

The frame was cycled to ±5% drift after both braces had fractured. The columns continued sustain yielding and local buckling, reaching the performance state of severe local buckling. After the test the frame was disassembled and it was noted that slight bolt hole elongation had occurred in the top and bottom holes in the beam web, as shown in Figure 4.69 and Figure 4.70. There was much less bolt hole deformation in this test than in Chevrons 4 and 5.

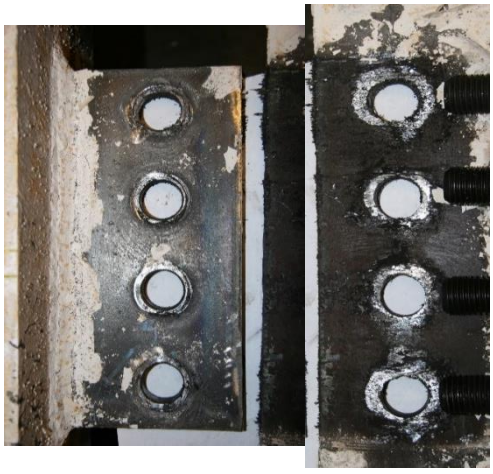

Figure 4.69 Final Condition South Beam Web and Shear Tab

Figure 4.70 Final Condition North Beam Web and Shear Tab

4.6 Single-Story Chevron Observation Comparison

A side by side comparison is provided in this section, of the six single story chevron frames, Chevron 1 through Chevron 6. For brevity, this section will make use of abbreviations to refer to different locations on the frame which are described in Table 4.13. For example, the north side of the the mid-beam gusset plate is defined as NMBG and the north corner column gusset is NCG. Table 4.14 provides a comparison of the performance of the six specimens at 1.4% drift (2.8% drift range).Table 4.15 provides a comparison of the performance of the six specimens at 2.5% drift (5% drift range). Table 4.16 provides a comparison of the performance of the six specimens at the end of each test. Note that this is a drift range of 6.3%, 6.3%, 7.2%, 9.1%, 6.5%, 6% for Chevrons 1 through 6 respectively.

Table 4.13 Single-story frame location designation meanings

Letter	Meaning
N	North
S	South
C	Corner
G	Gusset
B	Beam
Br	Brace
Co	Column
M	Middle
Pl	Plate
Sh	Shear

Table 4.14 Chevron performance at 1.4% story drift

Behavior	**Chevron 1**	**Chevron 2**	**Chevron 3**	**Chevron 4**	**Chevron 5**	**Chevron 6**
Max. Lateral Resistance	222 kips	195 kips	170 kips	148 kips	166 kips	200 kips
Max. Beam Deflection	1.0 in.	1.2 in.	1.6 in.	1.8 in.	1.4 in.	1.0 in.
Beam	n/a	Y1	Y1	Y1	Y1	Y1
						
Brace	B2	B2	B2	B2	B2	B2
						

Table continued on next page

Column		Y1	Y1	Y1	Y1	Y1	Y1
			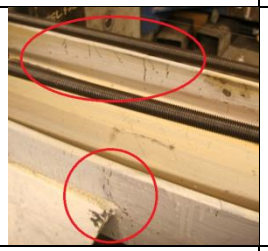	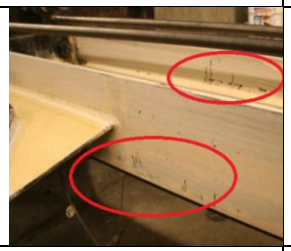			
Gusset Plate		Corner - Y1* Mid-span – Y2*	Corner - Y1 Mid-span – Y2	Corner - Y1 Mid-span – Y2	Corner – Y2 Mid-span – Y2	Corner - Y1 Mid-span – Y2	Corner - Y1 Mid-span – Y2
		No picture					
Shear Tab		Y1	Y1	Y1	Y1	Y1	Y1
							
Weld Crack	NMBG	--	1-1/2”	--	--	--	--
	SMBG	--	--	--	--	--	--
	NCG	--	--	--	--	--	--
	SCG	--	--	--	--	--	--

Table 4.15 Chevron performance at 2.5% story drift

Behavior	**Chevron 1**	**Chevron 2**	**Chevron 3**	**Chevron 4**	**Chevron 5**	**Chevron 6**
Max. Lateral Resistance	221 kips	206 kips	177 kips	152	175	205
Max. Beam Deflection	1.1 in.	1.7 in.	2.6 in.	3.0	2.3	-1.3
Beam	n/a	Y1 	Y1 	Y2 	Y1 	Y1 
Brace	B3-BC 	B3-BC 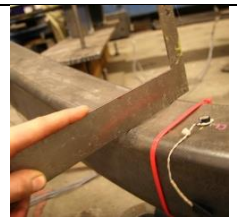	B3-BC 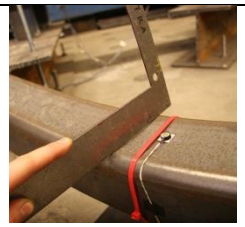	B3-BC 	B3-BC 	B3-BC 

Table continued on next page

Column		Y2/LB1	Y2/LB1	Y2/LB1	Y3	Y2/LB1	Y2/LB1
							
Gusset Plate		Corner – Y2 Mid-span – Y2	Corner – Y2 Mid-span – Y2	Corner – Y2 Mid-span – Y2	Corner – Y3 Mid-span – Y3	Corner – Y2 Mid-span – Y2	Corner – Y2 Mid-span – Y2
		No picture	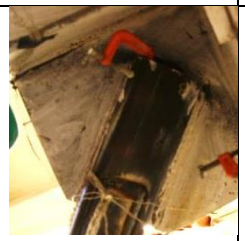	No picture			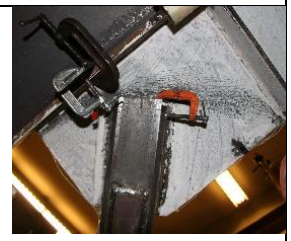
Shear Tab		Y1	Y1	Y1	Y1	Y1	Y1
							
Weld Crack	NMBG	2”	4”	3/4”	3-1/8”	1-1/2”	1/4”
	SMBG	--	2-1/2”	1/8”	2-7/8”	¼”	1/4”
	NCG	2”	1/4”	--	4-3/4”	1-3/4”	1/4”
	SCG	1/2”	1/4”	1/8”	2-3/4”	3”	1”

Table 4.16 Chevron performance at end of test

Behavior	**Chevron 1**	**Chevron 2**	**Chevron 3**	**Chevron 4**	**Chevron 5**	**Chevron 6**
Max. Lateral Resistance	233 kips	207 kips	177 kips	152	175	205
Max. Beam Deflection	1.1 in.	1.8 in.	3.0 in.	3.8 in	2.5 in	1.4 in
NBr deflection	17.0 in	18.1 in	18.4 in	21.5 in	18.0 in	19.0 in
SBr deflection	18.8 in	18.9 in	19.1 in	20.4 in	17.3 in	18.7 in
SCG OOP deflection	-2.4 in	-2.5 in	-2.5 in	-2.8 in	-2.3 in	-2.5 in
NCG OOP deflection	-2.6 in	-2.5 in	N/A	-2.8 in	-2.3 in	-2.4 in
Beam	No picture	Y1 	Y2 	Y2 	Y2 	Y2 

Table continued on next page

Brace	B4-BF	B4-BF	B4-BF	B4-BF	B4-BF	B4-BF
						
Column	Y3/LB2	Y3/LB1	Y3/LB3	Y3/LB3	Y3/LB2	Y3/LB1
	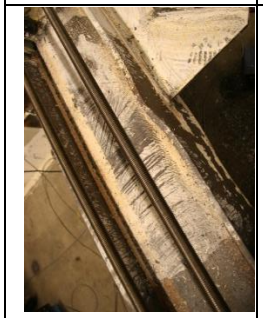					
Gusset Plate	Corner – Y2 Mid-span – Y2	Corner – Y2 Mid-span – Y2	Corner – Y2 Mid-span – Y2	Corner – Y3 Mid-span – Y3	Corner – Y2 Mid-span – Y2	Corner – Y2 Mid-span – Y2
	No picture	No picture	No picture			

Table continued on next page

		Y1	Y1	Y2	Y2	Y2	Y2
Shear Tab							
Weld Crack Length	NMBG	4”(WT3)	5-1/2”(WT3)	3” (WT2)	4.6” (WT3)	3” (WT2)	1/4" (WT1)
	SMBG	1-1/2”(WT2)	4”(WT3)	1/4” (WT1)	4-3/4” (WT3)	2-1/2” (WT1)	1-1/4” (WT1)
	NCG	5”(WT3)	3”(WT2)	2-1/4” (WT2)	7-1/4” (WT3)	4-1/4” (WT2)	1/2“ (WT1)
	SCG	1/2”(WT1)	3-1/2”(WT2)	2”(WT2)	7-1/4” (WT3)	4-1/8” (WT2)	3-3/4” (WT2)

As expected from the lower ductility of the braces, the brace out of plane deflection was lower in Chevron 5 than Chevron 3 since the lower ductility caused fracture at a lower strain range in the brace. This also led to a smaller beam midspan deflection Chevron 5 than Chevron 3. As expected from the higher stiffness of a deeper beam section, Chevron 6 beam had lower deflection and plastic deformation at the end of the test than Chevron 2. The difference in elastic deformation was proportional to the difference in beam stiffness. The beam stiffness of the W21 was 30% larger than the W14, and the beam plastic deflection was about 25% smaller than for the W14 beam. Further, the beam stiffness and brace ductility did not have a significant impact on the frames' maximum lateral resistance. The frame lateral resistance reduction was not proportional to the beam strength reduction. The reduction in strength for Chevrons 2, 3, and 4 compared to Chevron 1 was 12%, 24%, and 30%, respectively.

Bolt hole elongation in the Chevron 4 beam was much more significant than in any other specimen because of the much larger beam deflection. Finally, weld damage was much more prevalent in Chevron 4, which sustained the most damage and inelastic deformation and plate cracking only occurred in the frame specimens with iDCR below 2, where there was more rigidity in the connections.

CHAPTER 5
Single-Story Frame Experimental Analysis

5.1 Introduction

Chapter 4 presented the observed response of the three single-story chevron tests. This chapter builds on those results with the measured responses. Specifically, the data showing measured responses of each component of the frame (e.g., brace, beam, connections, and column) as well as the global response. Additionally, the salient responses for all six single-story frames are compared to investigate the impact of the beam strength and stiffness(i.e., iDCR) as well as the yield mechanics and failure modes. These results were used to design the 3-story test presented in Chapter 6.

5.2 Data Processing

5.2.1 LabView DAQ Data Processing

All of the instrument data except for NDI Optotrak was collected using the National Instruments Data Acquisition system and LabView software. The instruments were continuously sampled using a frequency of 1Hz. As such, there were spikes and unwanted readings during extended loading pauses used for observation of damage after the first positive and negative peak of each frame displacement. Thus, the data was post processed to remove spikes and data from test holds to facilitate analysis.

5.2.2 NDI Optotrak Data Processing

Optical sensor data was collected with the Northern Digital Inc. First Principles software. The 3-D position of each LED sensor was recorded on an arbitrary Cartesian coordinate system. In order

to interpret the data it was transformed into a relevant coordinate system using the beam's flanges as the x-z plane. Details of the transformation can be found in Ballard (2015).

5.2.3 NDI-DAQ Data Matching

The Optotrak data was coordinated in terms of time with the LabView DAQ data in order to directly compare beam and brace deformations and forces. The Optotrak system was also collecting data with a frequency of 1Hz. However, the system's collection rate was slightly faster than the DAQ's so post processing was required to remove Optotrak data points and achieve matching of the 2 systems' raw data. Then, the Optotrak and DAQ data was reduced simultaneously to remove data from test holds, and finally the two sets of data were independently filtered of spikes. An example of the vertical displacement measured at the center of the middle gusset plate of Chevron 4 using both systems is shown in Figure 5.1 to demonstrate the raw and processed data results.

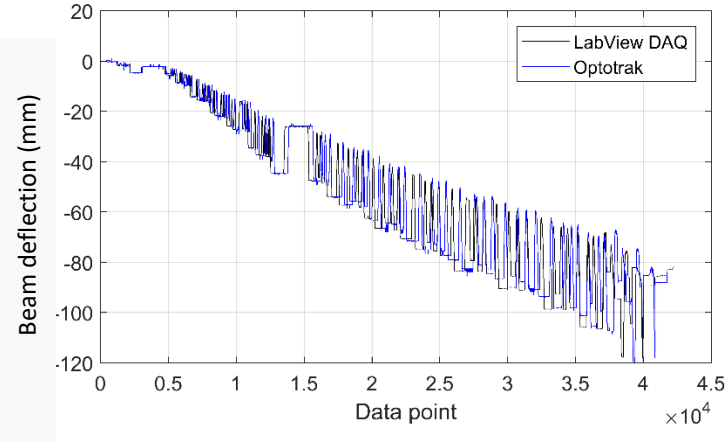

(a) Raw data

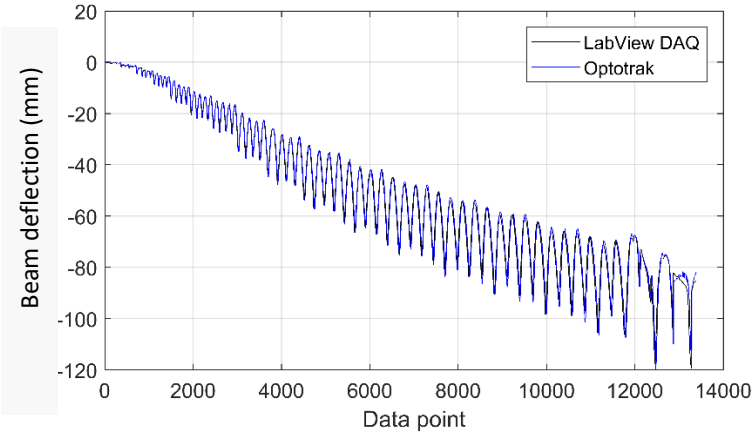

(b) Processed data

Figure 5.1 Example of data processing and matching

5.2.4 Backbone curves

Backbone curves will be used in this chapter to compare and highlight peak performance by taking the envelope of the hysteretic response and only using the peak value of the first cycle at each displacement amplitude tested. It should be noted that the backbone curves ignore shape and size of hysteretic loops. Additionally, only data from completed cycles is reflected in the envelope. An example of the backbone curve over hysteretic response is shown in Figure 5.2.

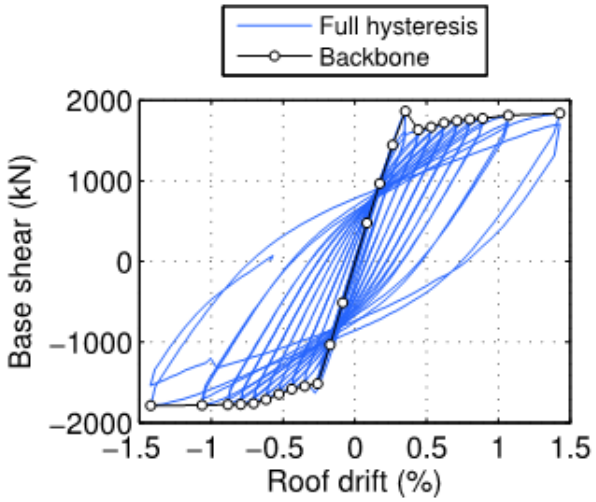

Figure 5.2 Backbone curve example (Sen 2014)

5.3 Parameter Definitions and Derivations

This section will establish salient parameters and expressions used to evaluate the response of each frame starting with a global frame view and transitioning to local response at each element.

5.3.1 Frame

The global frame experimental behavior is shown in Figure 5.3 at positive drifts. Actuator pulling in, represented a tensile force, and corresponded to positive frame drift. At positive frame displacement the north brace was in compression and the south brace was in tension. This corresponded to tension in the north half of the beam and compression in the south half of the beam.

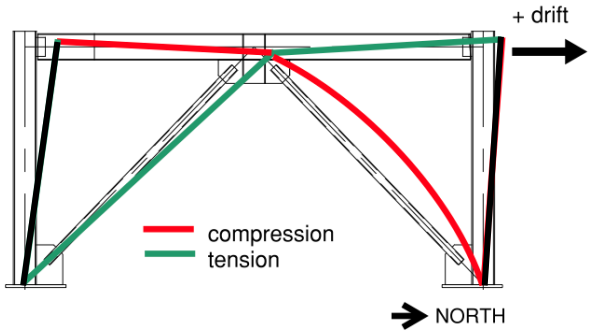

Figure 5.3 Frame behavior

5.3.2 Brace

The frame's lateral resistance will often be shown here normalized by the expected lateral resistance of the braces, $2P_{cr}Cos\theta$, (twice the horizontal component of the brace's expected compressive strength), calculated using the measured material properties given in Chapter 3. For reference, Appendix A contains several parameter definitions and the relevant material properties used for calculation. Salient brace strengths have been summarized in Table 5.1 and will be reference throughout this chapter. The expected brace strength, P_{cr}, was calculated using an effective length factor of K=1, where L was the end to end length of the braces and θ was the brace angle to the horizontal.

Table 5.1 Brace and Frame parameter summary

Behavior	Chevron 1-4	chevron 5	chevron 6
$2P_cCos\theta$ (kN)	685	650	741
$2P_{cr}Cos\theta$ (kN)	726	673	804
P_{cr} (kN)	519	484	570
P_t (kN)	1278	1112	1278

5.3.3 Beam

A reduced plastic moment capacity (M_p*) considering P-M interaction was calculated using the maximum measured axial force in the beam. This moment was determined by writing the AISC 2016b interaction equation used to design the beam to calculate the remaining flexural strength for the given values of P as shown in Eq 5.1(a). Similarly, a reduced yield moment (M_y*) is calculated using the stress in the beam as shown in Eq 5. 3. These adjusted moment capacities incorporate consideration of measured material properties and strength reduction from high initial axial demands on the beam and were used to normalize test results. The measured axial demands, P, and reduced plastic and yielding moments for Chevrons 1 through 6 are provided in Appendix D.

When $\frac{P}{P_c} \geq 0.2$

$$M_p^* = \left(\left(1.0 - \frac{P}{P_c}\right) * \frac{9}{8}\right) M_p \qquad \text{Eq 5.1(a)}$$

When $\frac{P}{P_c} < 0.2$

$$M_p^* = \left(\left(1.0 - \frac{P}{2P_c}\right)\right) M_p \qquad \text{Eq 5.2(b)}$$

$$M_y^* = \left(F_{y,exp} - \frac{P}{A}\right) S_x \qquad \text{Eq 5. 3}$$

Where

P = measured maximum axial load in beam

P_c = axial capacity of beam from measured material properties

M_p = plastic flexural capacity of beam from measured material properites

$F_{y,exp}$ = material yield stress from coupon tests

The beams for this test series were designed to achieve iDCR based on the expected vertical unbalanced load from the beam per AISC(2016a). Table 5.2 provides the maximum forces from the two analysis cases used for design, resulting from the unbalanced loads as were expressed in Chapter 3 Section 3.3. The expected unbalanced loads based on measured material properties are also included in this table and are denoted by the subscript "exp".The design loads for Chevrons 1 through 4 were all the same given their identical geometries, Chevrons 5 and 6 had different materials properties or geometry so the design loads vary from the rest.

Table 5.2 Beam Shear, Axial, and Flexural Design Demands

Behavior		Chevron 1-4	chevron 5	chevron 6
Total Vertical design force (kN)	$\mathbf{V_{br,d}}$	743	796	721
(case 2)	$\mathbf{V_{br,exp}}$	785	756	781
Total horizontal force (kN)	$\mathbf{H_{br,d}}$	1254	1281	1308
(case 1)	$\mathbf{H_{br,exp}}$	1257	1203	1304
Moment (kN-m)	$\mathbf{M_r}$	909	970	839
(case 1)	$\mathbf{M_{r,exp}}$	958	922	953

5.3.4 Column

The column's reduced plastic moment capacity (M_p*) was calculated using the average maximum measured axial load, which, occurred at the beginning of each test due to the post-tensioned gravity loading system. In the following sections, the moment in the column at the edge of the gusset plate $M_{col,gus}$, is reported because this is where plastic hinge formation was observed during the experiments. The measured axial demands and reduced yielding moments are provided in Appendix D.

5.3.5 Verification of member forces

Verification of forces calculated from strain gauge data was performed through equilibrium checks and comparison of forces derived from different sets of strain gauges. Generally, the lateral resistance of the beams, braces, and columns agreed with the applied actuator forces. The vertical

unbalanced loads from the braces and the total shear in the beam did not agree as well. A detailed study of the forces is provided in Appendix D.

5.4 Measured Response of Chevron 4 (iDCR = 4.3)

This section will include a detailed review of salient beam, brace, and column forces calculated from the data collected during experimental testing of Chevron 4. A global view of the frame response will set precedent for a discussion of the local response at each element of the frame that contributed to the frame behavior. For clarity, all measurement histories, except base shear response, are shown up to initial brace fracture.

5.4.1 Frame Response

The force-drift hysteresis of Chevron 4 in Figure 5.4 shows that brace buckling occurred at 0.28% drift and the system achieved a peak lateral resistance of 99% of the expected strength with 719 kN. The frame resistance plateaued after brace buckling around 1.5% story drift until initial brace tearing, when there was a loss of strength. The maximum drift range was 9.1%, with brace fracture of the south brace at 4.4% story drift and north brace fracture at -4.7% story drift.

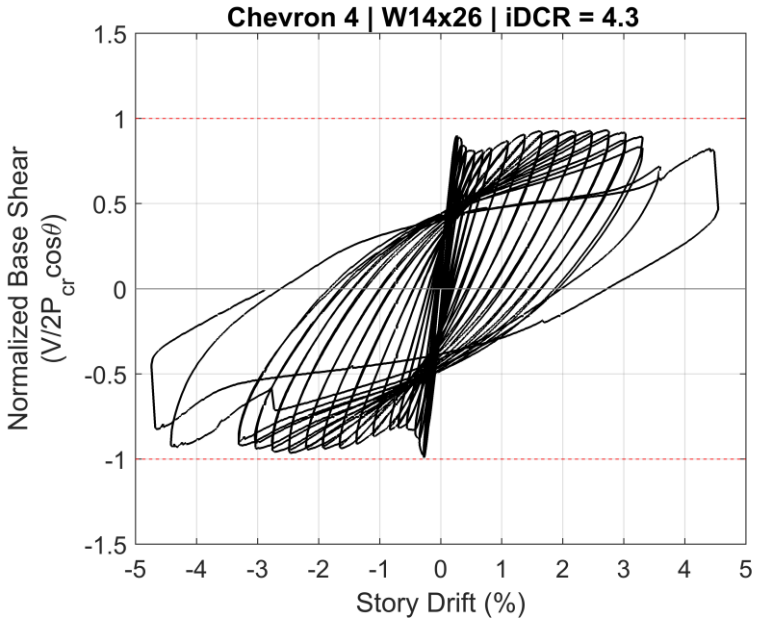

Figure 5.4 Chevron 4 base shear-story drift hysteresis

5.4.2 Brace Response

The brace axial force vs. frame deformation hysteresis in Figure 5.5 and the hysteretic plot of brace deformation vs brace axial force normalized by P_{cr} in Figure 5.6 highlights the following:

- Positive drift frame deformation corresponded to fame movement towards the north, so the north brace was in compression first and the south brace in tension.
- The two braces buckled at approximately the same drift and force of 0.28% and 610kN.
- The north brace, which experiences tension at negative drifts developed higher tensile forces than the south brace. The peak tensile strength of the north brace was approximately 40% of the expected tensile strength (P_t) and the south brace peak tensile strength was 0.37 P_t at incipient brace buckling
- The braces' compressive strength degraded to 11% and 20% of the expected compressive strength (P_{cr}) for the South and North braces respectively
- Both braces reached a stable tensile demand of 450kN ($0.87P_{cr}$).
- The brace deformation was entirely in brace shortening, with only 4 mm of elongation in either of the braces and 145 mm of shortening.

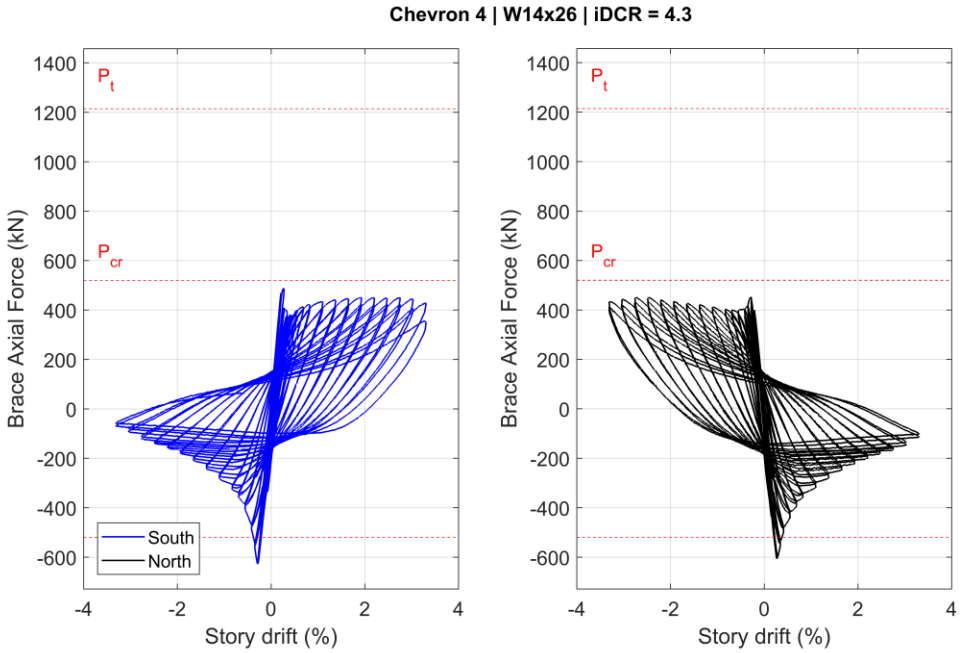

Figure 5.5 Chevron 4 brace axial force vs story drift hysteresis

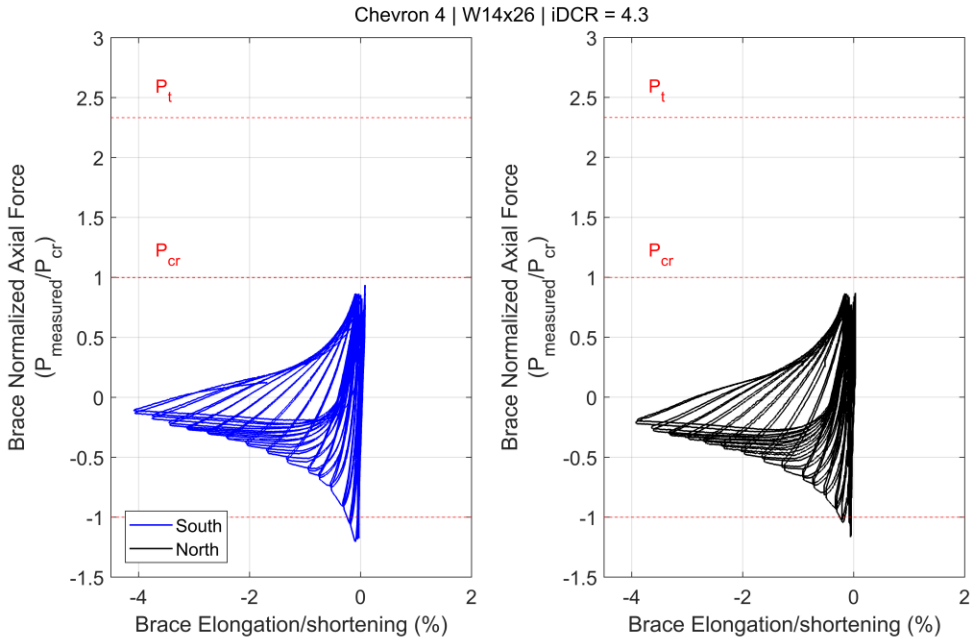

Figure 5.6 Chevron 4 Brace elongation and shortening vs. normalized axial force hysteresis

Figure 5.7 shows the out of plane deflected shape of the south brace along its length, at various drift cycle peaks. This plot was constructed using Z direction movement from LED's located on one half of the brace and mirroring the data to visualize the other half of the brace. LEDs near the center of the brace were out of range of the cameras at some points during the test, so the full brace shape could not be reproduced at all drift levels of interest. However, the available information clearly demonstrates the gradual increase in deflection starting at 0.2% drift. It also shows the plastic hinge formation between 1.1% and 2.2% story drift, evident by the liner brace deflected shape. Thus, the complete brace shape at the highest shown drift was produced (dashed portion of the plot) and resulted in an approximation of 470 mm of brace OOP deflection at 3.0% story drift.

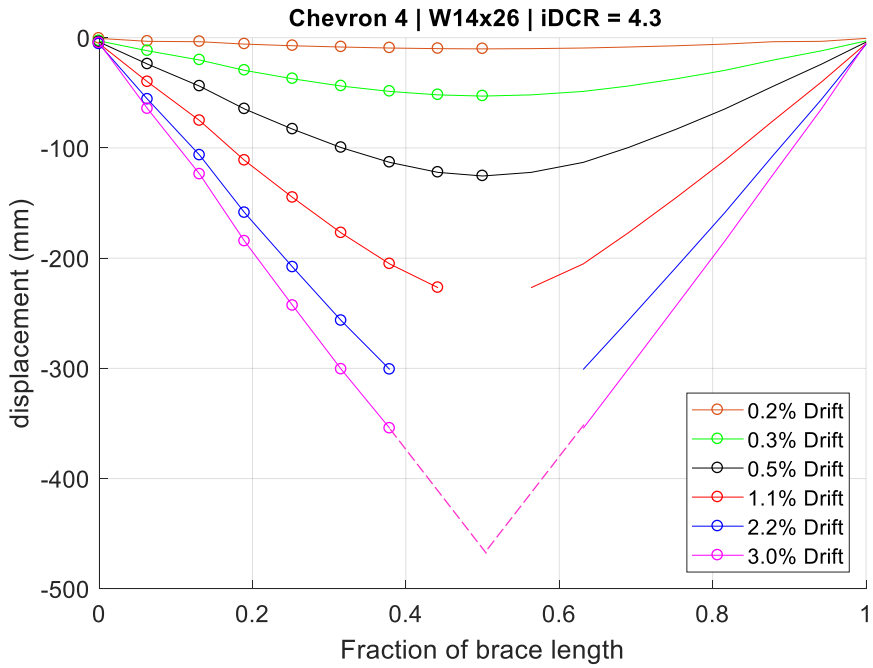

Figure 5.7 Chevron 4 South brace out of plane deformation

5.4.3 Beam Response

Figure 5.8 shows that the vertical force (measured in the braces) vs the deflection at the midspan of the beam. The figure shows:

- The initial unbalanced force was upwards but did not result in beam deflection.
- A downward deflection resulted from an upward force
- The force-deflection response of the beam was not linear
- The vertical force from the braces reverses with each cycle, pushing the beam up but never to the previously unloaded position.

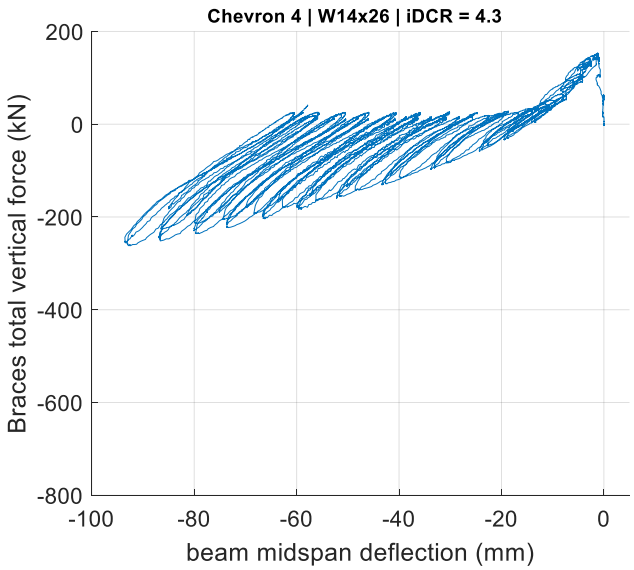

Figure 5.8 Chevron 4 Beam deflection vs. unbalanced vertical load hysteresis

The beam response backbone curves for moment, shear, and axial forces calculated using the beam strain gauges as described in Chapter 3 are shown in Figure 5.9 show the following:

- The north side of the beam is in tension at positive drifts, which corresponds with the north brace in compression. Similarly, the south side of the beam is in compression, corresponding to the south brace in tension.
- The force was not evenly distributed on the two sides of the beam as was assumed for design.
- The axial force on the side of the beam in tension plateaued and stabilized after brace buckling, but the force in the beam in compression degraded.
- The shear force was higher on the side of the beam in tension, as was the moment.
- The moment response curves suggests that the beam reached the reduced yield moment (M^*_y) at 1% story drift and plateaued after reaching the plastic moment (M^*_p). This is consistent with observed behavior.

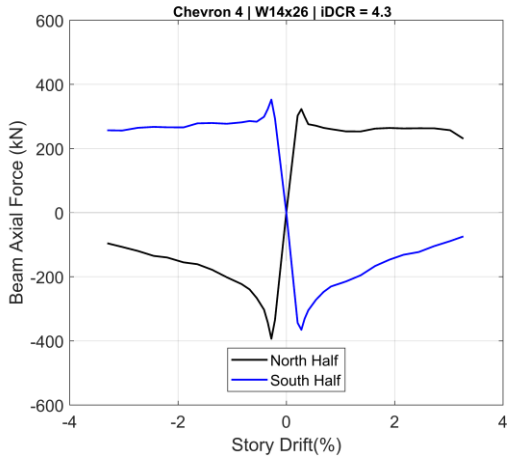

(a) Beam axial force backbone curve

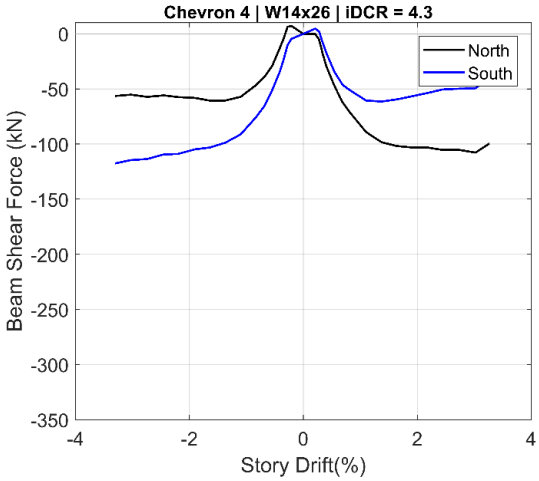

(b) Beam shear force backbone curve

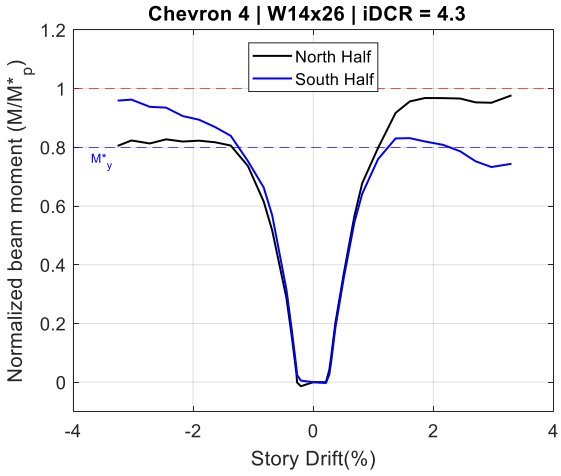

(c) Beam normalized moment backbone curve

Figure 5.9 Chevron 4 beam response envelopes

5.4.4 *Connection Response*

The deflection of the gusset plate, measured with string potentiometers at the corner gussets and Optotrak sensors at the beam midspan gussets, are shown in Figure 5.10. The deflection values in these plots are shown as positive but gusset plates were bending downward, consistent with brace out of plane deflection. It is clear to see from these that the behavior of all the plates was consistent. The maximum deflection at the middle gussets was about 10mm less than at the corners, but the plastic deformation is larger as seen from the higher deflections at the corresponding brace tension cycle.

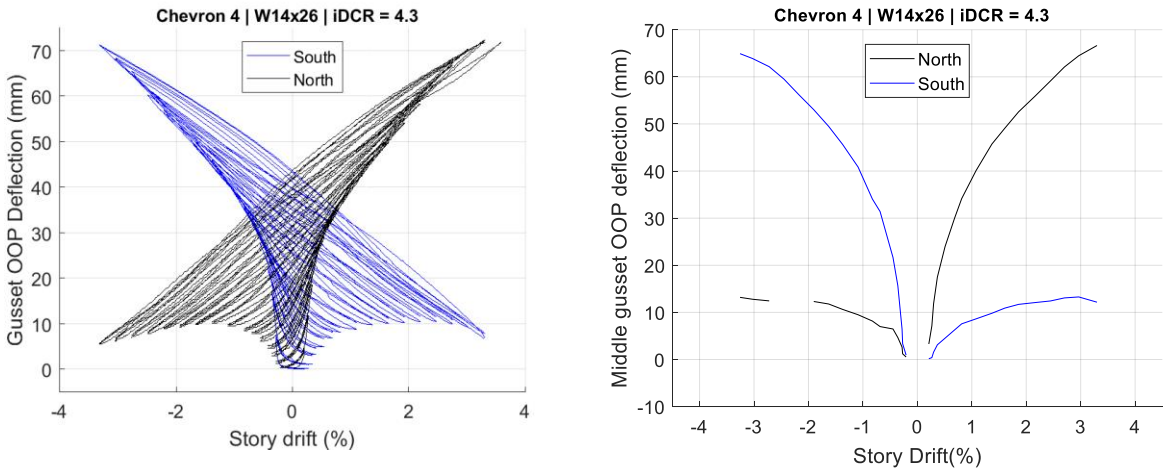

(a) Corner gussets (b) Middle gusset

Figure 5.10 Chevron 4 Gusset plate deflection

5.4.5 *Column Response*

The column shear force hysteretic plots for main test cycles and post fracture cycles, and the column axial force backbone curve are shown as part of Figure 5.11. The column shear in the main cycles reversed very quickly after brace buckling when the braces no longer had enough strength and stiffness to carry the entire load of the actuator. The stiffness of the columns remained approximately equal throughout the test and into the post fracture cycles. As expected from the previous tests, the columns started with a high axial load and gradually shortened, causing the prestress force to reduce.

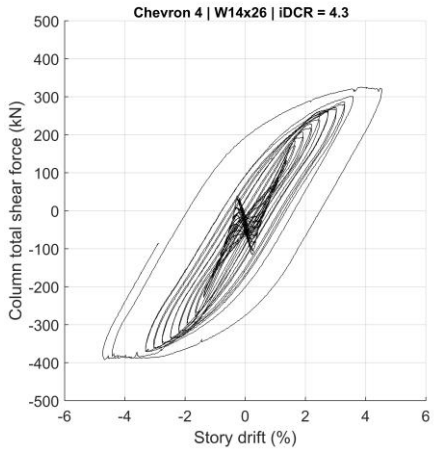

(a) Total column shear hysteresis during main test cycles

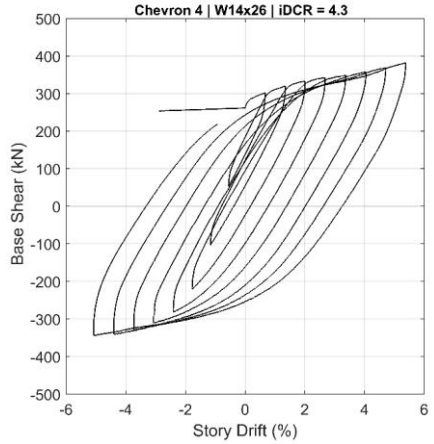

(b) Total column shear hysteresis during post fracture cycles

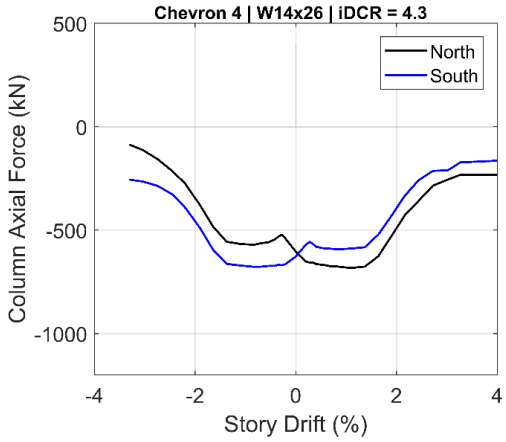

(c) Column axial force backbone curves

Figure 5.11 Chevron 4 measured column response

5.5 Measured Response of Chevron 5 (iDCR = 3.0)

This section will include a detailed review of salient beam, brace, and column forces calculated from the data collected during experimental testing of Chevron 5. A global view of the frame response will set precedent for a discussion of the local response at each element of the frame that contributed to the frame behavior.

5.5.1 Frame Response

The force-drift hysteresis of Chevron 5 in Figure 5.12 shows that brace buckling occurred at 0.28% drift and the system achieved a peak lateral resistance of 116% of the expected strength with 780 kN. The maximum drift range was 6.5%, with brace fracture of the north brace at -3% story drift and south brace fracture at 3.5% story drift, resulting in asymmetric frame deformation.

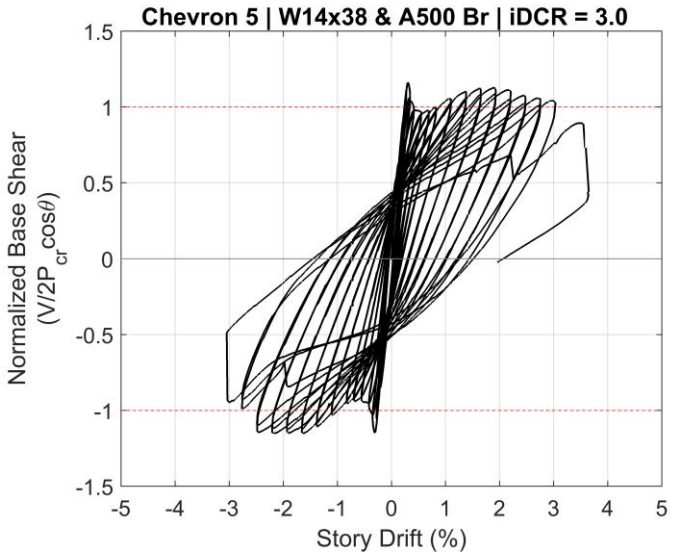

Figure 5.12 Chevron 5 base shear-story drift hysteresis

5.5.2 Brace Response

The brace axial force vs. frame deformation hysteresis in Figure 5.13 and the hysteretic plot of brace deformation vs brace axial force normalized by P_{cr} in Figure 5.14 highlights the following:

- The two braces buckled at approximately the same drift and force of 0.28% and 550kN.

- Post buckling response of the braces highlights the asymmetric frame deformation. The north brace, which experiences tension at negative drifts developed lower tensile forces than the south brace. The peak tensile strength of the south brace was approximately 50% of the expected tensile strength (P_t) near 1% drift, while the north brace peak tensile strength was 0.45 P_t and occurred at incipient brace buckling (~0.3% story drift)
- The braces' compressive strength degraded to 17% and 5% of the expected compressive strength (P_{cr}) in the South and North braces respectively
- There was a 20% loss of strength immediately after brace buckling. The North brace reached a stable tensile demand of 500kN ($1.0P_{cr}$) but did not stabilize in the south brace.
- The brace deformation was entirely in brace shortening, with only 4 mm of elongation in either of the braces and 107 mm of shortening.

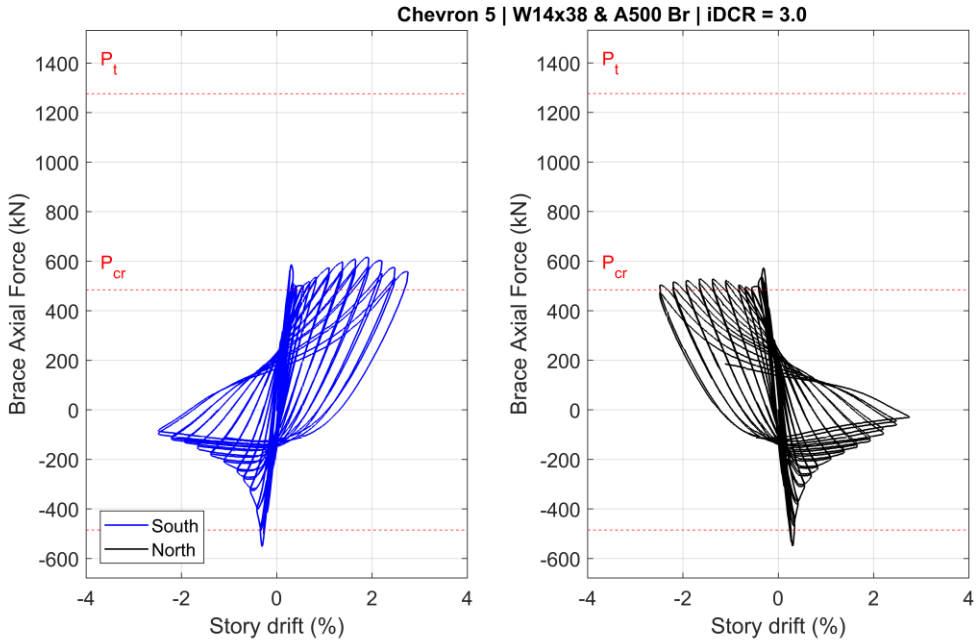

Figure 5.13 Chevron 5 brace axial force vs story drift hysteresis

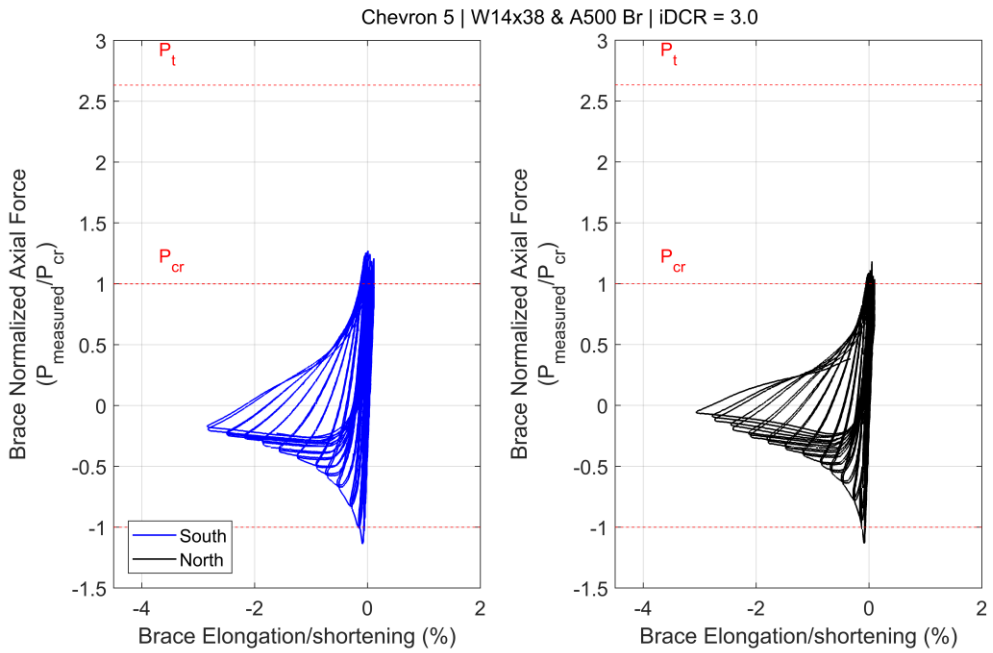

Figure 5.14 Chevron 5 Brace elongation and shortening vs. normalized axial force hysteresis

The Optotrak LEDs near the center of the brace used to plot the deformed south brace shape at severalstory drift levels in Figure 5.15were out of range of the cameras at some points during the test, so the full brace shape could not be reproduced at all drift levels of interest. However, the available information clearly shows the increase in deflection after brace buckling between 0.3% and 0.5% story drift and plastic hinge formation between 1.1% and 2.2% story drift, differentiated by the liner brace deflected shape. Thus, the complete brace shape at the highest shown drift was produced, (represented by the dashed portion of the plot) and resulted in an approximation of 430 mm of brace OOP deflection at 3.0% story drift.

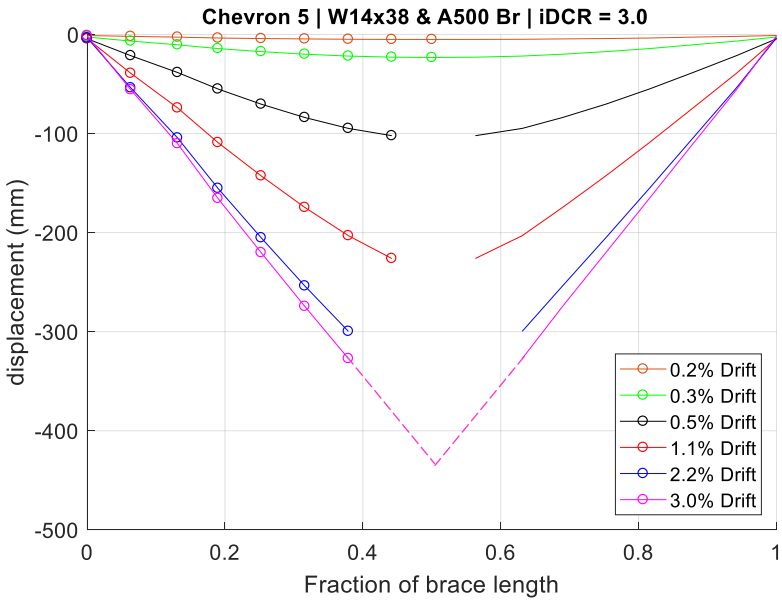

Figure 5.15 Chevron 5 South brace out of plane deformation

5.5.3 Beam Response

Figure 5.16 shows that the vertical force (measured in the braces) vs the deflection at the midspan of the beam. The figure shows:

- A downward deflection resulted from a downward force
- The force-deflection response of the beam was not linear
- The vertical force from the braces reverses with each cycle, pushing the beam up but never to the previous position.

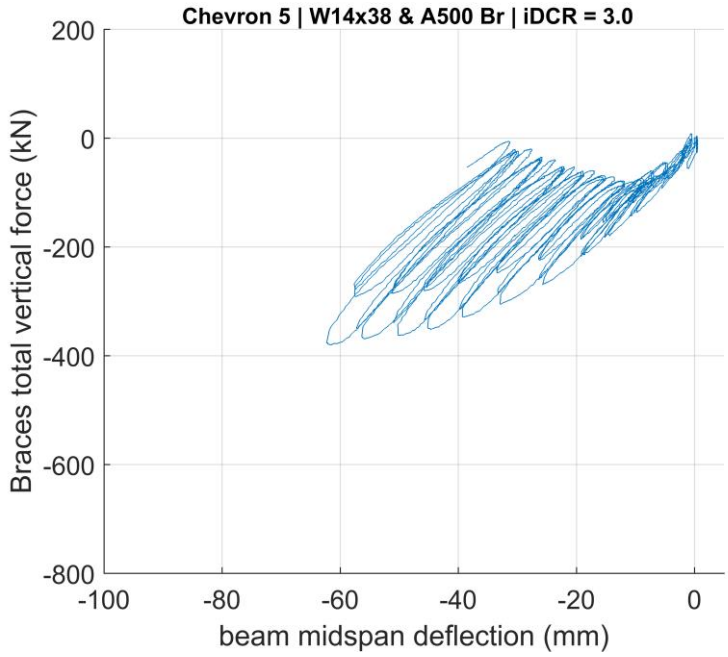

Figure 5.16 Chevron 5 Beam deflection vs. unbalanced vertical load hysteresis

The beam response backbone curves for moment, shear, and axial forces calculated using the beam strain gauges as described in Chapter 3 are shown in Figure 5.17 show the following:

- The force was not evenly distributed on the two sides of the beam as was assumed for design.
- The axial force on the side of the beam in tension plateaued and stabilized after brace buckling, but the force in the beam in compression degraded until brace fracture.
- The shear force and moment curves reflect at a greater magnitude the asymmetric behavior in the two sides of the frame. The shear force was larger in the side of the beam in tension, but the moment demand was always higher on the north side of the beam.
- The moment response curves suggests that the beam reached the reduced yield moment (M^*_y) at 1 % story drift on the north side but did not surpass it on the south side. This is inconsistent with extensive observed yielding during the experiment.
- The moment inconsistencies and difference in North beam behavior at positive and negative drifts suggests an error in the experimental results.

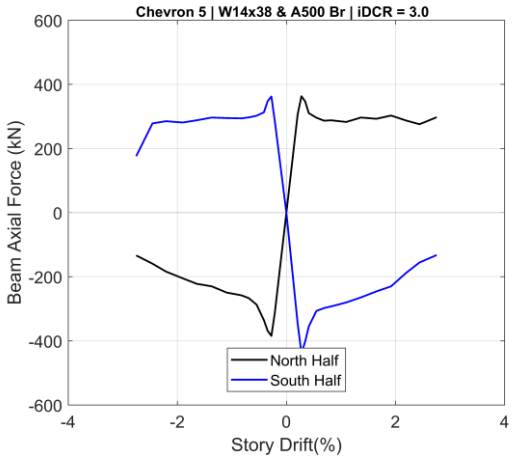

(d) Beam axial force backbone curve

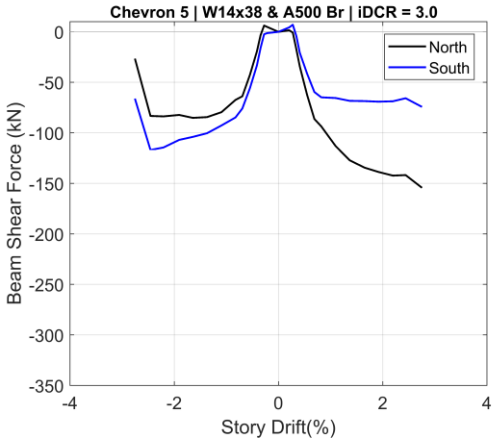

(e) Beam shear force backbone curve

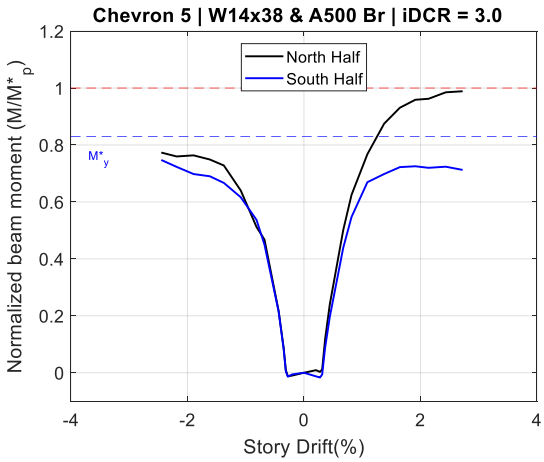

(f) Beam normalized moment backbone curve

Figure 5.17 Chevron 5 beam response envelopes

5.5.4 Connection Response

The deflection of the gusset plates in Figure 5.18 show very consistent behavior at the middle and corner gussets. The maximum deflection at the middle gussets was about 5 mm less than at the corners. The plastic deformation was also very similar as shown by the deformation when the corresponding brace was in tension.

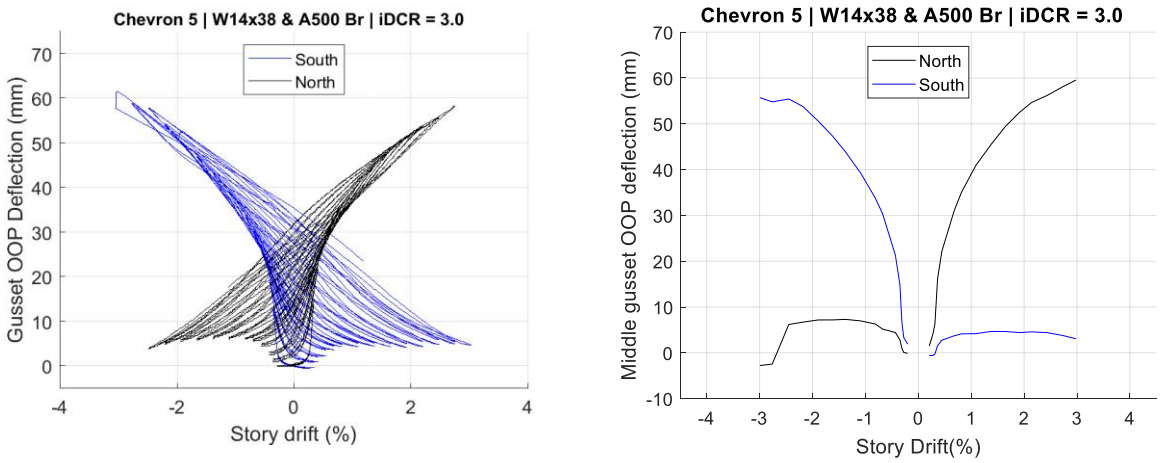

(c) Corner gussets (d) Middle gusset

Figure 5.18 Chevron 5 gusset plate deflection

5.5.5 Column Response

The column shear force hysteretic plots for main test cycles and post fracture cycles, and the column axial force backbone curve are shown as part of Figure 5.19. The column shear in the main cycles reverses very quickly after brace buckling. The stiffness of the column remained approximately equal throughout the test and into the post fracture cycles. As expected from the previous tests, the columns started with a high axial load and gradually shortened, causing the prestress force to reduce.

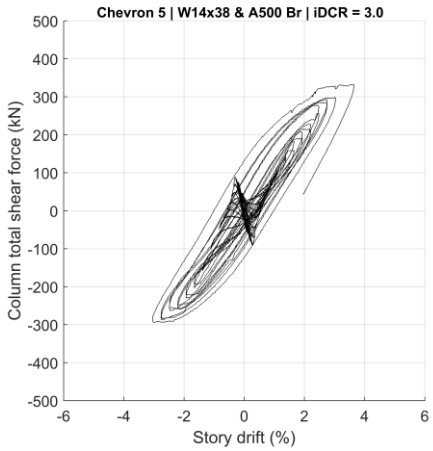

(d) Total column shear hysteresis during main test cycles

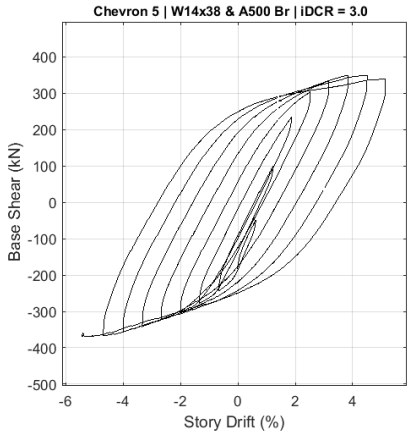

(e) Total column shear hysteresis during post fracture cycles

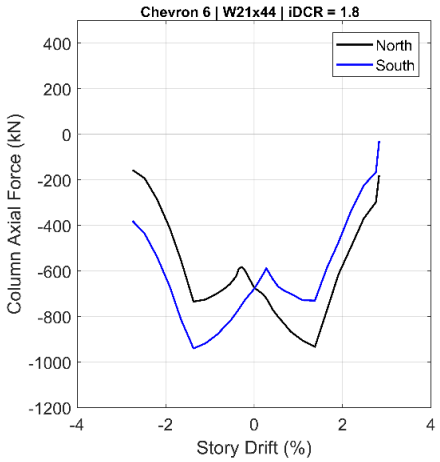

(f) Column axial force backbone curves

Figure 5.19 Chevron 5 measured column response

5.6 Measured Response of Chevron 6 (iDCR = 1.8)

This section will include a detailed review of salient beam, brace, and column forces calculated from the data collected during experimental testing of Chevron 6. A global view of the frame response will set precedent for a discussion of the local response at each element of the frame that contributed to the frame behavior.

5.6.1 Frame Response

The force-drift hysteresis of Chevron 6 in Figure 5.20 shows that brace buckling occurred at 0.28% drift and the system achieved a peak lateral resistance of 113% of the expected strength with 911 kN. The maximum drift range was 6%, with brace fracture of the south brace at 3% story drift and north brace fracture at -3% story drift.

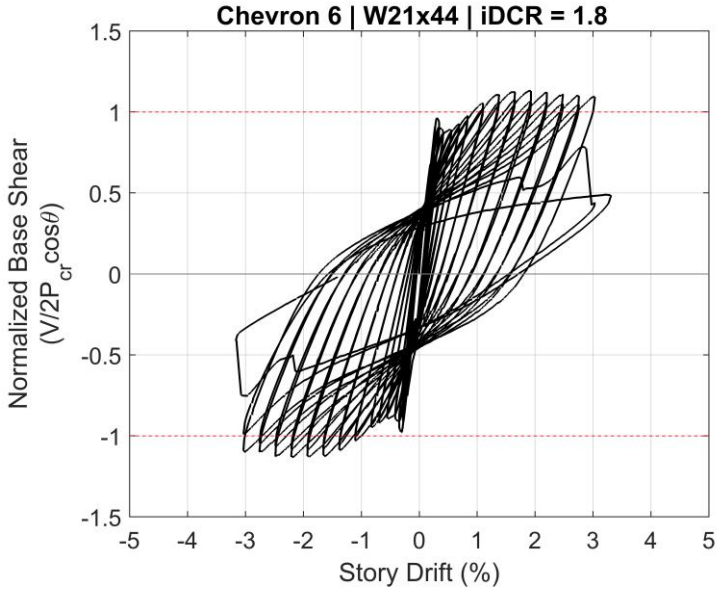

Figure 5.20 Chevron 6 base shear-story drift hysteresis

5.6.2 Brace Response

The brace axial force vs. frame deformation hysteresis in Figure 5.21 and the hysteretic plot of brace deformation vs brace axial force normalized by P_{cr} in Figure 5.22 highlights the following:

- The two braces buckled at approximately the same drift and force of 0.28% and 700kN.

- Post buckling response of the braces included a peak tensile strength of approximately 76% of the expected tensile strength (P_t)
- The braces' compressive strength degraded to 25% and 23% of the expected compressive strength (P_{cr}) for the South and North braces respectively
- The braces reached stable tensile demand of 919kN ($1.63P_{cr}$) in the South brace and 880kN ($1.54P_{cr}$)
- Additionally, the compressive force at brace buckling is higher than the force in the tension brace, resulting in the large unbalanced upward load discussed in Section 5.3.5.
- There three times more shortening of the braces than elongation.

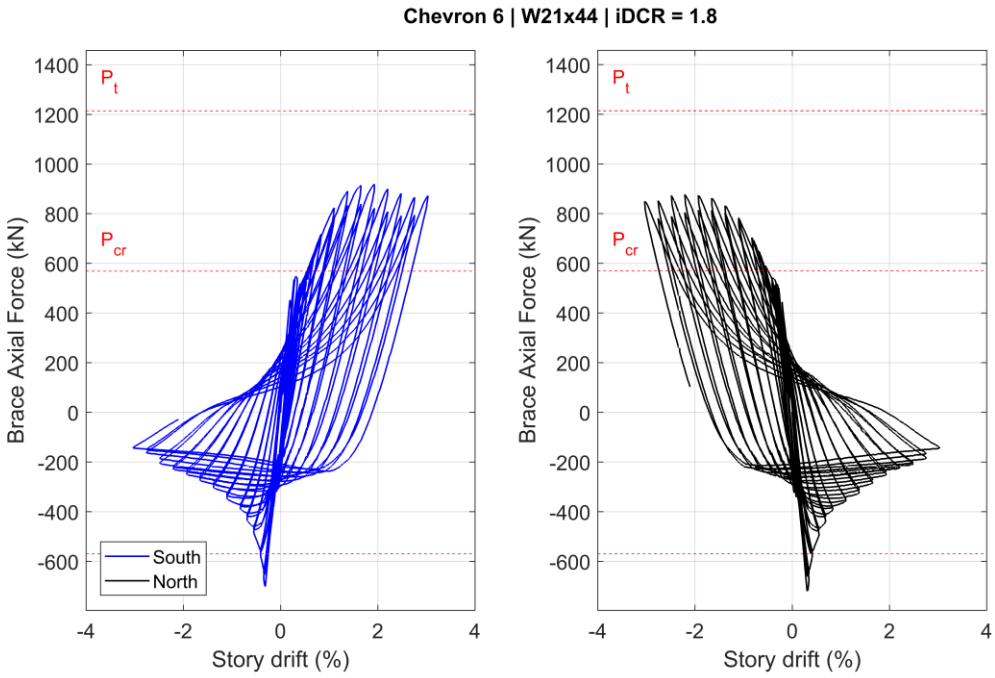

Figure 5.21 Chevron 6 brace axial force vs story drift hysteresis

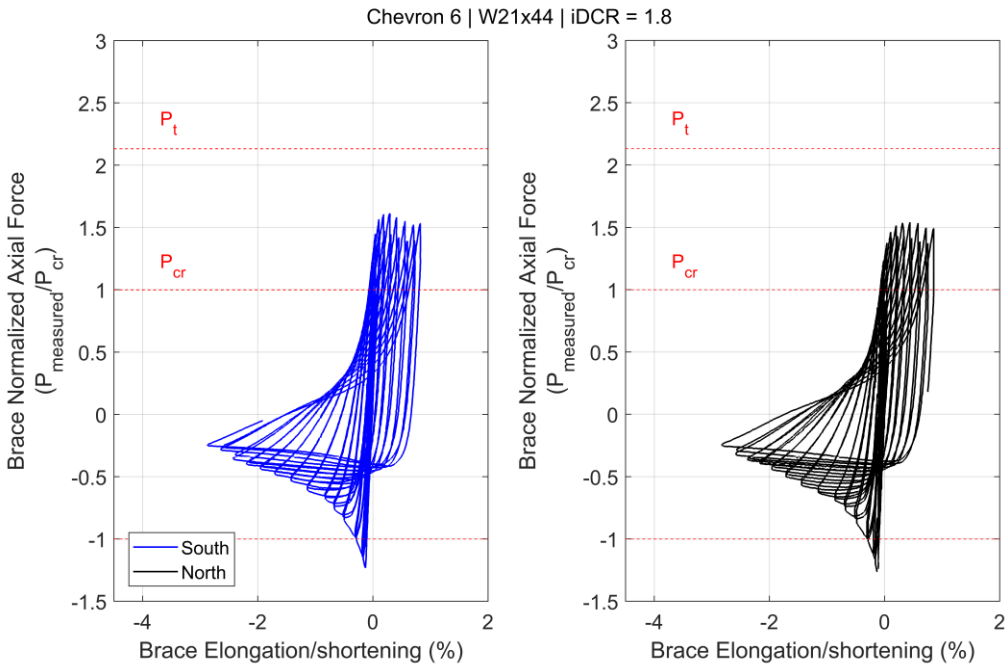

Figure 5.22 Chevron 6 Brace elongation and shortening vs. normalized axial force hysteresis

The Optotrak LEDs near the center of the brace used to plot the deformed brace shape at several story drift levels in Figure 5.23 were out of range of the cameras at some points during the test, so the full brace shape could not be reproduced at all drift levels of interest. However, the available information clearly shows the increase in deflection after brace buckling between 0.3% and 0.5% story drift and plastic hinge formation between 1.1% and 2.2% story drift, differentiated by the liner brace deflected shape. Thus, the complete brace shape at the highest shown drift was produced (represented by the dashed portion of the plot) and resulted in an approximation of 445 mm of deflection at 3.0% story drift.

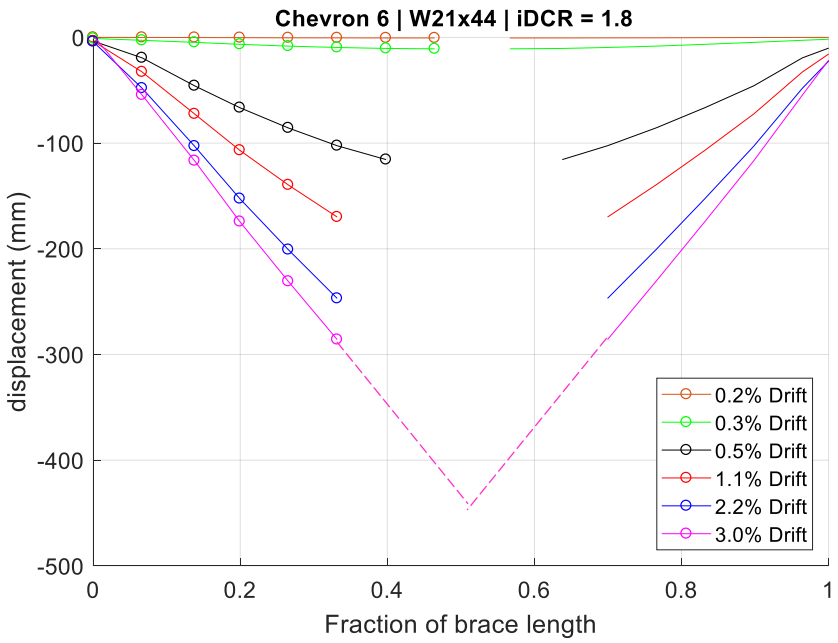

Figure 5.23 Chevron 6 South brace out of plane deformation

5.6.3 Beam Response

Figure 5.24 shows that the vertical force (resulting from the braces) vs the deflection at the midspan of the beam. The figure shows:

- The initial unbalanced force was upwards but did not result in beam deflection.
- A downward deflection resulted from a downward force
- The force-deflection response of the beam was not linear
- The vertical force from the braces reverses with each cycle, pushing the beam up close to its initial position.

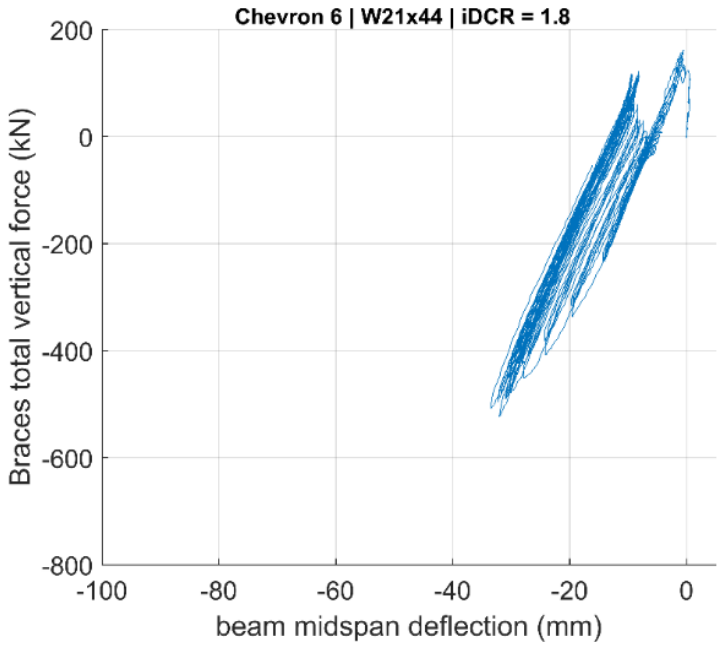

Figure 5.24 Chevron 6 Beam deflection vs. unbalanced vertical load hysteresis

The beam response backbone curves for moment, shear, and axial forces calculated using the beam strain gauges as described in Chapter 3 are shown in Figure 5.25 show the following:

- The force was not evenly distributed on the two sides of the beam as was assumed for design.
- The axial force on the side of the beam in tension plateaued and stabilized after brace buckling, but the force in the beam in compression degraded.
- The shear force was higher on the side of the beam in tension, as was the moment.
- The moment response curves suggests that the beam reached the reduced yield moment M^*_y at 1.75% story drift on the north side but did not surpass it on the south side and the moment demand was larger at positive drifts than negative drifts. This is inconsistent with the observed yielding on both sides of the beam during the experiment.

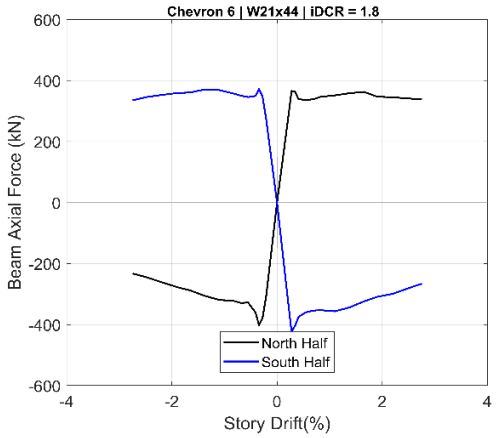

(g) Beam axial force backbone curve

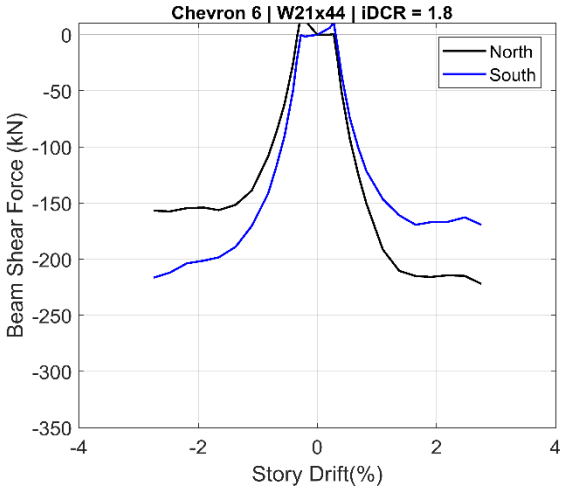

(h) Beam shear force backbone curve

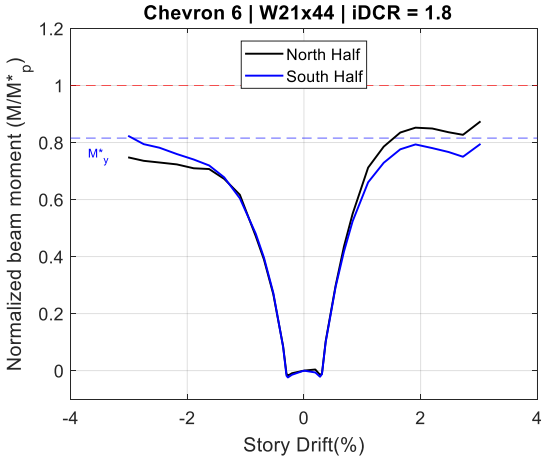

(i) Beam normalized moment backbone curve

Figure 5.25 Chevron 6 beam response envelopes

5.6.4 Connection Response

The deflection of the gusset plates in Figure 5.26 show very consistent behavior at the middle and corner gussets. The maximum deflection at the middle gussets was about 5 mm less than at the corners. The plastic deformation was also very similar as shown by the deformation when the corresponding brace was in tension.

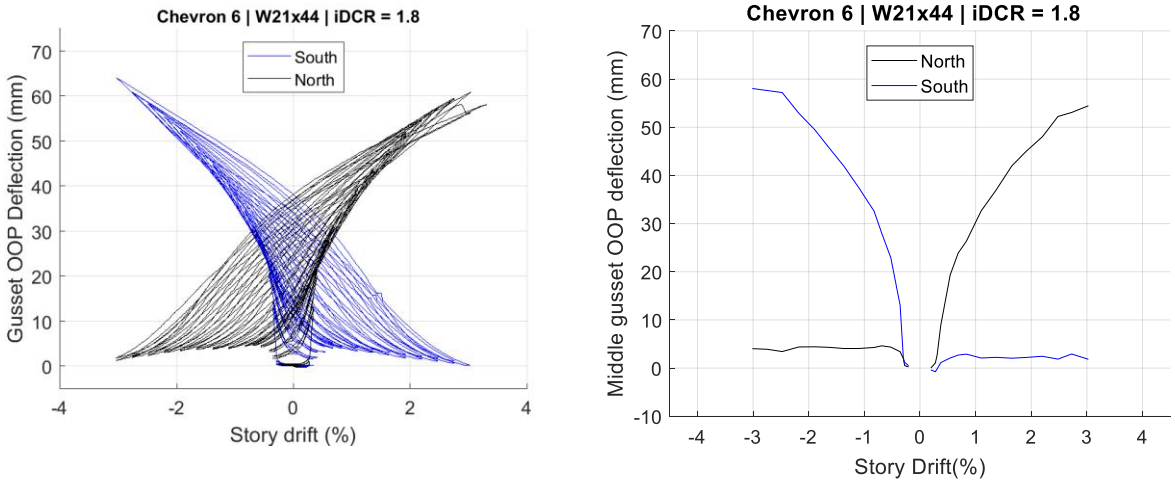

(e) Corner gussets (f) Middle gusset

Figure 5.26 Chevron 6 gusset plate deflection

5.6.5 Column Response

The column shear force hysteretic plots for main test cycles and post fracture cycles, and the column axial force backbone curve are shown as part of Figure 5.19. The column shear in the main cycles reverses gradually after brace buckling. The stiffness of the column remained approximately equal throughout the test and into the post fracture cycles. As expected from the previous tests, the columns started with a high axial load and gradually shortened, causing the prestress force to reduce.

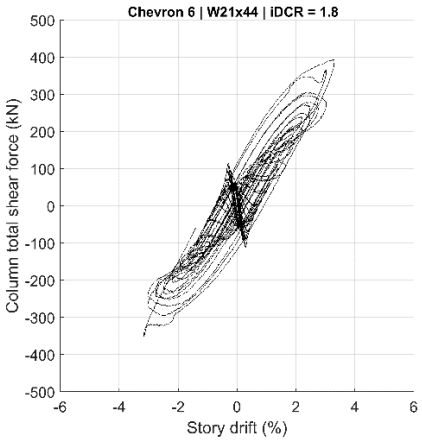

(g) Total column shear hysteresis during main test cycles

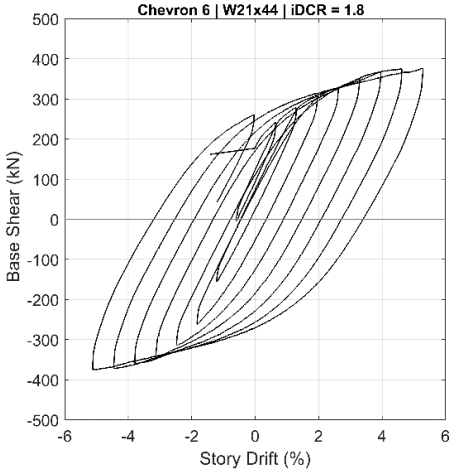

(h) Total column shear hysteresis during post fracture cycles

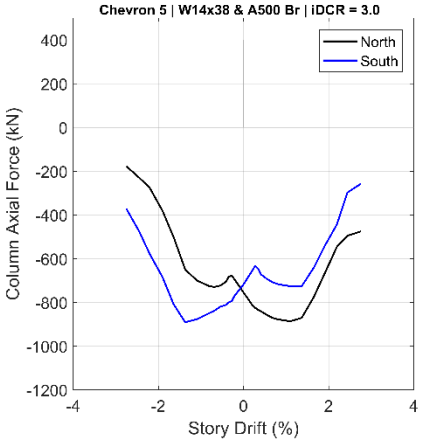

(i) Column axial force backbone curves

Figure 5.27 Chevron 6 measured column response

5.7 System Comparison

This section will compile results from Terpstra (2017) on Chevrons 1 through 3 for a full comparison of all single story chevrons tested to study the behavior of chevron SCBFs with yielding beams. Chevrons 1 through 4 have progressively weaker beams, Chevrons 2 and 6 have equal beam iDCR's but different beam stiffness, and Chevrons 3 and 5 have similar iDCRs but different brace ductility.

5.7.1 Force Drift Response

A summary of frame response is provided in Table 5.3 and Figure 5.28 shows the backbone curve of the base shear vs. story drift response normalized by the expected frame lateral resistance ($2P_{cr}Cos\theta$). These results show that all but Chevron 4 met or exceeded their expected lateral strength. All frames exhibited high ductility and reached drift ranges of 6% or greater, and in all instances the frame sustained 30 to 45% of the frame's lateral strength after brace fracture. Figure 5.29 shows that the initial elastic stiffness of the frames, calculated from the first peak force and displacement, was very similar for all the braces between 80 and 95 kN/mm. The frame with A500 braces had higher initial stiffness than the frame with same iDCR but A1085 braces, but lower ductility with 8% lower drift range.

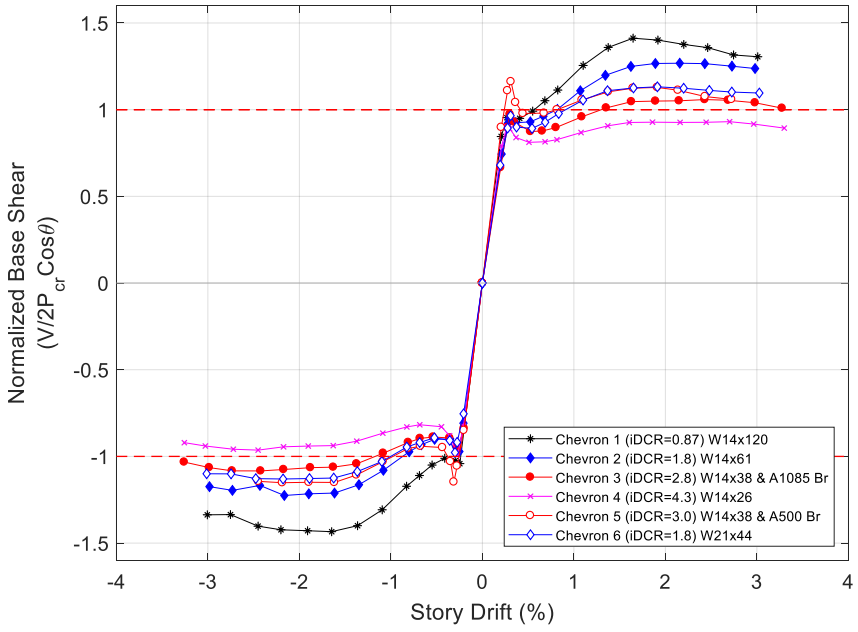

Figure 5.28 Base Shear- story drift backbone curve for Chevrons 1 through 6

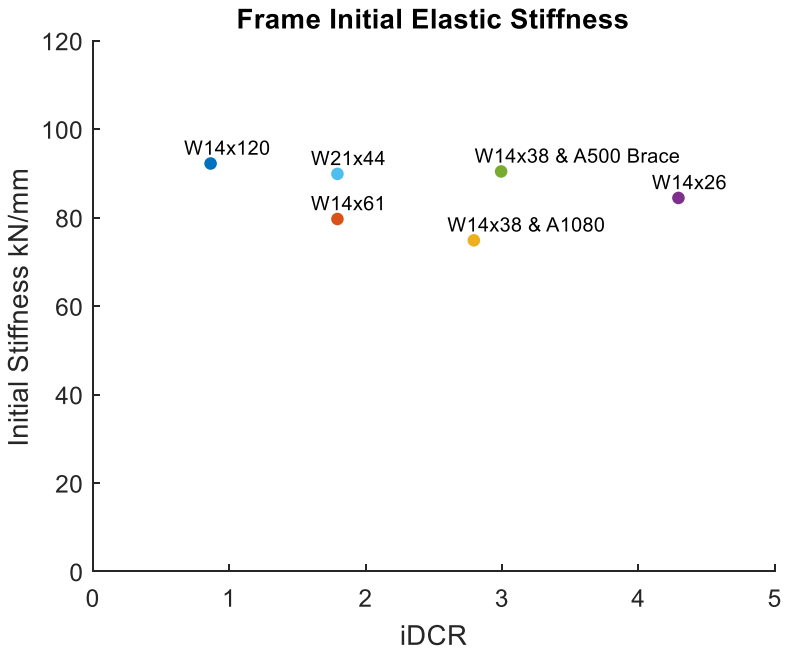

Figure 5.29 Frame initial elastic stiffness

Table 5.3 Summarized Test Results

Chevron	**1**	**2**	**3**	**4**	**5**	**6**
Beam iDCR	0.9	1.8	2.8	4.3	3.0	1.8
Max Lateral Resistance (kN)	1040	919	786	719	780	911
Max. Lateral Resistance / 2PcrCos(theta)	1.43	1.27	1.08	0.99	1.16	1.13
Max. Lateral Resistance / 2PcCos(theta)	1.52	1.34	1.15	1.05	1.20	1.23
Drift at 1st Brace Fracture	3 (S)	3 (S)	-3.6 (N)	4.4 (S)	-3 (N)	3 (S)
Drift at 2nd Brace Fracture	-3.3 (N)	-3.3 (N)	3.6 (S)	-4.7 (N)	3.5 (S)	-3 (N)
Max Drift Range	6.3	6.3	7.2	9.1	6.5	6
Max Post Fracture	84.8	83.4	74.4	85.9	83.1	84.8
Column Action	0.33	0.38	0.41	0.48	0.45	0.41

5.7.2 Brace Response

5.7.2.1 Axial Force and Elongation

The comparison of all the braces elongation and shortening in Figure 5.30 shows that as iDCR increased the elongation decreased and shortening increased. This is due to the increasing residual deflection of the beam. As the stiffness of the beam decreases and deflects it prevents the braces from elongating, which also results in lower maximum tensile forces being developed in the braces. Therefore, it would seem surprising that Chevron 6, which had a stiffer beam than Chevron 2 developed slightly lower tensile forces in the braces than Chevron 2. However, the braces in Chevron 6, did develop larger compressive forces than in Chevron 2, as expected. Table 5.4 provides a summary of brace elongation and maximum forces measured in each brace and is normalized in Table 5.5. Where $P_{t,exp}$ is the maximum measured tensile force in the braces and $P_{cr,exp}$ is the maximum measured compressive force in the braces. Maximum compressive forces, used to define brace buckling, were used to back-calculate the effective length factor, K. The expression used to calculate K is included in Appendix A and uses the end-to-end length of the braces. These results would suggest that in all cases the boundary conditions were more rigid than assumed for design.

Table 5.6 summarizes the measured unbalanced vertical and horizontal components of the forces measured in the braces, normalized by the demands used to design the beam based on the idealized unbalanced brace forces per Seismic Provisions (AISC 2016a). The design forces used were previously given in Table 5.2. These results show that the peak vertical unbalanced force decreased about 20% with each decrease in iDCR but the peak horizontal unbalanced force (brace lateral resistance) only decreased by 16% from from Chevrons 1 and 2 and remains stable for continued decrease of beam strength.

Table 5.4 Brace Axial force and Elongation Summary

Chevron		1	2	3	4	5	6
iDCR		0.87	1.81	2.83	4.32	3.02	1.77
Max. Tensile Elongation	S	42	25	13	3	4	29
(mm)	N	41	25	13	4	4	30
Max. Compressive	S	-104	-107	-136	-148	-103	-100
Shortening (mm)	N	-92	-106	-130	-142	-111	-97
Max. Tensile Force	S	1187	920	534	489	617	919
$P_{t,exp}$(kN)	N	1152	889	593	453	574	878
Max. Compressive Force	S	-631	-634	-544	-627	-551	-701
$P_{cr,exp}$(kN)	N	-612	-583	-610	-606	-550	-720
Effective Length factor,	S	0.89	0.88	0.97	0.89	0.91	0.86
K	N	0.91	0.93	0.91	0.91	0.91	0.84

Table 5.5 Normalized Brace Axial Force Results

Chevron	1	2	3	4	5	6
iDCR	0.87	1.81	2.83	4.32	3.02	1.77
Max($P_{t,exp}$)/P_t	2.29	1.77	1.14	0.94	1.25	1.61
Max($P_{t,exp}$)/P_{cr}	0.93	0.72	0.46	0.38	0.50	0.72

Table 5.6 Brace experimentally measured forces

Chevron	1	2	3	4	5	6
iDCR	0.87	1.81	2.83	4.32	3.02	1.77
max total horizontal force (kN)	957.0	758.6	742.2	746.7	780.1	887.4
max total vertical force (kN)	725.0	562.5	375.8	236.2	347.3	507.2

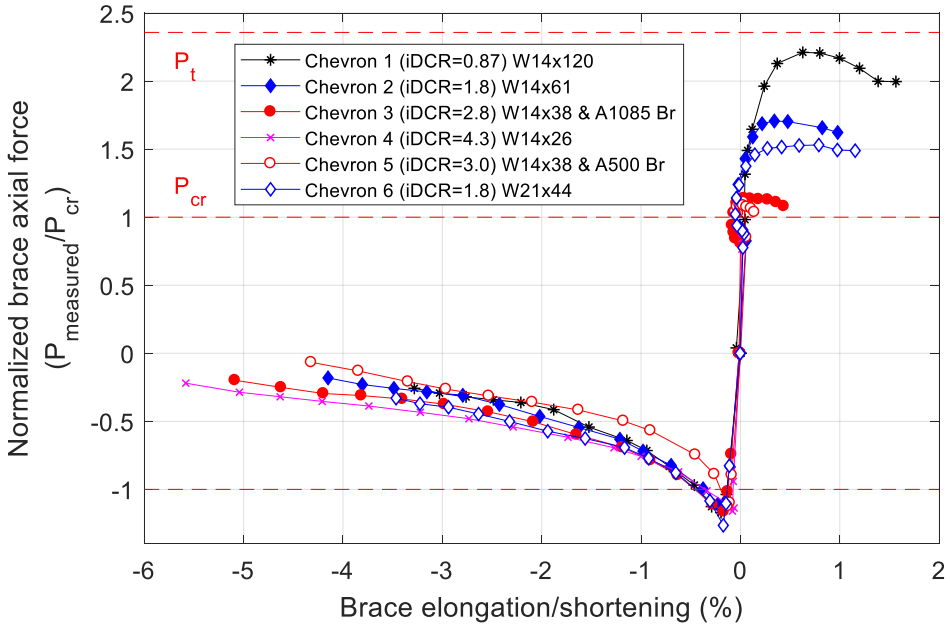

(a) North brace

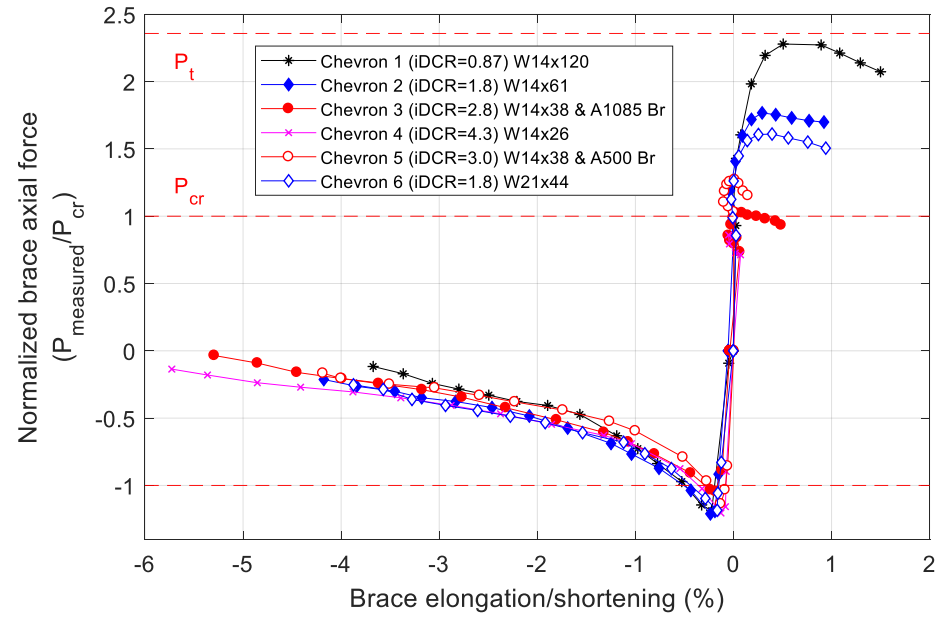

(b) South brace

Figure 5.30 Brace elongation and shortening vs normalized brace axial force backbone curves

5.7.2.2 Out of plane deformation

The braces deflected out of plane more with increasing beam iDCR to accommodate the increased brace shortening discussed in the previous section. The maximum deflection at the brace midpoint for each frame is shown in Table 5.7. In considering only maximum brace deflection there is not much difference for Chevrons 1 to 3. The deformation increases much more between Chevrons 3 and 4. Chevrons 2 and 6 have very similar brace deformation. Chevron 5, which has the A500 braces and is comparable to Chevron 3 has lower elongation and shortening, indicative of its lower ductility. Brace deflected shape plots for Chevrons1 through 3 can be referenced in Appendix C.

Table 5.7 Maximum brace out of plane deflection

Chevron	1	2	3	4	5	6
iDCR	0.87	1.81	2.83	4.32	3.02	1.77
Max North brace deflection (mm)	431	460	468	546	457	483
Max south brace deflection (mm)	477	481	485	519	439	475

5.7.3 28Beam Response

5.7.3.1 Deflection

With increasing beam iDCR and decreasing beam stiffness the maximum beam deflection increases. These maximum deflection values are presented in Table 5.8 and Figure 5.31. This data shows that the beam deflection between chevrons with iDCR between 2 and 3.

Table 5.8 Maximum Beam deflection

Chevron	1	2	3	4	5	6
iDCR	0.87	1.81	2.83	4.32	3.02	1.77
Max beam deflection (mm)	27.9	45.7	76.2	96.5	63.5	35.6
Max beam residual deflection (mm)	9.3	13.3	46.9	90.5	38.9	10.5

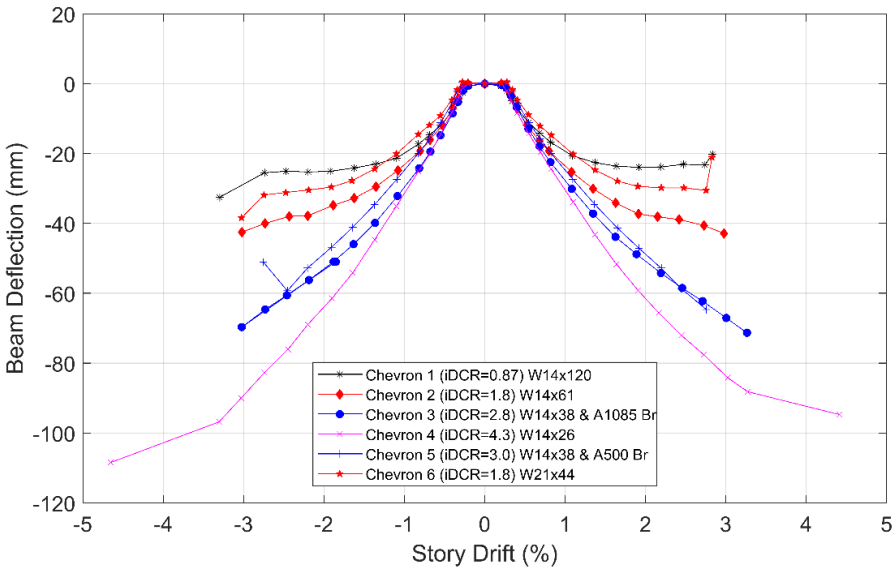

Figure 5.31 Beam vertical deflection envelope

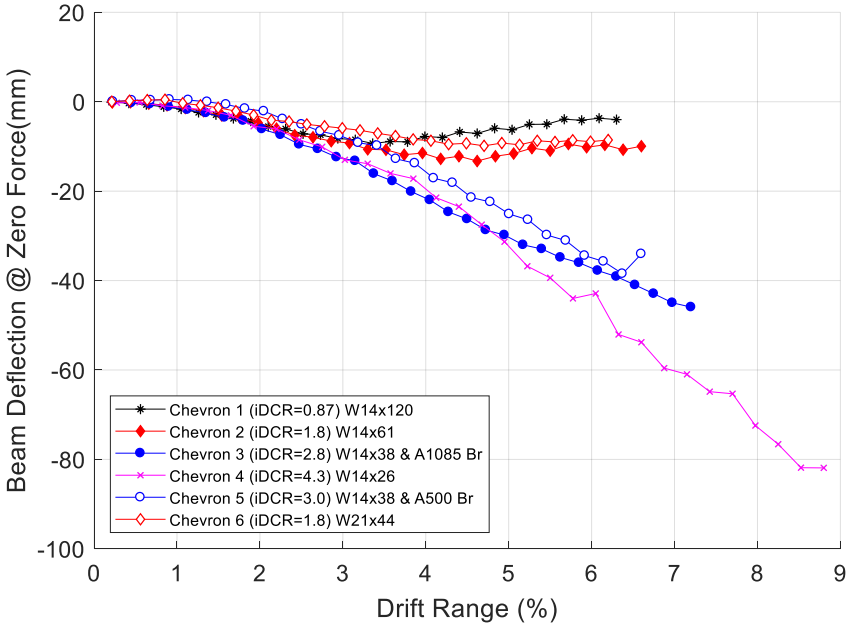

Figure 5.32 Beam residual deflection

The beam residual deflection values given in the Table 5.8 and Figure 5.32 corresponds to zero-force points of the loading cycle. The fact that the beam residual deflection decreases after 1.5% story drift in chevrons with iDCR less than 2 reflects the brace hardening that occurred in these frames at the same story drift. It can also be seen from this figure that the beam plastic deformation is very similar for all chevrons tested until approximately 1.5% story drift, and begin to diverge past this point in the tests. The difference become more significant between chevrons with iDCR below and above 2 after 2% story drift. The final residual deflection of chevrons with IDCR=3 is 250% more than chevrons of iDCR=2 and Chevron 4 had a final residual deflection twice as large as Chevron 3.

Although Chevron 6 had a stiffer beam than Chevron 2, and the same beam iDCR, and maximum deflections were 10mm larger for Chevron 2, the two had almost the same residual deflection at the end of the test.

5.7.3.2 Beam Shear

Comparing the measured forces in the beam to the design forces (theoretical brace unbalanced force) from procedures in the Seismic Provisions (AISC 2016a), in Table 5.2, is useful to illustrate the global effect of reducing beam strength on brace force development. The total horizontal and vertical forces in the beam, determined by adding the forces on both sides of the beam, were normalized by design values previously discussed in Section 5.3.3. The results are shown in Table 5.9 and presented in Figure 5.33 and Figure 5.34. The maximum beam forces in each test have are normalized and summarized in Table 5.9. The maximum horizontal force in the beam (axial) is relatively consistent for all the specimens developing around 60% of the design load. Chevron 1 is an exception, which at 78% develops a larger proportion of the design load. However, the beam axial strength degradation does increase with increasing iDCR and is much faster in Chevron 4. The total shear developed by the beam is consistent with the reduction in beam strength. Chevron 2 with approximately one half the beam design strength develops 60% of the design shear load. Similarly, Chevrons 3 and 4 develop 1/3 and ¼ of the shear and moment demands.

Table 5.9 Beam experimentally-measured forces

Chevron	1	2	3	4	5	6
iDCR	0.87	1.81	2.83	4.32	3.02	1.77
max total axial force (kN)	974.2	782.8	725.6	774.1	827.2	839.3
max total vertical force (kN)	689.8	473.2	219.5	188.5	246.5	442.7
max beam moment at gusset edge (kN-m)	889.9	575.3	292.7	212	332	514

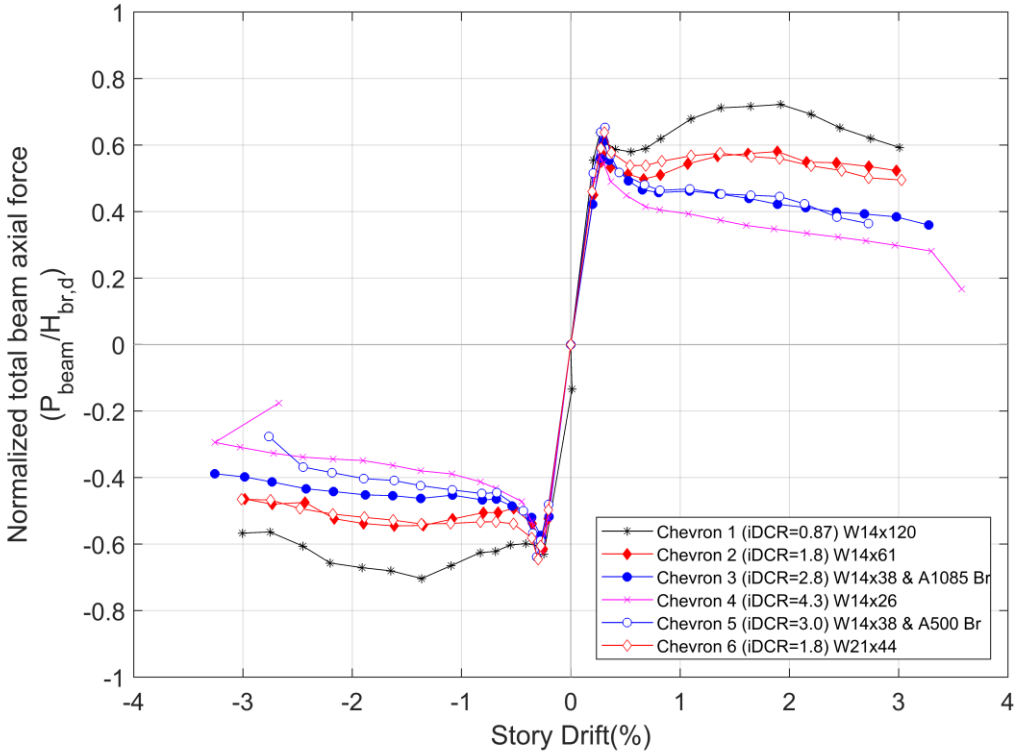

Figure 5.33 Beam normalized total axial load backbone curves

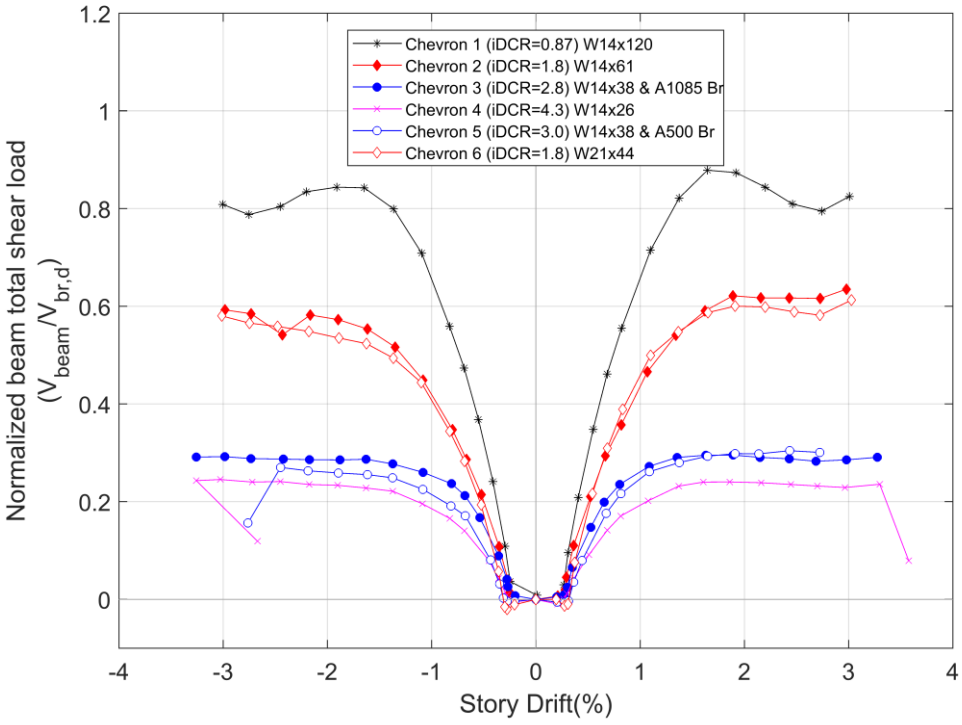

Figure 5.34 Beam normalized total shear load backbone curves

5.7.4 Column Response

The proportion of shear carried by the columns increased with an increase in iDCR as shown in Figure 5.35. The columns ultimately developed the same shear forces in each test, but due to the decrease in developed forces in the braces with increasing beam iDCR, the columns contributed a larger proportion of the strength. The column contribution was slightly lower in the Chevron 6 frame than in Chevron 2 due to a slightly larger development in brace forces in Chevron 2, as discussed in Section 5.7.2. The columns had essentially the same strength contribution in Chevrons 3 and 5. The column shear history is somewhat asymmetric, and increases with increasing iDCR. There is also more divergence in contribution between different iDCR frames in negative drift than in positive drift (movement of frame towards the north). This is likely due to the fact that the loading beam was offset to the north side of the spreader beam in the test setup.

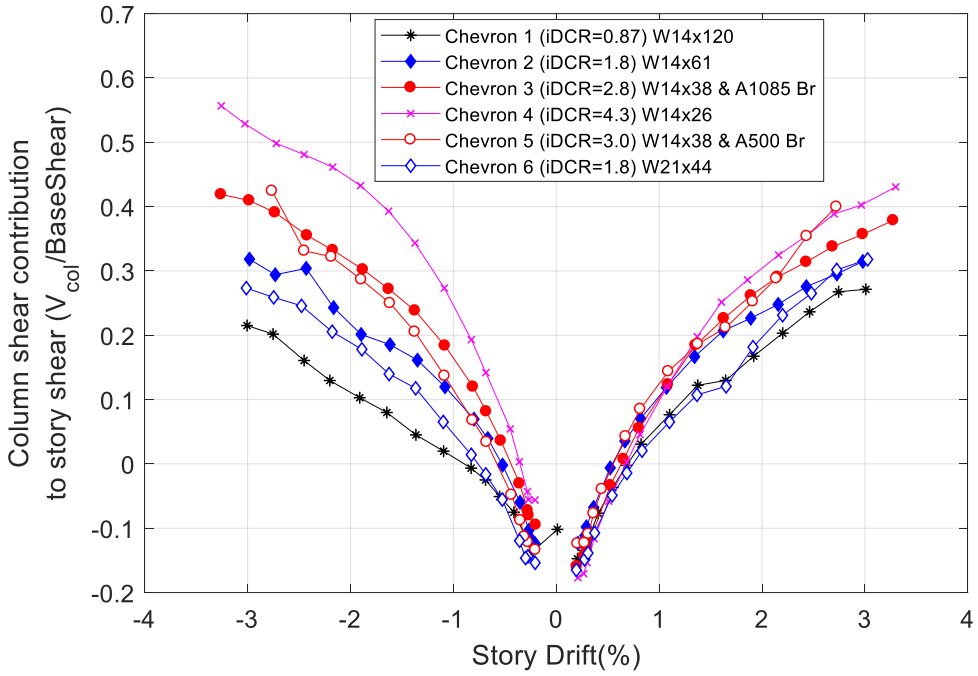

Figure 5.35 Column contribution to lateral resistance

Figure 5.36 show the backbone curves of the north and south column moment at the edge of the corner gusset plate normalized by the reduced plastic moment discussed in Section 5.3.4. These curves show that the moment demand increased more rapidly for chevrons with beam iDCRs. Chevron 1 moment remained close to zero until brace buckling at about 0.3% story drift, but the moment demand in the column of Chevron 4 was already about 10% of M^*_p by the time the braces buckled. Very consistently, the column reached the plastic moment about 1.25% story drift, which is consistent with test observations of column yielding beginning at 1.1% story drift.

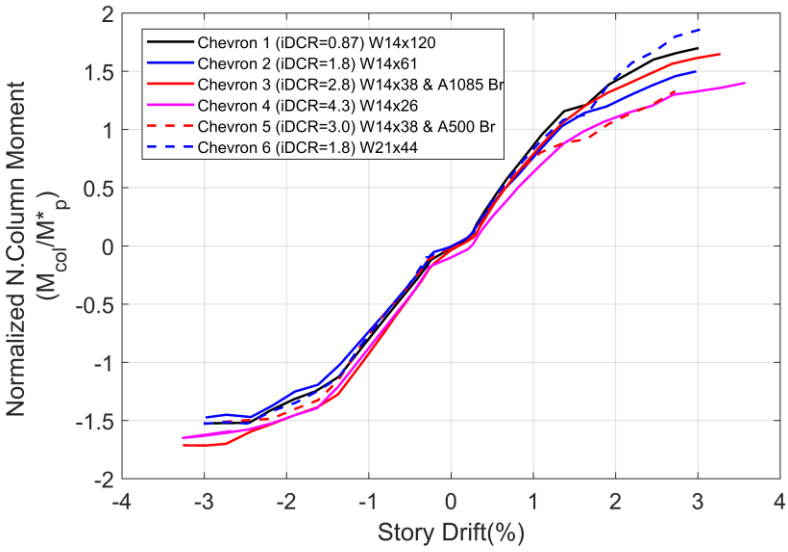

(a) North column normalized moment response envelope

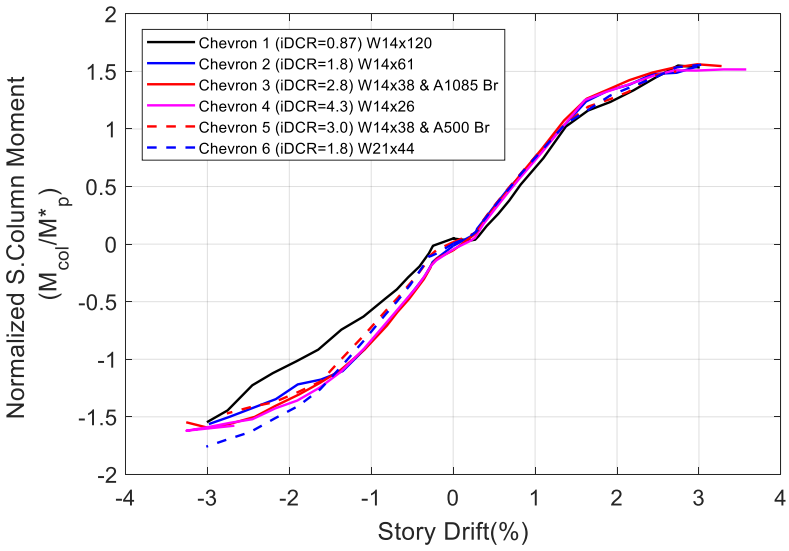

(b) South column normalized moment response envelope

Figure 5.36 Column moment backbone curve

CHAPTER 6
Three-Story Chevron Test

6.1 Introduction

This Chapter describes Part III of the experimental program which involved one 3-story chevron SCBF, Chevron 7 (Figure 6.1). Each story of the test had a chevron configuration but the top story was designed to remain essentially elastic to transfer the forces. This specimen was designed to investigate the system response of chevron braced frames with beams that yield under the brace demand. The test frame had composite slabs with gusset plates at the beam column connections; these two aspects of the configuration were expected to simulate a more realistic behavior.

6.2 Specimen Design

The column, brace, and beam design requirements are the same for single and multi-story SCBF's. The boundary conditions for the multi-story frame result in restrained beam-to-column connections at the gusset plate locations and a different expected beam yielding mechanism than for the single story frame because chevron bracing results in a corner gusset plate connection at all beam-to-column connections. For details on Seismic Provisions (AISC 2016a) requirements on the columns and braces refer to Chapter 3.

Figure 6.1 Chevron 7 overview picture (prior to testing)

6.2.1 Basic Geometry and Strategies

The geometry and configuration of the test frame was chosen to be similar to that used by Lumpkin (2009) and Sen (2014), because this permitted comparison with prior tests and reuse of the test setup, including out-of-plane restraint and instrumentation layout and supports.

After a preliminary design, numerical studies in ABAQUS were performed by Andrew Sen and Ruyue Liu to estimate the expected performance of the test frame, and to determine the adequacy of the design in meeting the test objectives listed below.

Objectives:

- Capture local damage of the beam at the plastic hinge locations.
- Evaluate the performance of the partially composite beam under cyclic loading.
- Evaluate the deflection in the beam and slab effects.
- Evaluate the load in the braces and maximum unbalanced loads developed.
- Evaluate the concentration from soft story effect.

6.2.2 General Constraints

The design of the frame was meant to satisfy the test objectives within the limitations of the laboratory setup established by Lumpkin (2009) for the TCBF2 test series. The TCBF2 series consisted of three story frames with double story X-bracing on the first two stories and a chevron configuration the third story.

A design was completed with the same general geometry as used in Lumpkin's frames in order to reuse the same test setup. A summary of the steel sections used in the tested frame is in Table 6.1 and Figure 6.2 shows the frame configuration and dimensions. Notable aspects of the specimen and lateral support include:

- The bottom two beams were expected to have significant vertical and horizontal deflections, and lateral rotational restraint was required for the beams of the steel frame.
- The beam at the top level was a W24x94 designed to remain elastic.

- The beams at the first and second floor levels were W14x30 designed to fully hinge at the cross section.
- The transverse beams were W14x26 sections.
- The columns were W12x106 sections, sized to develop the full expected brace forces
- All beam-column connections were welded flange-welded web connections
- The top slab was 200mm thick with steel fiber reinforce concrete and steel edge beams along the entire length. The top slab was heavier, stiffer, and stronger due to numerous shear studs on the continuous edge beam in order to ensure force transfer.
- A 150 mm composite deck was used on the first and second stories. Normal weight concrete was used and shear studs were spaced at 305mm to achieve partially composite action. The metal deck ridges were parallel to the W14x30 beams.
- Gusset plates were 13mm thick and designed using the BDP.

Table 6.1 Chevron 7 Design Summary

Specimen Name	Chevron 7
First Story Beam	W14x30
Second Story Beam	W14x30
Third Story Beam	W24x94
First Story Slab	150 mm
Second Story Slab	150 mm
Third Story Slab	200 mm
Brace Size	HSS5x5x1/2
Column Size	W12x106
Brace ASTM Designation	A1085

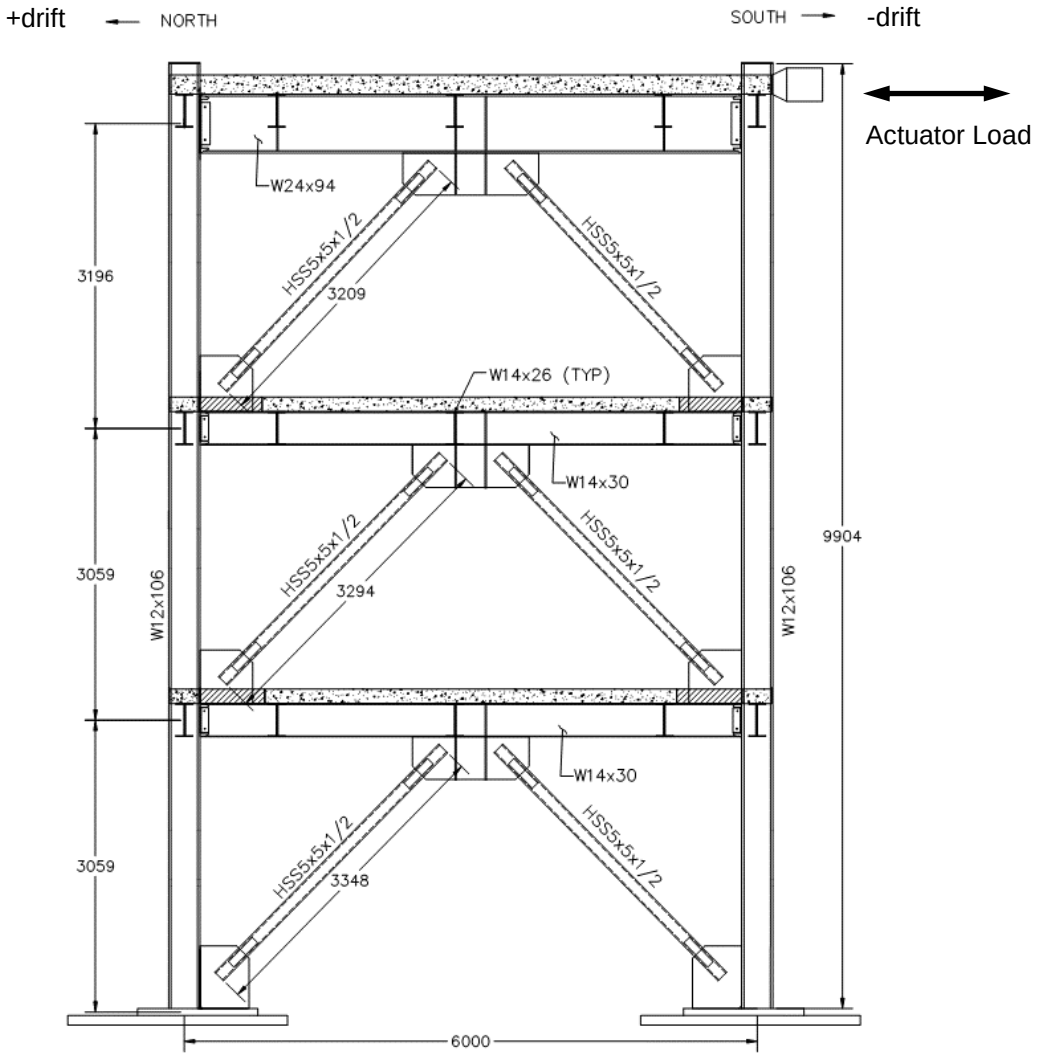

Figure 6.2 Chevron 7 dimensioned drawing

6.2.3 Beam

Experimental results of Chevrons 1 through 4 and numerical analysis of the single-story frames showed that the lateral resistance of the frame was not decreased proportionately to the beam strength reduction and frames with beams of the aforementioned strength could still meet or exceed the frames' design lateral resistance. It was proposed, and corroborated by numerical analyses that in the multi-story frame with gusset plates above the beam-to-column connection, welded flange-

welded web (WFWW) moment connections, and partially composite slab would increase the overall stiffness and strength of the system and result in twice the internal work of the simply supported beam in the single-story. Thus, it was determined that a 3-story frame with a W14x30 would exhibit seismic performance between that of Chevrons 2 and 3, which showed desirable ductility, strength, and little strength degradation. Based on a simple span plastic collapse mechanism, with a beam length from the end of the beam to the edge of the midspan gusset plate, and not considering composite action, the resulting iDCR for the bottom two stories would have been 5.8.

The top beam of the frame was designed with a very low iDCR because lateral loads from the test actuators were brought into the frame through the slab and beam of the top level. The beams selected for the test specimen complied compactness criteria for moderately ductile members after brace buckling per the Seismic Provisions (AISC 2016a).

6.2.4 Braces

The size of the braces was limited by actuator capacity and the availability of A1085 tube sizes. The b/t ratio of these braces was 7.0, lower than the single-story tests which had b/t = 9.8 and the highly ductile compactness criteria limit from the Seismic Provisions is 14.0. This compactness combined with the Chevron 1 through 6 test results suggested it was unlikely that the braces would fracture during the test.

6.2.5 Columns

The columns were designed to meet Seismic Provisions (AISC 2016a) to resist the expected brace resistance and were W12x106 shapes. The columns were cut to the full height of the frame to avoid column splices. With local slenderness values of $h/t_w = 15.9$ and $b/2t = 6.17$ the column sections also comply with compactness criteria for highly ductile members before and after brace buckling as required by the AISC 2016a. The columns and connections were checked for the maximum axial and lateral demands developed by the braces using compression forces of P_{cre} and $0.3P_{cre}$ (initial buckling and full degradation of the compressive force) since the lateral contribution of the frame strength was expected to increase significantly once the braces buckled.

6.2.6 Connections

The corner and mid-beam gusset plates at every story were designed using the BDP as explained in Chapter 3. With elliptical clearance at the corner gussets and linear offset at the mid-beam gusset plates. The details for the gusset plate connections are shown in Figure 6.4,Figure 6.7, andFigure 6.8.

Given the change in boundary conditions at the beam ends, simple shear tab connections were no longer adequate given the existence of moment at the beam end due to the rigidity provided by the gusset plate of the floor above. In such conditions, where a gusset plate connect to both a column and beam at a beam-column connection, Seismic Provisions (AISC 2016a) the connection must meet one of the following:

a) be a simple connection with rotation capacity of 0.025 rad.
b) be designed to resist the lesser of a moment of magnitude 1.1RyMp, corresponding to the expected beam flexural strength multiplied by 1.1 and the sum of the expected column flexural strengths multiplied by 1.1.

Several beam to column connections were considered for Chevron 7 including variations of bolted shear plates that would meet requirement (a) as stipulated above. Additionally, results from the ABAQUS analyses mentioned in Section 6.2.1 showed that a connection of a bolted web shear tab with welded beam flanges would have provided sufficient strength and rotation. Ultimately, a welded flange welded web (WFWW) moment resisting connection was chosen for all the beam to column connection due to its preferred use by practicing engineers. The details for this connection at the first, second, and third story beams are shown in Figure 6.5 and Figure 6.6. At these beam-to-column connections, the weld runoff was cut off from the bottom flange weld and the backing bars were left in place as shown in Figure 6.3.

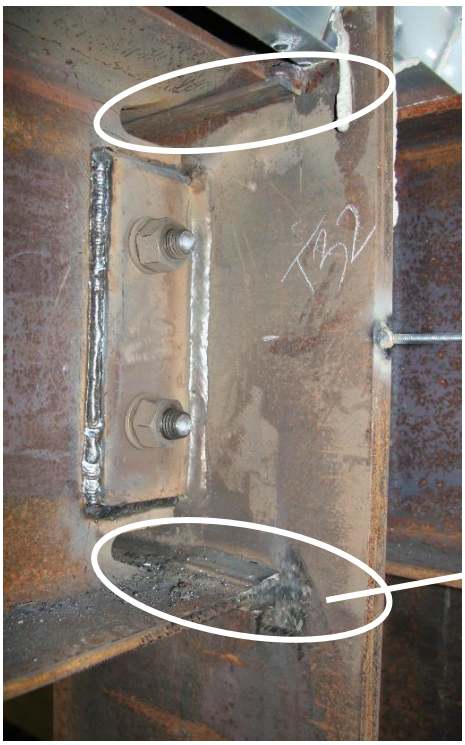

(a) backing bars on welded connection

(b) cut and ground weld runoff on bottom flange weld

Figure 6.3 Typical beam-to-column connection

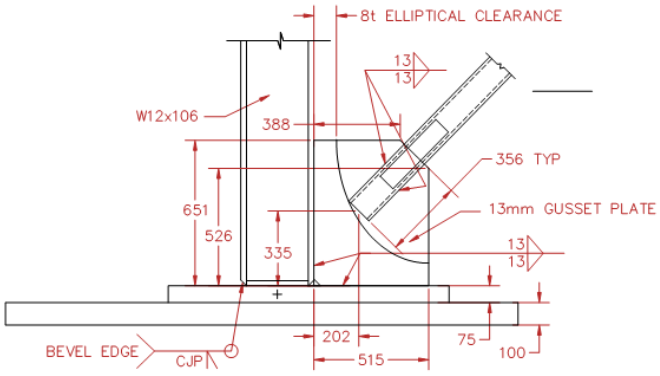

Figure 6.4 First Story corner gusset plate detail

(all dimensions in mm)

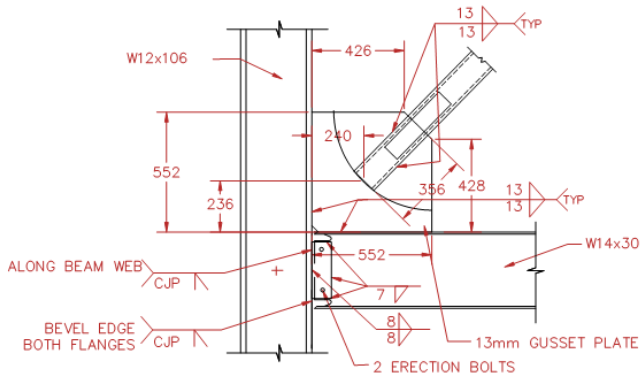

Figure 6.5 First and second story corner gusset plate detail

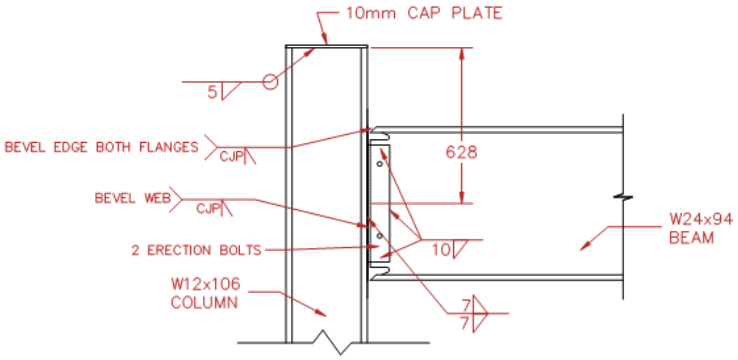

Figure 6.6 Third story beam to column detail

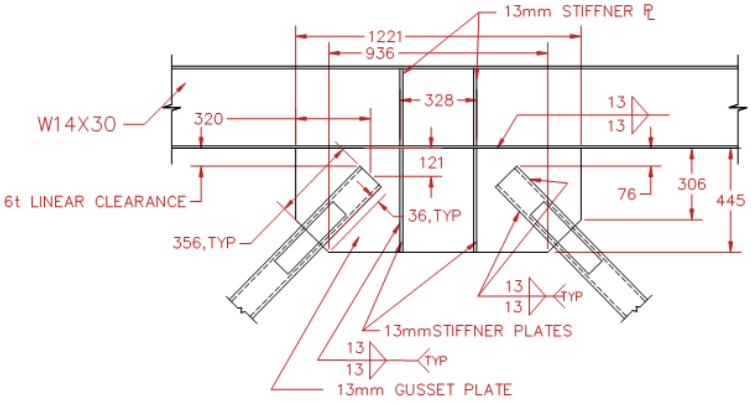

Figure 6.7 First and second story mid-span gusset plate detail

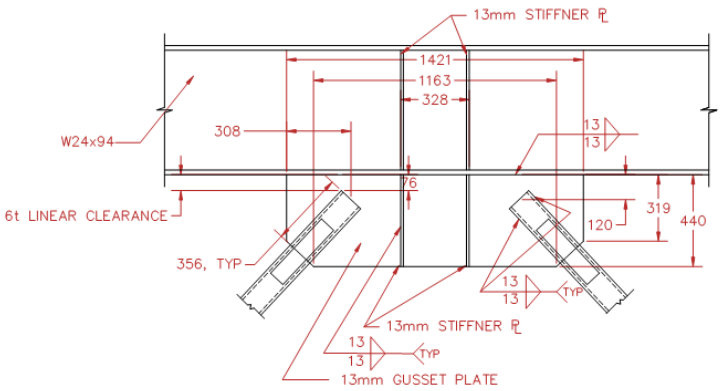

Figure 6.8 Third story mid-span gusset plate detail

6.2.7 Component Material Properties

The measured material properties of the structural sections and plates used are given in Table 6.2. The wide flange sections used for the beams and columns, and the tubes used for the braces in the test specimen were shipped to Taiwan from the U.S so they had ASTM material designations and U.S. dimensions. The plates used for gusset plates and stiffeners were from Taiwan and, thus, have Taiwanese material designations; but they were selected to closely match an A572 Grade 50 material. The yield and ultimate tensile strengths, F_y and F_u, measured from on-site tensile coupon tests per ASTM E8/E8M (ASTM Standards) are provided along with overstrength factors, i.e., the ratio of measured to nominal strengths. Table 6.3 shows the 8 day, 28 day, and test-day compressive strength of the Chevron 7 concrete slabs. These were determined from cylinder compression tests performed on-site per ASTM C39/C39M.

Table 6.2 Steel measured material properties

Section	Material	F_y		F_u		F_y/F_{ynom}	F_u/F_{unom}
		(MPa)	(ksi)	(MPa)	(ksi)		
W14x30	A992 Gr. 50	385	55.8	510	74	1.12	1.14
W12x106	A992 Gr. 50	379	55	521	75.6	1.10	1.16
W24x94	A992 Gr. 50	416	60.4	534	77.5	1.21	1.19
HSS5x5x1/2	A1085	490	71.0	552	80.1	1.42	1.23
13mm plate	SN490B	390	56.5	532	77.2	1.20	1.19
10mm plate	SN490B	370	53.6	534	77.4	1.14	1.19

Table 6.3 Concrete measured material properties

Story	Days since cast	Avg f'_c (MPa)	(psi)
1,2	8	36.7	5323
3	8	34.9	5057
1,2	28	40.0	5801
3	28	37.3	5410
1,2	34	38.1	5526
3	34	35.9	5207

6.3 3-Story Frame Experimental Setup

The experimental setup was designed by NCREE researchers Te-Hung Lin and An-Chien Wu. The setup was very similar to that used for the TCBF2 test series, explained in detail by Lumpkin (2009), and included the adapted modifications used for the TNCBF series explained in Sen (2014). The geometry of Chevron 7 was based on the TCBF2-HSS geometry. The two frames had equal bay width and total frame height but slightly different story heights. The modifications used by Sen (2014) as well as in this experiment included the use of only 3 – 100 metric ton actuators, a modified roller system to prevent twisting of the top beam and slab, and discontinuous edge beams at the first and second floor to prevent adding an unrealistic rigidity to the midspan of the composite beam. However, the slabs ultimately had some added rigidity from aluminum angles, as seen in Figure 6.12, used for formwork and left in place for testing.

This test setup was intended to provide realistic loading and boundary conditions of a multi-story SCBF.

6.3.1 Test Layout

The various components of the test layout, as shown in Figure 6.9 to Figure 6.11, include the actuators, out-of-plane frame, edge beams, and rotational restraints. Complete drawings of the experimental setup are included in Appendix B.

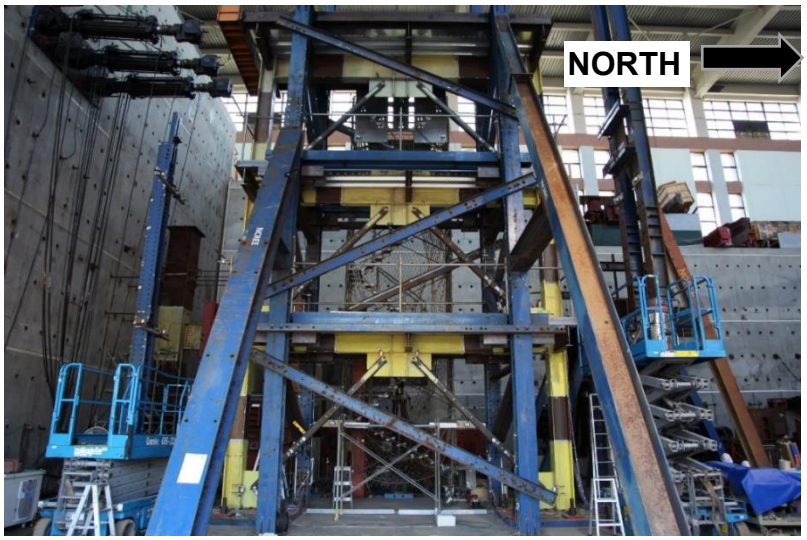

Figure 6.9 Photo of test specimen with out-of-plane frame (in blue)

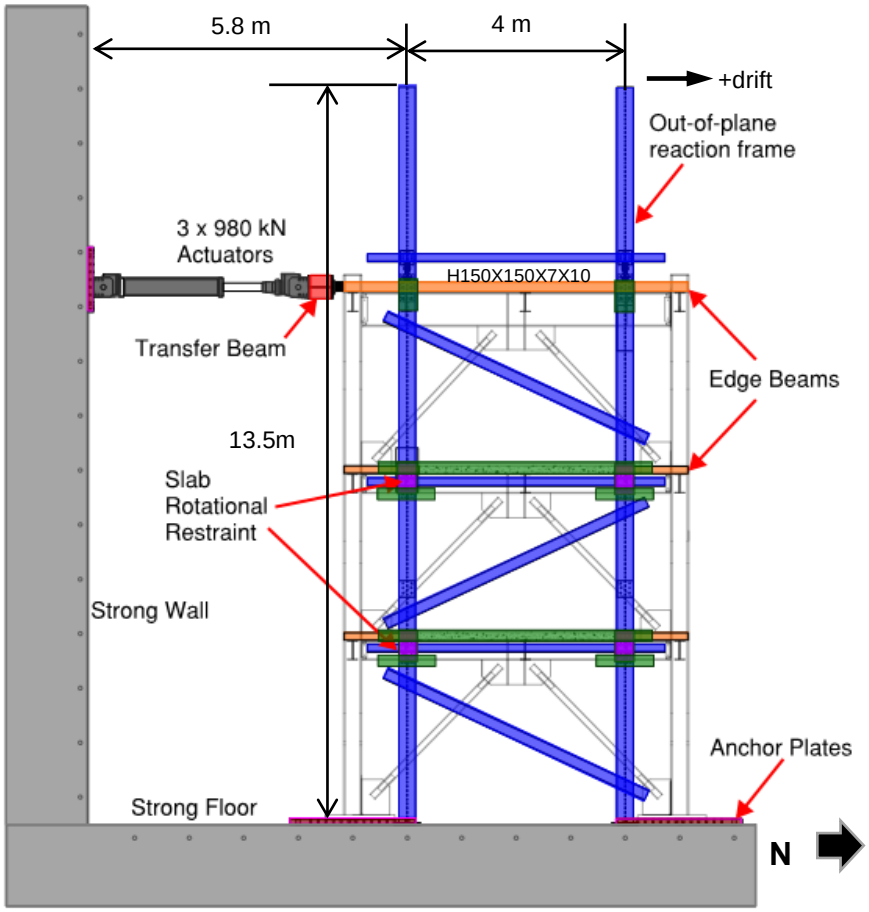

Figure 6.10 East elevation of test setup

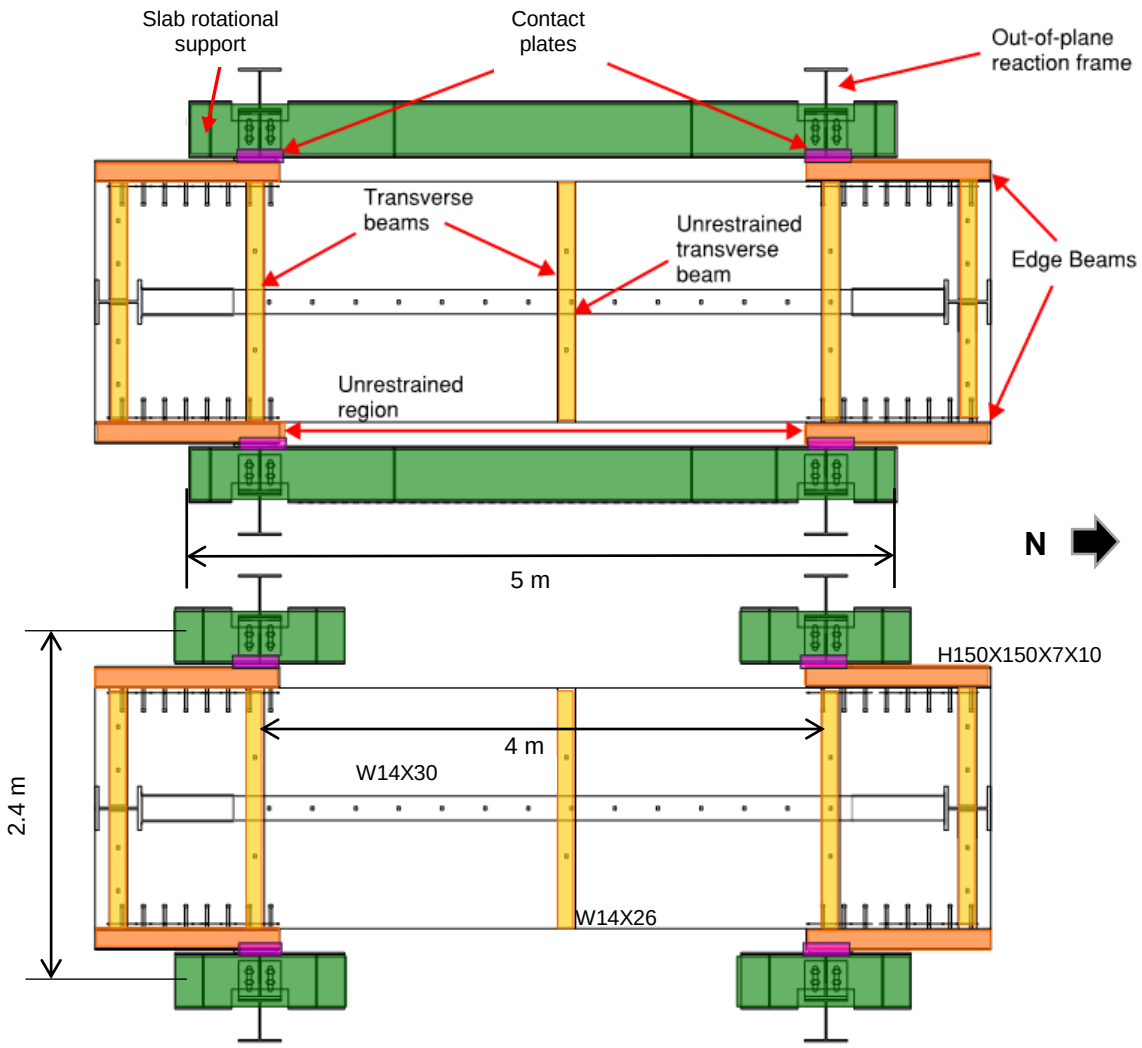

Figure 6.11 Typical floor and ceiling plan of the test setup at lower beams

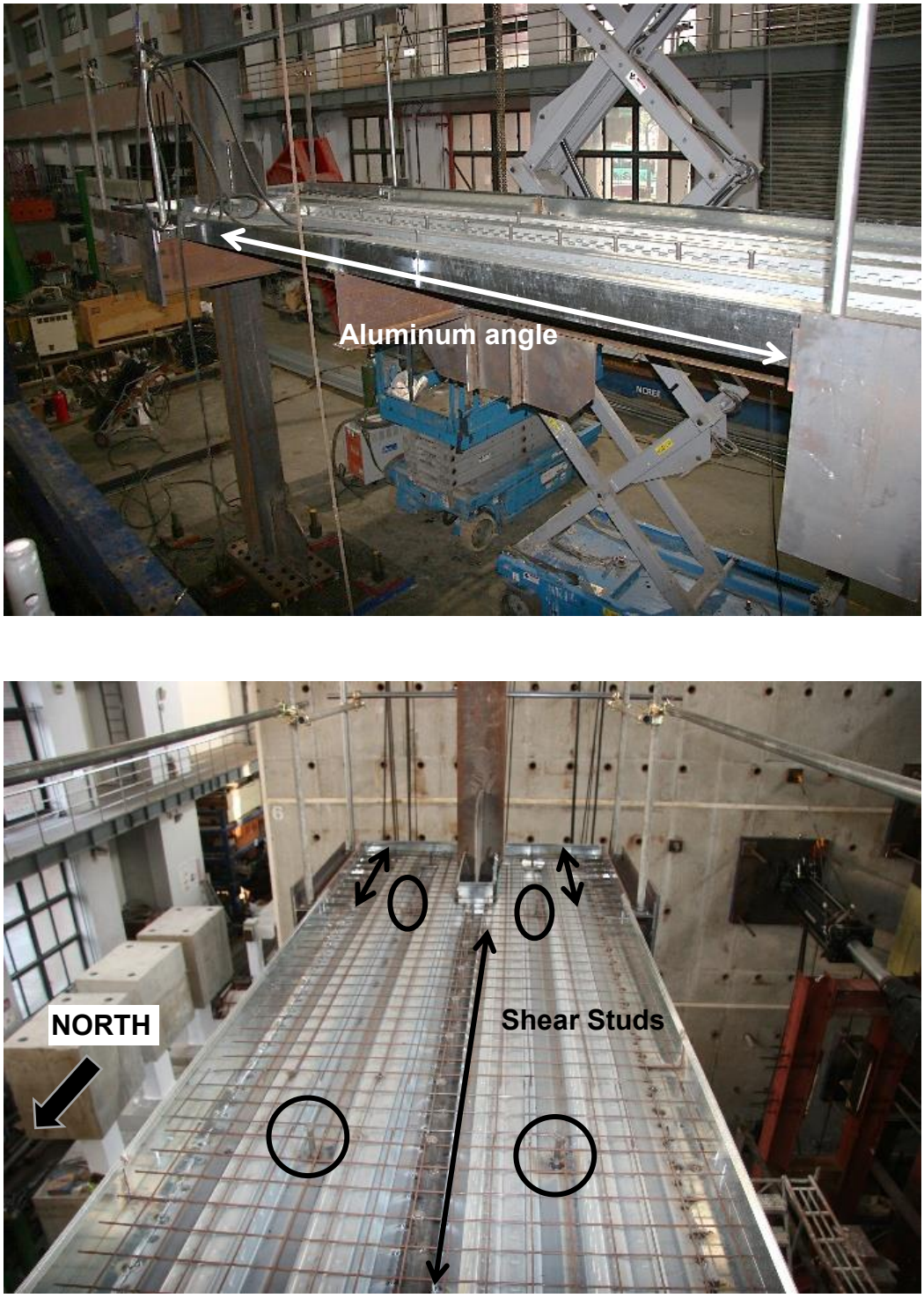

Figure 6.12 Typical metal deck for first and second story slabs

6.3.2 Out-of-Plane (OOP) Reaction Frame

It is noteworthy that the first and second story beam and slabs were restrained only at the beam quarter points, as shown in Figure 6.11. The slab rotational restraints at the first story (Figure 6.10 andFigure 6.11), consisting of two points of contact of the transverse beams with the OOP frame are pictured in Figure 6.13. This was a primary difference with Sen (2014) and Lumpkin (2009) tests as there were no slab rotational restraints over a 4 m section of the slab on the first and second stories. This absence of rotational support and edge beams in the inner portion of the beams and slab resulted in a stiff end condition between the two exterior transverse beams and a much more flexible interior section. This condition was used to accommodate the larger vertical deflections at midspan of the beam with yielding chevron beams, and it was compounded by inadvertent changes to the test setup for this test.

The top slab, pictured in Figure 6.14 had rotational and lateral restraint over its entire length. At the top slab, the rollers meant to provide rotational restraint were too close to the edge beam and got stuck during testing as shown in Figure 6.14. This resulted in slight bending of the top story edge beam and movement of the OOP frame during loading. As a result, these rollers were removed halfway through the test to prevent additional OOP frame movement.

(a) First story rotational supports (b) Edge plate and rotational support

Figure 6.13 Slab out-of-plane rotational restraint

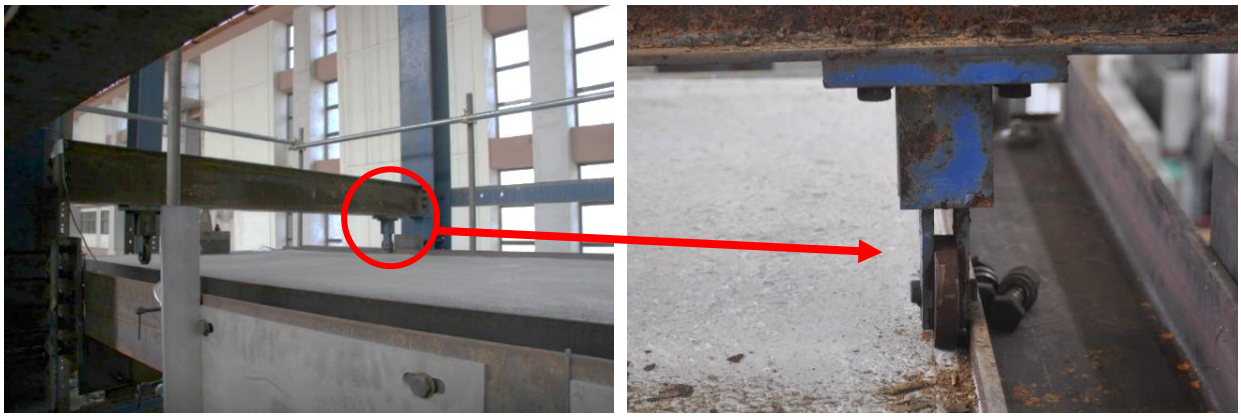

(a) Guide and roller (b) roller

Figure 6.14 Top floor slab rotational restraint

6.3.3 Actuator Load Path and Edge Beams

The specimen's lateral load path is outlined in Figure 6.15. The force from the actuators was transferred through the transfer beam to the two continuous edge beams in Figure 6.10 at the third story. Then, a shear force was delivered to the slab through the shear studs spaced at 150 mm and the resulting load was transferred to the braced frame through the shear studs, also at 150mm o.c., on the third story beam. The three actuators, located on the south side of the frame, pushed out (actuators extended in compression) towards the north on the frame to incite a positive drift. As they pulled in (actuators retracted in tension) and moved the frame in the south directions, this corresponded to a negative frame drift. Of the three actuators, the center one was controlled by a preprogrammed displacement protocol, and the east and west ones were slaved to the displacement of the middle actuator.

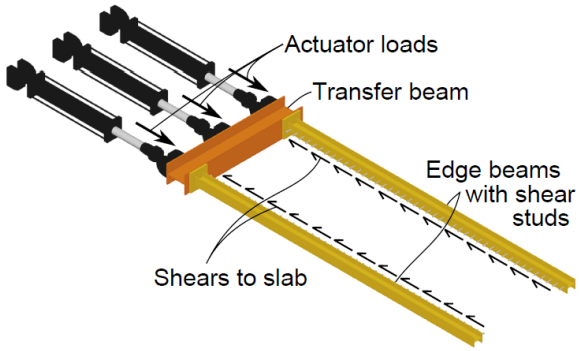

Figure 6.15 Actuator-to-specimen load path at third story (Sen 2014)

Figure 6.16 Top slab edge beam

6.3.4 Loading Protocol

The actuators were programmed to follow a displacement-controlled cyclic loading protocol shown in Table 6.4. The program was based on the roof drift, however since the stiffness of the three stories varied, the drift was not distributed evenly along the height of the building and the individual story drifts differ from those shown on the table. A Temposonic LVDT aligned with the center of the top slab at the north column flange was used as reference to control the displacement. The protocol was based on a brace buckling yield drift, Δ_y, of 29mm estimated from preliminary analyses and Part I tests. The specimen was subjected to two cycles at each target displacement; the intention of this protocol is to capture cyclic strength degradation. Each target displacement

was set as a multiple of the yield displacement. Nineteen full cycles were completed until a column fracture on the South column prevented further cyclic loading. After column fracture the frame was monotonically loaded towards the south to -4.0% roof drift (the direction closing the column crack).

Table 6.4 Chevron 7 Loading Protocol

Load type	Cycle	Avg. ductility Δ/Δ_y	Roof disp Δ (mm)	% Roof drift
	1,2	±0.25	± 7.3	±0.08
	3,4	±0.5	± 14.6	±0.15
	5,6	±.75	±21.9	±0.23
	7,8	±1.0	±29.2	±0.3
	9,10	±1.5	±43.7	±0.45
Cyclic	11,12	±2.0	±58.3	±0.6
	13,14	±3.0	±87.5	±0.9
	15,16	±4.5	±131	±1.35
	17,18	±6.0	±175	±1.8
	19	±7.5	±219	±2.25
	19.25		+91	+0.95
Monotonic	19.75		-390	-4.0

6.4 Instrumentation

Physical and optical sensors were installed at various locations on the specimens for data collection during the experiments. Instruments used and their purpose are outlined in Table 6.5. The full instrumentation plan for all the specimens is included in Appendix B.

Table 6.5 Overview of sensor descriptions and uses

Sensor	Photo	Locations	Derived quantity
Uniaxial strain gauge	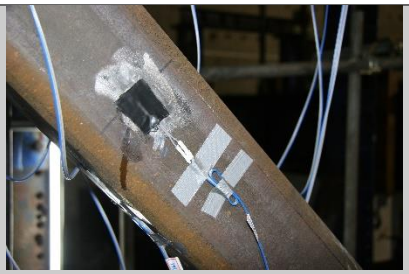	Braces …….	Axial force
		Beams …….	Axial & shear force, moment
		Columns …….	Axial & shear force, moment
		Slabs ……	Shear force
Triaxial strain gauge rosette	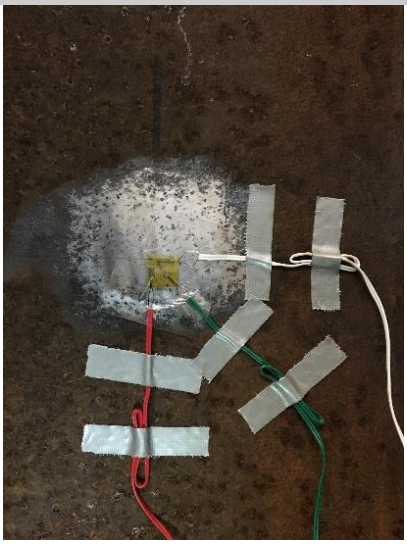	Columns ……	Shear force
		Beams ……	Shear force
Linear variable displacement transducer (TML)		Beams …….	Mid span deflection
		Gusset plates ……	OOP rotation
Linear variable displacement transducer (Temposonic)		3F slab end ……..	3F lateral displacement

String potentiometer		1F and 2F slabs ……... 1F Braces …….. 2F Braces ……. 3F Gusset plates ……..	Lateral displacement Elongation & shortening, OOP displacement Elongation & shortening, OOP rotation
Inclinometer (Jewell)		Beams ……. Columns ……. Slabs ……...	In-plane-rotation In-plane rotation OOP rotation
Dial gauge (Peacock)		*Base plates* …….. *Anchor plates* ……	Slip, uplift Slip, uplift
Internal load cell (MTS)	n/a	Actuator ……	Applied lateral force

NDI Optotrak LED markers		*1F Beam* ……..	3D displacement & rotation
		1F Braces ……..	OOP displacement, rotation
		1F Mid Gusset plates ..	OOP rotation
OptiTrack retroreflective markers and Prime 41 cameras		*2F beam* …….	3D displacement & rotation
		2F braces ……	OOP displacement, rotation
		2F Mid gusset plates .	OOP rotation

6.4.1 Optical Systems

Two independent optical systems were used to gather 3D data on this test. The NDI Optotrak system, used also for the single-story tests was used to gather information about the first story beam and brace deformations. The OptiTrack system was used to gather information about the second story beam and brace deformations. The layout of markers at the two stories was the same, with the omission of conflicting markers on the second story. A detailed plan of the marker layout is provided in Appendix B.

6.4.2 Frame

The internal load cells in the actuators were used to determine the base and story shear forces. Since the force was only applied at the roof, the base and story shears are equivalent. A Temposonic linear variable displacement transducer (LVDT) was positioned on a reference column on the north side of the frame, opposite the actuators, to measure the roof displacement. This measurement was used to control the actuator displacement and ensure the target frame roof drifts were reached since the actuator internal displacement could include slip and uplift of the actuators, or loading beam deformations. String potentiometers were mounted on reference columns at the north and south ends of the frame to monitor the frame displacement at each story. All the sensors were aligned with the corresponding floor's slab mid-depth.

6.4.3 Beams

LVDT's were mounted to measure the vertical deflection at the midpoint of each of the three beams as shown in Figure 6.17. However, several issues with the instruments at these three locations throughout the test rendered the data unreliable. One such issue was that the needle of the LVDT was bent due to out of plane movement of the beam and did not measure vertical displacements accurately. Thus, the reported beam deflection was determined from NDI Optotrak and OptiTrack optical sensor data for the first and second story beams respectively. The optical data was also used to calculate beam torsional rotation.

Inclinometers were installed along the length of the beam at connection regions with the intention to investigate the deflection and in plane rotation of the beam. The beams were also instrumented with triaxial and uniaxial strain gauges in an effort to determine axial force, shear, and moment distributions in the same manner as for the single-story frames described in Chapter 3.

(a) Second Story beam (b) Third story beam

Figure 6.17 Beam deflection LVDTs

6.4.4 Slabs

In an attempt to determine the concrete slab contribution to the beam strength, concrete surface strain gauges were installed on the slab. Five strain gauges were spaced across the width of the slab at four different locations along the length of the beam as shown in Figure 6.18. It is expected that the measured strains will provide some information about the effective width of the composite beam, the extent of composite action at each location, and the point at which composite action between the beam and slab was lost.

Inclinometers were also placed at each of the 4 edge faces of the first and second story slabs to measure out of plane rotation. On the west and south slab faces, the inclinometers were in line with the beam midspan. On the north and south faces, the inclinometers were positioned as illustrated in Figure 6.19.

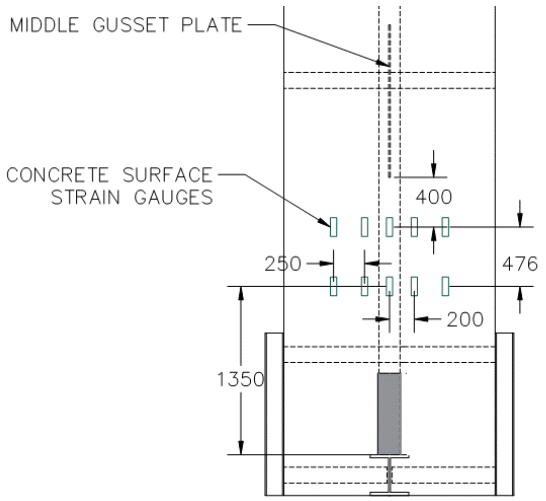

Figure 6.18 Typical concrete strain gauge layout plan on south side of the frame

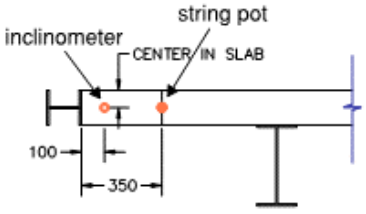

Figure 6.19 Typical inclinometer and string potentiometer locations on south and north slab elevation

6.4.5 Columns

Rosette strain gauges installed at the center of the column webs, away from areas of expected yielding, and were used to calculate the shear forces in the columns. These shear forces were verified using the calculated column moments obtained from strain gauges on the flanges of the columns at the top and bottom of the each story and the distance between the gauge groups. Figure 6.20 demonstrates the rationale for the derivation of column shear forces.

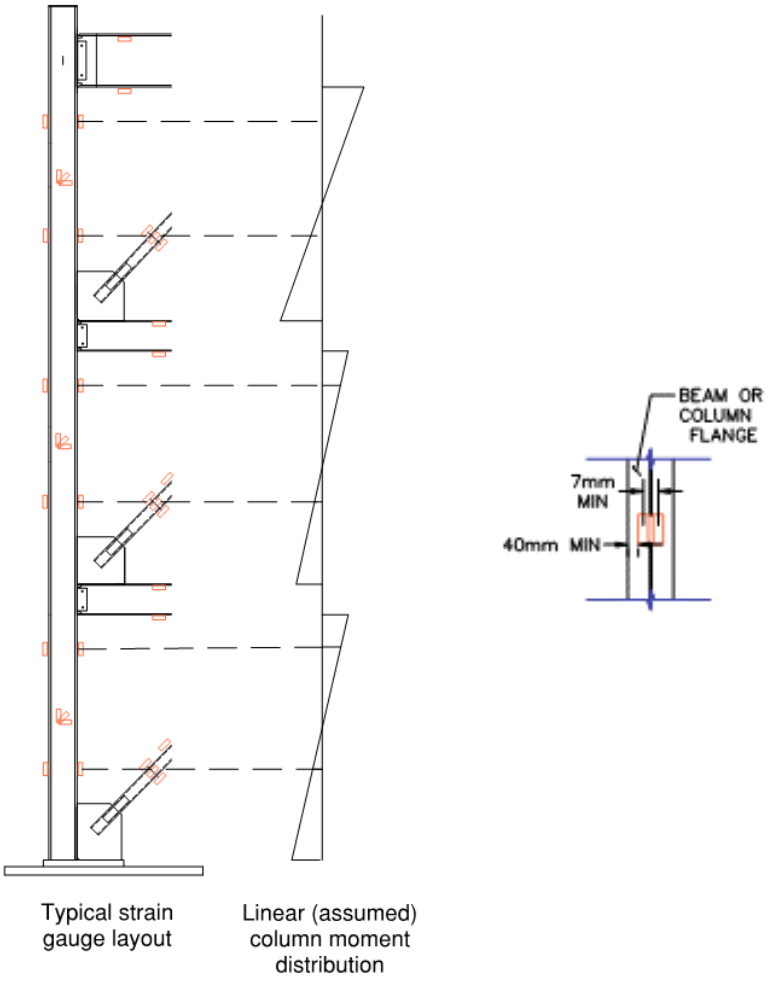

Figure 6.20 Column strain gauge schematic and derived shear and moment fields

6.4.6 Braces

Each brace was instrumented with 8 strain gauges at approximately ¼ and 1/3 from the end of the brace. The gauges were installed in sets of 4 at each of the two locations. One gauge was centered on each face of the square brace at each location. The cyclic behavior of the gauge readings from the test suggested the strain gauges were functional throughout the experiment, but they display a large bifurcation of stresses when the braces buckled. This complicated brace axial force calculation. The reported brace forces for Chevron 7 were derived by assuming a bilinear stress-strain relationship in steel and that was fitted to stress-strain curves from coupon tension tests. Several corrections to the data validated by statics and Phase I and II test results were also made and are justified in Section 6.6.3.

String pots attached to the column and beam webs parallel to the braces were used to measure the brace elongation and shortening. The reported elongation and shortening is the change in length from brace end to end. On the first and third stories, string pots were used to record brace out of plane deformation. At the second story optical markers along the brace gathered data on brace deformation.

6.4.7 Whitewash

Regions on the frame with expected inelastic behavior were painted with a thin layer of whitewash, a lime and water mixture. When hot-rolled steel yields, mill scale on the surface of the member cracks and flakes off when yield occurs. The whitewash layer flakes off with the mill, making initial and progression of yielding visually detectable. The whitewash mixture was tinted yellow to enhance the contrast of the paint on the bare steel sections and improve visual detection of yielding. The painted regions included the beam ends and center, gusset plates, and column base and connections.

6.5 Experimental Observations

This section provides performance state definitions, an overview of experimental findings and a detailed account of test observations. This frame was only loaded at the roof, thus the shear forces at each story are equivalent to the actuator load. The drift is the ratio of lateral displacement to the height of the relevant location. In the following sections roof drift, and story drifts will be

referenced, which were and were calculated as shown in Eq 6. 1 to Eq 6. 4. Figure 6.21 provides a lateral displacement schematic and story heights used.

$$\delta_{roof} = \frac{\Delta_r}{9722}\ x\ 100\% \quad \text{Eq 6. 1}$$

$$\delta_1 = \frac{\Delta_1}{3311}\ x\ 100\% \quad \text{Eq 6. 2}$$

$$\delta_2 = \frac{\Delta_2}{3059}\ x\ 100\% \quad \text{Eq 6. 3}$$

$$\delta_3 = \frac{\Delta_3}{3353}\ x\ 100\% \quad \text{Eq 6. 4}$$

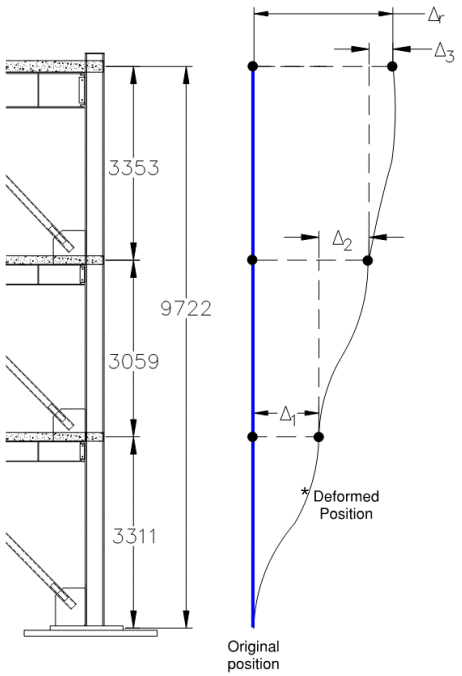

*The deformed position is for reference and not representative of the real deflected shape

Figure 6.21 Roof and story heights

6.5.1 Overview of response

On March 17, 2018 the multi-story SCBF Chevron 7 was tested at NCREE. The load and displacement histories are shown in Figure 6.22 and Figure 6.23. The frame's maximum lateral resistance was -2425kN. The frame sustained cyclic loading for nineteen full cycles before a fracture in the inner flange of the second story south column, at the beam-to-column moment connection CJP weld prevented further cyclic loading. The crack originated at the bottom flange weld of the second story beam-to-column connection, behind the backing bar that was left in place. The fracture occurred as the frame was pushed in the north direction (positive drift movement). Upon fracture, the frame sustained a 30% loss in resistance in the positive loading direction but it remained stable. The frame was deemed stable enough to load in the negative-drift direction. As the frame was pushed south, the gap at the flange fracture closed.

The relationships of frame base shear vs story drift is shown in Figure 6.24. The red line at $2P_c\cos\theta$ denotes the design (using nominal strengths) lateral resistance. Before column fracture, the drift range for the first and second stories were 6.4% and 6.2% respectively. The maximum drift range when accounting for the monotonic loading was 9.2% and 8.5% at the first and second stories. However, cyclic loading was stopped due to column fracture and not brace fracture. All four lower story braces had buckled, but none of those braces had the local cupping that precedes brace fracture, so they could have resisted further cyclic inelastic deformation.

Before column flange fracture, the maximum beam vertical deflection was 106 mm and 93mm at the first and second story beams, respectively. The sequence of brace buckling and fracture is shown in Table 6.6 along with the drift at which it occurred. The first-story south brace buckled first at -0.42% story drift and then the north brace buckled at the first story at +0.51% story drift. The second story braces followed buckling, first the south brace and then the north brace. Brace buckling was evident a sudden out of plane deflection in the braces.

The inelastic deformation was approximately evenly distributed among the first and second stories and the third story remained essentially elastic. The drift distribution and peak lateral resistance can be examined in detail in Table 6.7. The gusset plate connections experienced moderate weld

damage at story drifts exceeding 2.5%. As expected, the beams developed plastic hinges at the ends of the gusset plates as observed by the severe local buckling of the beam web and flange at these locations. Cracks in the slab were concentrated at each end of the slab and near the blockout. This is reasonable since the edge beams transferring the force to the slab ended just past the blockout, where the beam studs began.

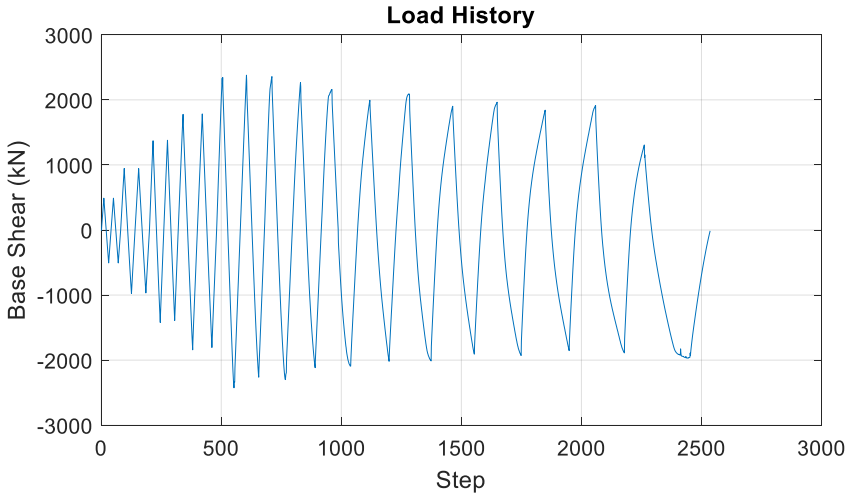

Figure 6.22 Chevron 7 load history

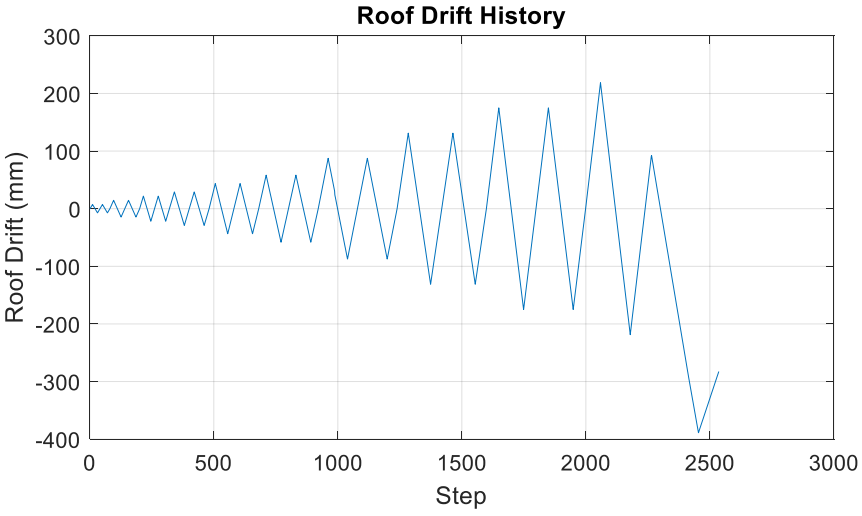

Figure 6.23 Chevron 7 roof drift history

Table 6.6 Significant events during test

Location	Event	Roof Drift (%)	Story drift (%)	$P_{cr,exp}$
1F north brace	buckling	0.42	0.50	-1768
1F south brace	buckling	-0.43	-0.42	-1610
2F north brace	buckling	0.56	0.52	-1749
2F south brace	buckling	-0.58	-0.62	-1575
2F top south column	fracture	0.95	1.23	n/a

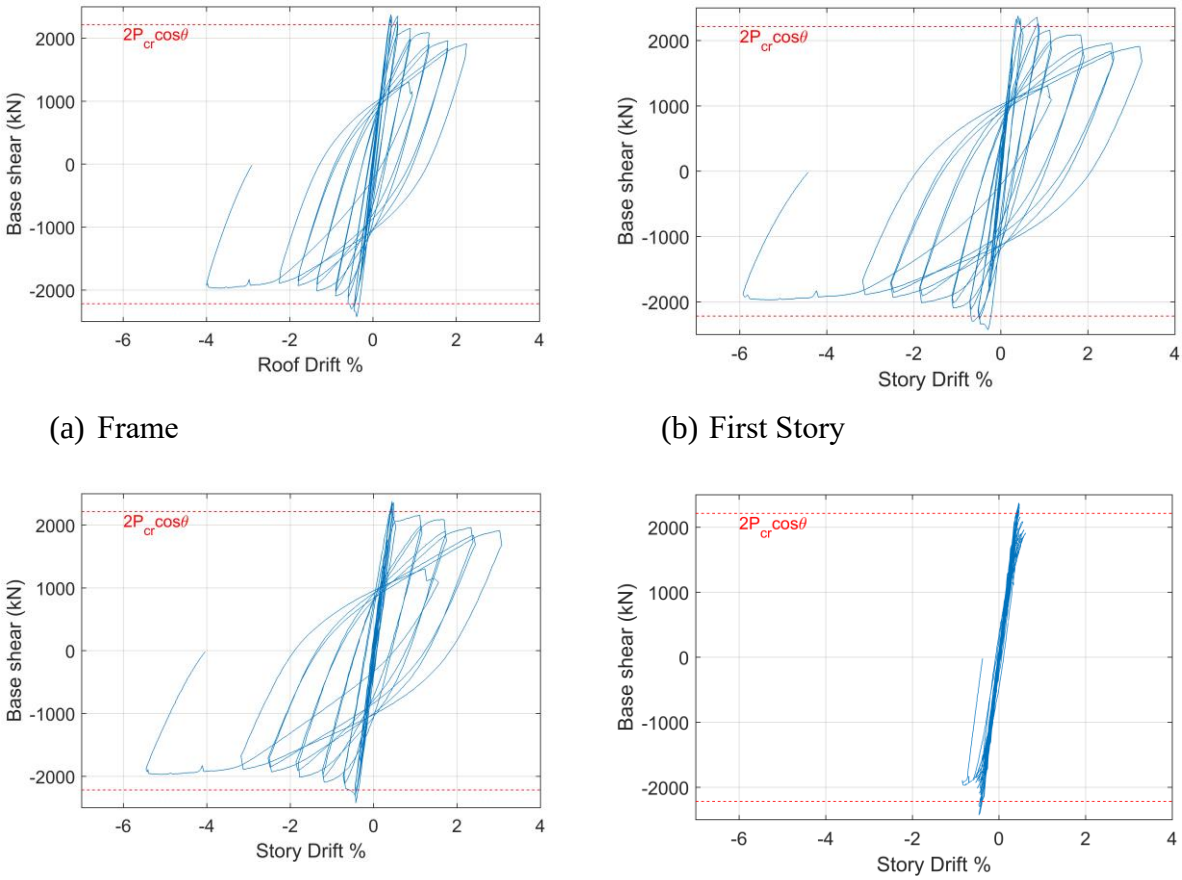

(a) Frame (b) First Story

(c) Second Story (d) Third Story

Figure 6.24 Chevron 7 base shear- drift hysteresis

Table 6.7 Peak lateral resistances and drifts

Cycle	Resistance (kN)		Roof Drift (%)		1F drift (%)		2F drift (%)		3F drift (%)	
	Max.	Min.	Max.	Min.	Max.	Min.	Max.	Min.	Max.	Min.
1	489	-506	0.07	-0.07	0.06	-0.07	0.08	-0.07	0.09	-0.08
2	489	-507	0.07	-0.07	0.06	-0.07	0.08	-0.07	0.09	-0.08
3	946	-975	0.15	-0.15	0.12	-0.13	0.16	-0.15	0.17	-0.16
4	944	-967	0.15	-0.15	0.12	-0.13	0.16	-0.16	0.17	-0.16
5	1371	-1421	0.22	-0.22	0.18	-0.19	0.24	-0.23	0.25	-0.25
6	1379	-1391	0.22	-0.22	0.19	-0.19	0.23	-0.22	0.25	-0.25
7	1777	-1842	0.30	-0.30	0.25	-0.26	0.32	-0.31	0.33	-0.33
8	1784	-1805	0.30	-0.30	0.26	-0.26	0.32	-0.30	0.33	-0.33
9	2345	-2425	0.45	-0.39	0.45	-0.29	0.45	-0.43	0.45	-0.46
10	2379	-2262	0.43	-0.45	0.39	-0.49	0.44	-0.42	0.45	-0.42
11	2358	-2299	0.60	-0.52	0.83	-0.65	0.48	-0.45	0.47	-0.45
12	2266	-2116	0.58	-0.60	0.86	-0.68	0.41	-0.70	0.46	-0.42
13	2160	-2092	0.90	-0.90	1.13	-1.09	1.11	-1.18	0.48	-0.45
14	1993	-2018	0.90	-0.90	1.14	-1.09	1.14	-1.20	0.45	-0.43
15	2091	-2012	1.29	-1.35	1.73	-1.82	1.62	-1.77	0.55	-0.50
16	1902	-1908	1.35	-1.35	1.87	-1.80	1.71	-1.82	0.50	-0.47
17	1964	-1929	1.80	-1.80	2.54	-2.48	2.34	-2.45	0.58	-0.54
18	1842	-1854	1.80	-1.80	2.53	-2.46	2.39	-2.48	0.54	-0.52
19	1913	-1888	2.25	-2.25	3.19	-3.12	3.02	-3.13	0.61	-0.59
20	1307	-1968	0.86	-3.67	1.08	-5.30	1.23	-5.08	0.31	-0.79

6.5.2 Performance State Overview

Various performance states pertaining to yielding, buckling, and connection damage established by Terpstra (2017). These performance states were used in Chapter 4 to describe the damage of the single-story frames and will be used again in this chapter to describe the damage of the 3-story frame in Table 6.9 as observed throughout loading of the specimen.

6.5.3 Frame Location Designations

Throughout the rest of this chapter, references will be made to locations on the Chevron 7 specimen. For convenience each location of significance on the frame has been assigned an acronym for reference. The location designations are illustrated in Figure 6.25 and described in Table 6.8.

Table 6.8 Chevron 7 location designation meanings

Letter or Number	Meaning
1	First Story
2	Second Story
3	Third Story
N	North
S	South
C	Corner
M	Middle
F	Far
L	Lower
U	Upper
B	Beam
Br	Brace
Co	Column
G	Gusset
Cn	Connection
(SL)	Slab

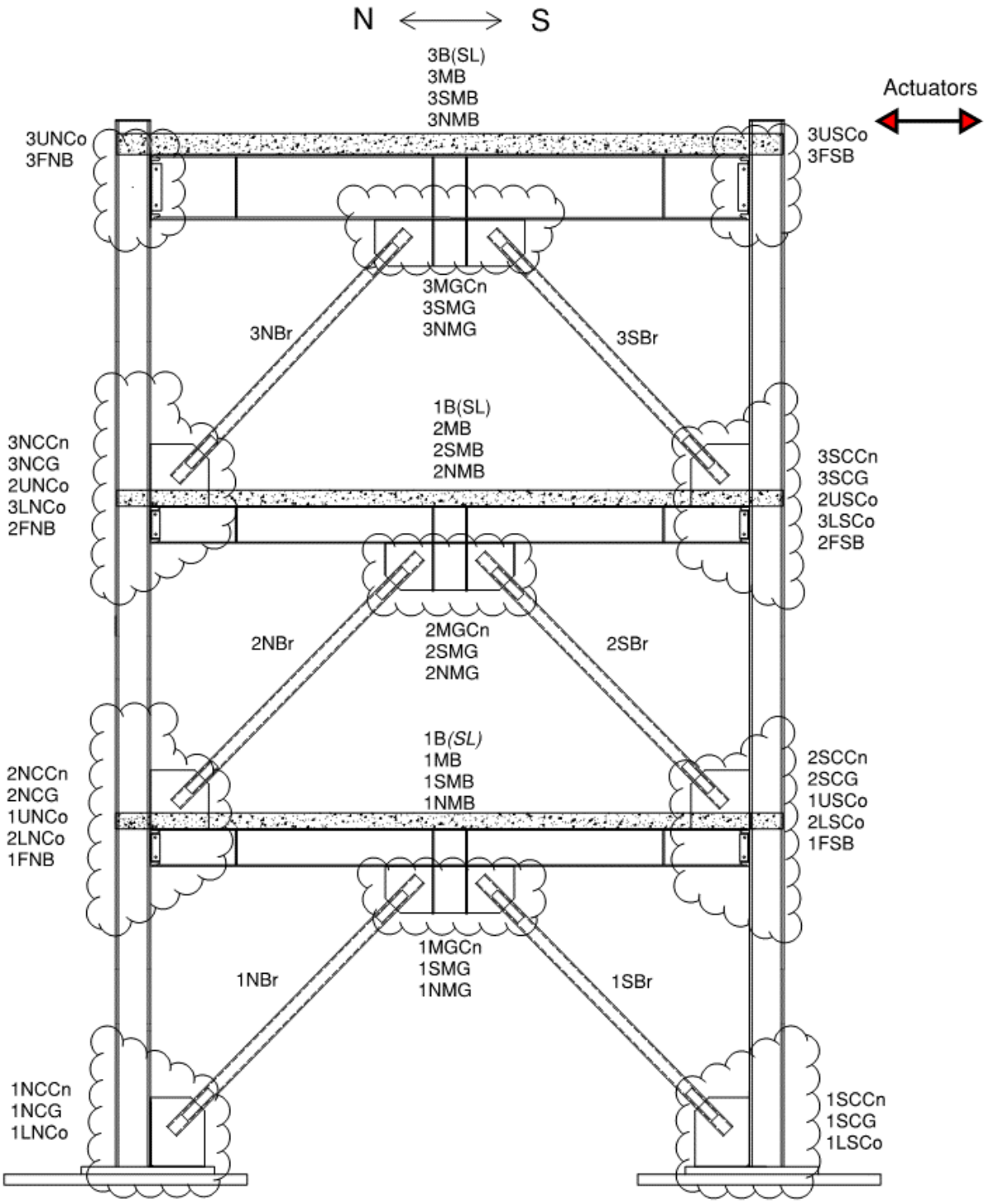

Figure 6.25 Chevron 7 location designations on west elevation

6.5.4 Detailed Cyclic Response

The following sections describe the progression of yielding and buckling of the SCBF components. Detailed review of the cyclic response is divided in three sections based on the extent of damage. In the initial state, global-frame response is largely elastic. The next part describes moderate damage of the frame after the braces have buckled. The frame then enters severe damage state when components have begun to sustain severe yielding and buckling and an ultimate fracture leads to instability. Discussion and test pictures focus on the first and second stories since inelastic action only occurred in these stories, as designed. For reference, images showing the initial condition of the frame are presented in Figure 6.26.

6.5.4.1 Initial Conditions (Roof Drift ≤ 0.45%) (individual story drift uniform)

Drift (%)				Observed Damage
Roof	**1F**	**2F**	**3F**	
0.15	0.12	0.16	0.17	• Yield lines near the toe of brace-to-gusset weld on east and west faces of the gusset plate at 1NCG, 1SCG, 2NCG, 2SCG as shown in Figure 6.27 (a), and (b). This is likely from welding heat effects on the plate
0.22	0.19	0.24	0.25	• Yield lines at the toe of the brace-to-gusset weld on east and west faces of the gusset plate at 1NMG 1SNMG 2NMG 2SMG, 2NMG, 3NMG, 3SNMG
0.30	0.26	0.32	0.33	• Yielding at the corner of the gusset plate at 1SCG and 1NCG, 2SCG and 2NCG • Initial beam yielding at 1SMB, 1NMB, 2SMB, and 2NMB on the flange at the edge of the mid gusset plate weld as shown in Figure 6.27 (d).
0.43	0.49	0.45	0.45	• 1st story braces buckle, first south (first cycle) then north (second cycle). There was a large and sudden deformation upon initial buckling evident in Figure 6.27 (e) and (f). • Yielding of beam web at 1MB and 1FSB and of flanges at 1SMB 1NMB, shown in Figure 6.27 (c). • Initial yielding of beam flanges at 2SMB 2NMB and beam web at 2MB and 2FSB and 2FNB • yielding on outer and inner flange above the gusset plates at 1LSCo and 1LNCo

(a)1LNCo

(b) 1SCG

(c)1MB

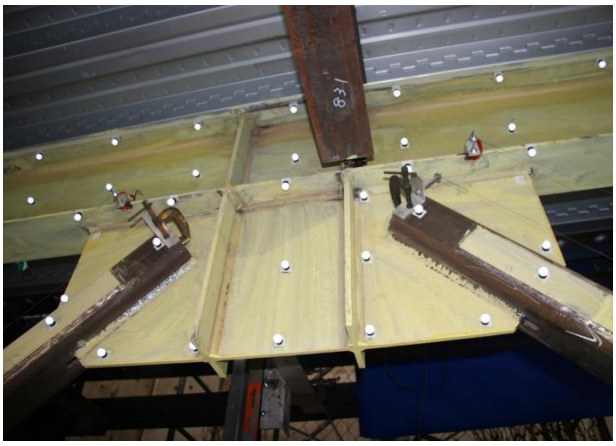

(d)2MB

(e)2NCG

(f)2SCG

(g)3MB

(h)3SCG

(i) 3NCG

Figure 6.26 Initial Conditions

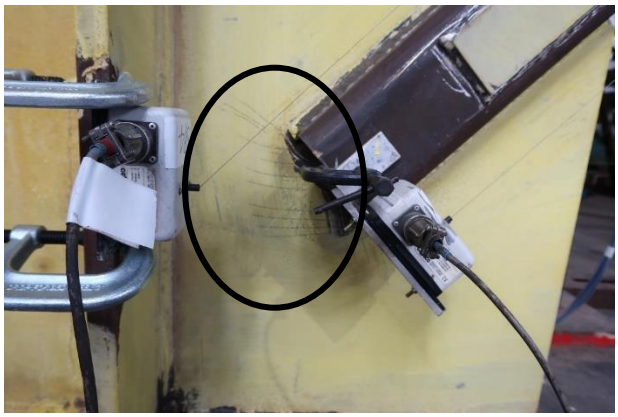

(a) 1SCG

(b) 1NCG

(c) 1MB

(d) 2MB

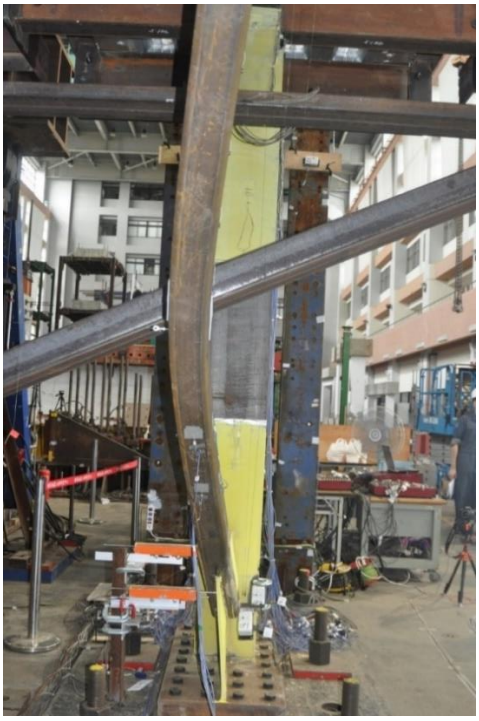

(e) 1NBr buckled at 0.45% roof drift

(f) 1SBr buckled at -0.45% roof drift

Figure 6.27 Story damage at low roof drifts
(Circled regions indicated observation of yield lines)

6.5.4.2 Moderate Damage State

Moderate damaged is defined to occur between 0.6% and 1.35% roof drift, which approximately corresponds to 0.7% and 1.8% first and second story drift. Images of the deformed brace shape at each cycle are shown in Figure 6.32 through Figure 6.34

Drift (%)				Observed Damage
Roof	**1F**	**2F**	**3F**	
0.60	0.86	0.70	0.46	• 2LNCo yielding on outer and inner flange above the gusset plates • 2LSCo yielding of bottom flange at 1FSB and 1FNB • 2NBr and 2SBr buckle, first at the south then the north. The deformation is evident in Figure 6.34 (a)
0.90	1.14	1.15	0.45	• Yielding at the bottom flange of 2FSB and 2FNB and top flange at 2MB and 2FNB and 2FSB. The damage at the first story was consistent with the second story at these locations as shown in Figure 6.28 and Figure 6.29 (c) (d) and (e) • Initial yielding at 1UNCo • Local buckling in 2SMB flange • Moderate yielding at gusset plates and beams, shown in Figure 6.29 (a) (b) (e)
1.35	1.80	1.71	0.50	• Visible separation of deck and top beam flange at 1B(SL) • Initial buckling of flange at 2NMB • Moderate local buckling of top and bottom flanges on 1FNB and 1FSB. Buckling at beam ends begins just past the edge of the second story corner gusset plate shown in Figure 6.30 (c) • Continued yielding of 1LNCo and 1LSCo at the web, shown in Figure 6.30 (a) • 2LSCo initial yielding near corner gusset • 2USCo and 2UNCo flange yielding at beam-column connection, shown in Figure 6.30 (b) • Moderate yielding at beams and gussets on first and second stories as seen in Figure 6.30 (b) and (d) and Figure 6.31 (a)(c)(d)

(a) 1NMB

(b) 1FNB

(c) 1SCG

(d) 1LNCo

Figure 6.28 1st story damage at 0.9% roof drift

(a) 2NCG

(b) 2SCG

(c) 2FNB

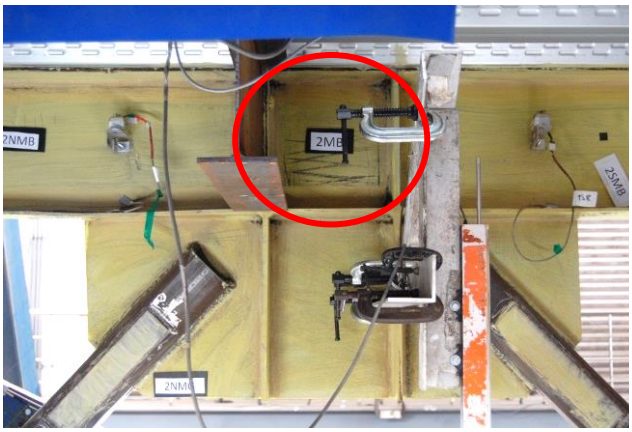

(d) 2MB

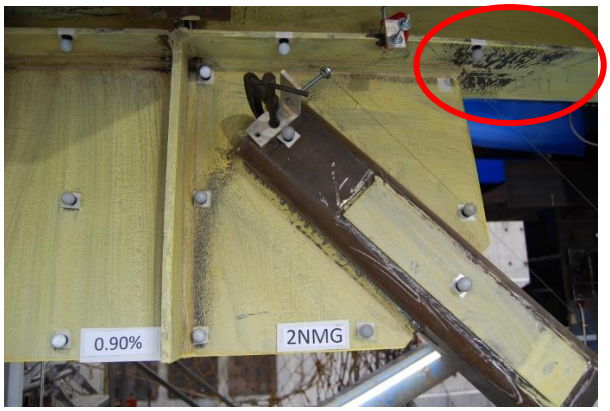

(e) 2NMG

(f) 1B(SL) south

Figure 6.29 2nd Story damage at 0.9% drift

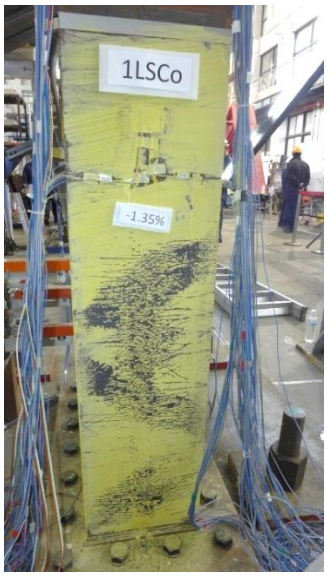

(a) 1LSCo

(b) 1SCG

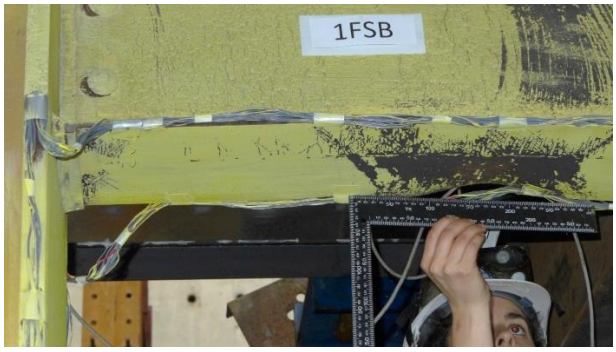

(c) 1FSB

(d) 1MB

Figure 6.30 1st story damage at 1.35% roof drift

(a) 2NCG

(b) 2UNCo

(c)2FSB

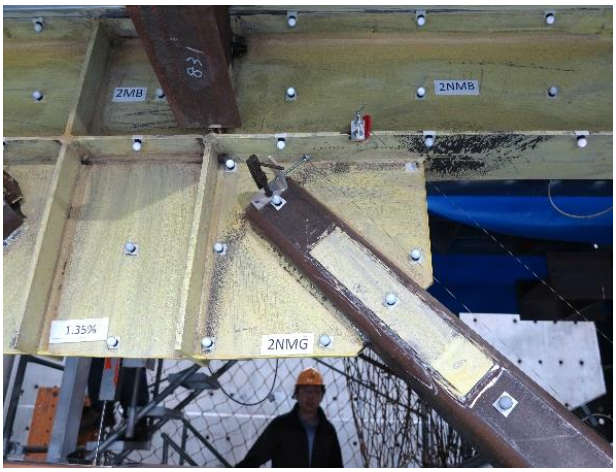

(d) 2MB

Figure 6.31 2nd story damage at 1.35% roof drift

(a) 0.6% roof drift

(b) 0.9% roof drift

(c) -1.35 % roof drift

Figure 6.32 First story buckled braces at moderate roof drifts

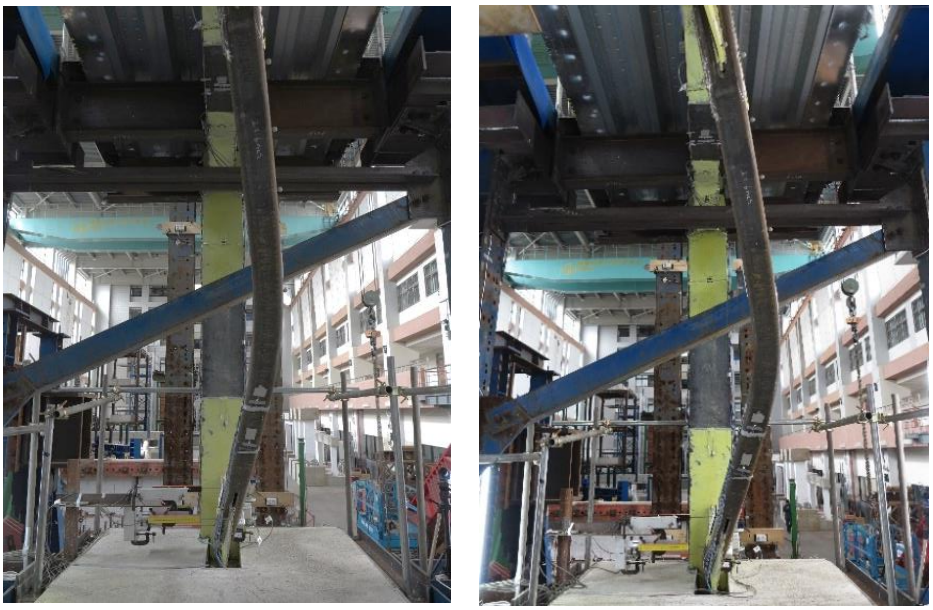

(a) 0.9% roof drift (b) 1.35 % roof drift

Figure 6.33 2NBr buckled braces at moderate roof drifts

(a) -0.6% roof drift (b) -0.9% roof drift (c) -1.35% roof drift

Figure 6.34 2SBr buckled braces at moderate roof drifts

6.5.4.3 Severe Damage State (Roof Drift ≥ 1.8%)

Severe damaged is defined to occur above 1.8% roof drift, which approximately corresponds to 2.5% first and second story drift. Images of the deformed brace shape at each cycle are shown in Figure 6.39 and Figure 6.40.

Drift (%)				**Observed Damage**
Roof	**1F**	**2F**	**3F**	
1.80	2.50	2.40	0.54	• Initial local buckling at 1LNCo flanges and severe yielding shown in Figure 6.35 (a) • Severe local buckling at flanges of 1FNB and 1FSB (24mm) shown in Figure 6.35 (b) • 2MB separation with slab • 1FSB and 1FNB web local buckling and severe flange local buckling and severe yielding evident in Figure 6.35 (c) and (d) • 1FMB max beam to slab separation at the end of the middle transverse beam was 90mm • Initial yielding at 2UNCo web at the moment connection seen in Figure 6.36 (b)
2.25	3.15	3.02	0.61	• Minimal cupping @ 1NBr and 1SBr • 13mm separation between 1MB and slab • Buckling of bottom flange at 2SMB is 38mm • Severe yielding at beam middle and ends, and at the first story columns • There was little yielding 2LNCo and 2LSCo • Severe yielding at 2USCo and 2UNCo inner flanges shown in Figure 6.37 (a) and (b) • Moderate yielding at 2USCo and 2UNCo web at the moment connection seen in Figure 6.37 (c) • When moving toward the second peak of +2.25% roof drift the 2USCo flange fractured behind the bottom beam flange backing bar at the moment connection shown in Figure 6.41. The crack propagated halfway through the web of the column as seen in image (d)
-4.0	-5.9	-5.4	-0.84	• Little cupping at 2SBr shown in Figure 6.38

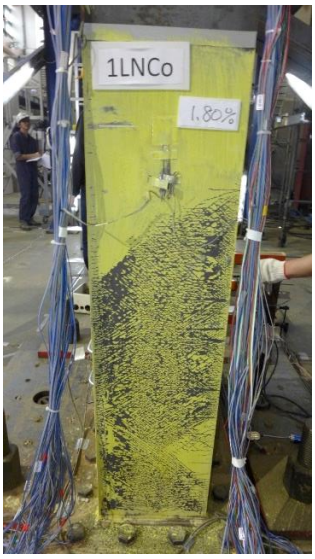

(a) 1LNCo

(b) 2SMB

(c) 1FNB

(d) 1FSB

Figure 6.35 1st Story damage at 1.8% roof drift

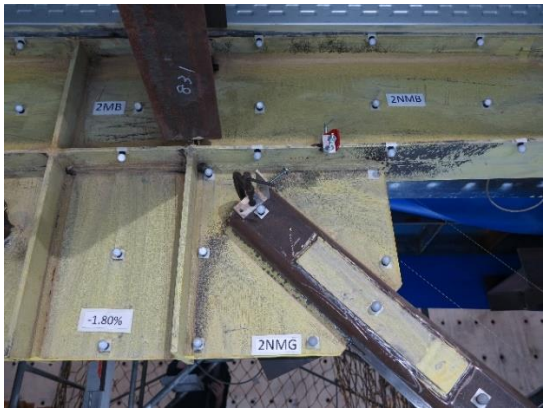

(a) 2NMG

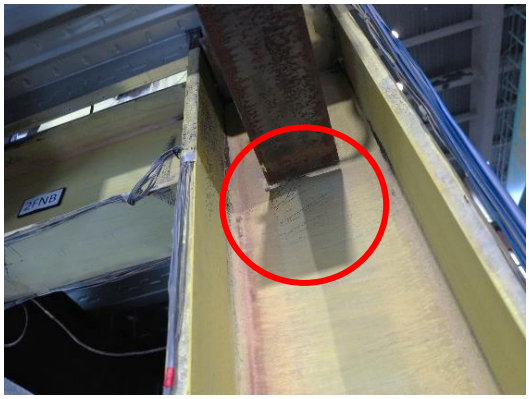

(b) 2UNCo

(c) 2NCG

(d) 2SCG

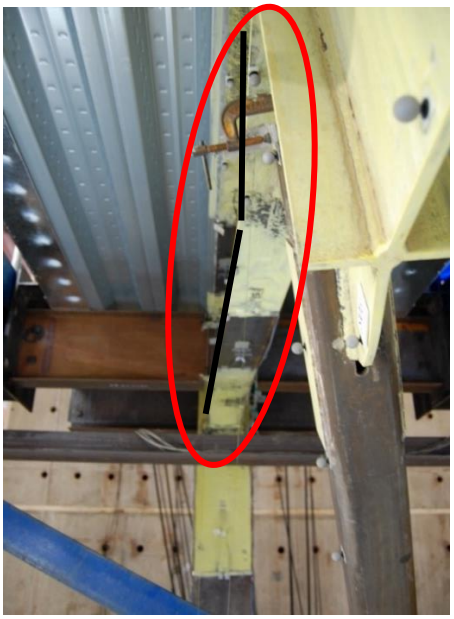

(g) 2B bending out of plane

Figure 6.36 2nd story damage at 1.8% roof drift

(a) 2USCo

(b) 2UNCo

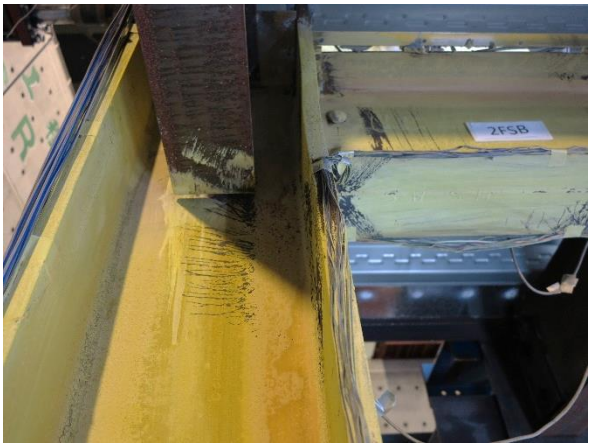

(c) 2USCo

Figure 6.37 2nd Story damage at 2.25% roof drift before column fracture

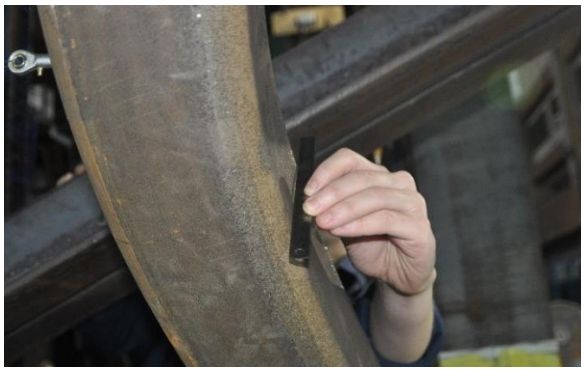

(a) 1NBr at +2.25% roof drift with minimal cupping

(b) 2SBr at -3% roof drift

Figure 6.38 Brace local buckling

(a) 1NBr 1.8% roof drift

(b) 1SBr -2.25% roof drift

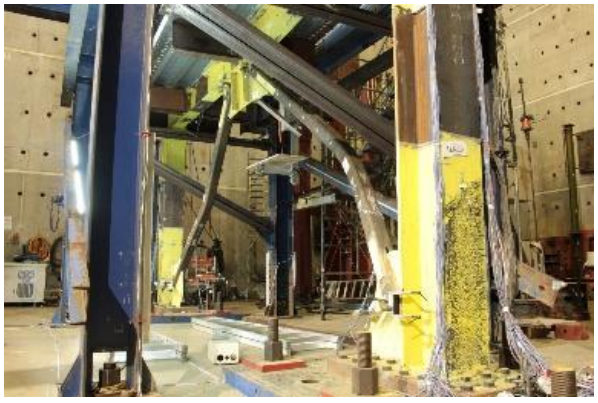

(c) 1.8% roof drift

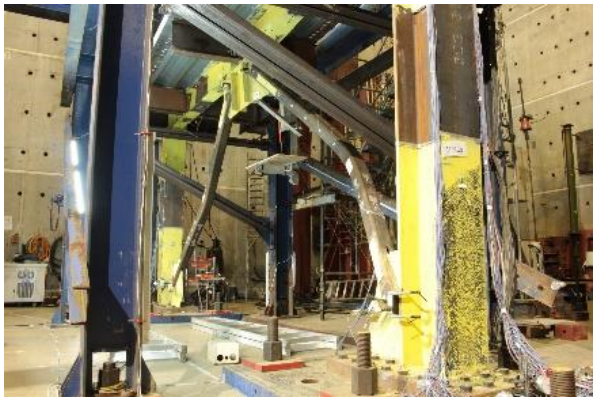

(d) 2.25% roof drift

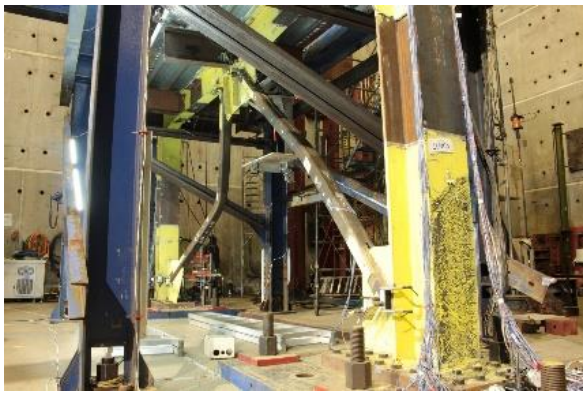

(e) - 1.8% roof drift

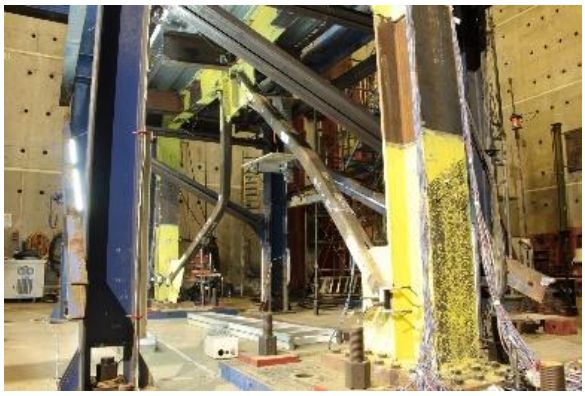

(f) -2.25 % roof drift

Figure 6.39 1st story buckled braces at high roof drifts

(a) 2SBr -1.8% roof drift

(b) 2SBr -2.25% roof drift

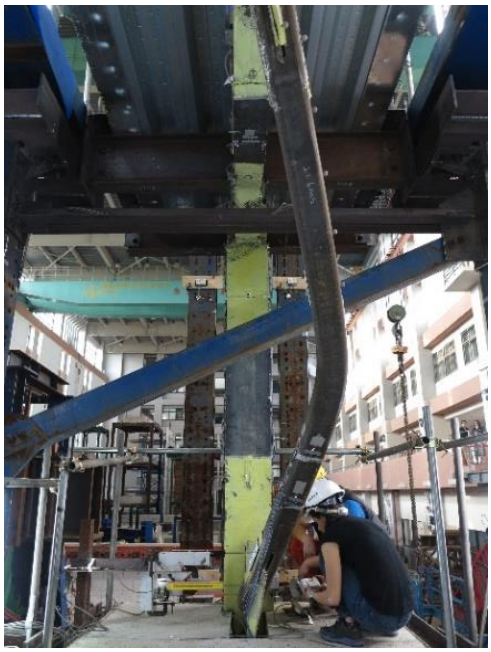

(c) 2NBr 1.8% roof drift

(d) 2NBr 2.25% roof drift

Figure 6.40 2nd Story buckled braces at high roof drifts

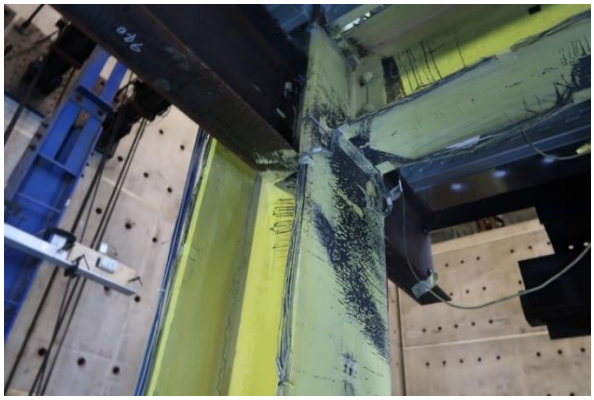

(a) 2USCo

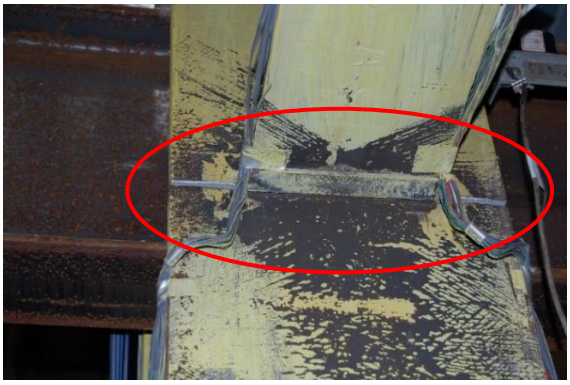

(b) fracture across the column flange

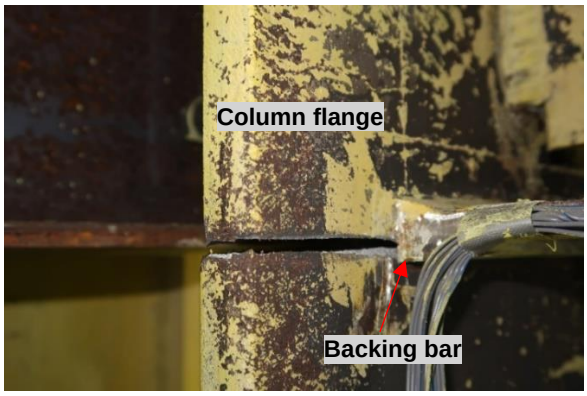

(c) fracture at backing bar

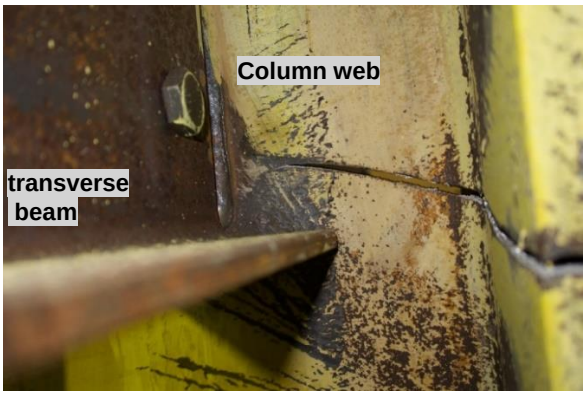

(d) fracture on column web

Figure 6.41 Fracture at 2USCo

6.5.4.4 Final observations and comments

1st Story

- Severe yielding of lower column and beam flanges and web, and severe local buckling of flanges and webs at plastic hinge location as seen in Figure 6.42 (a) (b) (e) and (f)
- Both braces bucked in the same direction towards the west
- Only initial yielding incurred at col 1USCo and the column web at the moment connection
- Yielding on the beam was concentrated around the edges of the gusset plates
- Shear stud separation from the concrete occurred between the two outer transverse beams as seen in Figure 6.42 (c) and (d) where 10 studs pulled out. When the studs elongated, the slab cracked longitudinally.
- The slab and beam rotated significantly, in the final condition the east side was lower than the west as shown in Figure 6.42 (g)
- The plastic hinge formed on the at 1NMB, which is distinguishable in Figure 6.42 (c) and (d)

2nd Story

- Severe yielding of upper columns, beam, and corner gusset plates and severe buckling at beam plastic hinge locations evident form the images in Figure 6.43
- Moderate yielding of middle gusset plates clearly seen in Figure 6.43 (h) (i) (j) and (k)

- Severe beam top flange buckling at the edge of the mid gusset plate at 2NMB west side, denoting the beam midpoint plastic hinge distinguishable from the comparison of Figure 6.43 (d) (e) and (g)
- The braces buckled in opposite direction. 2NBr buckled toward the east and the 2SBr buckled toward the west
- 2SBr local buckling (minimal cupping)
- 2MB deck to beam final separation of 25mm
- Less separation of the beam and slab than on the first floor beams seen in Figure 6.43 (d) and (e). Only 8 studs pulled out of the concrete slab.
- The slab and beam rotated significantly, in the final condition the east side was lower than the west as seen from Figure 6.43 (l)

3rd Story

- Behavior remained largely elastic Figure 6.44 (a)
- There was no discernible yielding on the beams and very little at the columns shown in Figure 6.44 (d)
- Minimal yielding (horizontal yield lines) in the gusset plate concentrated at the toe of the brace to gusset plate welds Figure 6.44 (b) and (c)

Global Comparison

- More yielding was observed on 1LSCo than 1LNCo
- More yielding was observed at 2UNCo than at 2USCo outer flange
- More yielding was observed on 2USCo than 2UNCo column web at the beam-to-column moment connection and inner flange
- There was little to no yielding of 2LNCo and 2LSCo
- More yielding was observed at 3LNCo than 3LSCo outer flange
- Beam flange buckling and yielding at the beam-end plastic hinges was more severe at the first story than the second story

- Top and bottom beam flange buckling at the end of the beam, in both the first and second stories, which indicates the beam experiences both positive and negative moment at the ends in cyclic loading, characteristic of a sway mechanism (Figure 6.42 (e)(f)).
- More yielding was observed on the corner gusset plates than the middle gusset plates. Likely because the rigidity was different. The corner gussets welded to the column and beam were more rigid than the mid-beam gusset plate since the beam rotated along with the gusset plates. The middle gusset plate did not rotate independently as much as the corner gussets. This is corroborated by gusset plate rotation data in the results section.
- It was observed that there was generally less yielding at the outer flange of the south column than the north column. This is reasonable because the south column fractured, and the frame was pushed much farther monotonically in negative drift.

(a) 1LNCo

(b) 1LSCo

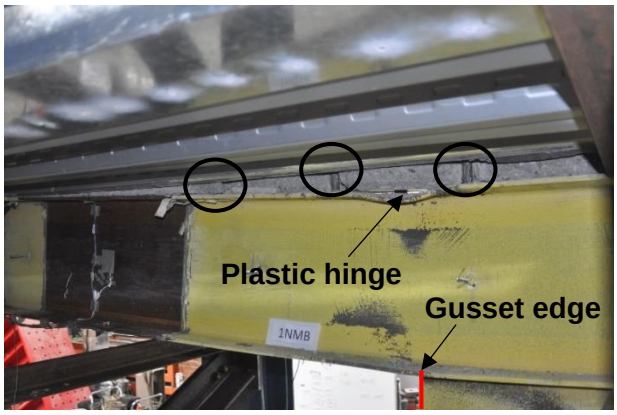

(c) 1NMB

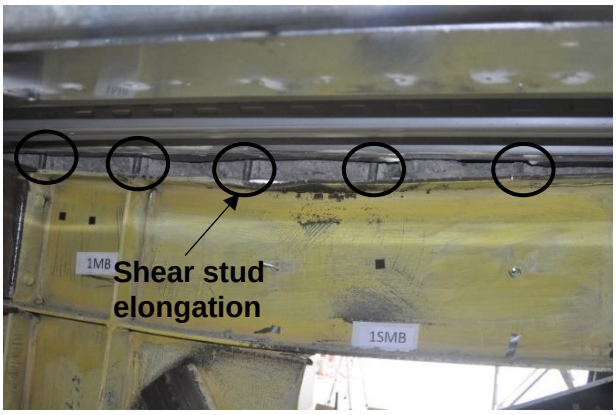

(d) 1SMB

(e) 1FNB

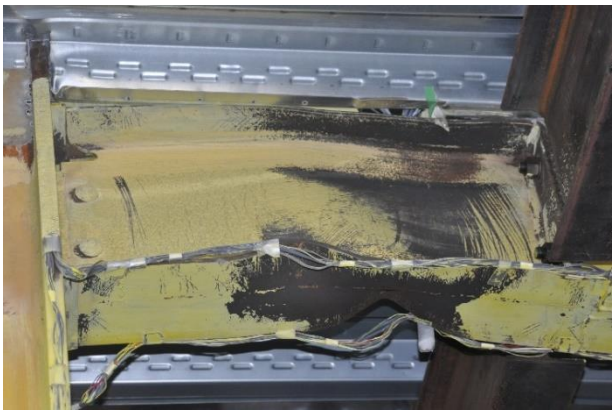

(f) 1FSB

(g) 1st story north elevation

(h) 1MB

Figure 6.42 Final condition of 1st story

(a) 2USCo

(b) 2UNCo

(c) 2LNCo

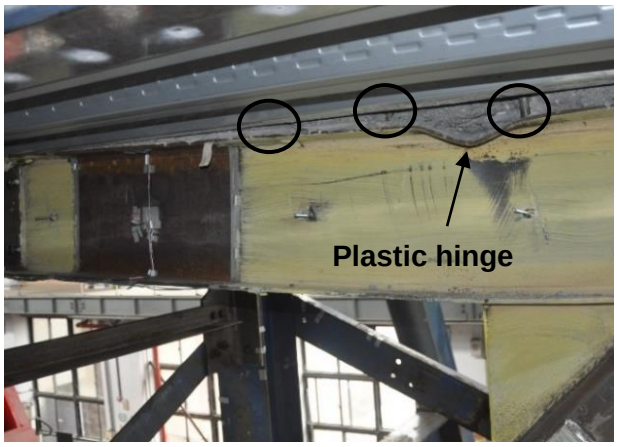

(d) 2NMB (west elevation)

(e) 2SMB

(f) 2FNB

(g) 2NMB (east elevation)

(h) 2SMG

(i) 2NMG

(j) 2NCG

(k) 2SCG

(l) Second story north elevation

Figure 6.43 Final condition of 2nd story

(a) 3NCo

(b) 3MB

(c) 3SCG

(d) 3LNCo

Figure 6.44 Final condition of 3rd story

6.5.5 Performance State Progression Table

Table 6.9 Chevron 7 Performance State Progression

		Low Drift					Moderate Drift			High Drift		
	Full Cycle #	1-2	3-4	5-6	7-8	9-10	11-12	13-14	15-16	17-18	19	20
% Drift (+/-)	**Roof Drift**	0.07	0.15	0.22	0.30	0.43	0.60	0.90	1.35	1.80	2.25	-4
	1F	0.06	0.12	0.19	0.26	0.49	0.86	1.14	1.80	2.50	3.15	-6
	2F	0.08	0.16	0.24	0.32	0.45	-0.70	1.15	1.71	2.40	3.02	-6
	3F	0.09	0.17	0.25	0.33	0.45	0.46	0.45	0.50	0.54	0.61	-1
Braces	**1S**					B1		B2				B3
	1N					B1		B2				
	2S						B1	B2				
	2N						B1	B2				
	3S											
	3N											
Corner Gusset	**1S**				Y1			Y2			Y3	
	1N				Y1			Y2			Y3	
	2S				Y1			Y2			Y3	
	2N				Y1			Y2			Y3	
	3S											
	3N											
Mid-Span Gusset	**1S**				Y1			Y2				
	1N				Y1			Y2				
	2S					Y1		Y2				
	2N					Y1		Y2				
	3S											Y1
	3N											Y1

(Table continues on next page)

		Low Drift					Moderate Drift			High Drift		
	Full Cycle #	1-2	3-4	5-6	7-8	9-10	11-12	13-14	15-16	17-18	19	20
% Drift (+/-)	**Roof Drift**	0.07	0.15	0.22	0.30	0.43	0.60	0.90	1.35	1.80	2.25	-4
	1F	0.06	0.12	0.19	0.26	0.49	0.86	1.14	1.80	2.50	3.15	
	2F	0.08	0.16	0.24	0.32	0.45	-0.70	1.15	1.71	2.40	3.02	
	3F	0.09	0.17	0.25	0.33	0.45	0.46	0.45	0.50	0.54	0.61	

Beam	**1 End**					Y1	LB1	Y2	LB2/Y3	LB3		LB3
	1 Midspan				Y1			Y2/LB1		Y3		
	2 End					Y1	LB1	Y2	LB2/Y3	LB3		
	2 Midspan				Y1			Y2/LB1		Y3		LB3
	3 End										Y1	
	3 Midspan										Y1	

Column	**1S-L**					Y1			Y2	Y3		
	1S-U							Y1				
	1N-L					Y1			Y2	Y3/LB1		
	1N-U								Y1			
	2S-L								Y1			
	2S-U								Y1	Y2	Y3/CF*	
	2N-L									Y1		
	2N-U								Y1	Y2	Y3	
	3S											Y1
	3N											

*CF denotes column flange fracture

6.6 Experimental Analysis

This section includes limited analysis of the data collected from the multi-story specimen. The collected data were analyzed to determine local and global movements, component forces, and force distributions The frame stories are compared with careful consideration of brace, beam, column, and connection cyclic behavior. Analysis focuses on the first and second stories because this is where the inelastic action occurred as designed.

Some of the results in this section are presented as backbone curves, or hysteretic envelopes, for more efficient comparison of the data at load cycle peak forces. Only peaks of complete cycles are reflected in these curves, and the hysteretic loop shape and size is lost. Additionally, since drift distribution was not consistent among the three stories, the behavior at story drift of the three stories is not directly comparable. Drift distribution throughout the test can be referenced in Table 6.7 of Section 6.5.1. Data processing and verification processes are included in Appendix C.

6.6.1 System Response

The normalize force-drift response envelopes for Chevrons 1 through 4 and 7 in Figure 6.45 show the frame lateral resistance of Chevron 7 peaked at incipient brace above the expected lateral strength. From the previously presented force-drift plots at each story (Figure 6.24) its noted first two stories achieved large drift ranges of approximately 6% in cyclic loading and the frame reached a roof drift range of 6% after loading monotonically. This deformation capacity is larger than that expected from conventional Chevron braced frames and premature fracture of the southern column resulted in an asymmetric, post-fracture drift history. Chevron 7 performed in a similar strength range as Chevron 4, which had the smallest beam of the single-story tests. Although initial strength is larger in Chevron 7 than the other frames, shortly after the first and second story braces buckled, (after 0.7% story drift) the strength quickly degrades below all the single story specimens.

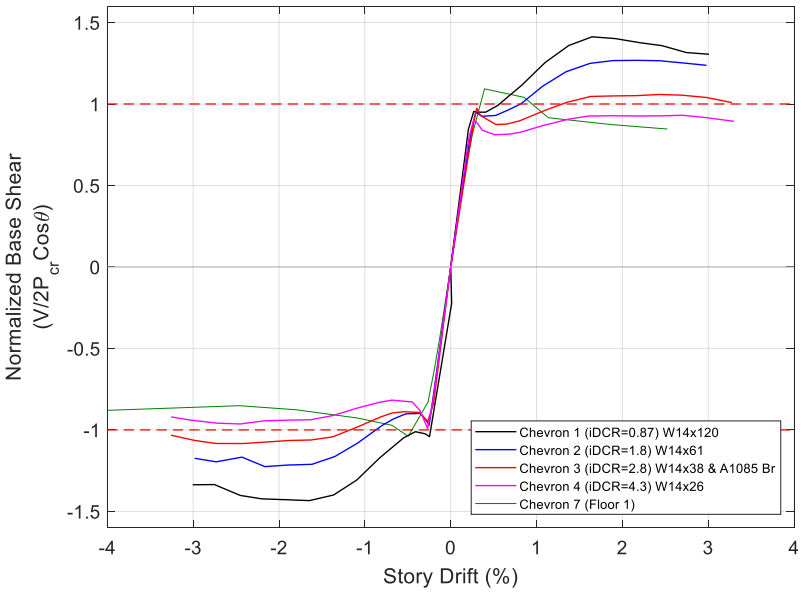

Figure 6.45 Normalized frame response envelope for Chevrons 1-4 and 7

6.6.2 Beam Response

6.6.2.1 Vertical displacement

The beam deflection data comes from Optotrak and OptiTrak data collection for the first and second story beams respectively. The sensor used for both measurements was number N30 as shown in Figure 6.49, located at the bottom flange of the midpoint of the beam. The displacement backbone curves in Figure 6.48 show that the beams did not experience deflection until the braces buckled and had similar deflection at each cycle peak. After cyclic loading, the first floor beam deflection was 10% larger than at the second story at 106mm. The monotonic loading increased the deflection significantly to 182mm, 18% larger than at the second floor. These large beam deflections caused significant separation of the steel beam from the concrete slab. The beam deflection hysteretic behavior at the first and second story shown in Figure 6.46 suggest that the inelastic deformation of both beams increased rather linearly but to a lesser magnitude in the second story. The first story residual deflection when there was zero force in the actuator shown in Figure 6.47 more clearly corroborates this observation. It should be noted that the residual

deflection does not include the effects of monotonic loading, the drift range only considers cyclic loading.

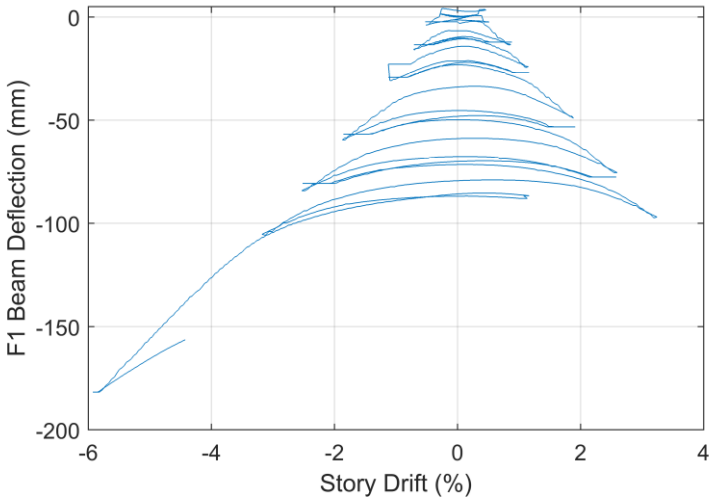

(a) First story

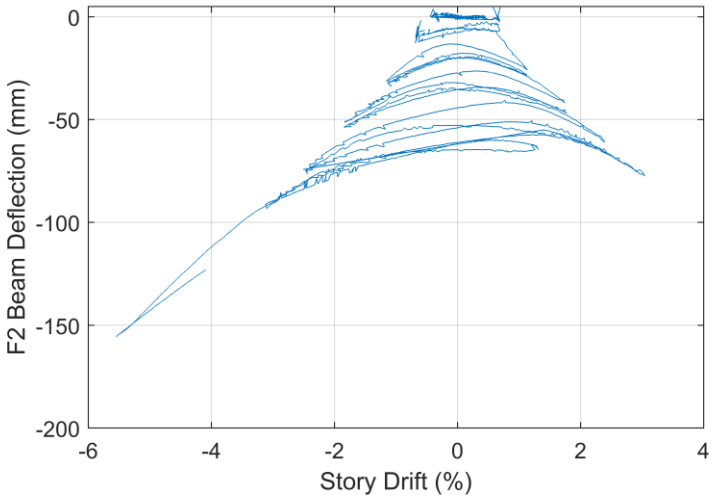

(b) Second story

Figure 6.46 Beam mid span vertical deflection hysteresis

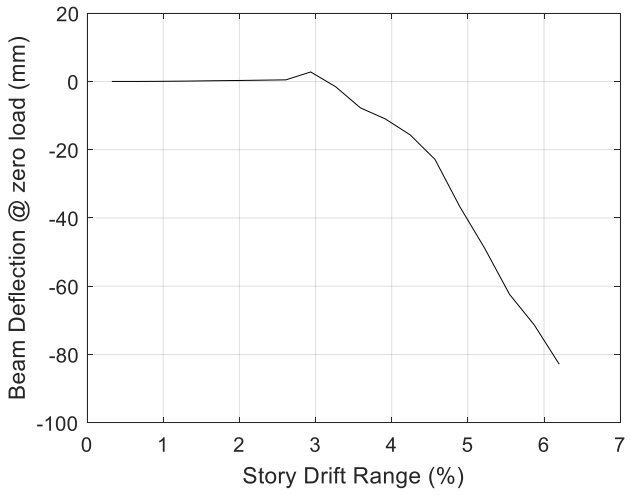

Figure 6.47 First story beam residual deflection

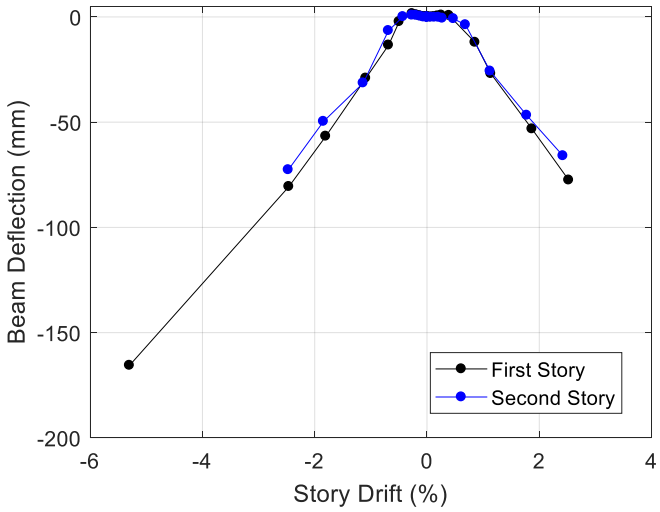

Figure 6.48 Beam mid span vertical deflection backbone

6.6.2.2 Torsion - Out of plane rotation

As previously explained in in the description of the out-of-plane reaction frame in Section 6.3.2, the first and second story beams and slabs were essentially unrestrained from rotational torsion at

all location along the length of the beam except at the beam quarter points. This condition allowed a large and unexpected rotation of the beam. The composite concrete slab should have provided the beam's lateral bracing, but the single stud connecting the transverse beams and concrete slab pulled out of the slab, allowing up to 12 cm of separation between the two by the end of the test. This means there was little restraint provided by the slab after the elastic cycles. Due to the rotation of the beam, the brace was also rotating about a higher point than the real brace end, resulting in a larger effective length than as built, or $K > 1$. Thus, the buckling strength of the braces in reality was lower than the design capacity, which would mean that the frame's lateral resistance exceeded the expected capacity of the system by a larger margin than reflected in Figure 6.24.

Evaluation of the beam out of plane rotation at the first story verifies this observation. Figure 6.50 and Figure 6.51 illustrate the out of plane movement of the beam, gusset plate, and brace at negative drift cycle peaks up to 3.7% roof drift. The figure's x-axis is the absolute displacement in the out of plane direction out of plane of the frame. The figure's y-axis is used to show the position in space of each marker on the y-axis based on an arbitrary reference point and does not reflect displacement in the y-direction (downward deflection). 3D data from Optotrak LED markers 21, 20, 14, and 12, was used to calculate the out of plane movements of the beam and gusset plate. These markers were located on the same line perpendicular to the x-axis on the x-y plane of the beam as detailed in Figure 6.49 and shown on the right vertical axis of Figure 6.50. The locations correspond to the beam's top flange, center of the web, bottom flange, and the corner of the middle gusset plate respectively, on the south side of the frame. LED markers 6, 5, 4, and 3 on the brace were used to determine brace out of plane movement shown in Figure 6.51. The illustration of the out of plane movement highlights the simultaneous initiation of rotation of the gusset plate and beam. Proving that the brace was effectively longer and rotating about a point higher than the actual brace end. This also proves that shortly after both braces had buckled the beam was rotating about its top flange.

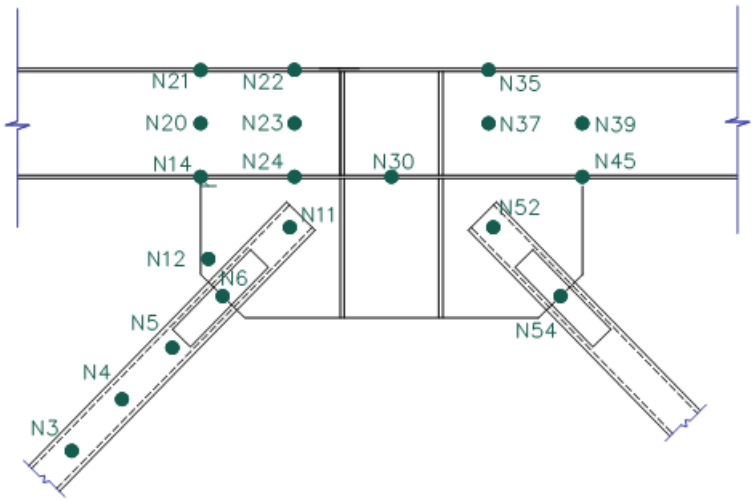

Figure 6.49 Sensor locations on the beam used for out of plane movement calculation

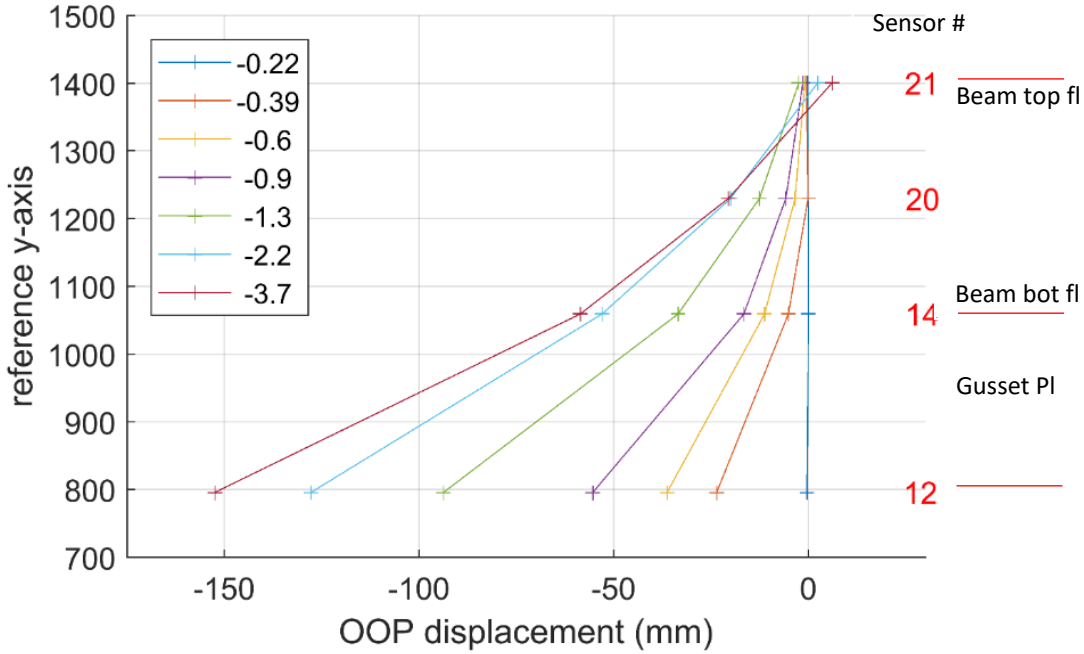

Figure 6.50 Out of plane movement of beam and gusset plate

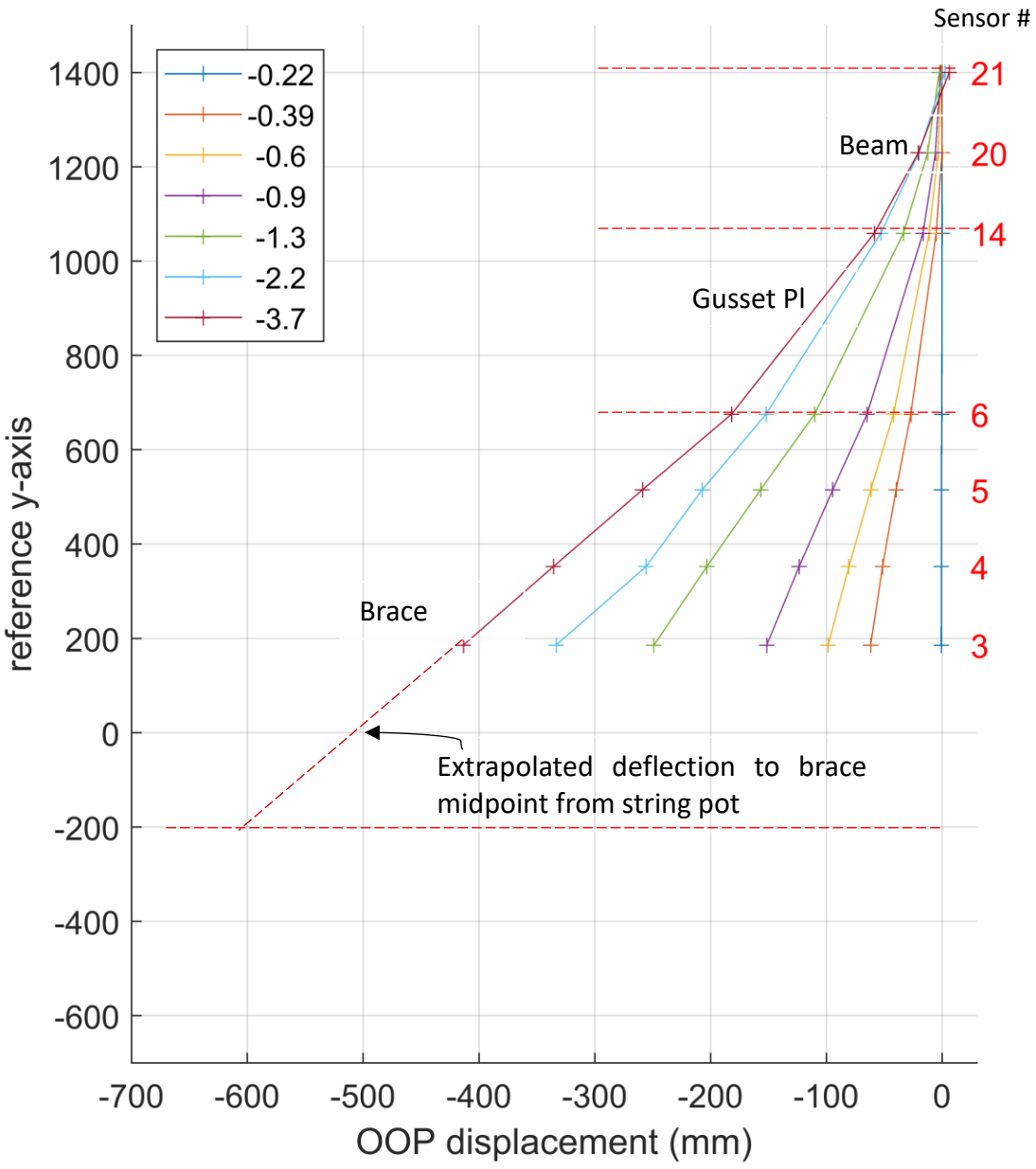

Figure 6.51 Out of plate movement of beam, busset plate, and south brace

Beam torsional rotation buckling is important to prevent in order to avoid lateral-torsional buckling. This is particularly important in chevron braced frames due to an out of plane force that develops from the braces when they buckle. As seen in the observations section and the previous plot of the out of plane movement of the beam and gusset plate, the torsional rotation was significant in this

experiment. The beam's torsional rotation can be calculated using Optotrak LEDs located on the beam flanges and web as shown in Figure 6.52. The 3D output data from the Optotrak system was used to determine the angle between the two sensors of interest at each time step, i, by using the x and y coordinates and Eq 6. 5. The angle of rotation of the beam could then be calculated using Eq 6. 6.

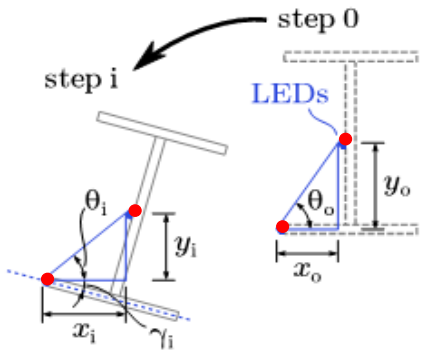

Figure 6.52 Beam torsional rotation geometry (Sen 2016)

$$\theta = atan\left(\frac{y}{z}\right) \quad \text{Eq 6. 5}$$

$$\gamma_i = \theta_o - \theta_i \quad \text{Eq 6. 6}$$

As roof drift and brace deformations increased, the braces rotated bout their longitudinal axis within the unrestrained section shown in Figure 6.11. This torsional rotation of the beam was calculated at the north and south edges of the middle gusset plate using the LED pairs 20 and 14, and 39 and 45 located as shown in Figure 6.49. The rotation on the north side of the beam is smaller than on the south because the transverse beam was offset towards the north at the center of the beam, making the section slightly more rigid in this section.

Although the optical 3D data for the second story beam has not been fully processed and beam torsional rotation is not reported, observations showed that the rotation was of a smaller magnitude. This was in part due to the braces buckling in opposite directions, which pushed and pulled the beam each cycle, minimizing out of plane deformations.

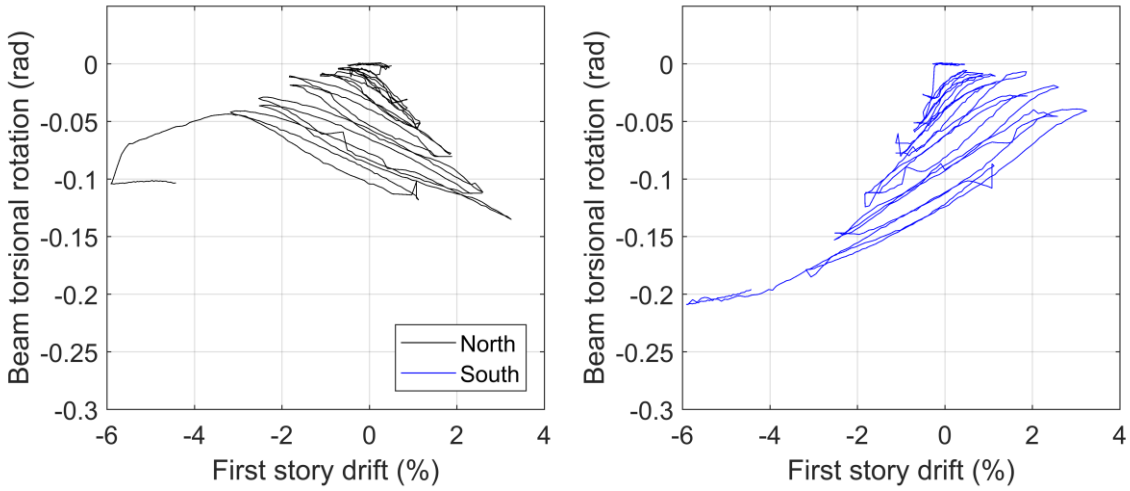

Figure 6.53 First story beam torsional rotation

6.6.3 Brace Response

Table 6.10 Provides a summary of the expected lateral strength of the braces ($2P_{cr}Cos\theta$) and the design unbalanced loads, $H_{br,d}$ and $V_{br,d}$, prescribed by the Seismic Provisions (AISC 2016a).

Table 6.10 Expected and design brace forces

	1FN	**1FS**	**2FN**	**2FS**	**3FN**	**3FS**
P_{cr}	1513	1513	1540	1540	1583	1583
$2P_{cr}Cos\theta$ (kN)	2117	2117	2155	2155	2216	2216

$$H_{br,d} = (P_{te} + P_{cre})Cos\theta = 2758\ kN$$

$$V_{br,d} = (P_{te} - 0.3P_{cre})Sin\theta = 1313\ kN\ (down)$$

6.6.3.1 Axial Force

As evidenced by Chevron 2 through 6 tests it was expected that the braces would not yield in tension and buckle at their compressive capacity. In fact, not even Chevron 1, which met beam design strength requirements, sustained brace yielding. Upon brace buckling, the force in the compressive brace would then degrade while the force in the tensile brace would converge and

plateau. This would result in an unbalanced vertical load at the middle of the beam that would decrease with the decrease in the force in the compressive brace. The deflections at the beam mid spans suggest the large vertical force was present.

The observed limited yielding of the third story and apparent small beam deflections suggest elastic behavior and should have resulted in very small unbalanced vertical loads. However, the forces calculated from the strain gauges on the braces initially proved contradictory and were not justified by test observations and previous test results; hence, the strain gauge data were corrected to provide the results shown below. The reported brace forces for Chevron 7 were derived by assuming a bilinear stress-strain relationship in steel and that was fitted to stress-strain curves form coupon tension tests. A large offset in the strains that occurred just following brace buckling was removed. Additionally, only data from the four strain gauges closer to the corner gusset plate was used.

The hysteretic curves of brace axial force vs drift in Figure 6.54 show that the braces achieved or exceeded the expected brace buckling strength P_{cr} of 1424 kN, indicated by the red line, in tension and compression. At the first two stories, the braces developed similar forces at incipient brace buckling, which were incidentally the peak tensile and compressive forces. The compressive strength degradation is consistent with single story tests, but the tensile strength of the braces appears to degrade unexpectedly quickly. The degradation of the tensile force in the second-story braces is not as steep as the first–story braces. The north braces does not show as much loss of strength between peaks of the same drift as the south braces. Some of this unexpected brace force response could be attributed to unintended boundary conditions discussed in Section 6.2.7 or an under conservative beam yielding mechanism resulting in a weaker system than was expected. In general, the second-story outperformed the first even though the connections and beam strength were the same.

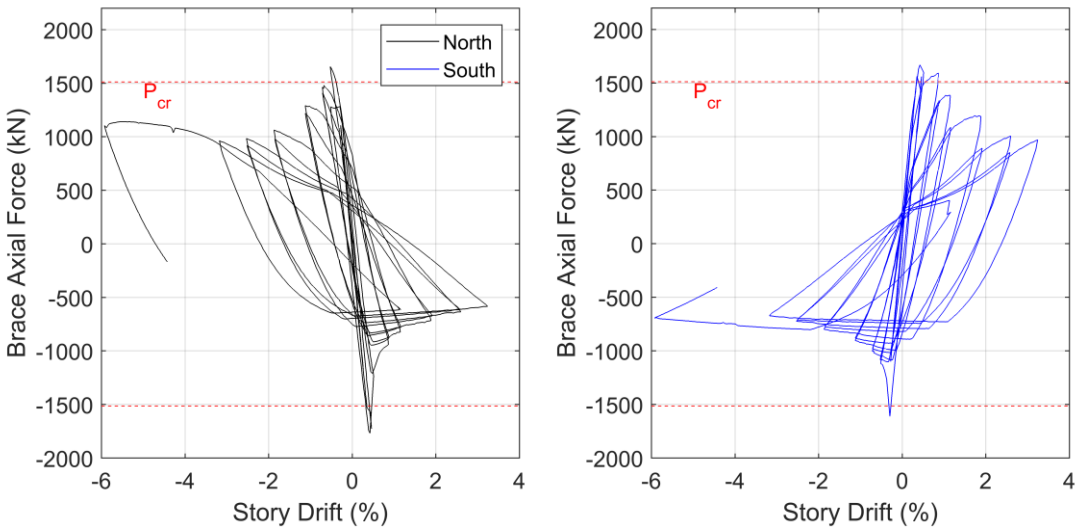

(a) First Story

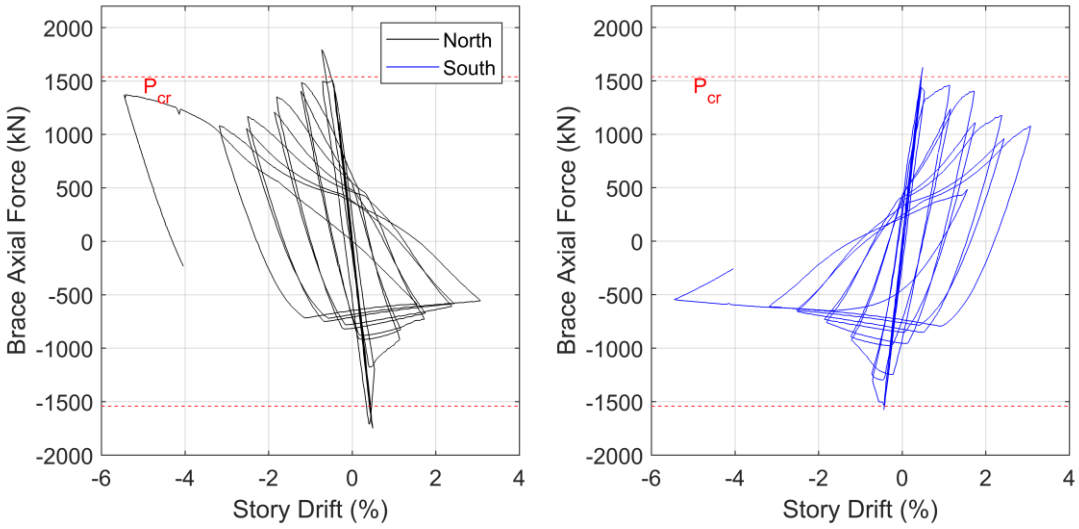

(b) Second Story

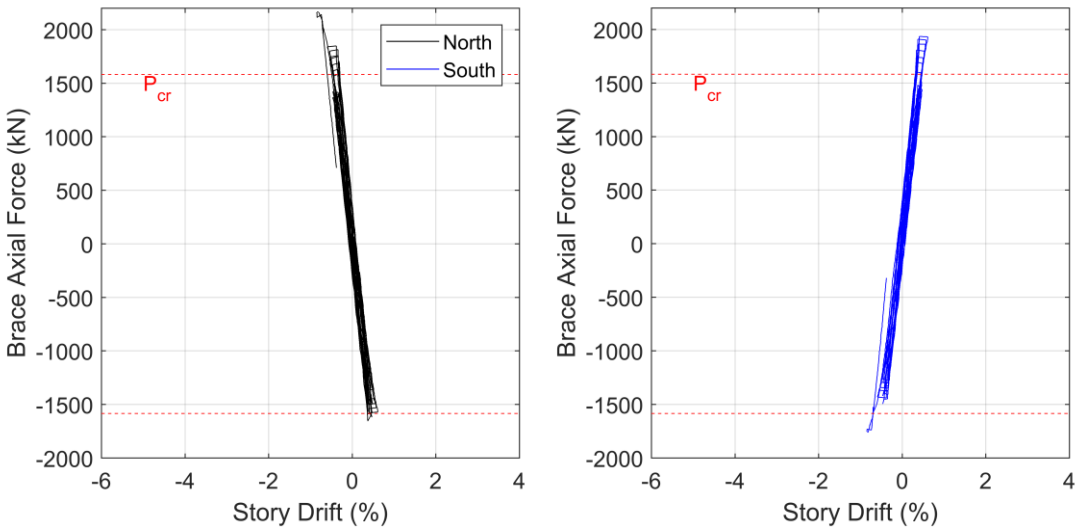

(c) Third Story

Figure 6.54 Brace axial force

6.6.3.2 Brace Effective length factors

The effective length factors, based on the measured buckling load of the braces and the end-to-end length of the braces at each story, were calculated and reported in Table 6.11 The calculated K factors agree with the buckling sequence at both stories and illustrate the effect of the offset transverse beam near midspan. The transverse beam was offset to the north, effectively stiffening the frame on this side, explaining the larger compressive forces in the south braces and later buckling even though they were loaded in compression first, and in a symmetric conditions would theoretically buckle first.

Table 6.11 Measured effective length factors

Location	Maximum tensile load in braces (kN) $P_{t,exp}$	Critical Buckling Load (kN) $P_{cr,exp}$ (kN)	Length L (mm)	Effective length factor, K	Story buckling sequence
1FN	1656	-1768	3348	0.85	2
1FS	1669	-1610	3348	0.94	1
2FN	1794	-1749	3294	0.87	4
2FS	1628	-1575	3294	0.98	3

6.6.3.3 Brace elongation

The brace elongation – brace force relationships in Figure 6.55 show that the brace is undergoing significant deformation, but it is almost exclusively in compressive shortening through out of plane deflection. Since the braces did not fracture or experience more than minimal local buckling they had the capacity for further shortening and out of plane bending. The first story plots show largely symmetric behavior of the north and south braces through cyclic loading with slightly less shortening of the north brace. At the second story, the south brace experienced about 30% more shortening than the north brace. The third story south brace elongation shows signs of shortening, suggesting incipient buckling, which would be expected due to the large post-fracture monotonic loading in negative drift.

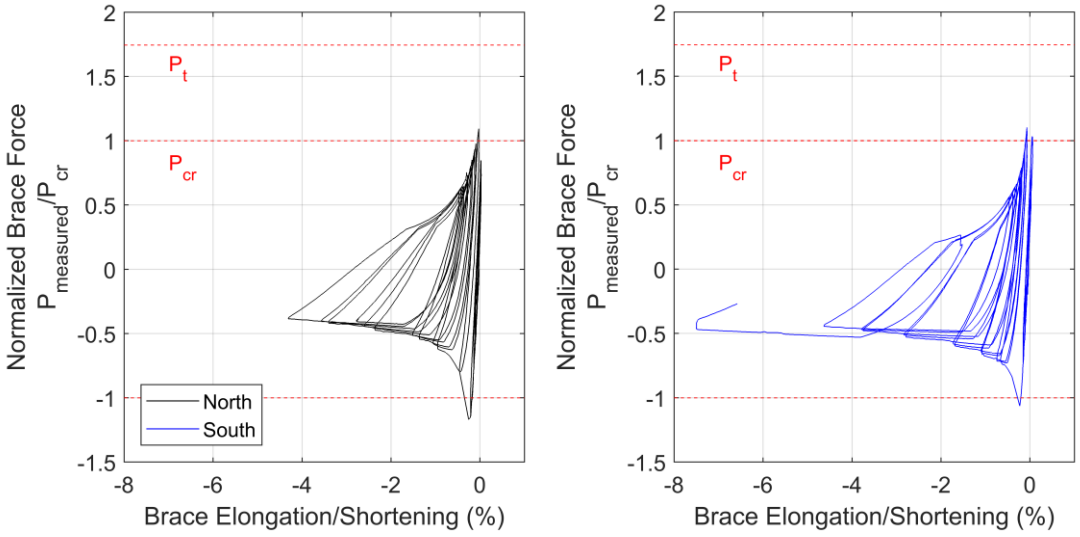

(a) First Story

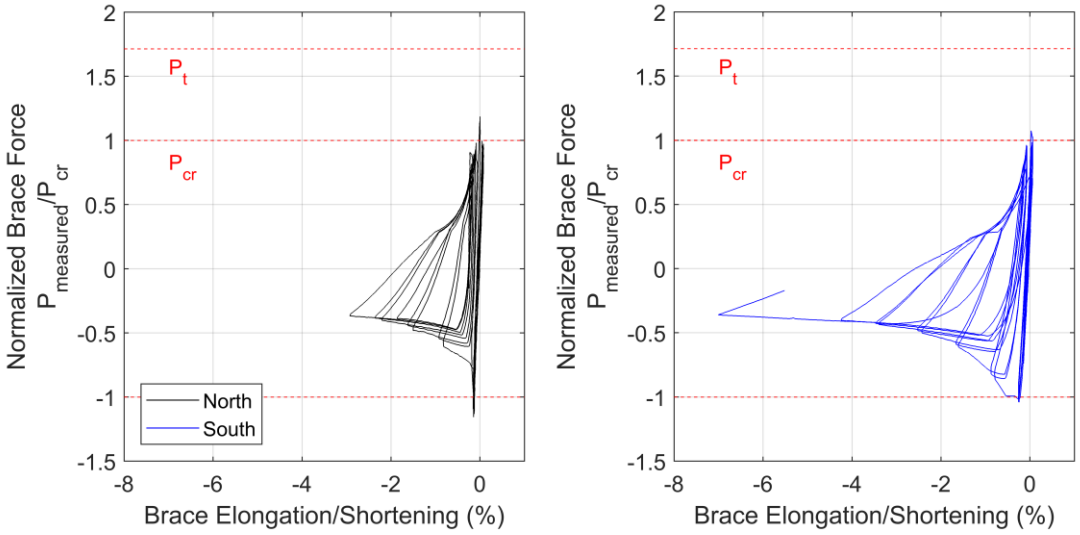

(b) Second Story

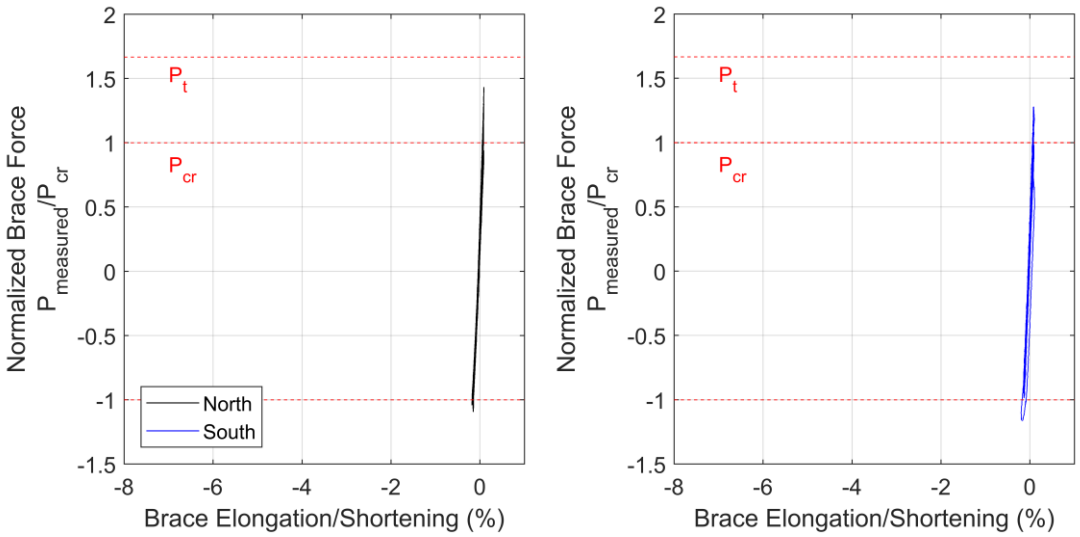

(c) Third Story

Figure 6.55 Brace elongation and shortening vs. brace axial force

6.6.3.4 Brace Unbalance – Beam Deflection Response

The relationship between brace vertical unbalanced force and beam mid-span deflection for the first story is shown in Figure 6.56. This illustrates how the unbalanced load does not fully reverse in each cycle after brace buckling, which corresponds to initiation of beam deflection. Although the downward load decreases in magnitude, the beam deflection continues to increase and never returns to its original position. This is likely due to premature beam yielding, suggesting that if the beam yields before the braces buckle the beam, or system, cannot regain strength, contributing to the continuous strength degradation noted in the previous results.

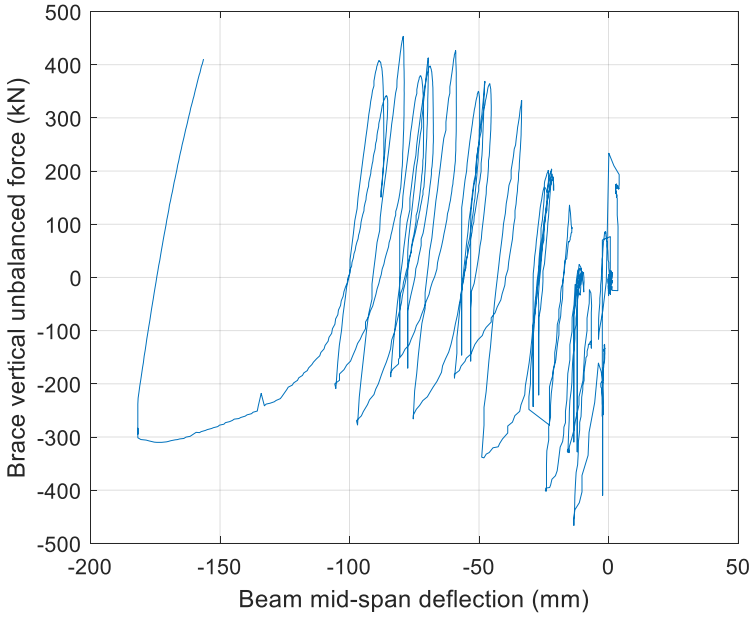

Figure 6.56 First story beam vertical deflection vs brace vertical unbalanced force

6.6.3.5 Brace OOP deflection

The out of plane deflection of the first and third story braces is shown in Figure 6.57. These deflections were measured with string potentiometers. The second floor brace data was measured with the OptoTrak, which remained unprocessed. The south and north braces at the first floor reached deformations of 450mm and 440mm respectively. The brace out of plane deformation of the third story also suggests that there was onset of brace buckling of the south brace during the monotonic loading that proceeded to 4% roof drift.

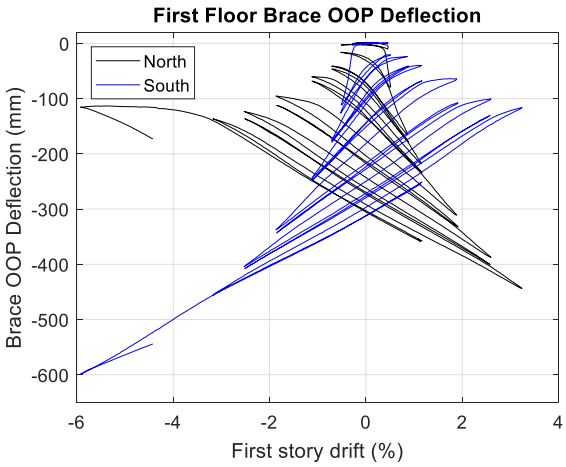

(a) First Story

(Not available)

(b) Second Story

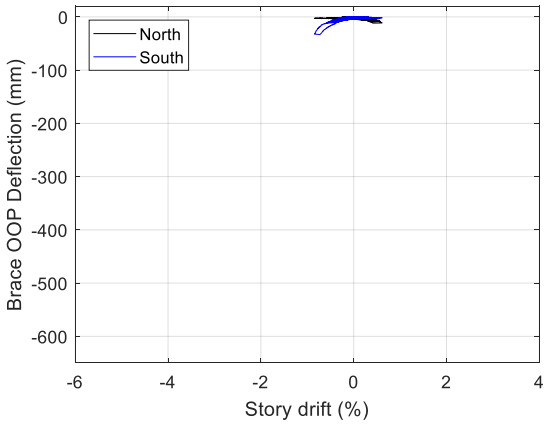

(c) Third story

Figure 6.57 Brace out of plane deformation

6.6.4 Column Response

Close evaluation of the column shears in Figure 6.58 shows that the column shear was approximately evenly distributed between the two columns at the first story, but the north carried more shear in positive drifts. At the second story in the elastic cycles, opposite to the first story, the south column provided more of the resistance in positive drift and the north column more in

negative drifts. There is also a brief reversal of shear direction when the second story braces buckle. In the third story, in the elastic range, the south column carries more load in positive drifts and vice versa. After the brace buckling, at around 0.5% roof drift, there is a permanent reversal of shear direction and the north column carries almost 50% more of the shear than the south column in negative drift, and the south column resists more in positive drifts.

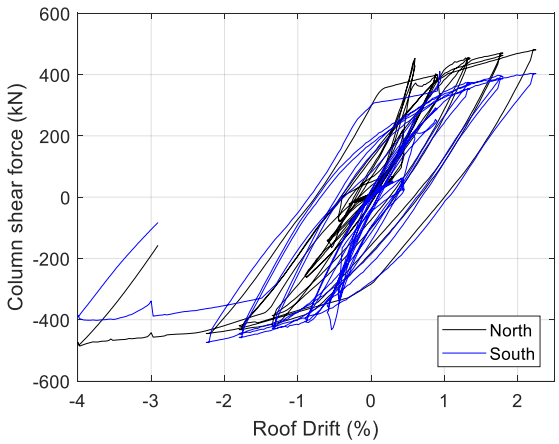

(a) First story

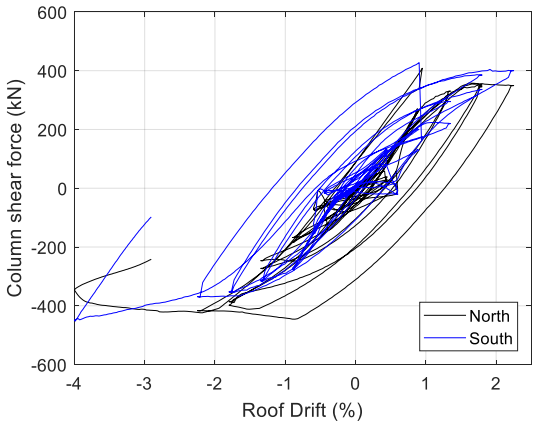

(b) Second story

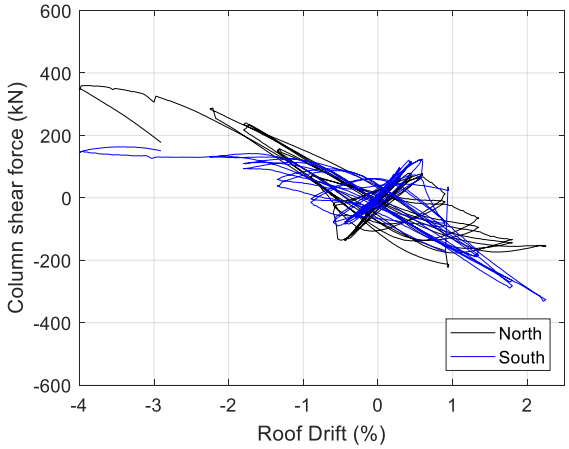

(c) Third story

Figure 6.58 Column shear force

The backbone curves of the total contribution of the columns to the lateral resistance of the braced frame is shown in Figure 6.59. The column shear contribution for the first and second stories as expected was less than 10% during the elastic response of the frame. Once the braces buckled at

around 0.5% roof drift the lateral resistance contribution started to increase gradually until towards the end of the test the columns carries almost 50% of the load. The third story shear in the elastic range is similar to the first and second stories; however, when the braces buckle the shear force was reversed and appears to have acted in the same direction rather than resisting the applied actuator force. This is likely due to the high stiffness of the third story, which acted like a rigid block over two soft stories. This large shear reversal between the second and third stories illustrates the issue that caused the south column to fracture at the second story moment connection.

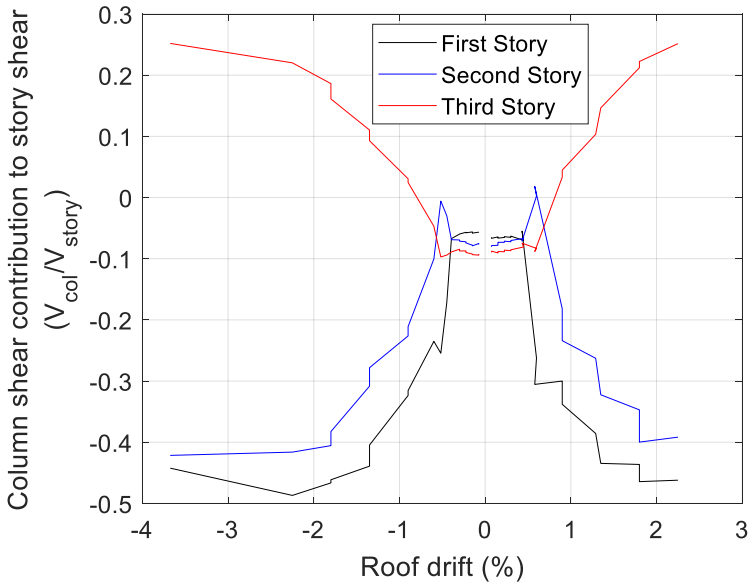

Figure 6.59 Column shear contribution to story shear backbone curve

6.6.5 Brace Unbalanced Force

In .Figure 6.60 and Figure 6.61 the measured horizontal and vertical components of the unbalanced force were normalized by the beam design loads required for chevron SCBFs per Seismic Provisions (AISC 2016a), provided in Table 6.10 ($H_{br,d}$ and $V_{br,d}$). These show that the maximum lateral resistance of the braces was approximately 90% of the design horizontal force. However, the brace resistance at the first and second stories began to degrade immediately after brace buckling to a final resistance of 50% of the design force. The brace unbalanced force vertical load at these bottom two stories reached about 36% of the design load before column fracture. Additionally, there is asymmetry in the response response of the vertical force in positive and negative displacements, particularly in the first story where the vertical load decreased at negative

drifts. This could be attributed to the stiffer north brace, where the brace tensile strength degraded more gradually.

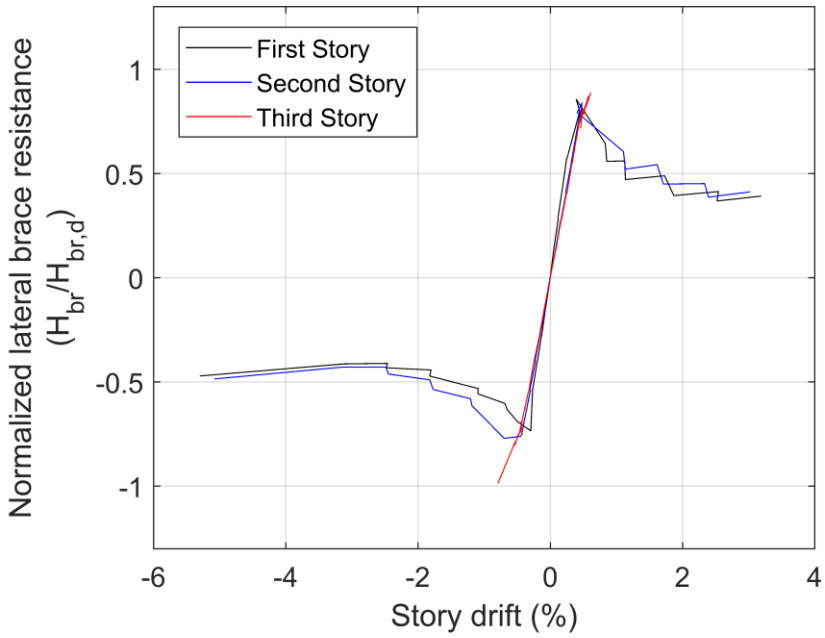

Figure 6.60 Normalized brace lateral resistance

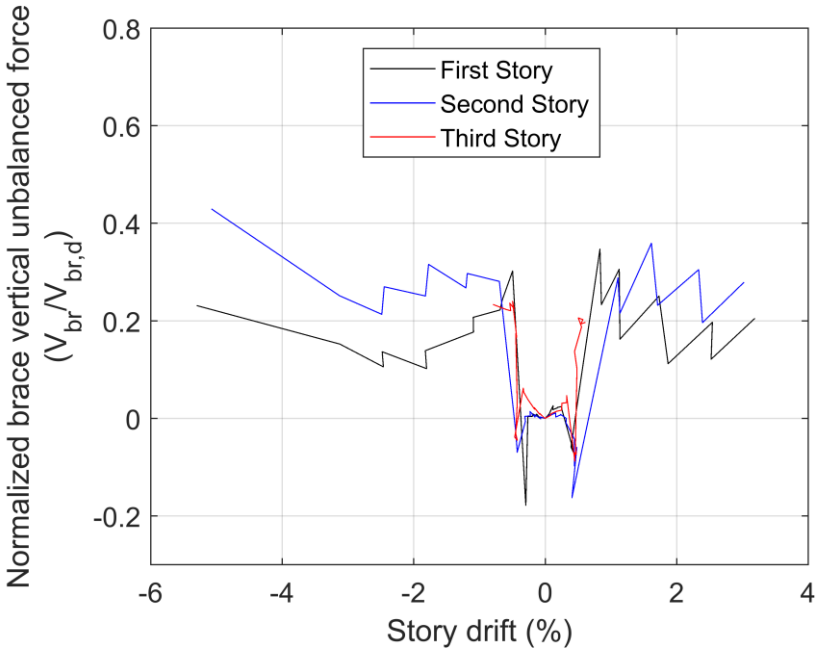

Figure 6.61 Normalized brace vertical unbalanced force

6.6.6 Connections

6.6.6.1 Gusset plate rotation

The rotation of the corner gusset plates was directly calculated from the LVDT measurements at the plate corners and brace end as shown in Figure 6.62 with Eq 6. 7 . Since the beam rotated significantly as shown in Section 6.6.2 the rotation at the gusset plate was measured using the geometry in Figure 6.63 with Eq 6. 8 and the beam rotation was subtracted from it. Corner gusset plate rotations are shown in Figure 6.64. These show that rotations and plstic deformation of the plates were larger at the first story by a small margin. The rotations are very symmetric on each floor.

The rotation associated with brace buckling at the top of the brace near the center of the beam was accommodated by beam rotations in addition to gusset plate rotations. Thus, as seen in Figure 6.65 the mid-beam gusset rotations were much smaller than for the corner gusset plates at the same story.

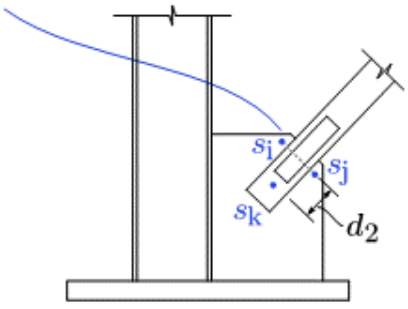

Figure 6.62 Corner Gusset plate rotation geometry (Sen 2014)

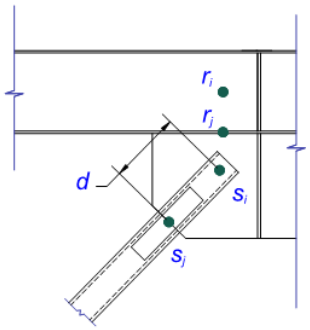

Figure 6.63 Middle gusset plate rotation geometry

$$\theta_{gp\_corner} = \text{atan}\left(\frac{\frac{s_i + s_j}{2} - s_k}{d_2}\right) \quad \text{Eq 6. 7}$$

$$\theta_{gp\_mid} = \text{atan}\left(\frac{\frac{s_i + s_j}{2}}{d}\right) - \gamma_i \qquad \text{Eq 6. 8}$$

Where γ is the beam torsional rotation calculated per Eq 6. 6 between points r_i and r_j

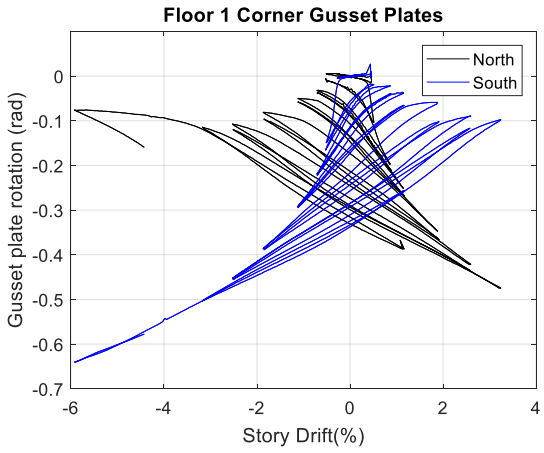

(a) First story

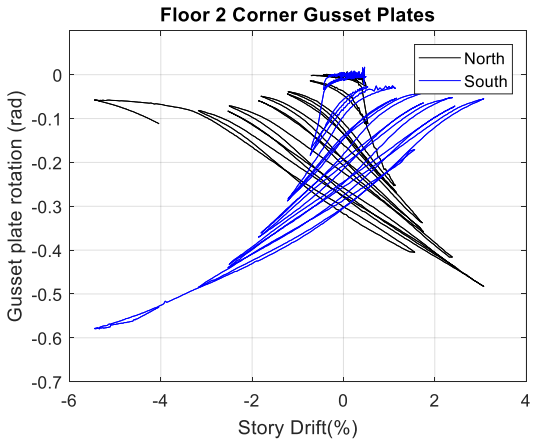

(b) Second story

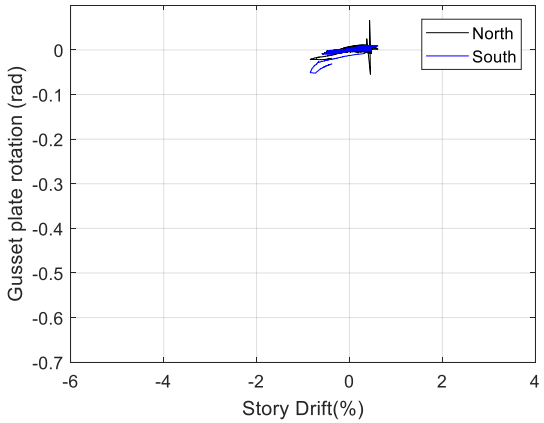

(c) Third story

Figure 6.64 Corner gusset plate rotation

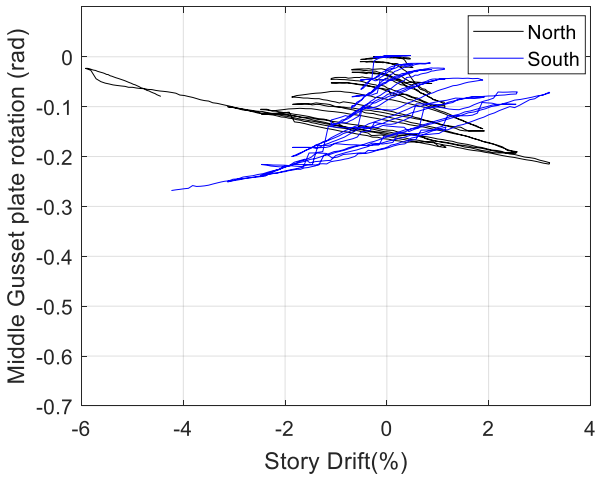

(a) First story

(Not available)

(b) Second story

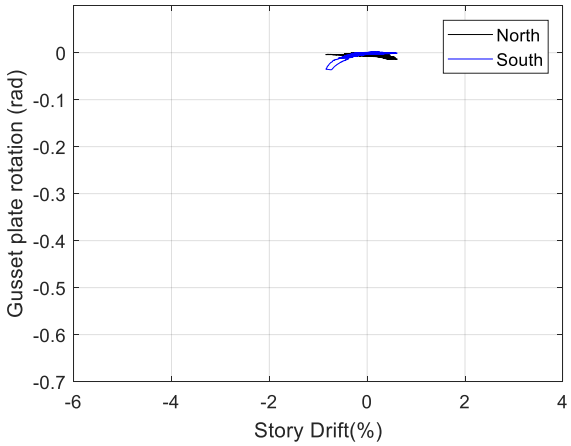

(c) Third story

Figure 6.65 Mid beam gusset plate rotation

CHAPTER 7

Summary, Conclusions, and Recommendations

7.1 Introduction

An experimental study was conducted to understand the impact of beam yielding on the seismic performance of chevron braced frames. Three single-story chevrons and one 3-story were tested. The single-story tests were performed in the University of Washington laboratories, and the 3-story test was performed in NCREE Laboratory in Taipei, Taiwan. The single-story specimens Chevrons 4 through 6 were a continuation of a series of single-story chevron SCBFs tested at the University of Washington (Terpstra 2017). Chevron 7 was a 3-story chevron SCBF designed based on the results from the previous six tests and supporting nonlinear numerical analysis by others with the objective of further investigating yielding beam effects with more realistic boundary conditions. The experimental results from these and the previously tested specimens were used to investigate the impact of various levels of chevron beam yielding, brace steel type, and beam stiffness on the seismic performance of the system.

7.2 Summary

Single-Story Specimens

The single-story specimens were tested to evaluate: the impact of a beam with ¼ the strength required by Seismic Provisions (AISC 2016a) (Chevron 4); the performance a frame with A500 braces relative to A1085 braces (Chevron 5); and the performance of a frame with a deeper, stiffer beam (Chevron 6).

All the single-story specimens had the same brace size, HSS 4x4x5/16, and column section, W12x50. All but Chevron 5 had braces of A1085 steel. To retain the specimen geometry the first

five specimens had W14 beams; Chevron 6 used a deeper beam section (W21), which caused slight changes in frame geometry. The strengths of the beams were quantified based on a simple span plastic collapse mechanism (single plastic hinge in beam on either side of the midspan gusset plate). The iDCR was calculated based on current AISC brace unbalanced loads occurring after deterioration of compressive resistance during post-buckling brace behavior. The three single story tests ended with brace fracture.

Chevron 4, with a beam iDCR of 4.32 had the weakest beam of the experimental program. It exhibited the highest ductility of all tested specimens with a maximum drift range of 9.1% story drift, and the resistance did not reach the expected lateral strength of the braces. The beam in this specimen began to yield at a low story drift and there was significantly large residual deformation of the beam of 80mm. This large beam deformation prevented brace elongation and contributed to the high story drift at brace fracture. This also resulted in the braces developing less than half their expected tensile capacity. The low lateral strength of this frame and the significant damage to the beam effectively establishing an experimental low bound for chevron behavior with yielding beams

Chevron 5, with a beam iDCR of 3.0, .having 1/3 of the current AISC required strength, had the same beam as Chevron 3 and A500 Gr.C braces since these section braces are more commonly used in construction and have been used in prior test programs. This specimen exceeded the expected lateral resistance with little strength degradation and demonstrated good but lower ductility than Chevron 3 with a 6.5% drift range. It also exhibited some dissimilar behavior of the north and south braces resulting in slightly higher resistance and inelastic deformation at positive drifts. The maximum tensile force in the braces was less than 50% of the expected tensile capacity which was equivalent to 1.2Pcr.

Chevron 6, with an iDCR of 1.8 and a beam of similar flexural strength to Chevron 2 but higher stiffness, behaved very similarly to Chevron 2. With the main difference being the elastic deflection of the beam, which was lower for the deeper W21 beam of Chevron 6 than the W14 beam of Chevron 2 and slightly lower ductility. Regardless, it demonstrated good ductility at 6% drift range. The peak strength well exceeded the design lateral resistance, and there was little

strength degradation. The maximum tensile force in the braces was about 3/4 of the expected tensile capacity.

3-Story Specimen

Chevron 7, the 3-story braced frame, was experimentally tested to investigate the system response of chevron braced frames with beams that yield under the brace demand, using more realistic boundary conditions including rigid beam-to-column connections and a concrete slab.

The frame was loaded at the top slab to provide constant story shear over the height of the structure. The bottom two stories of this frame were intended to evaluate the yielding beam chevron behavior. The beams on the lower two stories were W14x30 with partially composite slabs and had moment resisting connections at the column. If the beam had been designed based a simple span plastic collapse mechanism, with a beam length from the end of the beam to the edge of the midspan gusset plate, and not considering composite action, the resulting beam iDCR would have been 5.8.

During the test, the beams at the first and second stories experienced significant torsional rotation and midspan deflection of up to 100 mm at the first story beam. The lateral resistance of the frame exceeded the expected strength but there was immediate strength degradation upon brace buckling that continued until a column fracture impeded further cyclic loading of the frame. This column fracture was caused by the concentrated stress and strain caused by the relatively rigid top story; where brace buckling did not occur since the top beam and slab were designed to remain elastic in order to transfer actuator loads into the test frame. None of the braces fractured in this test and there was only incipient cupping at the braces, suggesting they could have resisted much larger deformations. The inelastic deformation was approximately evenly distributed amongst the bottom two stories. Ultimately, the bottom two stories, which were of most interest achieved high ductility, reaching 9.2% and 8.5% story drift range including displacement from a post-column-fracture monotonic loading, and the specimen response was near the limits of desirable performance when compared with single-story test results.

7.3 Conclusions

These tests demonstrated that the beam yielding mechanism improved the deformability of the SCBF without compromising the capacity of the system if beam yielding follows brace buckling. However, if the beam is too weak, the idealized lateral strength of the system using elastic analysis and design, corresponding to developing brace axial forces equal to the expected buckling capacity, cannot be achieved.

Lateral Resistance

- The lateral resistance of the frame decreases with beam yielding, but the decrease is smaller than the reduction in beam resistance. That is a 40% reduction in beam strength does not result in a 40% decrease in strength. In addition, the lateral resistance in chevrons with simply supported beams is consistently larger than the resistance required from a linear-elastic analysis using the design loads and calculations if the beam has an iDCR of 3 or less. However, the results suggest that if the iDCR exceeds 4, the lateral resistance was consistently smaller than the expected design resistance.

Deformation capacity

- SCBF's are considered to have good ductility with a drift range of 4% prior to brace fracture, and given the achieved drift ranges of above 6% in all the yielding beam specimens with A1085 braces, there was improved ductility for chevron-braced frames with beam yielding. The drift capacity was larger with increasing amounts of beam yielding (larger iDCR values).

Beam Performance

- Vertical deflections of the beam midspan increase with decreased beam strength, but the deflections were consistently smaller than would be expected given the reduction in beam resistance (most of the deformation was inelastic). Residual deflections at the end of the test were typically less than 25 mm or $^1/_{120}$ of the span length if the beam was strong enough to develop more than $^1/_3$ of the current strength requirements.

Brace Performance

- Chevron 5, with A500 Gr.C braces had a very similar strength response to its counterpart of equal iDCR, Chevron 3 with A1085 braces. In achieving a lower drift range before brace fracture than Chevron 3, it demonstrated the increased ductility resulting from using ASTM 1085 grade HSS section braces
- Braces buckle in compression for all iDCR values; the experimental results indicate that the degradation in compressive brace force is similar for all iDCR values. However, the tensile brace force decreases with increasing iDCR and approaches P_{cr} for braces in chevron frames with yielding beams.

3-Story Frame

- Prior research suggests that chevron-configured SCBF buildings concentrate nonlinear demands to a single story. However, the even distribution of inelastic deformation in the bottom two stories suggests that a soft story effect was not an issue for chevron frames with yielding beams.
- The concrete slab does not contribute much strength after the braces have buckled and caused the slab to crack significantly longitudinally, but the lack of lateral restraint at the center of the beam make definitive slab contribution inconclusive.

7.4 Recommendations for Future work

Based on limitations of the research presented further work is necessary to conclude the work and provide a proposed design procedure for the design of chevron braced frames with yielding beams.

Analysis of Experimental Results

- A very limited discussion of the 3-story frame results was presented in this thesis. Notably missing is analysis on the contribution of the concrete slab and the forces in the beam. It was originally postulated that the side of the beam in compression would carry most of the axial load and the even distribution of load to both sides of the beam for design purposes was not entirely realistic. Additionally, it would be useful for future studies, to determine the efficacy of concrete surface gauges, as were used in the 3-story experiment.

- Investigation of the connection deficiency observed in the multi-story test that resulted in column flange fracture. An X-Ray analysis of the two beam-to-column joints at the second story of Chevron 7 could provide a clear location of crack initiation.

Nonlinear Numerical Analysis

Refined numerical models created in ABAQUS and OpenSees using the three story test results for validation should be used to examine to examine important parameters related to chevron beam yield behavior and to optimize the design provisions for this behavior. Such parameters include:

- Experiment boundary conditions: In the 3-story test there were inadvertent changes in the boundary conditions resulting in inadequate out-of-plane restraint of the beams. ABAQUS models could be used to isolate the impact of the boundary conditions and beam strength. Boundary parameters of interest would include the number of shear studs on the transverse beams and slab torsional rotation support at the beam midspan.
- Beam plastic mechanism: The plastic mechanism used to calculate the iDCR for multi-story frames requires consideration of a coupled beam and sway mechanism since the unbalanced load occurs after significant lateral deflection. Additionally, the plastic mechanism used in the single-story iDCR calculation underestimates the moment resistance of the shear plate connection and overestimates the iDCR because the actual unbalanced loads are much smaller than suggested by the SCBF criteria when beam yielding occurs. This is due to the inability of the weaker beam to develop the brace idealized unbalanced forces.
- Connection requirements with yielding beams: Initial numerical analyses suggested that a less rigid welded-flange-bolted-web connection would have resulted in equal or better performance. However, the simple connection does not currently meet design requirements for chevron SCBFs and moment connections, such as the one used in the experiment based on recommendations from an Advisory Group, are commonly used in industry.
- Beam axial stress ratio: One significant difference between the single-story and 3-story frames was an axial stress ratio greater than 0.5 as compared to ratios of 0.25 or less. The maximum axial loads in the beam are not reduced by beam yielding, and so the

determination of the appropriate balance for this stress level could greatly benefit the design procedure.

- Beam-to-column flexural strength ratio. In the 3-story test, the column was designed to develop the full expected tensile and compressive capacity of the braces. However, with yielding beams in chevron braced frames the brace never develops its expected tensile force. The maximum tensile force in these systems is approximately the same as the magnitude of P_{cr}. Recognition of this in the column design requirements could result in significant cost savings for chevron braced frames. At the same time, the column strength benefits the performance of chevron braced frames by providing shear resistance due to reversed curvature in the column due to the gusset plate and beam-column connection. Nonlinear analysis of different beam to column strengths could provide great benefit to the design of these systems.

A final design recommendation required the refinement of the procedure for the design of the beam in chevron SCBFs that does not assume brace tensile yielding, but beam yielding and brace buckling in compression and would result in a lighter more economic beam section. The resulting beam section would necessarily experience larger deformation and allow the system to achieve the theoretical design strength and overall high ductility without strength degradation.

.

REFERENCES

AISC (1997). “Seismic provisions for structural steel buildings." AISC 341-97, American Institute of Steel Construction, Chicago, IL.

AISC (2010). “Seismic provisions for structural steel buildings." AISC 341-16, American Institute of Steel Construction, Chicago, IL.

AISC (2016a). “Seismic provisions for structural steel buildings." AISC 341-16, American Institute of Steel Construction, Chicago, IL.

AISC (2016b). “Specification for structural steel buildings." AISC 360-16, American Institute of Steel Construction, Chicago, IL.

ASTM Standards E8/E8M, 2018, “Standard Test Method for Tension Testing of Metallic Materials,” ASTM International, West Conshohocken, PA, 2018.

ASTM Standards C39/C39M, 2018, “Standard Test Method for Compressive Strength of cylindrical Concrete Specimens,” ASTM International, West Conshohocken, PA, 2018.

Ballard, Ryan. (2015) “Impact of Connection Type on Performance of Non-Seismic Concentrically Braced Frames” M.S. thesis, University of Washington, Seattle.

Foutch, D. A., Goel, S. C., and Roeder, C. W. (1987). “Seismic testing of full-scale steel building-part i." *Journal of Structural Engineering*, 113(11), 2111-2129.

Fukuta, T., Nishiyama, I., Yamanouchi, H., and Kato, B. (1989). “Seismic performance of steel frames with inverted v braces." *Journal of Structural Engineering,* 115(8), 2016-2028.

Goel, S. C. (1992). “Cyclic post buckling behavior of steel bracing members.” *Stability and ductility of Steel Structures under cyclic Loading,* CRC Press, Boca Raton, FL.

Kotulka, B. A. (2007). “Analysis for a design guide on gusset plates used in special concentrically braced frames." M.S. thesis, University of Washington, Seattle.

Lehman, D. E., Roeder, C. W., Herman, D., Johnson, S., and Kotulka, B. (2008). “Improved seismic performance of gusset plate connections." *Journal of Structural Engineering*, 134(6), 890-901.

Lumpkin, Eric J. (2009) “Enhanced Seismic Performance of Multi-Story Special concentrically Brace Frames using a Balanced Design Procedure.” M.S. thesis, University of Washington, Seattle.

Okazaki, Taichiro., Lignos, Dimitrios G., Hikino, Tsuyoshi., Kajiwara, Koichi. (2013). “Dynamic Response of a Chevron Concentrically Braced Frame.” *Journal of Structural Engineering* 139.4.515-25

Sabelli, Rafael. Roeder, Charles W., Hajjar, Jerome F. (2013). “Seismic Design of Steel Special Concentrically Braced Frame Systems. A Guide for Practicing Engineers.” NEHRP Seismic Design Technical Brief No.8.

Sen, Andrew D. (2014) “Seismic Performance of chevron Concentrically Braced Frames with Weak Beams.” M.S. thesis, University of Washington, Seattle.

Sen, Andrew D., Roeder, Charles W., Berman, Jeffrey W., Lehman, Dawn E., Li, Chao-Hsien, Wu, An-Chien, and Tsai, Keh-Chyuan. (2016). “Experimental Investigation of Chevron Concentrically Braced Frames with Yielding Beams”. *J. Struct. Eng*., 04016123

Roeder, Charles W. (1989) “Seismic Behavior of concentrically braced frames.” *Journal of Structural Engineering*, 115(8), 1837-1856.

Roeder, C. W., Lumpkin, E. J., and Lehman, D. E. (2011). “A balanced design procedure for special concentrically braced frame connections." *Journal of Constructional Steel Research,* 67(11), 1760-1772.

Terpstra, Clare (2017) “Impact of Beam Strength on Seismic Performance of Chevron Concentrically Braced Frames.” M.S. thesis, University of Washington, Seattle.

APPENDIX A
Sample Calculations

A.1 Variable Definitions

For the design of the specimens and iDCR calculations of Chevrons 4 through 6, nominal material properties and overstrength factors, R_y and R_t, were used to calculate expected brace strengths, denoted as P_{cre} and P_{te}. The expected brace strength in compression also includes the 1.14 factor. For analysis of experimental results, measured material properties were used to calculate expected strengths denoted as P_{cr} and P_t. The term "exp" indicates experimentally measured forces and stresses, such as the brace in the compression strength at buckling, $P_{cr,exp}$.

Table A.1 Brace Parameter Definitions

Description	Variable	Material Properties	Factors	Expression
Nominal yield strength	P_y	Nominal	none	$P_y = F_y A_g$
Expected tensile strength for design	P_{te}	Nominal	R_y	$P_{te} = R_y F_y A_g$
Actual expected tensile strength	P_t	Measured from coupon test	none	$P_t = F_{y,exp} A_g$
Nominal compressive strength	P_c	Nominal	none	$P_c = F_{cr} A_g$
Expected compressive strength/expected buckling load for design	P_{cre}	Nominal	1.14 and R_y	$P_{cre} = 1.14 F_{cr} A_g$
Actual expected compressive strength/expected buckling load	P_{cr}	Measured from coupon test	none	$P_{cr} = F_{cr} A_g$
Critical buckling load	$P_{cr,exp}$	-	-	Calculated from strain gauge test data

A.2 Single-Story Beam iDCR Calculation for Chevron 4

A.2.1 Brace Demands

Brace Parameters

Brace Section: HSS4x4x5/16
ASTM Standard: A1085
F_y = 50 ksi
F_u = 65 ksi
R_y = 1.25
R_t = 1.3
A_{br} = 4.36 in2
r = 1.48
b/t = 9.8
L_{br} = 143 in.
Brace angle (θ) = 45.9 °

Brace expected strength in tension:

$$P_{te} = R_y F_y A_g = 1.25(50 \text{ ksi})\left(4.36 \text{ in.}^2\right) = \mathbf{273 \text{ kips}}$$

Brace expected strength in compression:

$$F_e = \frac{\pi^2 E}{\left(\frac{KL}{r}\right)^2} = \frac{\pi^2 (29000 \text{ ksi})}{\left(\frac{143 \text{ in.}}{1.48 \text{ in.}}\right)^2} = 30.7 \text{ ksi}$$

$$\frac{R_y F_y}{F_e} = 2.0 < 2.25$$

$$F_{cr} = \left(0.658^{R_y F_y / F_e}\right) R_y F_y = \left(0.658^{1.25(50 \text{ ksi})/(30.7 \text{ ksi})}\right)(1.25)(50 \text{ ksi}) = 26.6 \text{ ksi}$$

$$P_{cre} = 1.14 F_{cr} A_g = 1.14(26.6 \text{ ksi})\left(4.36 \text{ in.}^2\right) = \mathbf{132 \text{ kips}}$$

Demand from brace unbalanced forces:

In the elastic case before braces buckle and both are at their maximum capacity

$$\text{Horizontal: } H_{br,d,e} = [P_{te} + P_{cre}]cos\theta = (273 + 132)\cos(45.9^O) = \mathbf{282\ kips}$$

$$\text{Vertical: } V_{br,d,e} = [P_{cre} - P_{te}]sin\theta = (273 - 132)\sin(45.9^O) = \mathbf{-101\ kips}$$

Post buckling case

$$\text{Horizontal: } H_{br,d,post} = [P_{te} + 0.3P_{cre}]cos\theta = \mathbf{217\ kips}$$

$$\text{Vertical: } V_{br,d,post} = [0.3P_{cre} - P_{te}]sin\theta = \mathbf{-167\ kips}$$

Maximum Moment Demand:

Assuming the beam remains rigid over gusset plate region and plastic hinges form at the edge of the gusset plate, the length form the end of the beam to the edge of the gusset L_g = 96 in.

Both braces at maximum capacity:

$$M_r = \frac{V_{br,d,e}L_g}{2} = \frac{101\text{ kips}(96\text{ in.})}{2} = \mathbf{403\ k\text{-}ft}$$

Post-buckling unbalanced load:

$$M_r = \frac{V_{br,d,post}L_g}{2} = \frac{167\text{ kips}(96\text{ in.})}{2} = \mathbf{669\ k\text{-}ft}$$

A.2.2 Beam Capacity

Beam Parameters

Section: W14x26
ASTM designation: A992
F_y = 50 ksi
F_u = 65 ksi
R_y = 1.1
A_b = 7.69 in^2
b/2t = 5.98
h/t_w = 48.1

$$\frac{KL_y}{r_y} = 38.9$$

$$\frac{KL_x}{r_x} = 20.3$$

Flexural Strength:
With the beam braced against flexural and lateral-torsional buckling:

$$\Phi M_p = 151 \text{ kip-ft}$$

Yield Strength:

$$\Phi P_y = 346 \text{ kips}$$

Effective Compressive Strength

$$\Phi P_n = 291 kips$$

A.2.3 Demand-to-Capacity Ratio (iDCR)

$$if \frac{P_r}{\phi_c P_n} < 0.2$$

$$iDCR = \frac{M_r}{M_c} + \frac{P_r}{2P_c}$$

$$if \frac{P_r}{\phi_c P_n} > 0.2$$

$$iDCR = \frac{8}{9}\frac{M_r}{M_c} + \frac{P_r}{P_c}$$

where

$$H_u = H_{br,d}$$

$$P_r = H_u/2$$

Both braces at maximum capacity:

$$\text{Axial DCR} = \frac{282/2}{291} = 0.48 > 0.2$$

$$\text{Flexural DCR} = \frac{403}{151} = 2.66$$

$$\text{Interaction DCR} = 8/9 * 2.66 + 0.48 = \mathbf{2.86}$$

Post-buckling unbalanced load:

$$\text{Axial DCR} = \frac{217/2}{291} = 0.37 > 0.2$$

$$\text{Flexural DCR} = \frac{669}{151} = 4.44$$

$$\text{Interaction DCR} = 8/9 * 4.44 + 0.37 = \mathbf{4.32}$$

A.3 Effective Length Factor

The effective length factor based on the experimentally measured axial forces in the braces was calculated as follows:

$$K = \frac{sqrt\left(\frac{\left(\pi^2 E r^2 * \log_b\left(\frac{P_{cr,exp}}{A_g F_{y,exp}}\right)\right)}{F_{y,exp}}\right)}{L_{brace}}$$

Where b = 0.658

APPENDIX B
Drawings

This appendix contains specimen construction and instrumentation drawings for all specimens tested by the author, Chevron 4, Chevron 5, Chevron 6, and Chevron 7. The construction drawings for Chevron 7, designated by “SK”, were used by professional fabricators to build the specimen at the National Center for Research on Earthquake Engineering in Taiwan. The instrumentation drawings, designated “IN”, were used to attach sensors and whitewash the specimens.The test setup drawings produced by An-Chien Wu and Te-Hung Lin for the 3-story test and test setup drawings produced by Terpstra for the single-story tests are included in this appendix.

B.1 Single-Story Frame Drawings

The specimen drawings for Chevron 4, Chevron 5, and Chevron 6 are found below. These include elevation and connection details, instrumentation plans and tables, and test setup plans and details.

B.1.1 Construction and Instrumentation Drawings

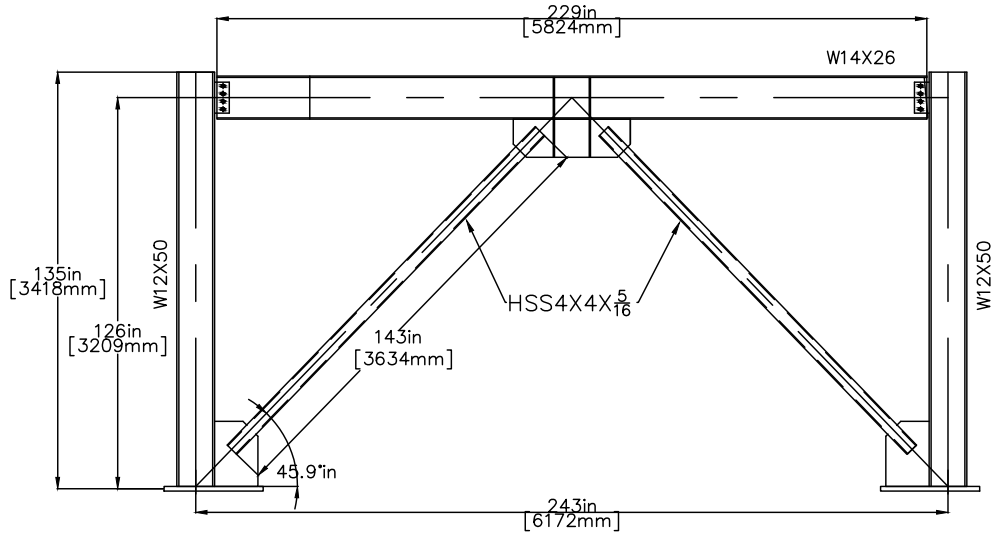

CHEVRON 4 ELEVATION

GENERAL NOTES:

1. ALL ROLLED SHAPES TO BE A992
2. ALL BOLTS TO BE A490 WITH THREADS EXCLUDED FROM THE SHEAR PLANE
3. ALL PLATE STEEL TO BE A572 GR 50
4. ALL WELDS AT GUSSET PLATE, HSS BRACES, BEAM TO COLUMN, AND BEAM TO BASE PLATE CONNECTIONS TO SATISFY AISC DEMAND CRITICAL REQUIREMENT (EQUIVALENT TO E7018, E71-T1, OR E71-T8)
5. ALL UNITS IN INCHES UNLESS OTHERWISE NOTED

FRAME ELEVATIONS	
SINGLE STORY SCBF WITH YIELDING BEAMS	DWG: SK-1
DRAWN BY: SMI DESIGNED BY: SMI DATE: 5/24/2018 CONTACT: SMIBARRA@UW.EDU	

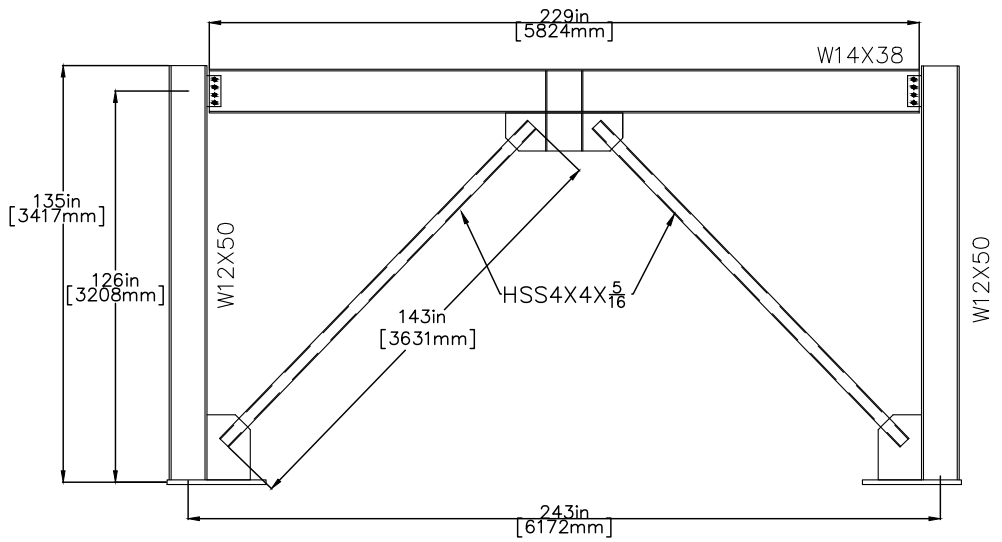

CHEVRON 5 ELEVATION

NORTH

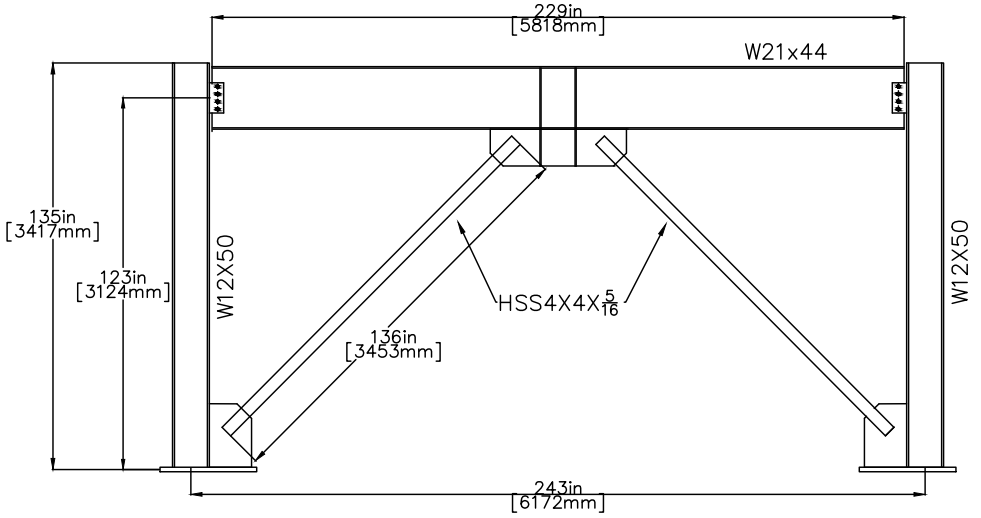

CHEVRON 6 ELEVATION

FRAME ELEVATIONS	
SINGLE STORY SCBF WITH YIELDING BEAMS	DWG: SK-2
DRAWN BY: SMI DESIGNED BY: SMI DATE: 5/24/2018 CONTACT: SMIBARRA@UW.EDU	

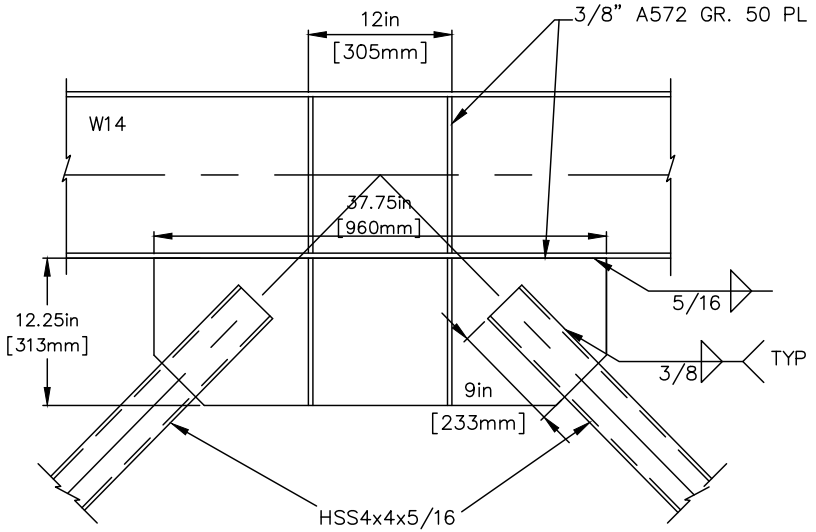

SHEAR TAB AND WEB DOUBLER

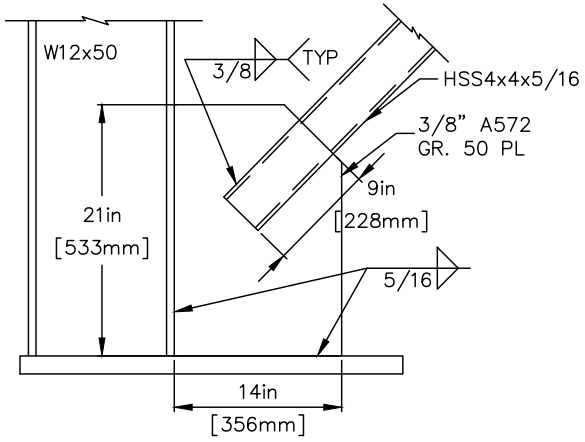

SHEAR TAB AND WEB DOUBLER

GUSSET PLATE CONNECTIONS W14	
SINGLE STORY SCBF WITH YIELDING BEAMS	DWG: SK-3
DRAWN BY: SMI DESIGNED BY: SMI DATE: 5/24/2018 CONTACT: SMIBARRA@UW.EDU	

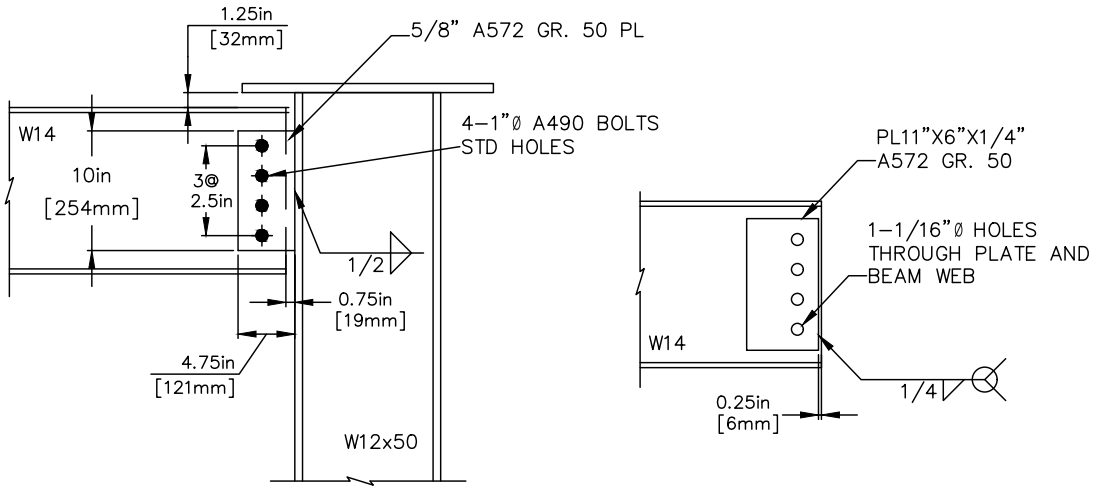

SHEAR TAB AND WEB DOUBLER

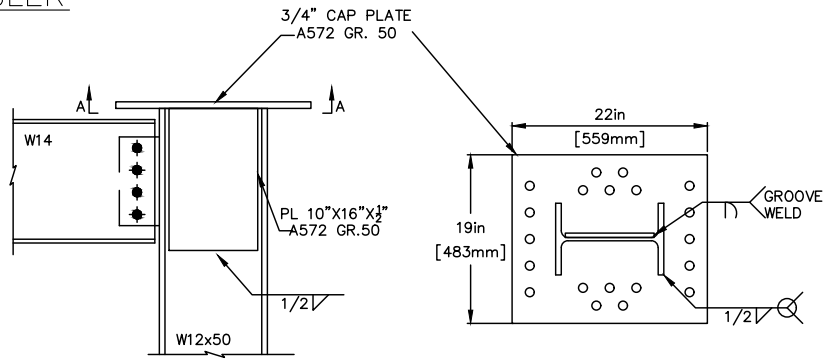

SECTION A–A

COLUMN DOUBLER AND CAP PLATE

W14 BEAM END CONNECTIONS	
SINGLE STORY SCBF WITH YIELDING BEAMS	DWG: SK-4
DRAWN BY: SMI DESIGNED BY: SMI DATE: 5/24/2018 CONTACT: SMIBARRA@UW.EDU	

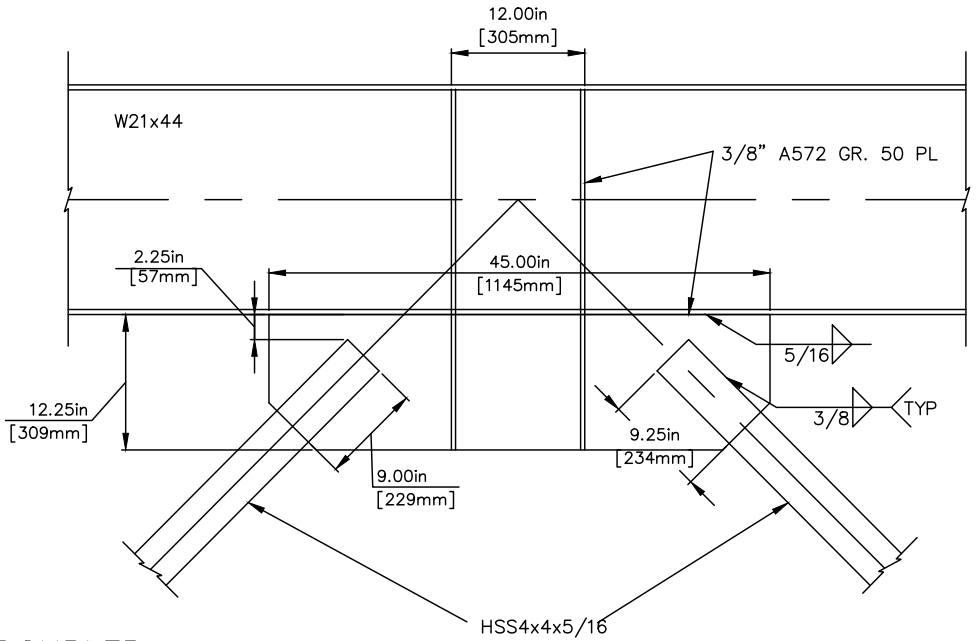

SHEAR TAB AND WEB DOUBLER

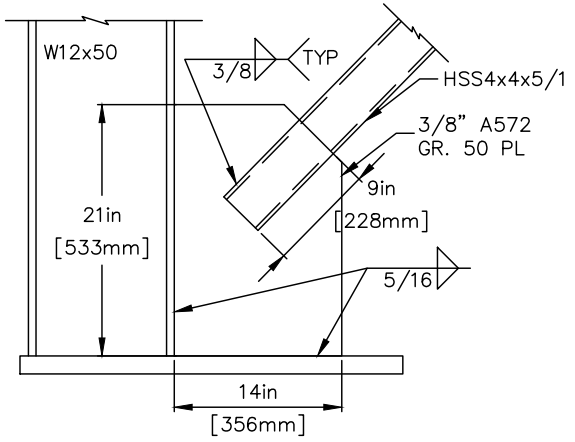

SHEAR TAB AND WEB DOUBLER

GUSSET PLATE CONNECTIONS W21	
SINGLE STORY SCBF WITH YIELDING BEAMS	DWG: SK-5
DRAWN BY: SMI DESIGNED BY: SMI DATE: 5/24/2018 CONTACT: SMIBARRA@UW.EDU	

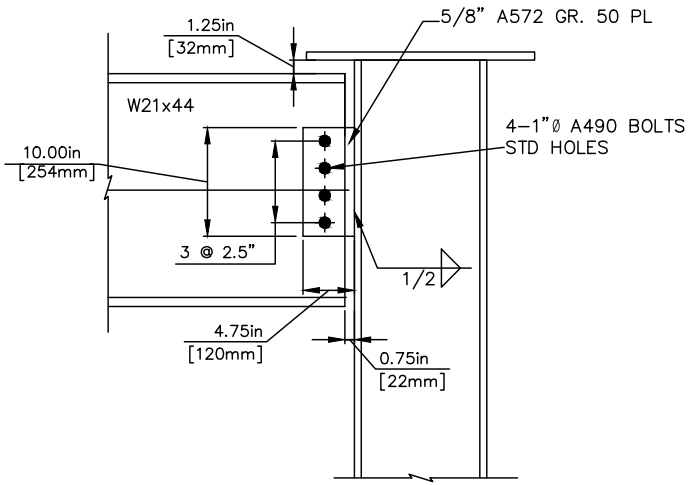

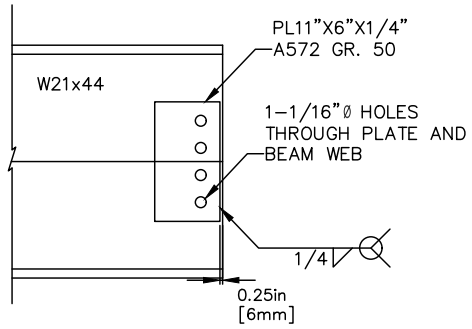

SHEAR TAB AND WEB DOUBLER

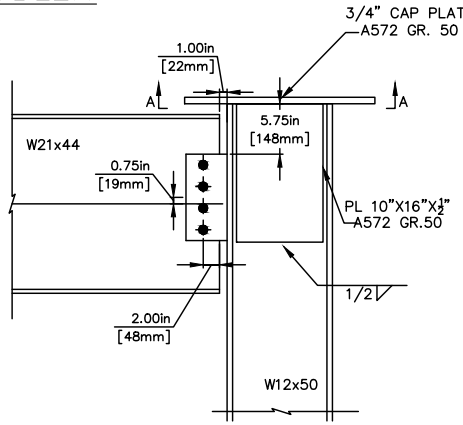

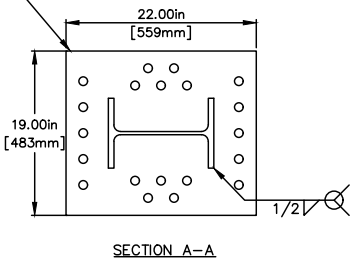

SECTION A–A

COLUMN DOUBLER AND CAP PLATE

W21 BEAM END CONNECTIONS	
SINGLE STORY SCBF WITH YIELDING BEAMS	DWG: SK-6
DRAWN BY: SMI DESIGNED BY: SMI DATE: 5/24/2018 CONTACT: SMIBARRA@UW.EDU	

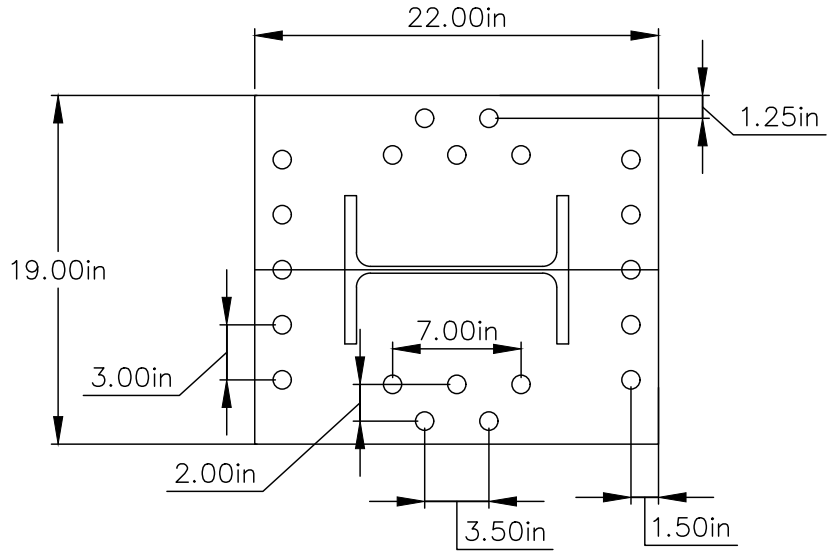

CAP PLATE DETAIL

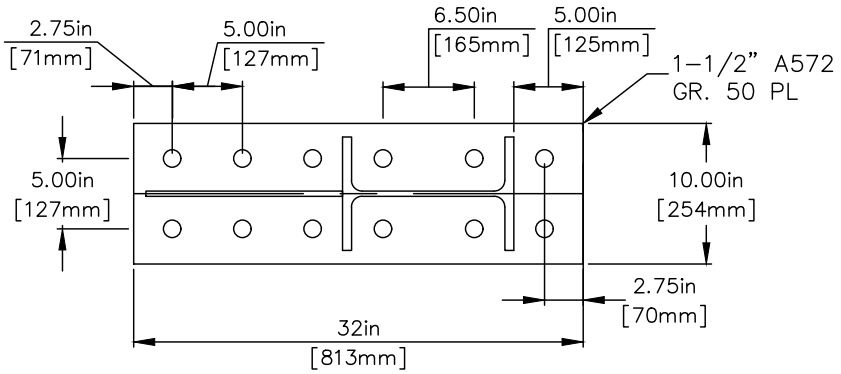

BASE PLATE DETAIL

BASE AND CAP PLATE DETAILS	
SINGLE STORY SCBF WITH YIELDING BEAMS	DWG: SK-7
DRAWN BY: SMI DESIGNED BY: SMI DATE: 5/24/2018 CONTACT: SMIBARRA@UW.EDU	

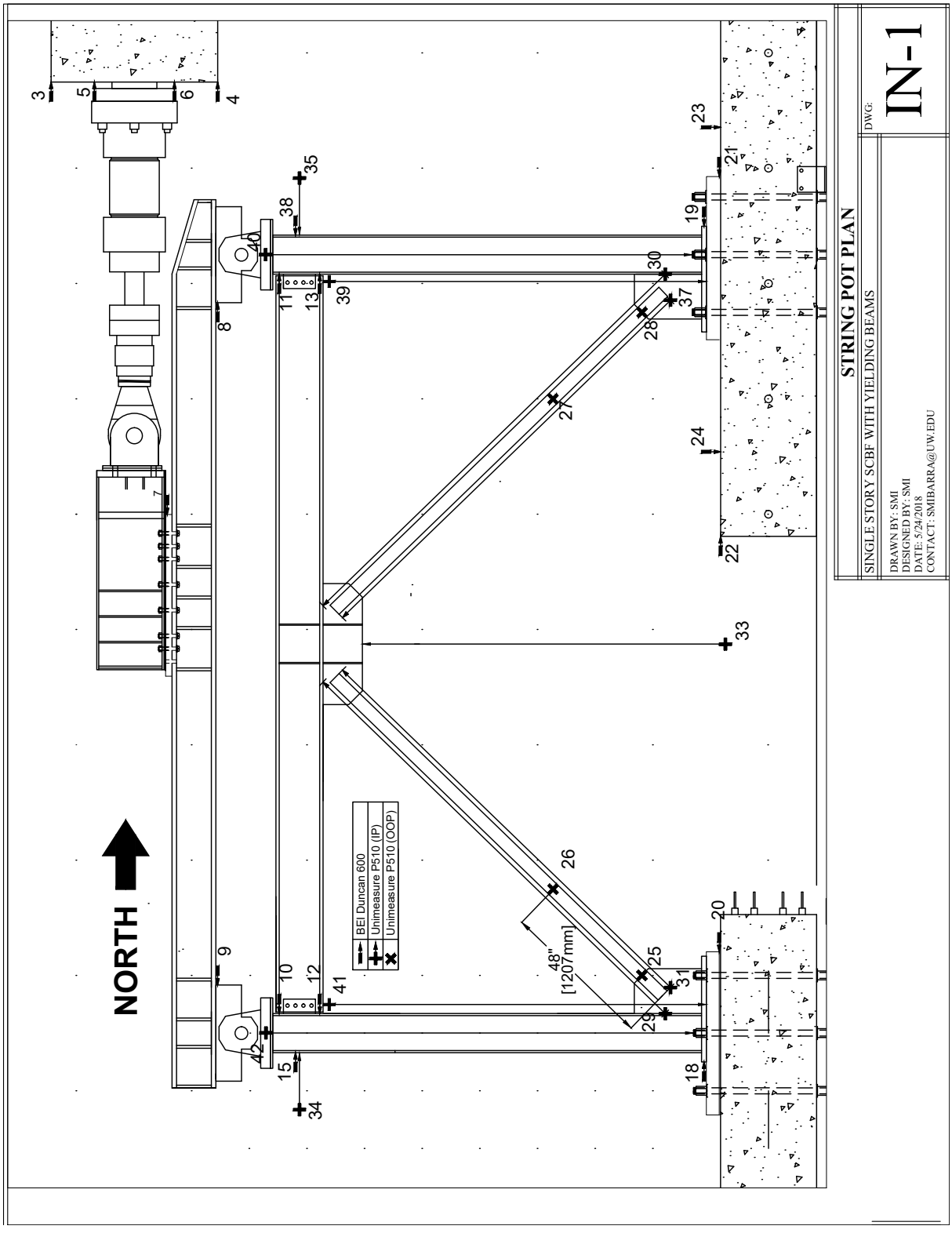
NORTH
BEI Duncan 600
Unimeasure P510 (IP)
Unimeasure P510 (OOP)
48"
[1207mm]
STRING POT PLAN
SINGLE STORY SCBF WITH YIELDING BEAMS
DRAWN BY: SMI
DESIGNED BY: SMI
DATE: 5/24/2018
CONTACT: SMIBARRA@UW.EDU
DWG:
IN-1

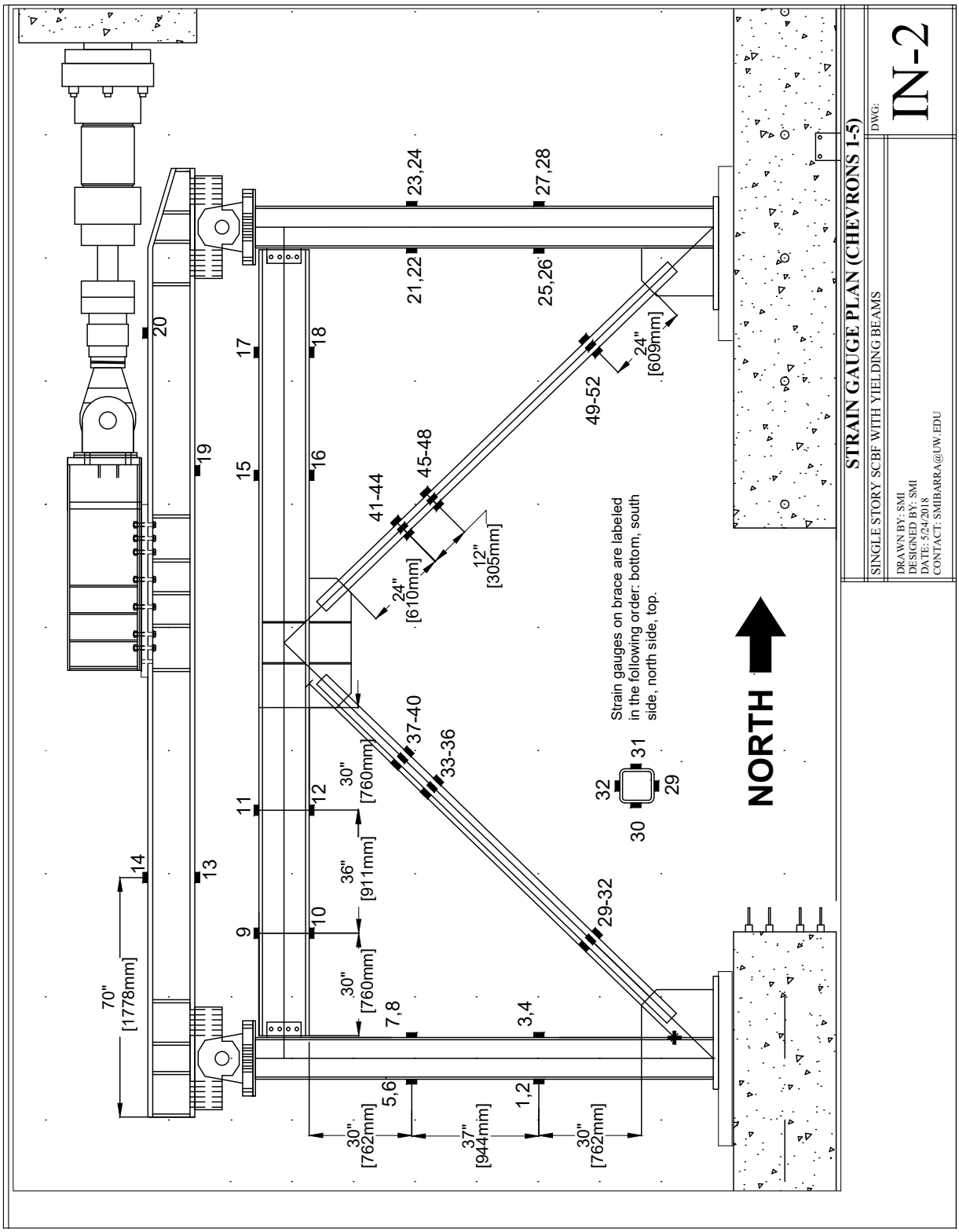
STRAIN GAUGE PLAN (CHEVRONS 1-5)
SINGLE STORY SCBF WITH YIELDING BEAMS
DRAWN BY: SMI
DESIGNED BY: SMI
DATE: 5/24/2018
CONTACT: SMIBARRA@UW.EDU
DWG:
IN-2
NORTH
Strain gauges on brace are labeled in the following order: bottom, south side, north side, top.
70" [1778mm]
30" [762mm]
37" [944mm]
30" [762mm]
30" [760mm]
36" [911mm]
30" [760mm]
24" [610mm]
12" [305mm]
24" [609mm]
1,2
3,4
5,6
7,8
9
10
11
12
13
14
15
16
17
18
19
20
21,22
23,24
25,26
27,28
29-32
33-36
37-40
41-44
45-48
49-52
29
30
31
32

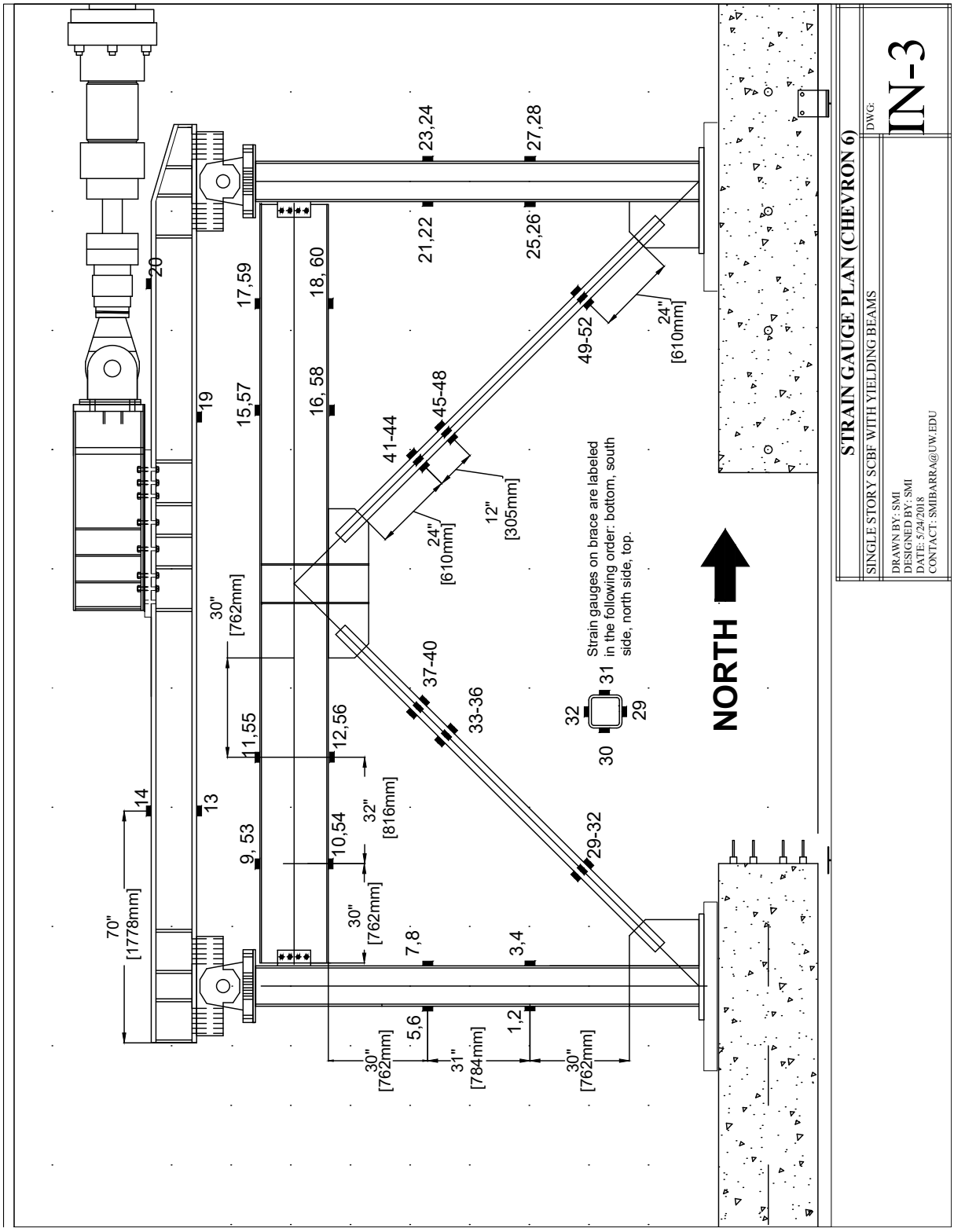
STRAIN GAUGE PLAN (CHEVRON 6)
SINGLE STORY SCBF WITH YIELDING BEAMS
DRAWN BY: SMI
DESIGNED BY: SMI
DATE: 5/24/2018
CONTACT: SMIBARRA@UW.EDU
DWG:
IN-3
NORTH
Strain gauges on brace are labeled in the following order: bottom, south side, north side, top.
70" [1778mm]
30" [762mm]
32" [816mm]
30" [762mm]
5,6
31" [784mm]
1,2
30" [762mm]
24" [610mm]
12" [305mm]
24" [610mm]
20
19
14
13
9, 53
10,54
11,55
12,56
15,57
16, 58
17,59
18, 60
21,22
23,24
25,26
27,28
7,8
3,4
29-32
33-36
37-40
41-44
45-48
49-52
30
31
32
29

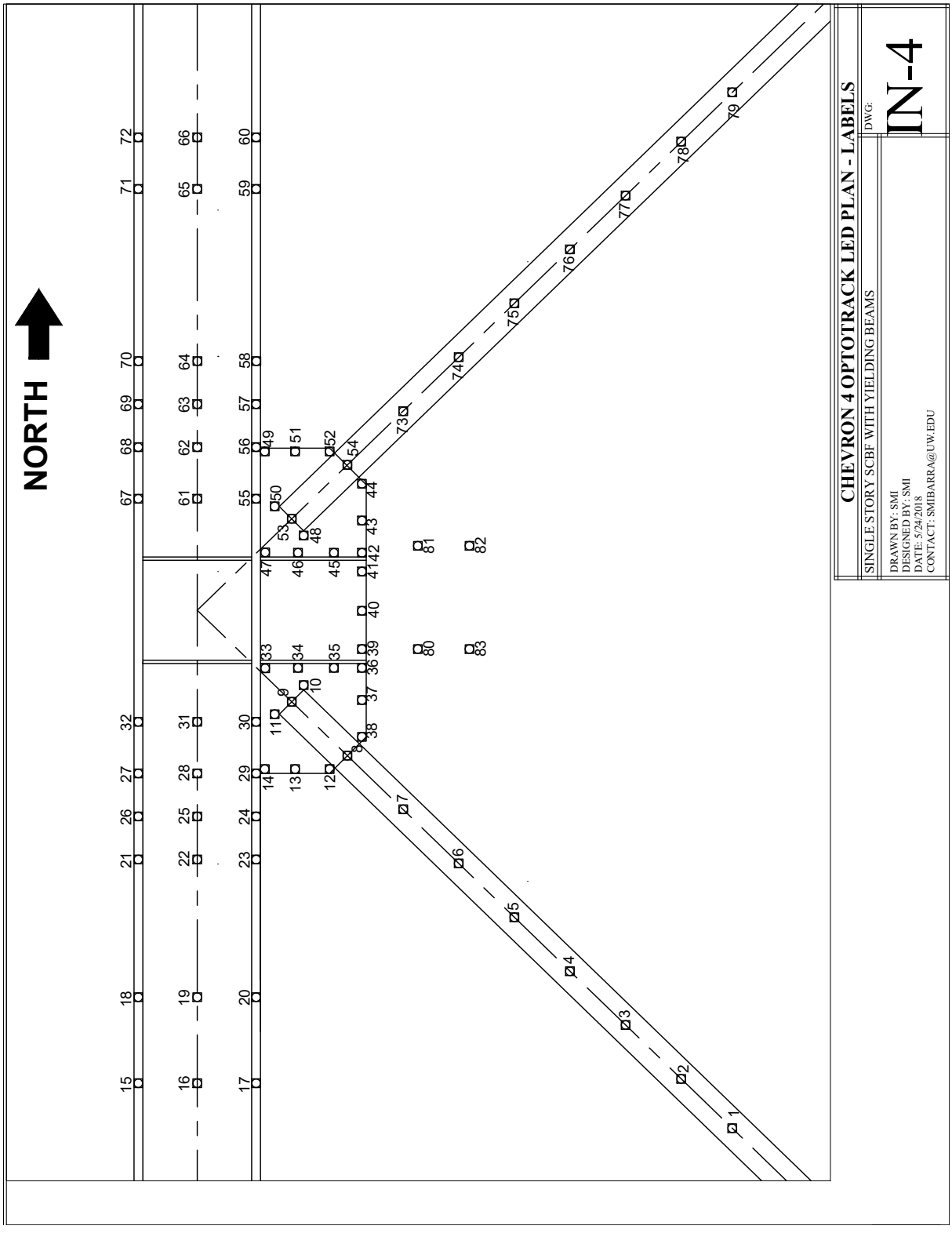
NORTH
CHEVRON 4 OPTOTRACK LED PLAN - LABELS
SINGLE STORY SCBF WITH YIELDING BEAMS
DRAWN BY: SMI
DESIGNED BY: SMI
DATE: 5/24/2018
CONTACT: SMIBARRA@UW.EDU
DWG:
IN-4

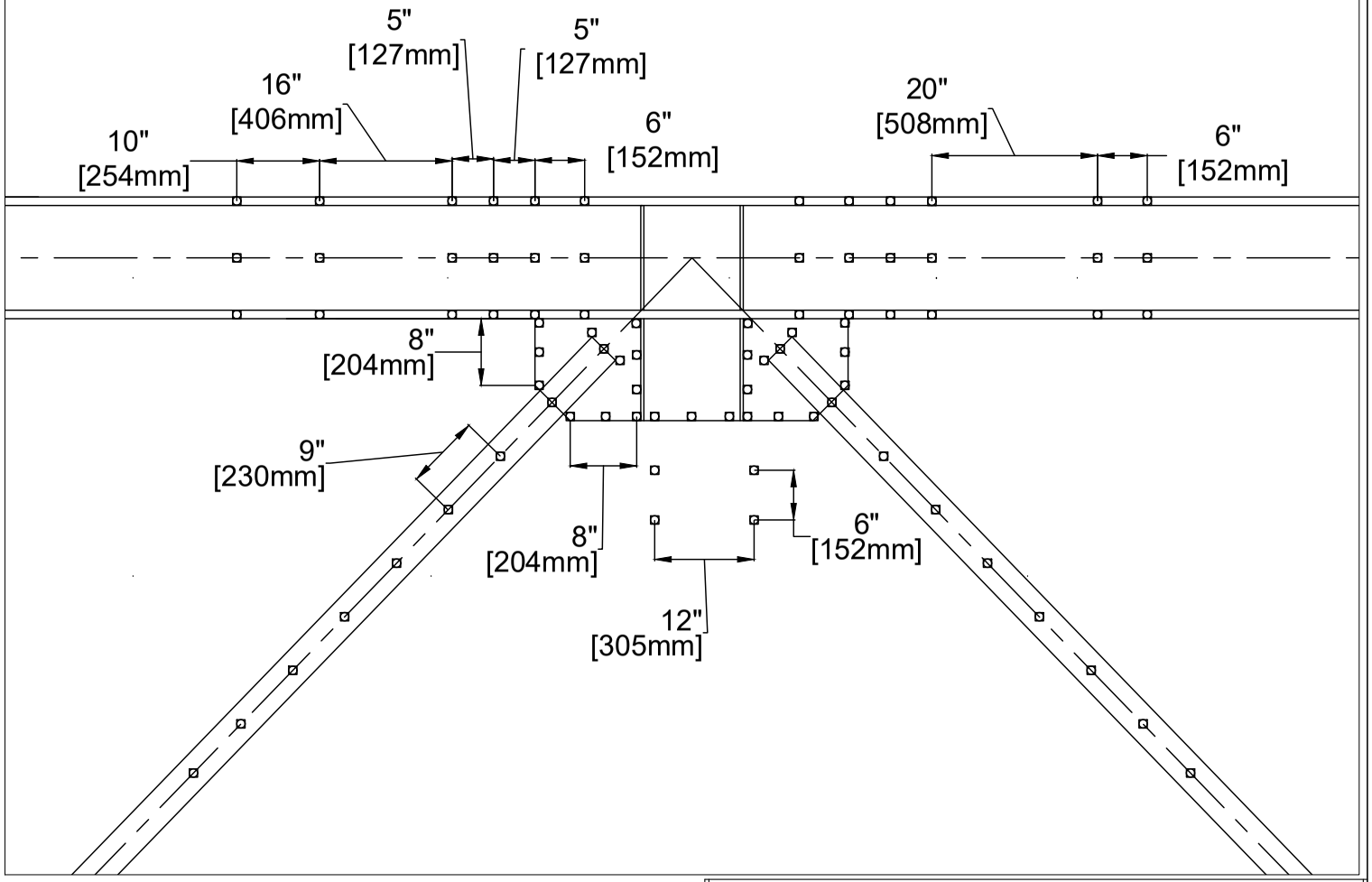

CHEVRON 4
OPTOTRAK LED PLAN

CHEVRON 4 OPTOTRACK LED PLAN - LOCATION

SINGLE STORY SCBF WITH YIELDING BEAMS

DWG: IN-5

DRAWN BY: SMI
DESIGNED BY: SMI
DATE: 5/24/2018
CONTACT: SMIBARRA@UW.EDU

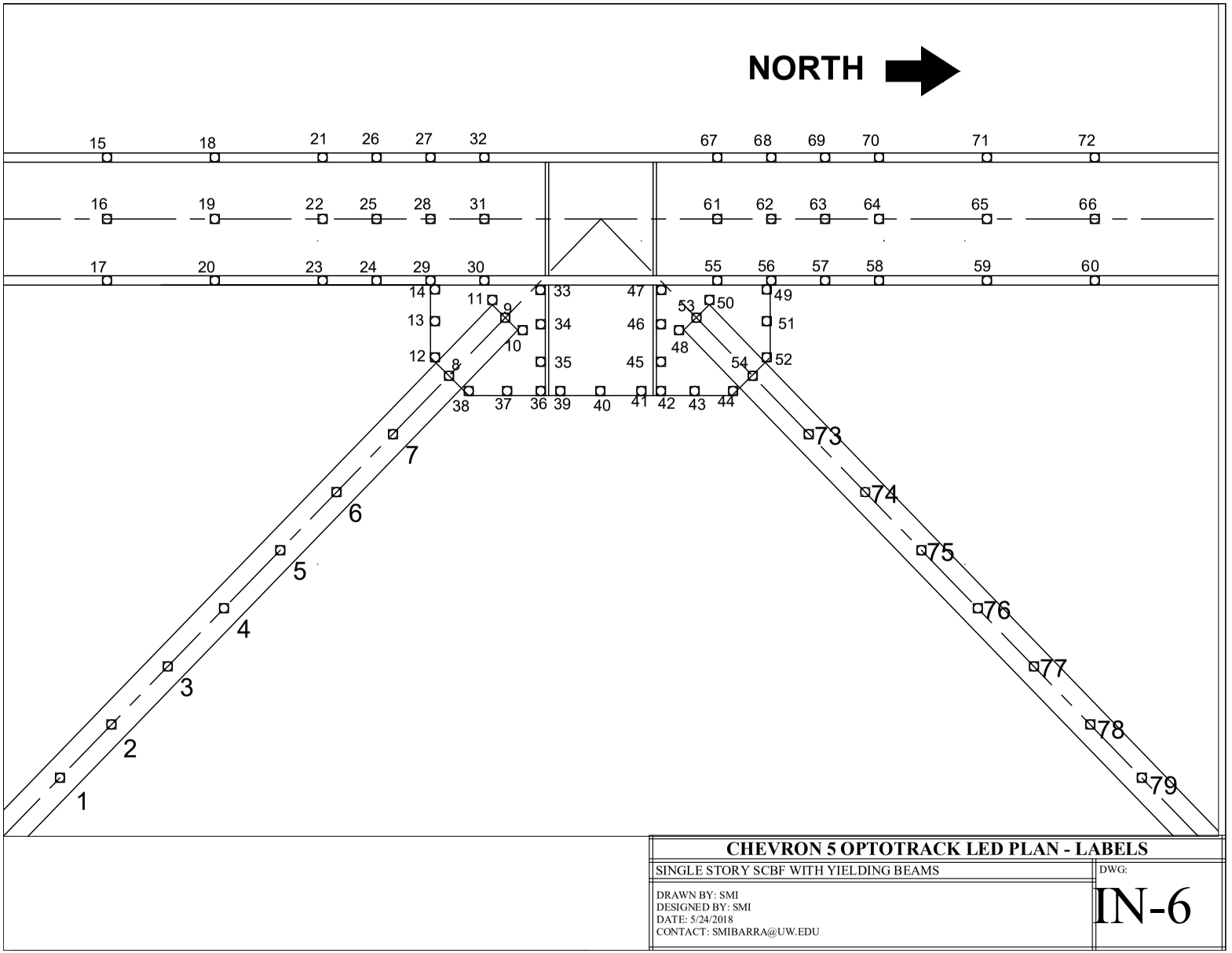

CHEVRON 5 OPTOTRACK LED PLAN - LABELS

SINGLE STORY SCBF WITH YIELDING BEAMS

DWG: IN-6

DRAWN BY: SMI
DESIGNED BY: SMI
DATE: 5/24/2018
CONTACT: SMIBARRA@UW.EDU

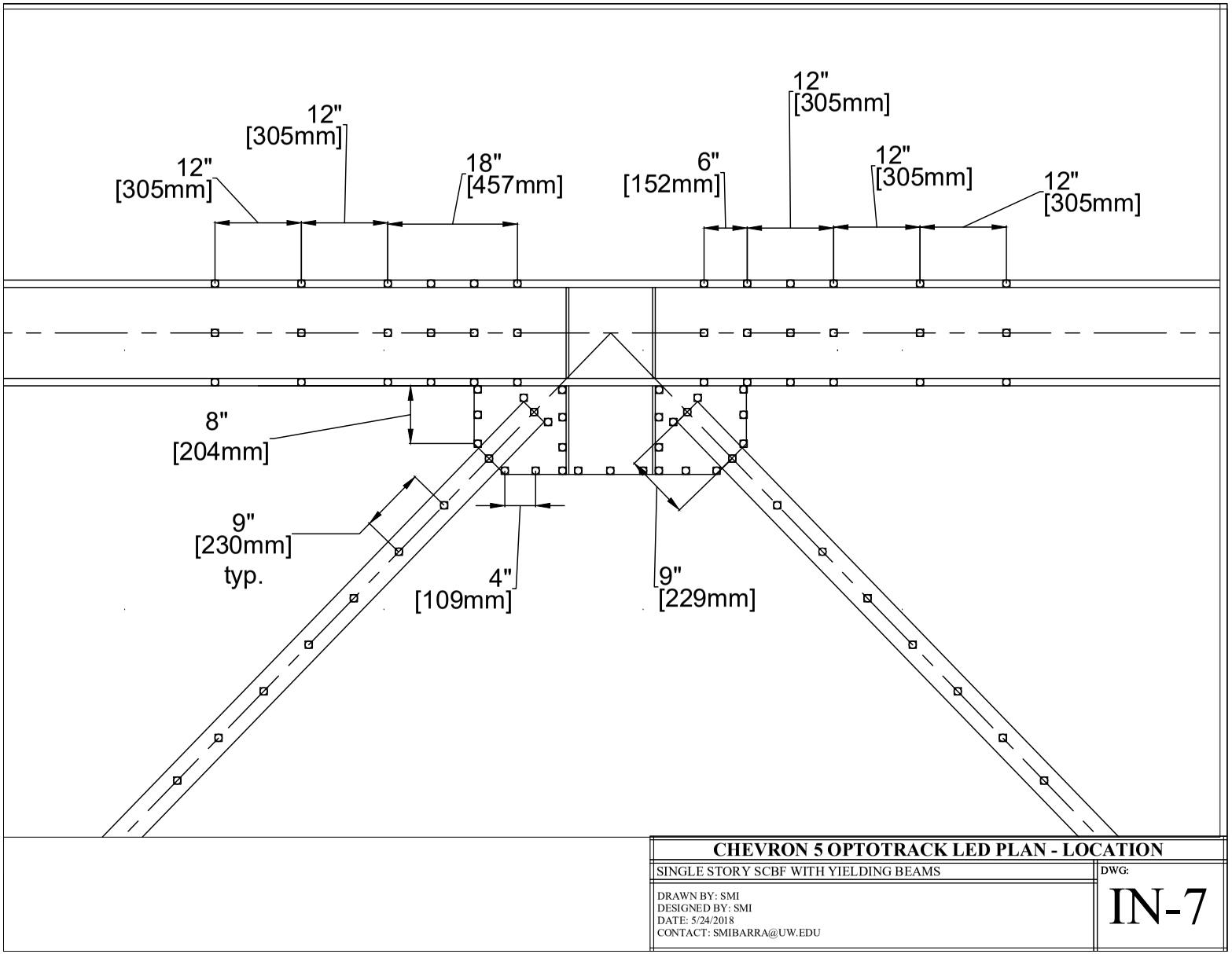

CHEVRON 5 OPTOTRACK LED PLAN - LOCATION

SINGLE STORY SCBF WITH YIELDING BEAMS

DWG: IN-7

DRAWN BY: SMI
DESIGNED BY: SMI
DATE: 5/24/2018
CONTACT: SMIBARRA@UW.EDU

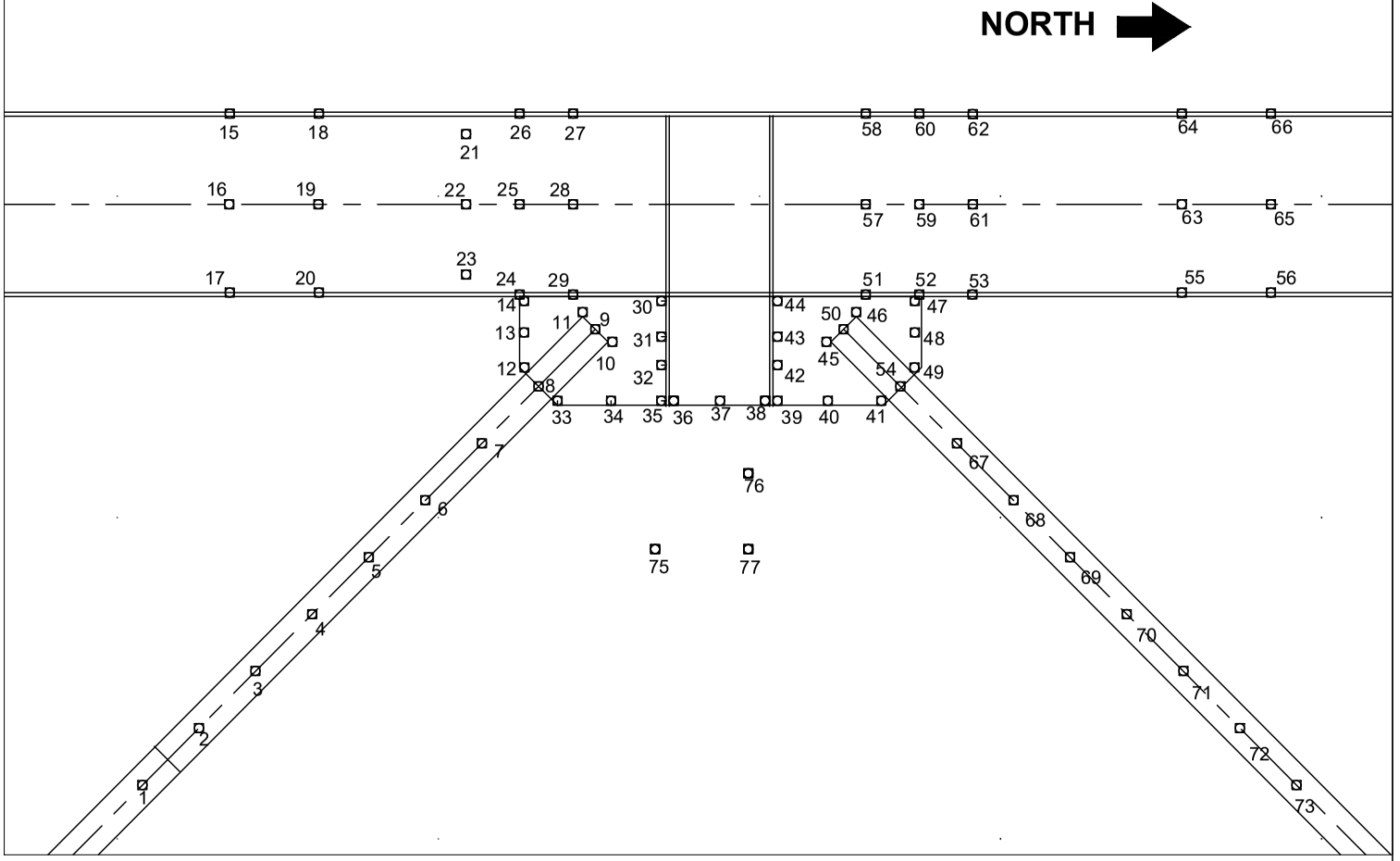

CHEVRON 6 OPTOTRACK LED PLAN - LABELS	
SINGLE STORY SCBF WITH YIELDING BEAMS	DWG: IN-8
DRAWN BY: SMI DESIGNED BY: SMI DATE: 5/24/2018 CONTACT: SMIBARRA@UW.EDU	

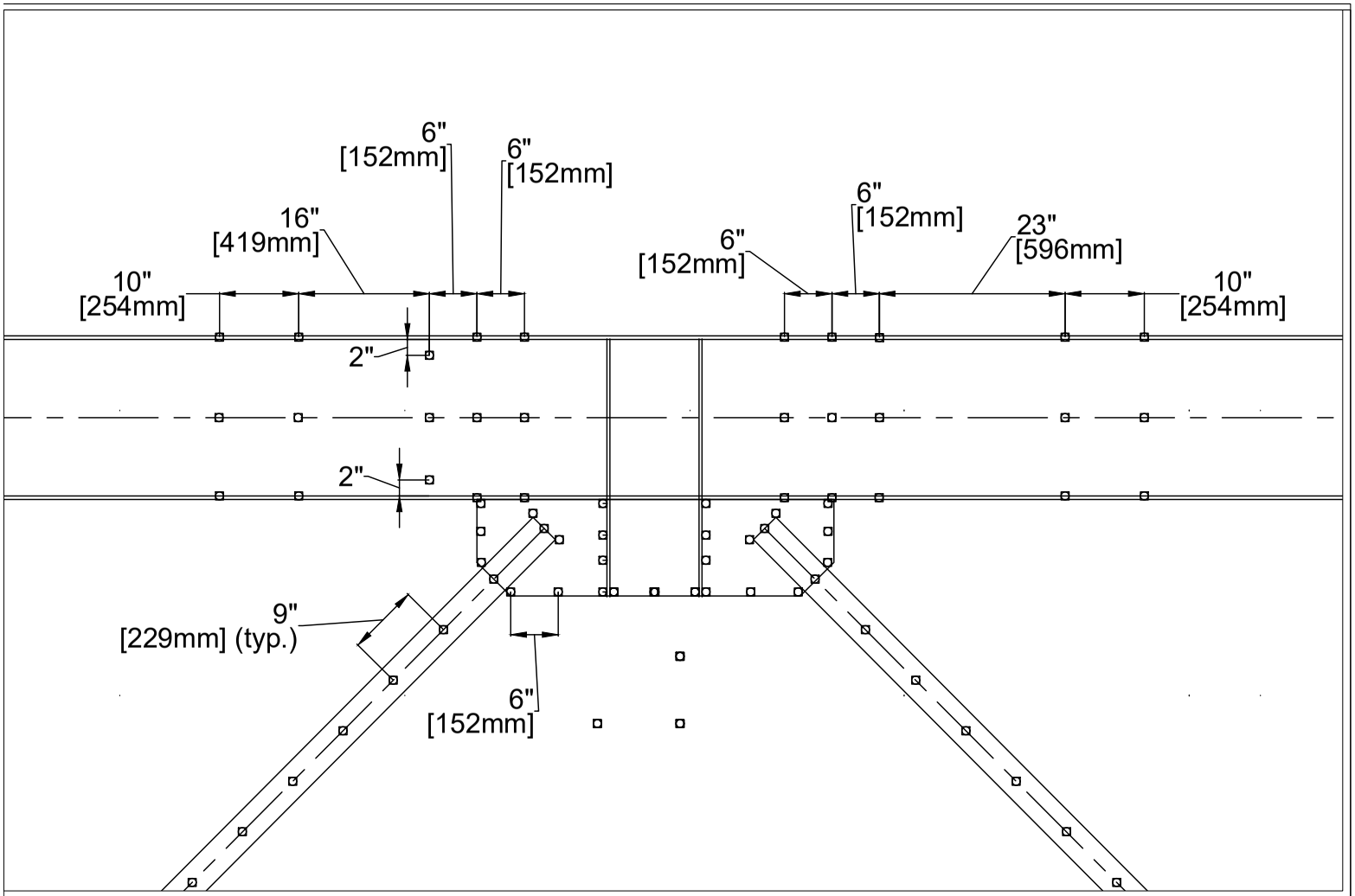

CHEVRON 6 OPTOTRACK LED PLAN - LOCATION

SINGLE STORY SCBF WITH YIELDING BEAMS

DWG: IN-9

DRAWN BY: SMI
DESIGNED BY: SMI
DATE: 5/24/2018
CONTACT: SMIBARRA@UW.EDU

Table B.1 String Pot index table for all single-story specimens

Label	Measurement	Labe	Measurement
1	Actuator Load	22	E Reaction Block Slip
2	Actuator Displacement	23	E Reaction Block Slip
3	N Reaction Block Slip W	24	E Reaction Block Slip
4	N Reaction Block Slip E	25	SE Gusset OOP Disp Displacement
5	Actuator Base Slip W	26	S Brace OOP Disp
6	Actuator Base Slip E	27	N Brace OOP Disp
7	Blue Beam Slip	28	NE Gusset OOP Disp
8	Clevis Slip N	29	S FL2FL Elongation
9	Clevis Slip S	30	N FL2FL Elongation
10	Beam End Rotation S	31	S Brace Elongation
11	Beam End Rotation N	32	n/a
12	Beam End Rotation S	33	Beam MidSpan Deflection
13	Beam End Rotation N	34	Frame Displacement S
14	n/a	35	Frame Displacement N
15	OOP restraint Slip S	36	n/a
16	n/a	37	N Brace Elongation
17	n/a	38	N OOP Restraint Slip
18	S Base Plate Slip	39	N Beam End Disp
19	N Base Plate Slip	40	N Col Elongation
20	S Interface Plate Slip	41	S Beam End Disp
21	N Interface Plate Slip	42	S Column Elongation

Table B.2 Strain Gauge Index (Chevrons 4 and 5)

Label	Location	Label	Location
1	S Col Bot Out 1	31	S Br Bot 31
2	S Col Bot Out 2	32	S Br Bot 32
3	S Col Bot In 3	33	S Br Mid 33
4	S Col Bot In 4	34	S Br Mid 34
5	S Col Top Out 5	35	S Br Mid 35
6	S Col Top Out 6	36	S Br Mid 36
7	S Col Top In 7	37	S Br Top 37
8	S Col Top In 8	38	S Br Top 38
9	Beam S TopFL 9	39	S Br Top 39
10	Beam S BotFL 10	40	S Br Top 40
11	Beam N TopFL	41	N Br Top 41
12	Beam SC BotFL 12	42	N Br Top 42
13	SprBeam S BotFL	43	N Br Top 43
14	SprBeam S Top FL	44	N Br Top 44
15	Beam NC Top FL 9	45	N Br Mid 45
16	Beam NC BotFL 10	46	N Br Mid 46
17	Beam N TopFL	47	N Br Mid 47
18	Beam N BotFL	48	N Br Mid 48
19	SprBeam S TopFL	49	N Br Bot 49
20	SprBeam N BotFL	50	N Br Bot 50
21	N Col Top In 21	51	N Br Bot 51
22	N Col Top In 22	52	N Br Bot 51
23	N Col Top Out 23		
24	N Col Top Out 24		
25	N Col Bot In 25		
26	N Col Bot In 26		
27	N Col Bot Out 27		
28	N Col Bot Out 28		
29	S Br Bot 29		
30	S Br Bot 30		

Table B.3 Strain Gauge Index (Chevron 6)

Label	Location	Label	Location
1	S Col Bot Out 1	31	S Br Bot 31
2	S Col Bot Out 2	32	S Br Bot 32
3	S Col Bot In 3	33	S Br Mid 33
4	S Col Bot In 4	34	S Br Mid 34
5	S Col Top Out 5	35	S Br Mid 35
6	S Col Top Out 6	36	S Br Mid 36
7	S Col Top In 7	37	S Br Top 37
8	S Col Top In 8	38	S Br Top 38
9	Beam S TopFL 9	39	S Br Top 39
10	Beam S BotFL 10	40	S Br Top 40
11	Beam N TopFL	41	N Br Top 41
12	Beam SC BotFL 12	42	N Br Top 42
13	SprBeam S BotFL	43	N Br Top 43
14	SprBeam S Top FL	44	N Br Top 44
15	Beam NC Top FL 9	45	N Br Mid 45
16	Beam NC BotFL 10	46	N Br Mid 46
17	Beam N TopFL	47	N Br Mid 47
18	Beam N BotFL	48	N Br Mid 48
19	SprBeam S TopFL	49	N Br Bot 49
20	SprBeam N BotFL	50	N Br Bot 50
21	N Col Top In 21	51	N Br Bot 51
22	N Col Top In 22	52	N Br Bot 51
23	N Col Top Out 23	53	Beam S TopFL 53
24	N Col Top Out 24	54	Beam S BotFL 54
25	N Col Bot In 25	55	Beam SC TopFL 55
26	N Col Bot In 26	56	Beam SC BotFL 56
27	N Col Bot Out 27	57	Beam N TopFL 57
28	N Col Bot Out 28	58	Beam N BotFL 58
29	S Br Bot 29	59	Beam NC TopFL 59
30	S Br Bot 30	60	Beam NC BotFL 60

B.1.2 General Test Setup

The general test setup was designed by Terpstra(2017) to test single-story chevron SCBFs at the University of Washington Structures Research Lab.

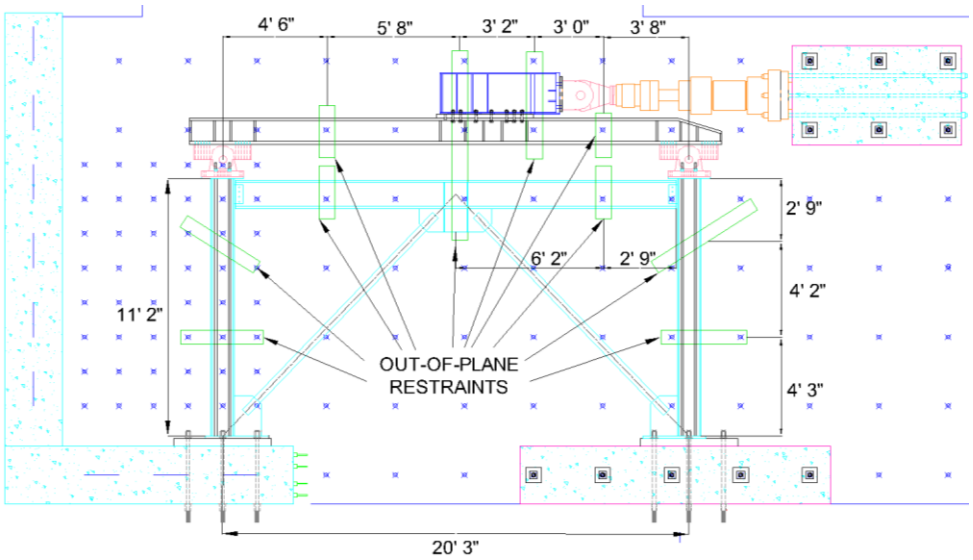

Figure B.1 Original OOP restraint arrangement (Terpstra 2017)

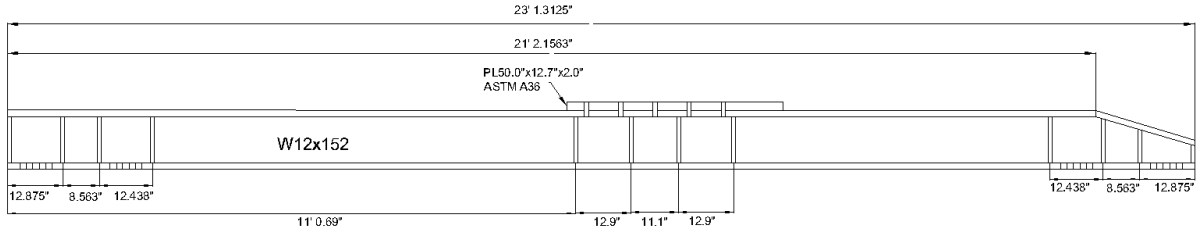

(a)

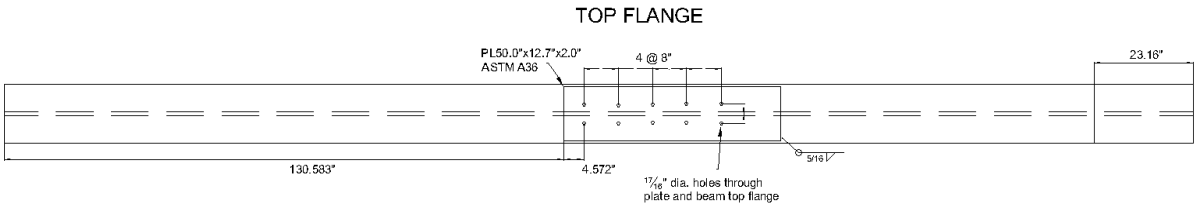

(b)

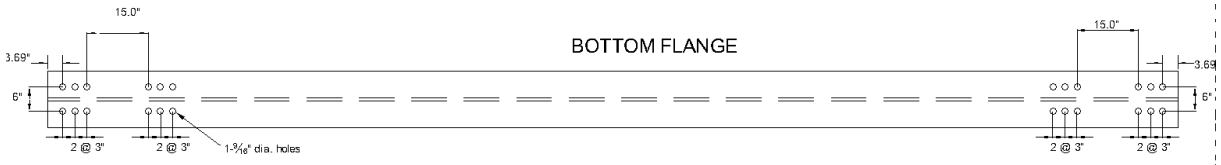

(c)

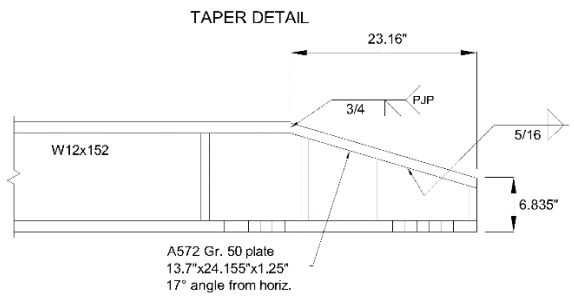

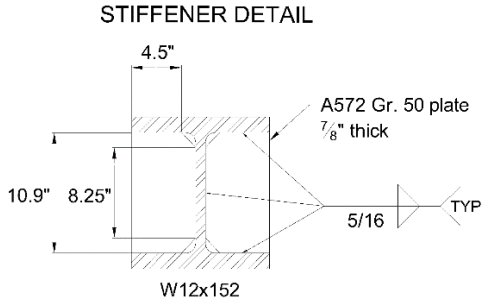

(d) (e)

Figure B.2 Load spreader beam details (Terpstra 2017)

B.2 Multi-Story Frame Drawings

The specimen drawings for Chevron 7 are found below. This was the fourth specimen tested by the author and only specimen of the series tested at NCREE so more detailed construction and instrumentation drawings are provided.

B.2.1 Construction and Instrumentation Drawings

DRAWING INDEX:

NOTES:

1. HSS5x5x1/2 BRACES TO BE A1085 OR EQUIVALENT
2. ALL ROLLED SHAPES TO BE A992 OR EQUIVALENT
3. ALL BOLTS TO BE A490 OR EQUIVALENT WITH THREADS EXCLUDED FROM THE SHEAR PLANE
4. ALL PLATE STEEL TO BE A572 GR 50 OR EQUIVALENT
5. FIRST AND SECOND FLOOR SLAB CONCRETE TO HAVE STRENGTH OF f'c=5000psi
6. TOP FLOOR SLAB TO HAVE STRENGTH OF f'c=5000psi AND CONCRETE TO INCLUDE 0.5% GLASS FIBER REINFORCING
7. ALL WELDS AT GUSSET PLATE, HSS BRACES, BEAM TO COLUMN, AND BEAM TO BASE PLATE CONNECTIONS TO SATISFY AISC DEMAND CRITICAL REQUIREMENT (EQUIVALENT TO E7018, E71-T1, OR E71-T8)
8. WELDS AT TRANSFER BEAMS CONNECTIONS MAY USE E70 ELECTRODE
9. ALL UNITS IN MILLIMETERS UNLESS OTHERWISE NOTED

SCALE:

GENERAL NOTES	
MULTI STORY SCBF WITH YIELDING BEAMS	DWG: SK-0
DRAWN BY: SMI DESIGNED BY: SMI DATE: 1/17/2018 CONTACT: SMIBARRA@UW.EDU	

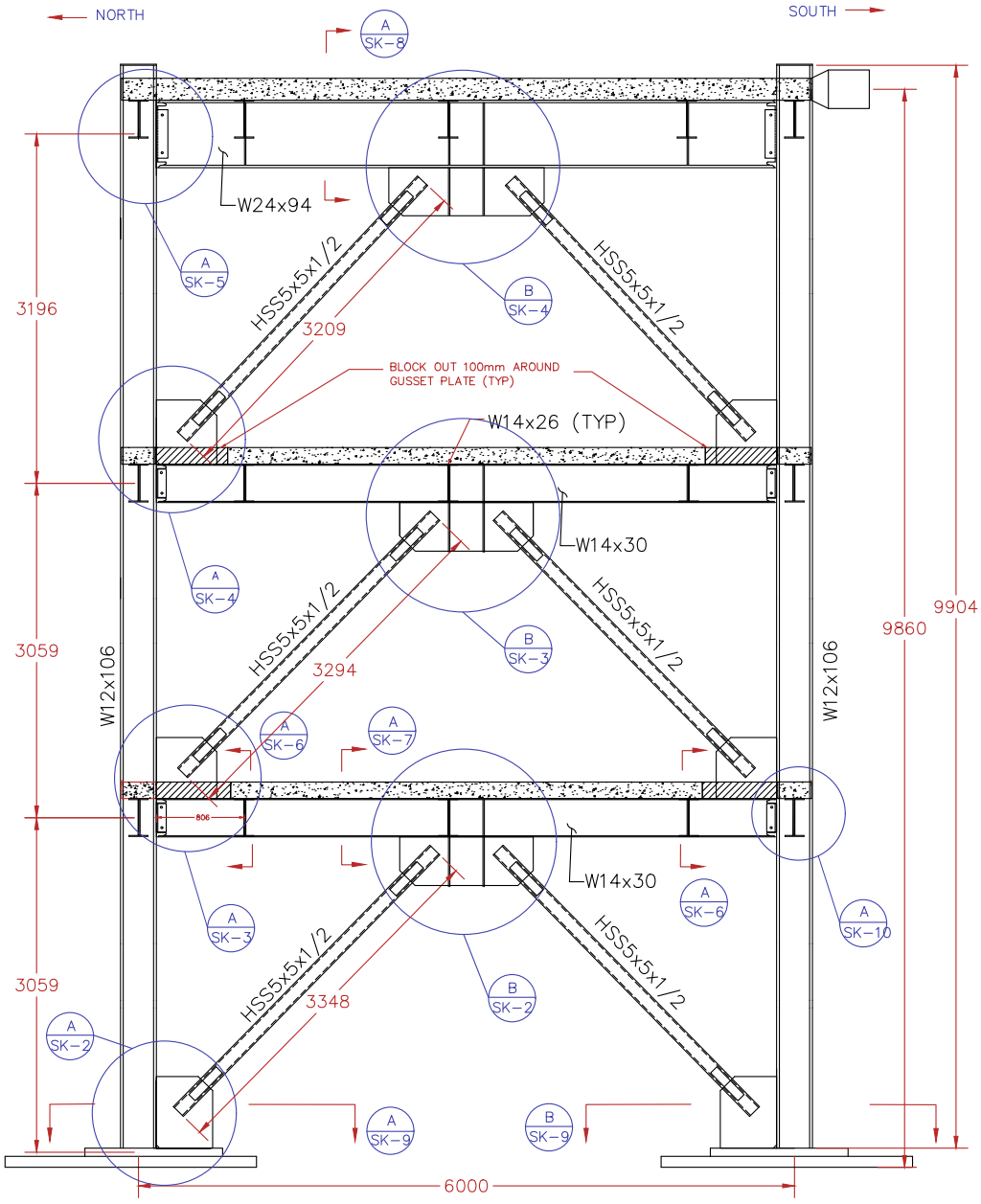

SCALE: 1mm = 50mm

SCBF ELEVATION WITH W14X30 BEAMS	
MULTI STORY SCBF WITH YIELDING BEAMS	DWG: SK-1
DRAWN BY: SMI DESIGNED BY: SMI DATE: 1/17/2018 CONTACT: SMIBARRA@UW.EDU	

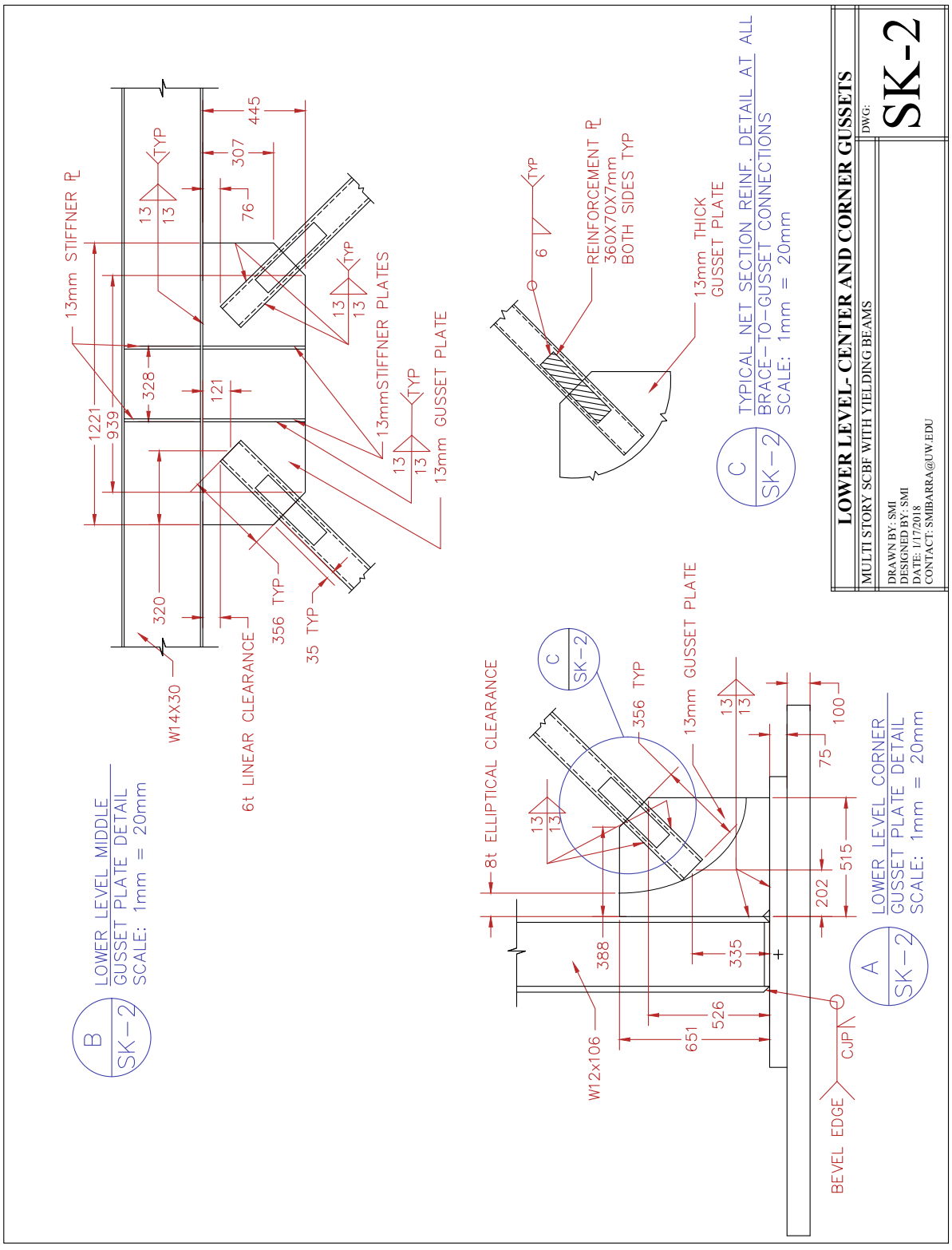
LOWER LEVEL- CENTER AND CORNER GUSSETS
MULTI STORY SCBF WITH YIELDING BEAMS
DRAWN BY: SMI
DESIGNED BY: SMI
DATE: 1/17/2018
CONTACT: SMIBARRA@UW.EDU
DWG:
SK-2
B SK-2 LOWER LEVEL MIDDLE GUSSET PLATE DETAIL SCALE: 1mm = 20mm
13mm STIFFNER PL
W14X30
6t LINEAR CLEARANCE
356 TYP
35 TYP
13mmSTIFFNER PLATES
13mm GUSSET PLATE
TYP
1221
939
328
121
320
445
307
76
13
C SK-2 TYPICAL NET SECTION REINF. DETAIL AT ALL BRACE-TO-GUSSET CONNECTIONS SCALE: 1mm = 20mm
REINFORCEMENT PL 360X70X7mm BOTH SIDES TYP
13mm THICK GUSSET PLATE
6
A SK-2 LOWER LEVEL CORNER GUSSET PLATE DETAIL SCALE: 1mm = 20mm
8t ELLIPTICAL CLEARANCE
W12x106
BEVEL EDGE
CJP
356 TYP
13mm GUSSET PLATE
388
651
526
335
202
515
75
100

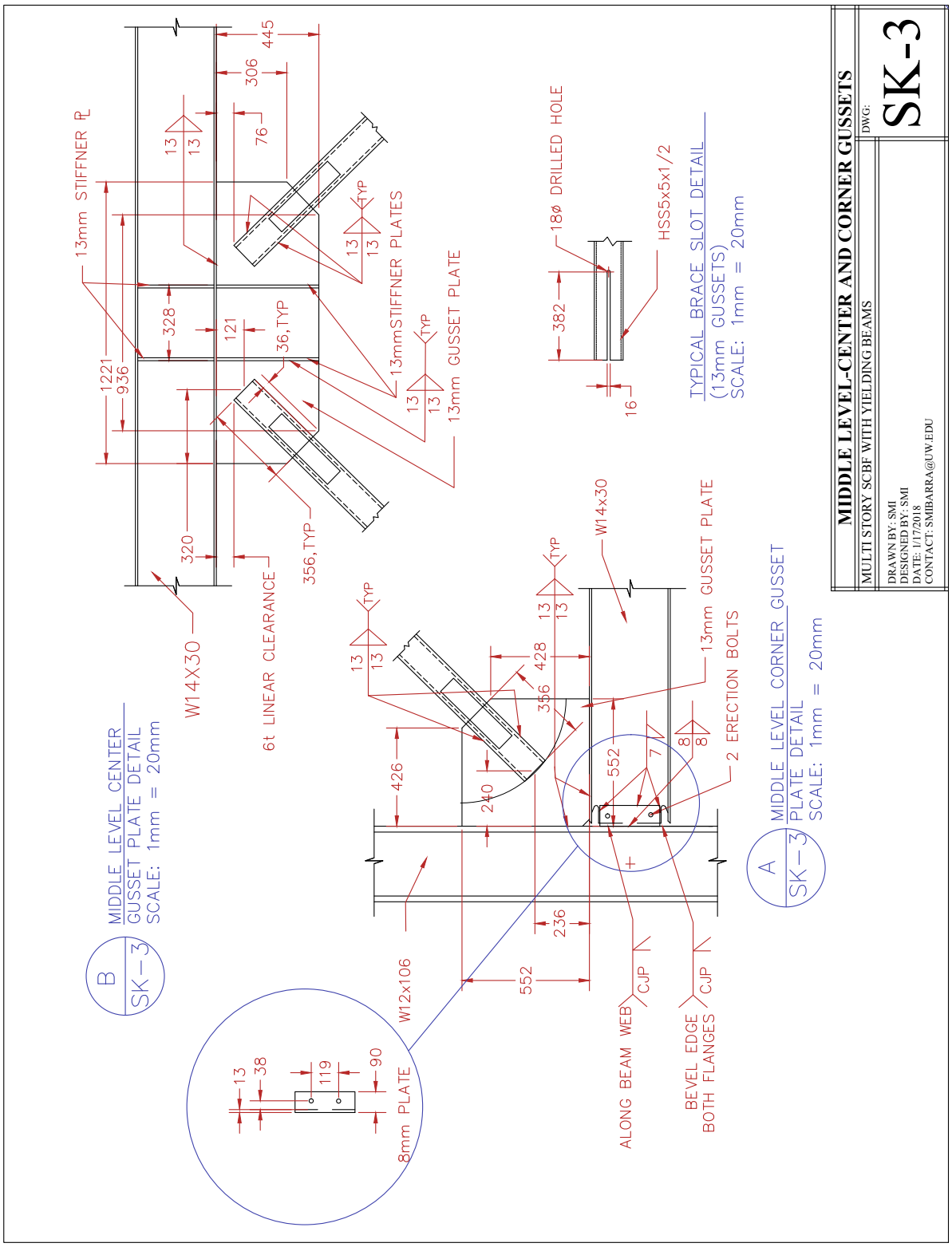
MIDDLE LEVEL-CENTER AND CORNER GUSSETS
MULTI STORY SCBF WITH YIELDING BEAMS
DWG: SK-3
DRAWN BY: SMI
DESIGNED BY: SMI
DATE: 1/17/2018
CONTACT: SMIBARRA@UW.EDU
13mm STIFFNER PL
W14X30
6t LINEAR CLEARANCE
356,TYP
13mmSTIFFNER PLATES
13mm GUSSET PLATE
18ø DRILLED HOLE
HSS5x5x1/2
TYPICAL BRACE SLOT DETAIL
(13mm GUSSETS)
SCALE: 1mm = 20mm
W14x30
13mm GUSSET PLATE
2 ERECTION BOLTS
W12x106
8mm PLATE
ALONG BEAM WEB
BEVEL EDGE
BOTH FLANGES
CJP
B
SK-3
MIDDLE LEVEL CENTER
GUSSET PLATE DETAIL
SCALE: 1mm = 20mm
A
SK-3
MIDDLE LEVEL CORNER GUSSET
PLATE DETAIL
SCALE: 1mm = 20mm

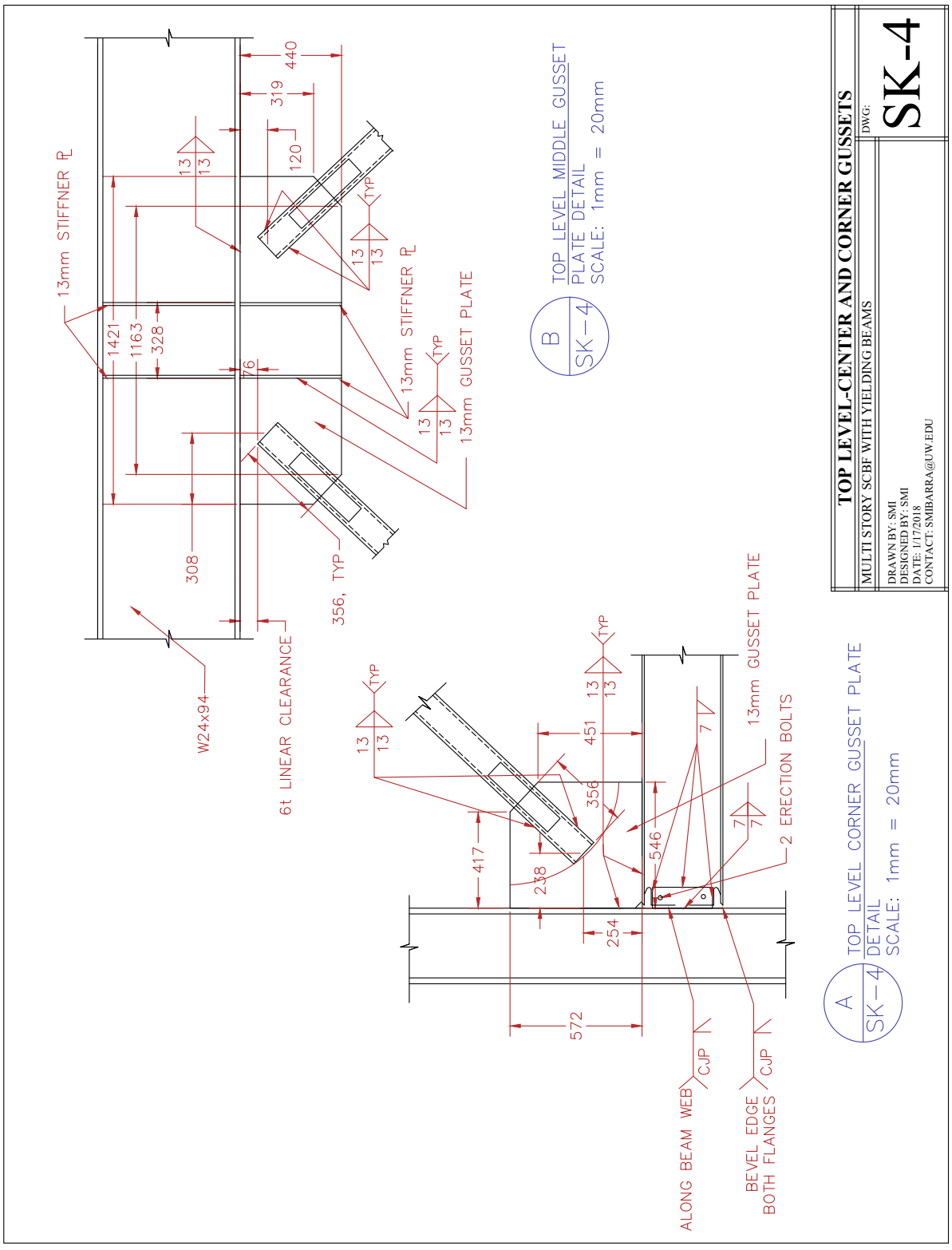
13mm STIFFNER PL
W24x94
6t LINEAR CLEARANCE
356, TYP
13mm STIFFNER PL
13mm GUSSET PLATE
TYP
13
13
440
319
120
1421
1163
328
308
76
B
SK-4
TOP LEVEL MIDDLE GUSSET
PLATE DETAIL
SCALE: 1mm = 20mm
451
356
417
238
254
572
546
7
2 ERECTION BOLTS
13mm GUSSET PLATE
ALONG BEAM WEB
CJP
BEVEL EDGE
BOTH FLANGES
CJP
A
SK-4
TOP LEVEL CORNER GUSSET PLATE
DETAIL
SCALE: 1mm = 20mm
TOP LEVEL-CENTER AND CORNER GUSSETS
MULTI STORY SCBF WITH YIELDING BEAMS
DRAWN BY: SMI
DESIGNED BY: SMI
DATE: 1/17/2018
CONTACT: SMIBARRA@UW.EDU
DWG:
SK-4

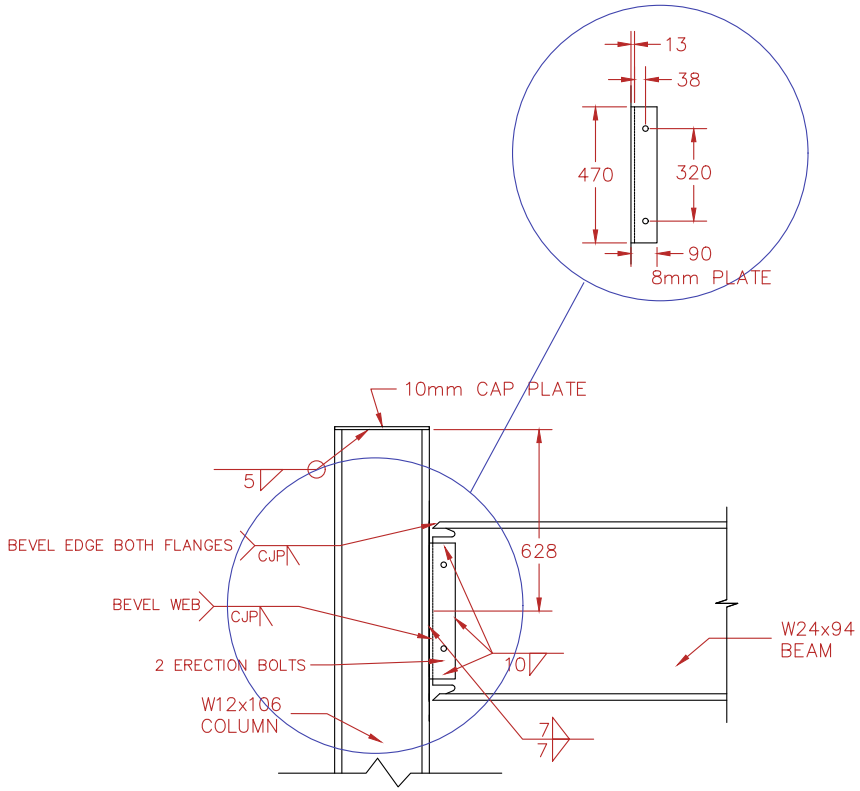

A
SK–5

TOP STORY CJP DETAIL
SCALE: 1mm = 20mm

TOP STORY COLUMN-TO-BEAM CONNECTION	
MULTI STORY SCBF WITH YIELDING BEAMS	DWG: SK-5
DRAWN BY: SMI DESIGNED BY: SMI DATE: 1/17/2018 CONTACT: SMIBARRA@UW.EDU	

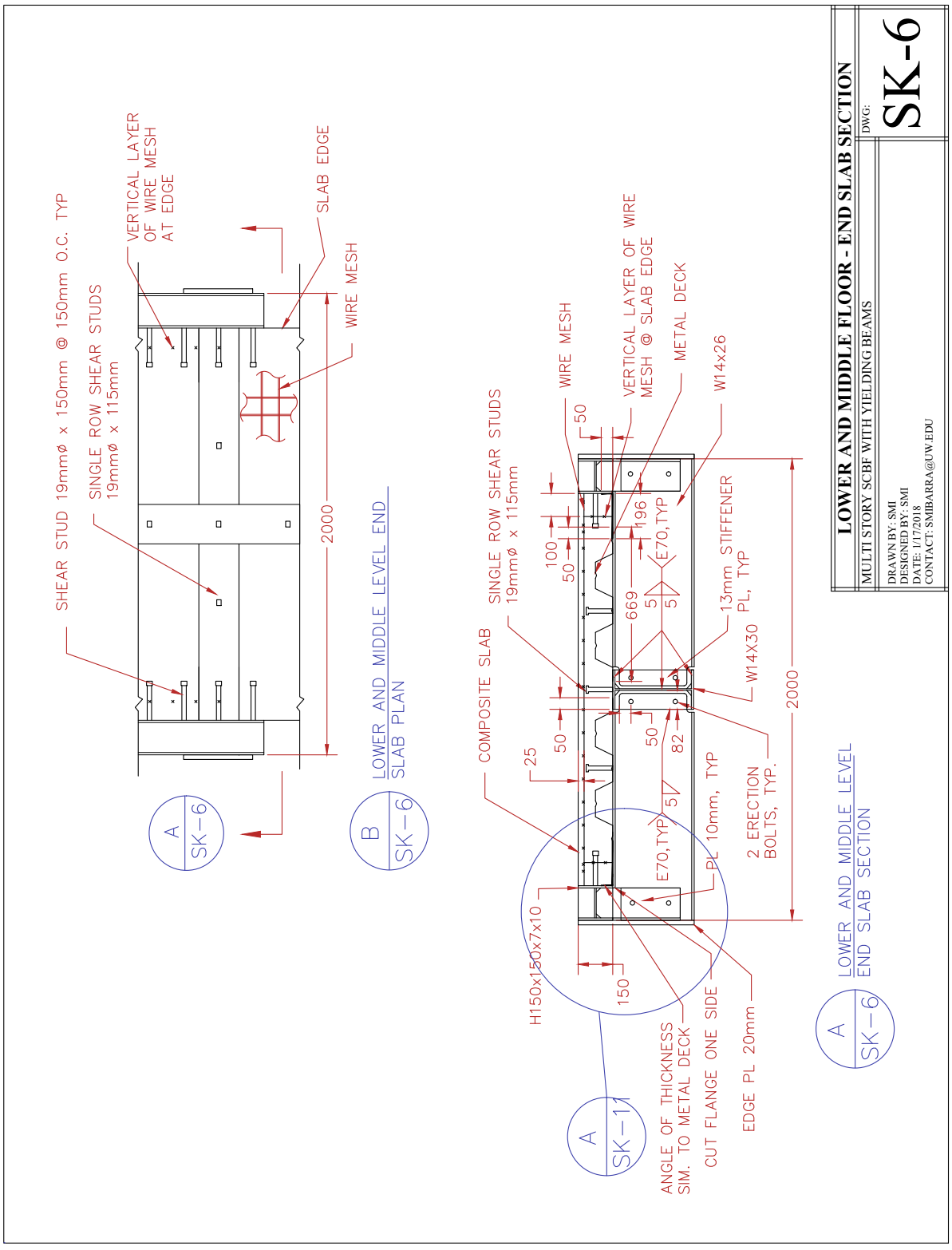
SHEAR STUD 19mmø x 150mm @ 150mm O.C. TYP
SINGLE ROW SHEAR STUDS 19mmø x 115mm
VERTICAL LAYER OF WIRE MESH AT EDGE
SLAB EDGE
WIRE MESH
2000
A SK-6
B SK-6
LOWER AND MIDDLE LEVEL END SLAB PLAN
COMPOSITE SLAB
SINGLE ROW SHEAR STUDS 19mmø x 115mm
WIRE MESH
VERTICAL LAYER OF WIRE MESH @ SLAB EDGE
METAL DECK
W14x26
13mm STIFFENER PL, TYP
W14X30
2000
2 ERECTION BOLTS, TYP.
PL 10mm, TYP
EDGE PL 20mm
CUT FLANGE ONE SIDE
ANGLE OF THICKNESS SIM. TO METAL DECK
H150x150x7x10
A SK-11
A SK-6
LOWER AND MIDDLE LEVEL END SLAB SECTION
25
50
100
196
669
82
E70, TYP
150
LOWER AND MIDDLE FLOOR - END SLAB SECTION
MULTI STORY SCBF WITH YIELDING BEAMS
DRAWN BY: SMI
DESIGNED BY: SMI
DATE: 1/17/2018
CONTACT: SMIBARRA@UW.EDU
DWG:
SK-6

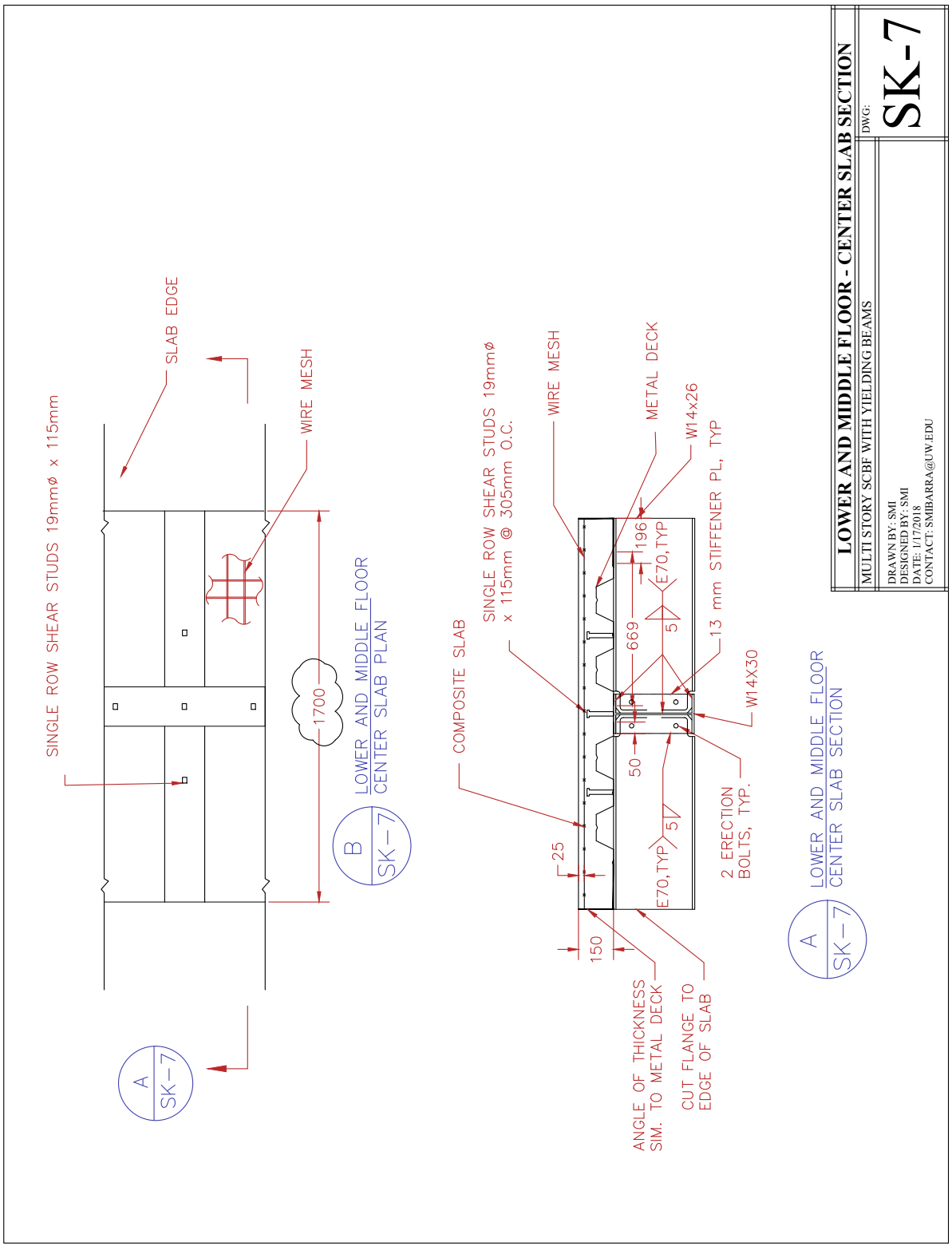
SINGLE ROW SHEAR STUDS 19mmø x 115mm
SLAB EDGE
WIRE MESH
1700
B
SK-7
LOWER AND MIDDLE FLOOR
CENTER SLAB PLAN
A
SK-7
COMPOSITE SLAB
SINGLE ROW SHEAR STUDS 19mmø
x 115mm @ 305mm O.C.
WIRE MESH
METAL DECK
W14x26
13 mm STIFFENER PL, TYP
W14X30
2 ERECTION
BOLTS, TYP.
196
669
50
25
150
5
E70, TYP
ANGLE OF THICKNESS
SIM. TO METAL DECK
CUT FLANGE TO
EDGE OF SLAB
A
SK-7
LOWER AND MIDDLE FLOOR
CENTER SLAB SECTION
LOWER AND MIDDLE FLOOR - CENTER SLAB SECTION
MULTI STORY SCBF WITH YIELDING BEAMS
DRAWN BY: SMI
DESIGNED BY: SMI
DATE: 1/17/2018
CONTACT: SMIBARRA@UW.EDU
DWG:
SK-7

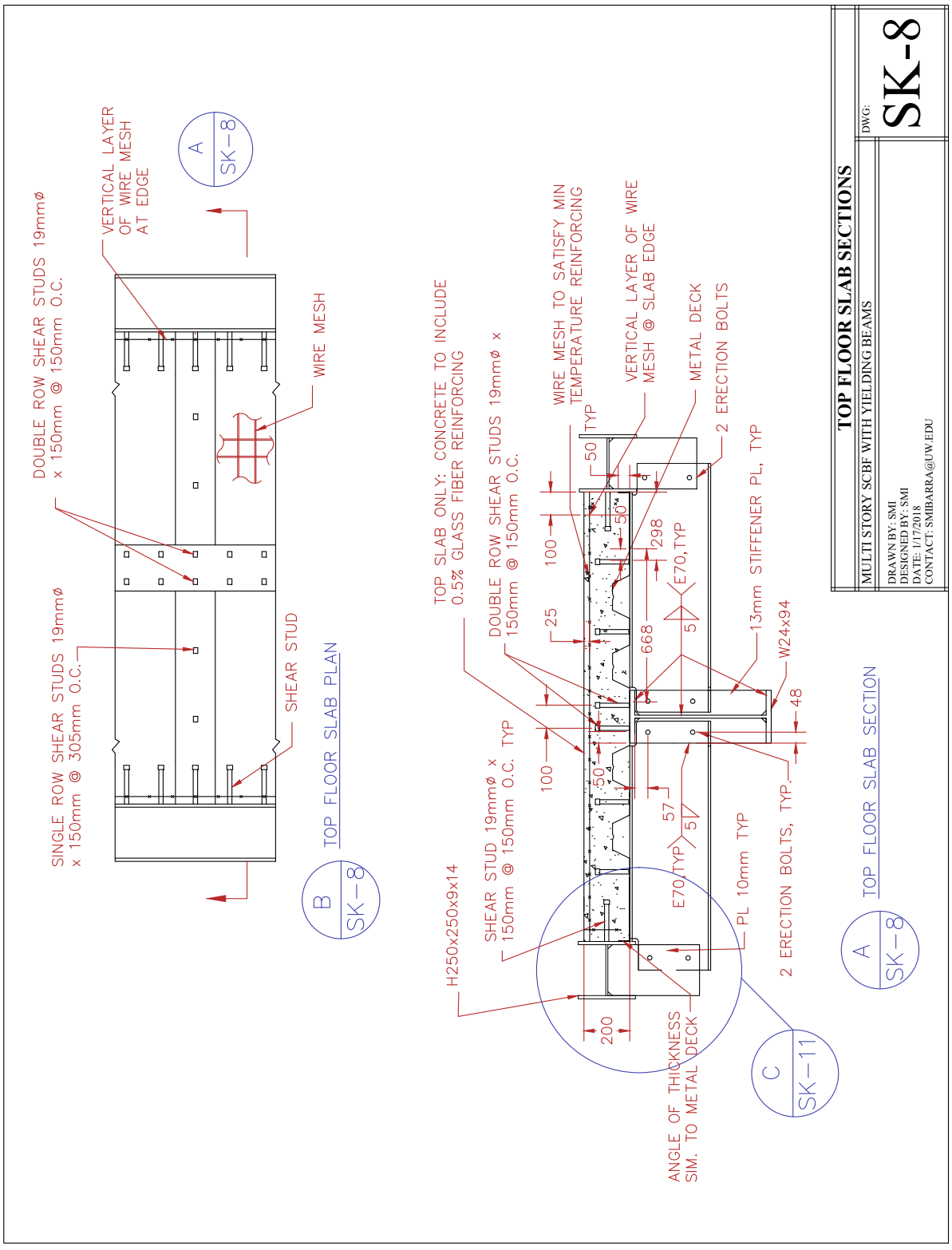
DOUBLE ROW SHEAR STUDS 19mmø
x 150mm @ 150mm O.C.
VERTICAL LAYER
OF WIRE MESH
AT EDGE
A
SK-8
SINGLE ROW SHEAR STUDS 19mmø
x 150mm @ 305mm O.C.
WIRE MESH
SHEAR STUD
B
SK-8
TOP FLOOR SLAB PLAN
TOP SLAB ONLY: CONCRETE TO INCLUDE
0.5% GLASS FIBER REINFORCING
DOUBLE ROW SHEAR STUDS 19mmø x
150mm @ 150mm O.C.
WIRE MESH TO SATISFY MIN
TEMPERATURE REINFORCING
VERTICAL LAYER OF WIRE
MESH @ SLAB EDGE
METAL DECK
2 ERECTION BOLTS
H250x250x9x14
SHEAR STUD 19mmø x
150mm @ 150mm O.C. TYP
100
25
50
TYP
100
50
50
298
668
E70, TYP
5
13mm STIFFENER PL, TYP
W24x94
48
57
5
E70, TYP
PL 10mm TYP
2 ERECTION BOLTS, TYP.
200
ANGLE OF THICKNESS
SIM. TO METAL DECK
C
SK-11
A
SK-8
TOP FLOOR SLAB SECTION
TOP FLOOR SLAB SECTIONS
MULTI STORY SCBF WITH YIELDING BEAMS
DRAWN BY: SMI
DESIGNED BY: SMI
DATE: 1/17/2018
CONTACT: SMIBARRA@UW.EDU
DWG:
SK-8

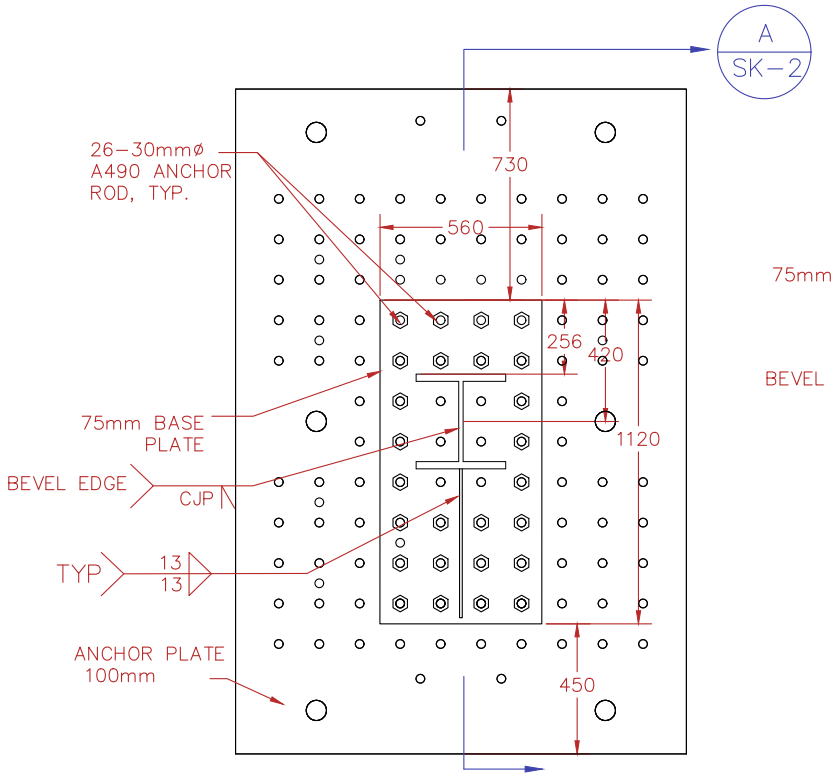

A SK–9 NORTH BASE PLATE PLAN VIEW
SCALE: 1mm = 20mm

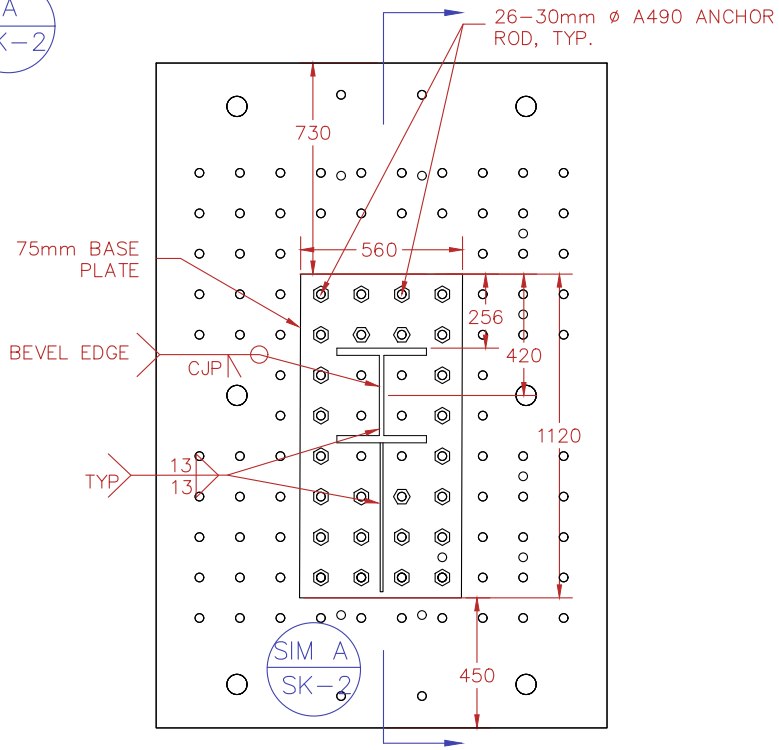

B SK–9 SOUTH BASE PLATE PLAN VIEW
SCALE: 1mm = 20mm

BASE PLATE CONNECTIONS	
MULTI STORY SCBF WITH YIELDING BEAMS	DWG: SK-9
DRAWN BY: SMI DESIGNED BY: SMI DATE: 1/17/2018 CONTACT: SMIBARRA@UW.EDU	

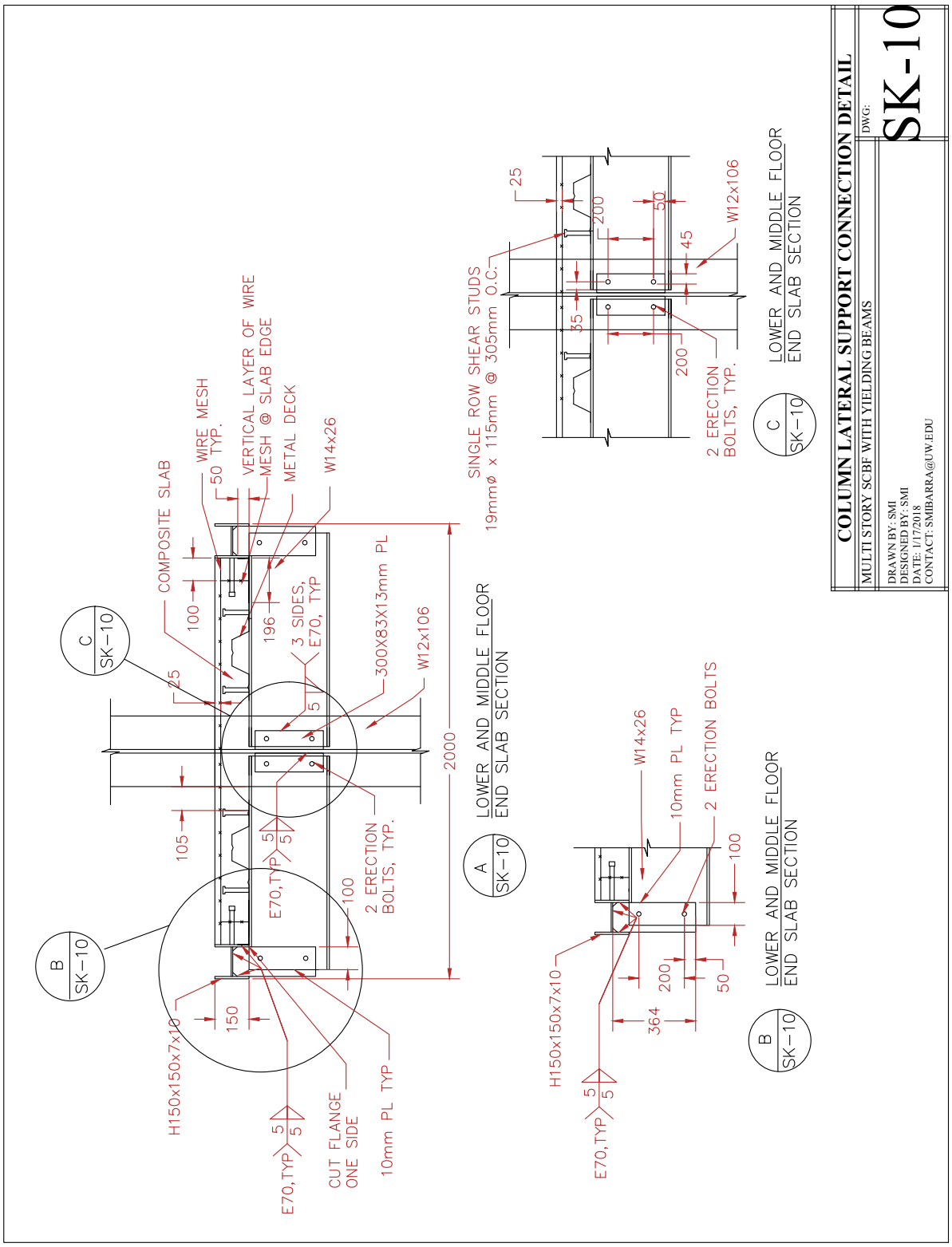
COLUMN LATERAL SUPPORT CONNECTION DETAIL
MULTI STORY SCBF WITH YIELDING BEAMS
DRAWN BY: SMI
DESIGNED BY: SMI
DATE: 1/17/2018
CONTACT: SMIBARRA@UW.EDU
DWG:
SK-10
COMPOSITE SLAB
WIRE MESH
50 TYP.
VERTICAL LAYER OF WIRE
MESH @ SLAB EDGE
METAL DECK
W14x26
3 SIDES,
E70, TYP
300X83X13mm PL
W12x106
2 ERECTION
BOLTS, TYP.
CUT FLANGE
ONE SIDE
10mm PL TYP
H150x150x7x10
E70,TYP
LOWER AND MIDDLE FLOOR
END SLAB SECTION
SINGLE ROW SHEAR STUDS
19mmø x 115mm @ 305mm O.C.
2 ERECTION BOLTS

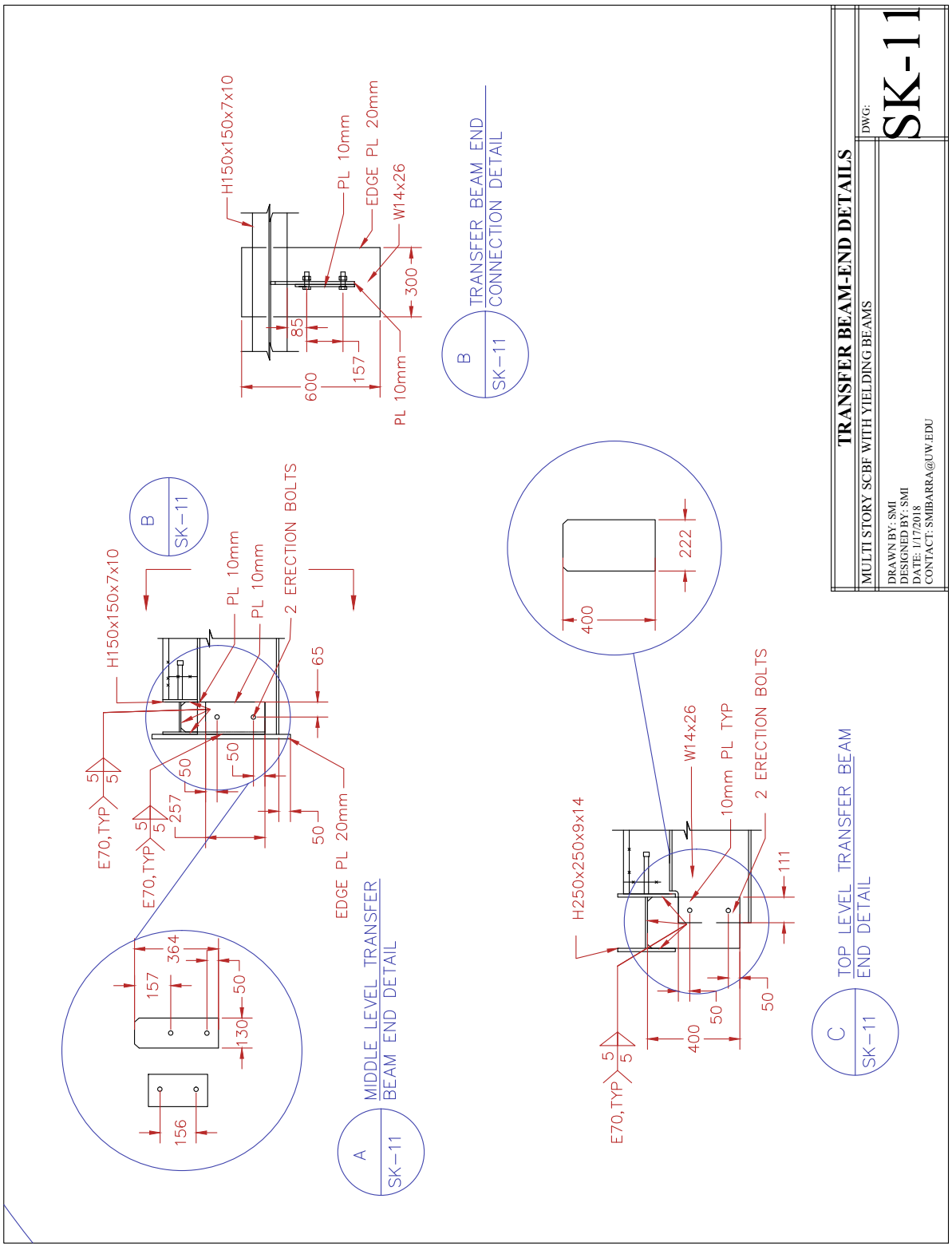
TRANSFER BEAM-END DETAILS
MULTI STORY SCBF WITH YIELDING BEAMS
DRAWN BY: SMI
DESIGNED BY: SMI
DATE: 1/17/2018
CONTACT: SMIBARRA@UW.EDU
DWG:
SK-11
H150x150x7x10
PL 10mm
EDGE PL 20mm
W14x26
PL 10mm
600
85
157
300
B
SK-11
TRANSFER BEAM END
CONNECTION DETAIL
H150x150x7x10
B
SK-11
PL 10mm
PL 10mm
2 ERECTION BOLTS
65
E70, TYP
5
5
E70, TYP
5
5
257
50
50
50
EDGE PL 20mm
157
364
50
130
156
A
SK-11
MIDDLE LEVEL TRANSFER
BEAM END DETAIL
222
400
H250x250x9x14
W14x26
10mm PL TYP
2 ERECTION BOLTS
111
E70, TYP
5
5
400
50
50
C
SK-11
TOP LEVEL TRANSFER BEAM
END DETAIL

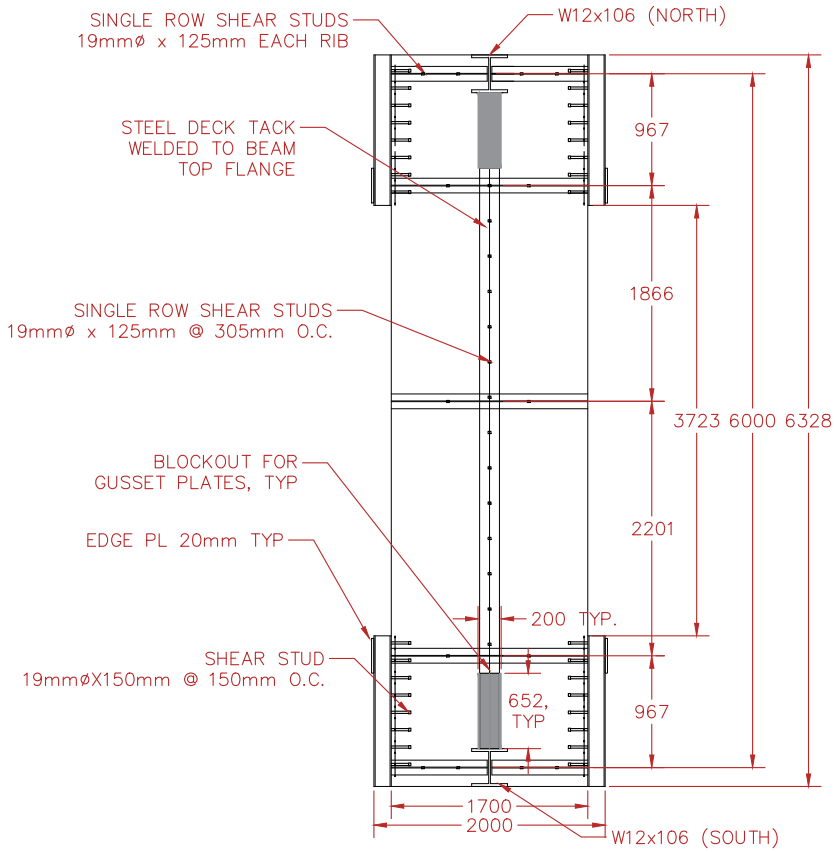

A
SK-12

TYPICAL INTERMEDIATE LEVEL PLAN VIEW
SCALE: 1mm = 50mm

INTERMEDIATE LEVEL PLAN VIEW	
MULTI STORY SCBF WITH YIELDING BEAMS	DWG: SK-12
DRAWN BY: SMI DESIGNED BY: SMI DATE: 1/2/2018 CONTACT: SMIBARRA@UW.EDU	

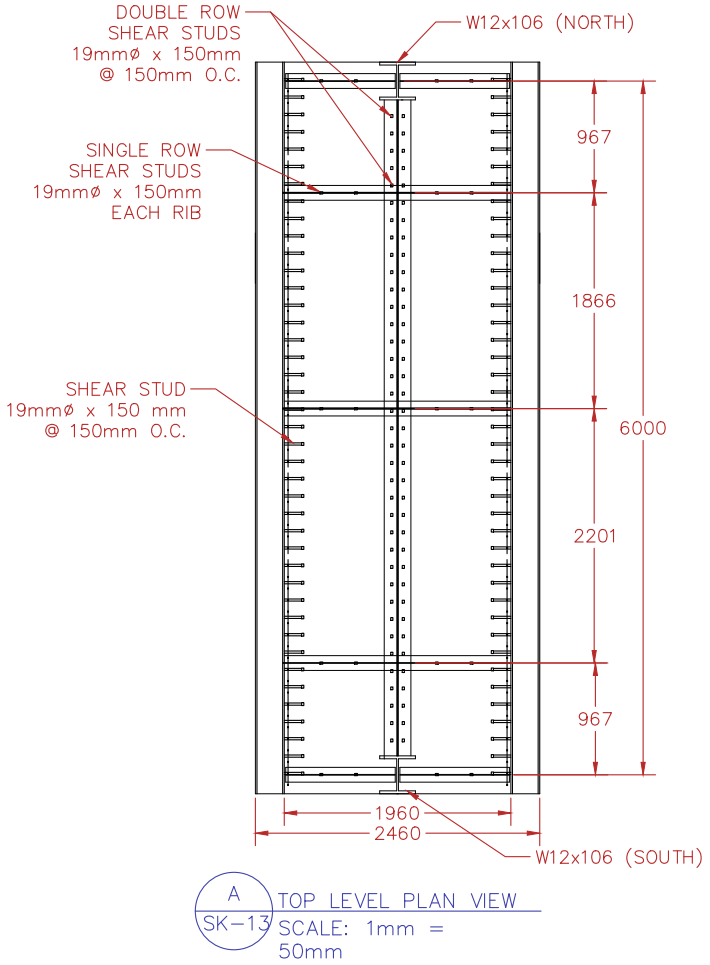

TOP LEVEL PLAN VIEW	
MULTI STORY SCBF WITH YIELDING BEAMS	DWG: SK-13
DRAWN BY: SMI DESIGNED BY: SMI DATE: 1/2/2018 CONTACT: SMIBARRA@UW.EDU	

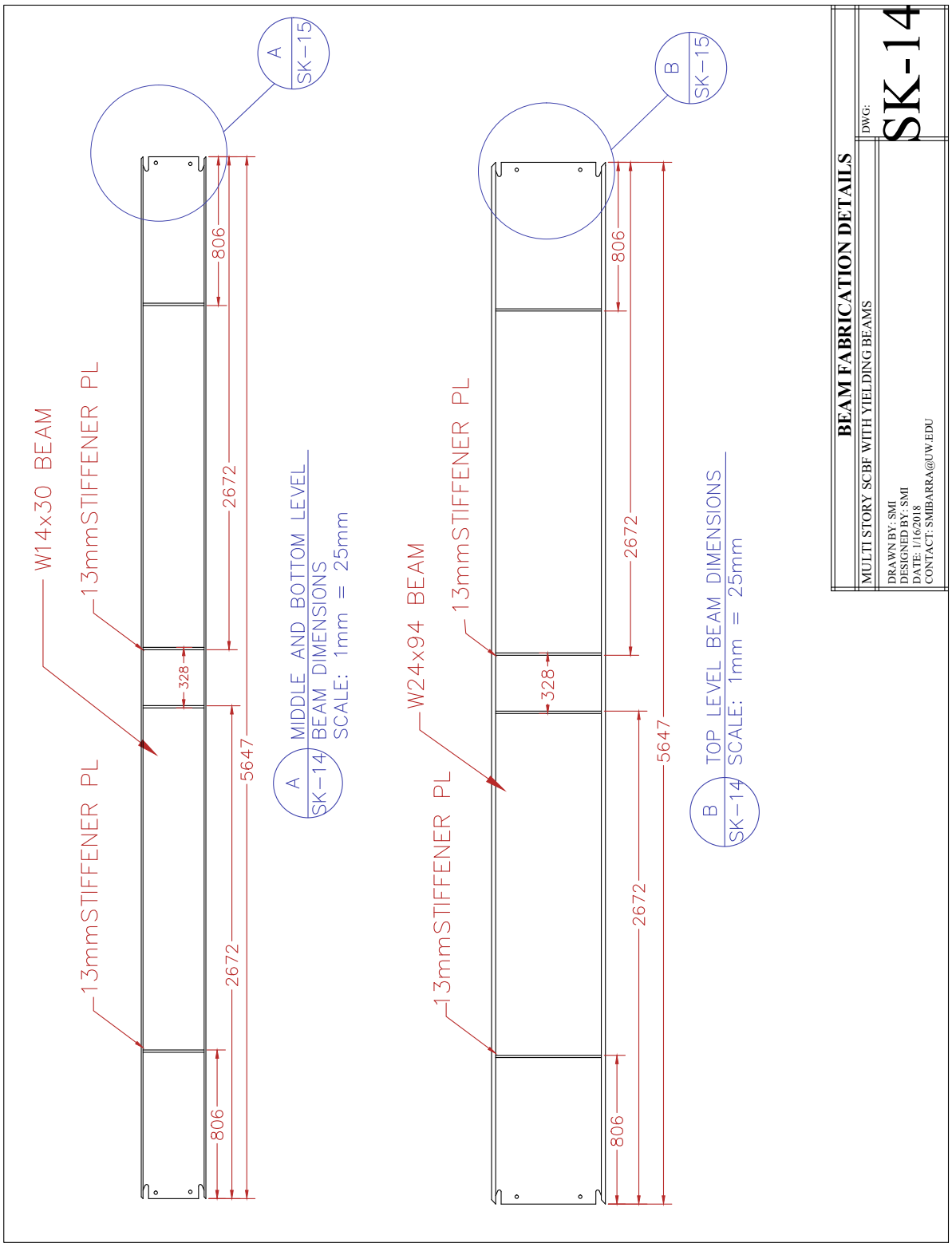
W14x30 BEAM
13mmSTIFFENER PL
13mmSTIFFENER PL
806
2672
328
5647
806
2672
A
SK-15
A
SK-14
MIDDLE AND BOTTOM LEVEL
BEAM DIMENSIONS
SCALE: 1mm = 25mm
W24x94 BEAM
13mmSTIFFENER PL
13mmSTIFFENER PL
806
2672
328
5647
806
2672
B
SK-15
B
SK-14
TOP LEVEL BEAM DIMENSIONS
SCALE: 1mm = 25mm
BEAM FABRICATION DETAILS
MULTI STORY SCBF WITH YIELDING BEAMS
DRAWN BY: SMI
DESIGNED BY: SMI
DATE: 1/16/2018
CONTACT: SMIBARRA@UW.EDU
DWG:
SK-14

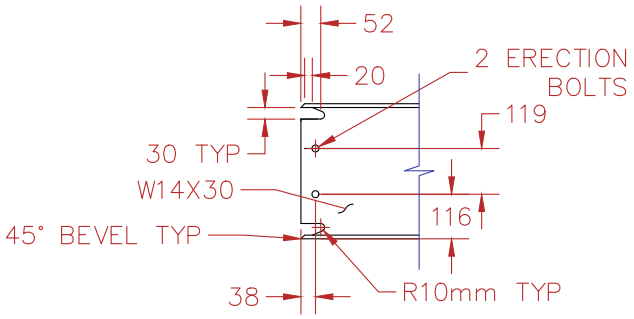

A / SK–15 MIDDLE AND BOTTOM BEAM END DETAIL
SCALE: 1mm = 15mm

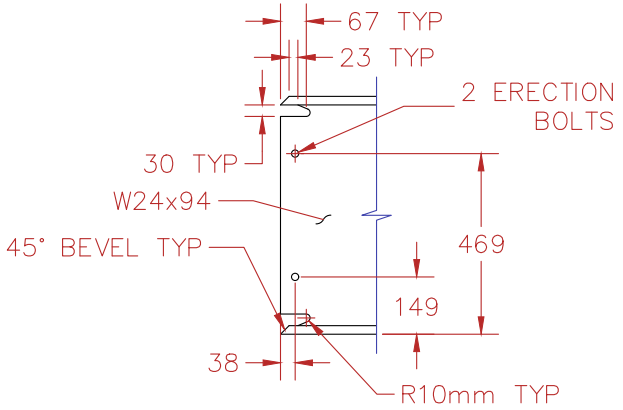

B / SK–15 TOP LEVEL BEAM END DETAIL
SCALE: 1mm = 15mm

BEAM-END FABRICATION DETAILS	
MULTI STORY SCBF WITH YIELDING BEAMS	DWG: SK-15
DRAWN BY: SMI DESIGNED BY: SMI DATE: 1/16/2018 CONTACT: SMIBARRA@UW.EDU	

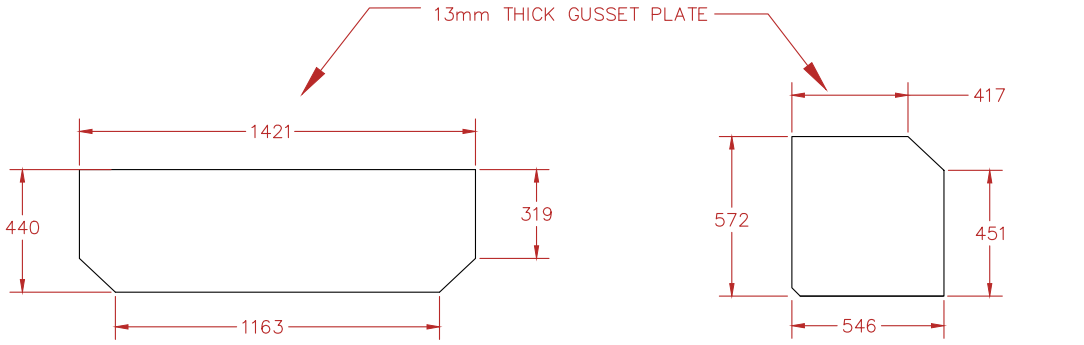

A / SK-16 TOP LEVEL MIDDLE GUSSET PLATE DIMENSIONS
SCALE: 1mm = 20mm

B / SK-16 TOP LEVEL CORNER GUSSET PLATE DIMENSIONS (X2)
SCALE: 1mm = 20mm

TOP LEVEL GUSSET PLATE FABRICATION DETAILS	
MULTI STORY SCBF WITH YIELDING BEAMS	DWG: SK-18
DRAWN BY: SMI DESIGNED BY: SMI DATE: 1/17/2018 CONTACT: SMIBARRA@UW.EDU	

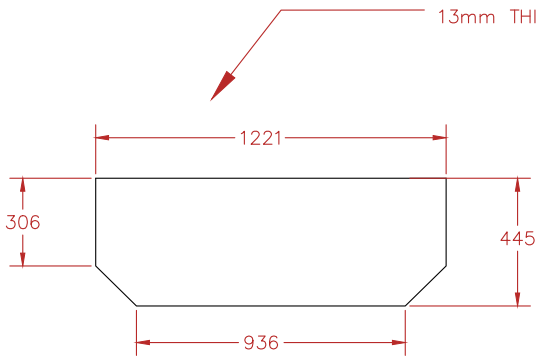

A
SK–17
MIDDLE LEVEL MIDDLE GUSSET PLATE DIMENSIONS
SCALE: 1mm = 20mm

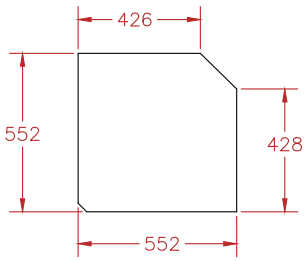

B
SK–17
MIDDLE LEVEL CORNER GUSSET PLATE DIMENSIONS (X2)
SCALE: 1mm = 20mm

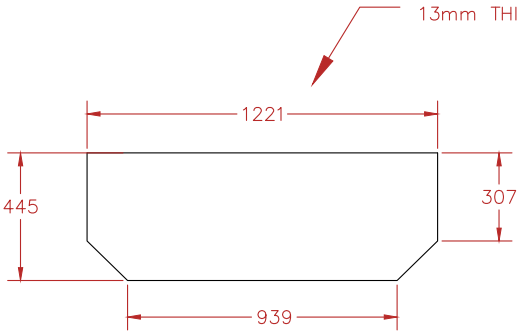

C
SK–17
BOTTOM LEVEL MIDDLE GUSSET PLATE DIMENSIONS
SCALE: 1mm = 20mm

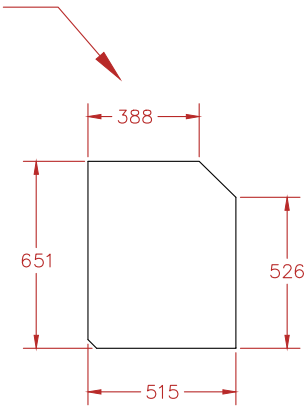

D
SK–17
BOTTOM LEVEL CORNER GUSSET PLATE DIMENSIONS (X2)
SCALE: 1mm = 20mm

INTERMEDIATE LEVELS GUSSET PLATE FABRICATION DETAILS	
MULTI STORY SCBF WITH YIELDING BEAMS	DWG: SK-17
DRAWN BY: SMI DESIGNED BY: SMI DATE: 1/17/2018 CONTACT: SMIBARRA@UW.EDU	

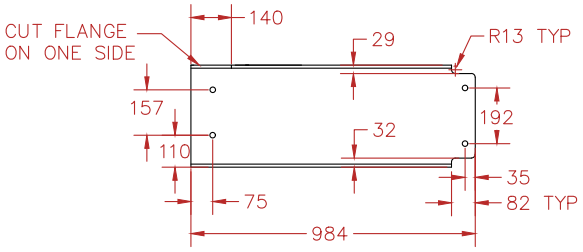

A
SK–18

LOWER AND MIDDLE LEVEL
(END) TRANSFER BEAM
FABRICATION DETAIL

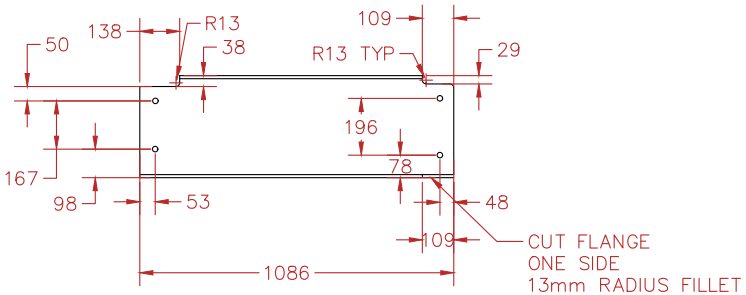

B
SK–18

TOP LEVEL TRANSFER BEAM
FABRICATION DETAIL

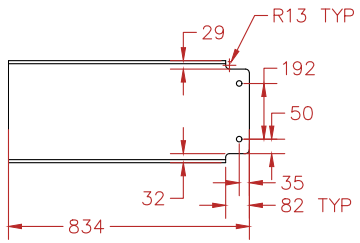

C
SK–18

LOWER AND MIDDLE LEVEL
(CENTER) TRANSFER BEAM
FABRICATION DETAIL

TRANSVERSE BEAMS FABRICATION DETAILS	
MULTI STORY SCBF WITH YIELDING BEAMS	DWG: SK-18
DRAWN BY: SMI DESIGNED BY: SMI DATE: 1/17/2018 CONTACT: SMIBARRA@UW.EDU	

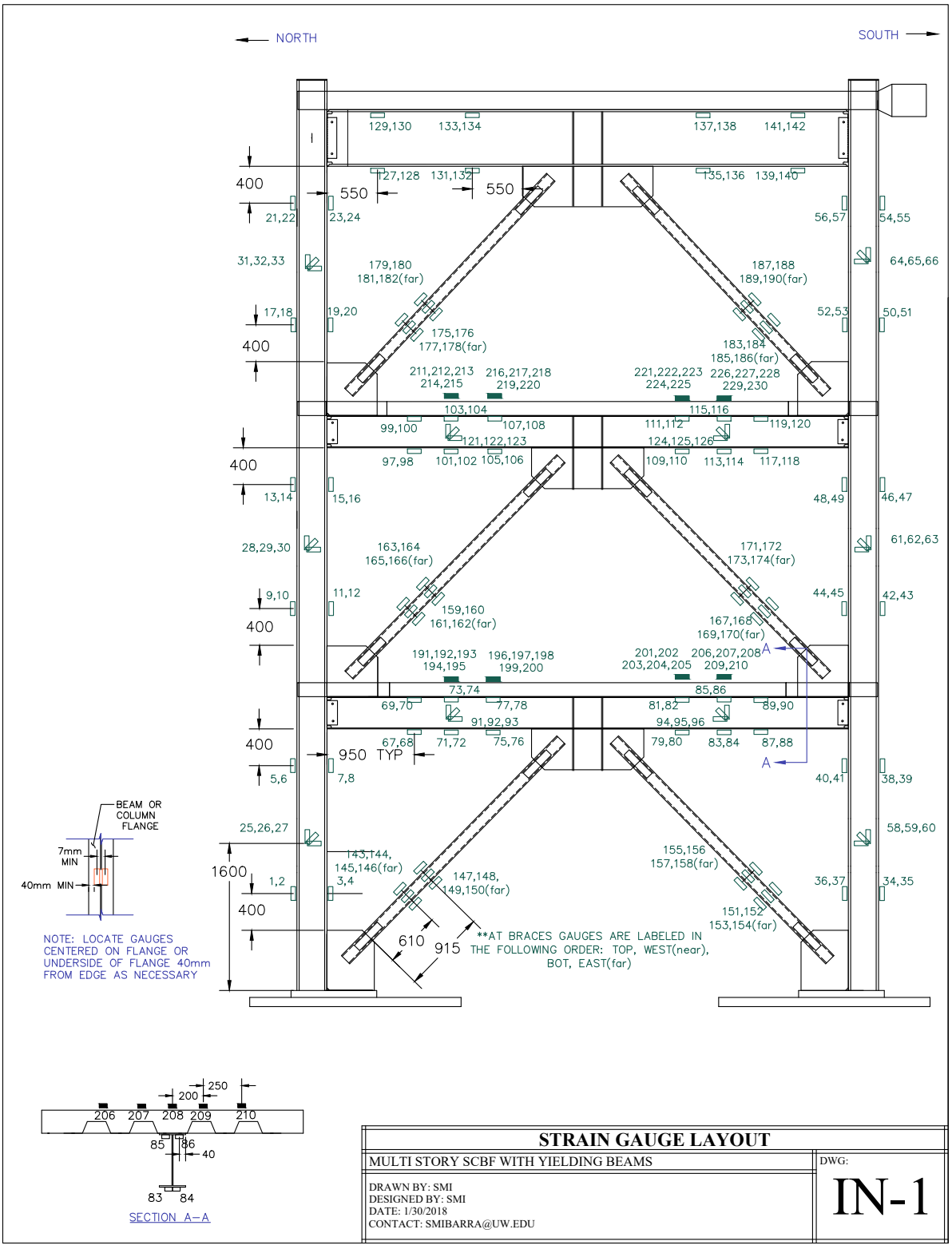

STRAIN GAUGE LAYOUT

MULTI STORY SCBF WITH YIELDING BEAMS

DWG: IN-1

DRAWN BY: SMI
DESIGNED BY: SMI
DATE: 1/30/2018
CONTACT: SMIBARRA@UW.EDU

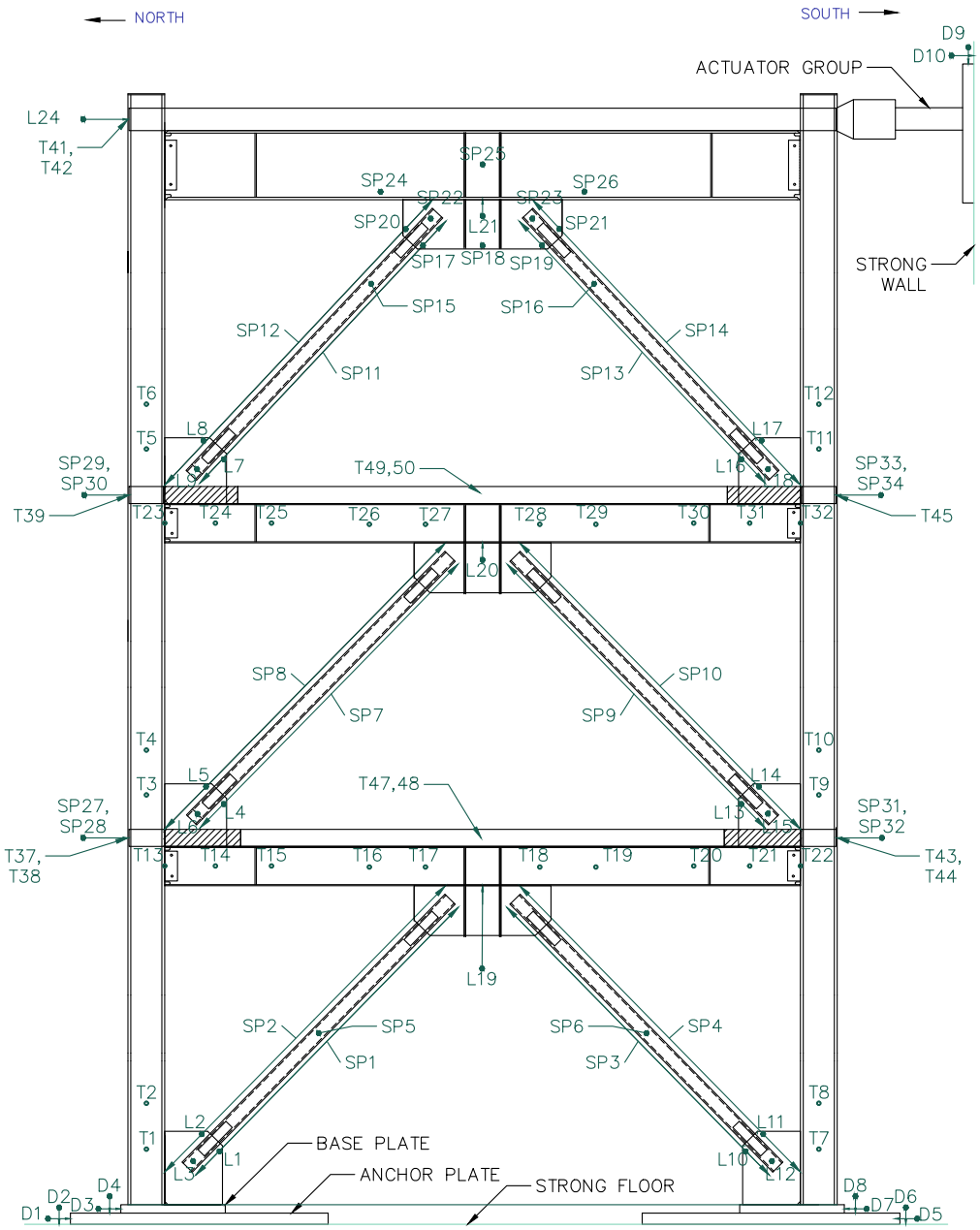

INSTRUMENTATION LAYOUT	
MULTI STORY SCBF WITH YIELDING BEAMS	DWG: IN-2
DRAWN BY: SMI DESIGNED BY: SMI DATE: 1/30/2018 CONTACT: SMIBARRA@UW.EDU	

●	DESCRIPTION	TYPE	RANGE +/−	FREEDOM
D1	N ANCHOR PL SLIP	DIAL	25mm	
D2	N ANCHOR PL UPLIFT	DIAL	25mm	
D3	N BASE PL SLIP	DIAL	25mm	
D4	N BASE PL UPLIFT	DIAL	25mm	
D5	S ANCHOR PL SLIP	DIAL	25mm	
D6	S ANCHOR PL UPLIFT	DIAL	25mm	
D7	S BASE PL SLIP	DIAL	25mm	
D8	S BASE PL UPLIFT	DIAL	25mm	
D9	ACTUATOR BASE PL SLIP	DIAL	25mm	
D10	ACTUATOR BASE PL UPLIFT	DIAL	25mm	

●	DESCRIPTION	TYPE	RANGE+/−	FREEDOM
SP1	N BOT BRACE DIAG	STRING	250mm	HORIZ
SP2	N BOT BRACE ELONGATION	STRING	250mm	HORIZ
SP3	S BOT BRACE DIAG	STRING	250mm	HORIZ
SP4	S BOT BRACE ELONGATION	STRING	250mm	HORIZ
SP5	N BOT BRACE MID PT	STRING	500mm	HORIZ
SP6	S BOT BRACE MID PT	STRING	500mm	HORIZ
SP7	N MID BRACE DIAG	STRING	250mm	HORIZ
SP8	N MID BRACE ELONGATION	STRING	250mm	HORIZ
SP9	S MID BRACE DIAG	STRING	250mm	HORIZ
SP10	S MID BRACE ELONGATION	STRING	250mm	HORIZ
SP11	N TOP BRACE DIAG	STRING	250mm	HORIZ
SP12	N TOP BRACE ELONGATION	STRING	250mm	HORIZ
SP13	S TOP BRACE DIAG	STRING	250mm	HORIZ
SP14	S TOP BRACE ELONGATION	STRING	250mm	HORIZ
SP15	N TOP BRACE MID PT	STRING	500mm	HORIZ
SP16	S TOP BRACE MID PT	STRING	500mm	HORIZ
SP17	N 3F GP OOP BOT EDGE	STRING	250mm	HORIZ
SP18	MID 3F GP OOP	STRING	250mm	HORIZ
SP19	S 3F GP OOP BOT EDGE	STRING	250mm	HORIZ
SP20	N 3F GP OOP N EDGE	STRING	250mm	HORIZ
SP21	S 3F GP OOP S EDGE	STRING	250mm	HORIZ
SP22	N 3F GP OOP CENTER	STRING	250mm	HORIZ
SP23	S 3F GP OOP CENTER	STRING	250mm	HORIZ
SP24	3F BEAM N OOP ROT	STRING	250mm	HORIZ
SP25	3F BEAM MID OOP	STRING	250mm	HORIZ
SP26	3F BEAM S OOP ROT	STRING	250mm	HORIZ
SP27	N 1F BEAM DRIFT W SIDE	STRING	500mm	
SP28	N 1F BEAM DRIFT E SIDE	STRING	500mm	
SP29	N 2F BEAM DRIFT W SIDE	STRING	500mm	
SP30	N 2F BEAM DRIFT E SIDE	STRING	500mm	
SP31	S 1F BEAM DRIFT W SIDE	STRING	500mm	
SP32	S 1F BEAM DRIFT E SIDE	STRING	500mm	
SP33	S 2F BEAM DRIFT W SIDE	STRING	500mm	
SP34	S 2F BEAM DRIFT E SIDE	STRING	500mm	

ABBREVIATIONS

N	NORTH
S	SOUTH
E	EAST
W	WEST
C	CENTER
BOT	BOTTOM
MID	MIDDLE
COL	COLUMN
COR	CORNER
BR	BRACE
PL	
OOP	OUT OF PLANE
DIAG	DIAGONAL
DISP	DISPLACEMENT
ROT	ROTATION
PT	POINT
WP	WORK POINT

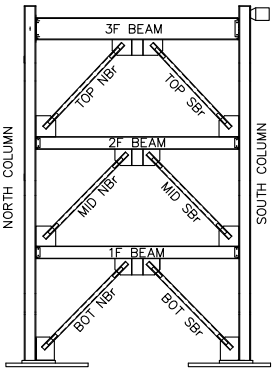

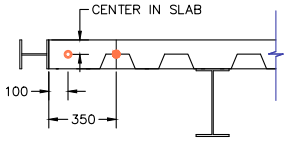

NOTE: LOCATE TILTMETERS ON OUTSIDE EDGE OF EACH SLAB

TYPICAL SLAB END INSTRUMENTATION DETAIL

INSTRUMENTATION DETAILS

MULTI STORY SCBF WITH YIELDING BEAMS

DRAWN BY: SMI
DESIGNED BY: SMI
DATE: 1/30/2018
CONTACT: SMIBARRA@UW.EDU

DWG: IN-3

●	DESCRIPTION	TYPE	RANGE+/−	FREEDOM
L1	N BASE GP OOP BOT	TML	100mm	
L2	N BASE GP OOP TOP	TML	100mm	
L3	N BASE GP OOP CENTER	TML	50mm	
L4	1F BEAM GP OOP BOT	TML	100mm	HORIZ
L5	1F BEAM GP OOP TOP	TML	100mm	HORIZ
L6	1F BEAM GP OOP CENER	TML	50mm	HORIZ
L7	2F BEAM GP OPP BOT	TML	100mm	HORIZ
L8	2F BEAM GP OOP TOP	TML	100mm	HORIZ
L9	2F BEAM GP OOP CENER	TML	50mm	HORIZ
L10	S BASE GP OOP BOT	TML	100mm	
L11	S BASE GP OOP TOP	TML	100mm	
L12	S BASE GP OOP CENTER	TML	50mm	
L13	2F BEAM GP OOP BOT	TML	100mm	HORIZ
L14	2F BEAM GP OOP TOP	TML	100mm	HORIZ
L15	2F BEAM GP OOP CENER	TML	50mm	HORIZ
L16	3F BEAM GP OPP BOT	TML	100mm	HORIZ
L17	3F BEAM GP OOP TOP	TML	100mm	HORIZ
L18	3F BEAM GP OOP CENER	TML	50mm	HORIZ
L19	1F BEAM VERT DISP	TML	150mm	HORIZ
L20	2F BEAM VERT DISP	TML	150mm	HORIZ
L21	3F BEAM VERT DISP	TML	150mm	HORIZ
L22	TOP ALUMINUM PL OOP N	TML	25mm	
L23	TOP ALUMINUM PL OOP S	TML	25mm	
L24	TOP BEAM DRIFT E SIDE	TEMPO	500mm	

○	DESCRIPTION	RANGE +/−	○	DESCRIPTION	RANGE +/−
T1	N COL BASE ROT	5°	T26	2F N SIDE CENTER BEAM ROT	15°
T2	N COL BASE ROT	10°	T27	2F N SIDE CENTER BEAM ROT	15°
T3	N COL 1F ROT	15°	T28	2F S SIDE CENTER BEAM ROT	15°
T4	N COL 1F ROT	15°	T29	2F S SIDE CENTER BEAM ROT	15°
T5	N COL 2F ROT	10°	T30	2F S SIDE BEAM ROT	10°
T6	N COL 2F ROT	15°	T31	2F S SIDE BEAM ROT	5°
T7	S COL BASE ROT	5°	T32	S COL FLANGE AT 2F BEAM	10°
T8	S COL BASE ROT	10°			
T9	S COL 1F ROT	15°			
T10	S COL 1F ROT	15°			
T11	S COL 2F ROT	10°			
T12	S COL 2F ROT	15°	T37	1F N SIDE SLAB ROTATION W	5°
T13	N COL FLANGE AT 1F BEAM	10°	T38	1F N SIDE SLAB ROTATION E	5°
T14	1F N SIDE BEAM ROT	5°	T39	2F N SIDE SLAB ROTATION W	5°
T15	1F N SIDE BEAM ROT	10°			
T16	1F N SIDE CENTER BEAM ROT	15°	T41	3F N SIDE SLAB ROTATION W	5°
T17	1F N SIDE CENTER BEAM ROT	15°	T42	3F N SIDE SLAB ROTATION E	5°
T18	1F S SIDE CENTER BEAM ROT	15°	T43	1F S SIDE SLAB ROTATION W	5°
T19	1F S SIDE CENTER BEAM ROT	15°	T44	1F S SIDE SLAB ROTATION E	5°
T20	1F S SIDE BEAM ROT	10°	T45	2F S SIDE SLAB ROTATION W	5°
T21	1F S SIDE BEAM ROT	5°			
T22	N COL FLANGE AT 1F BEAM	10°	T47	1F SLAB ROT MID W	15°
T23	S COL FLANGE AT 2F BEAM	10°	T48	1F SLAB ROT MID E	15°
T24	2F N SIDE BEAM ROT	5°	T49	2F SLAB ROT MID W	15°
T25	2F N SIDE BEAM ROT	10°	T50	2F SLAB ROT MID E	15°

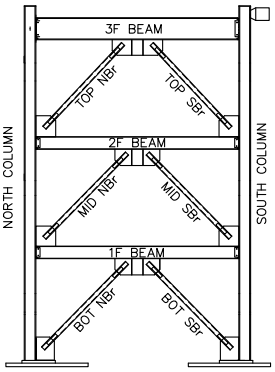

INSTRUMENTATION DETAILS

MULTI STORY SCBF WITH YIELDING BEAMS

DRAWN BY: SMI
DESIGNED BY: SMI
DATE: 1/30/2018
CONTACT: SMIBARRA@UW.EDU

DWG: IN-4

KEY
- STEEL UNIAXIAL STRAIN GAUGE
- CONCRETE UNIAXIAL STRAIN GAUGE
- TRIAXIAL STRAIN GAUGE

	LABEL	LOCATION		LABEL	LOCATION
1	SG 1	N COLUMN BOT	34	SG 34	S COLUMN BOT
2	SG 2	N COLUMN BOT	35	SG 35	S COLUMN BOT
3	SG 3	N COLUMN BOT	36	SG 36	S COLUMN BOT
4	SG 4	N COLUMN BOT	37	SG 37	S COLUMN BOT
5	SG 5	N COLUMN BOT	38	SG 38	S COLUMN BOT
6	SG 6	N COLUMN BOT	39	SG 39	S COLUMN BOT
7	SG 7	N COLUMN BOT	40	SG 40	S COLUMN BOT
8	SG 8	N COLUMN BOT	41	SG 41	S COLUMN BOT
9	SG 9	N COLUMN MID	42	SG 42	S COLUMN MID
10	SG 10	N COLUMN MID	43	SG 43	S COLUMN MID
11	SG 11	N COLUMN MID	44	SG 44	S COLUMN MID
12	SG 12	N COLUMN MID	45	SG 45	S COLUMN MID
13	SG 13	N COLUMN MID	46	SG 46	S COLUMN MID
14	SG 14	N COLUMN MID	47	SG 47	S COLUMN MID
15	SG 15	N COLUMN MID	48	SG 48	S COLUMN MID
16	SG 16	N COLUMN MID	49	SG 49	S COLUMN MID
17	SG 17	N COLUMN TOP	50	SG 50	S COLUMN TOP
18	SG 18	N COLUMN TOP	51	SG 51	S COLUMN TOP
19	SG 19	N COLUMN TOP	52	SG 52	S COLUMN TOP
20	SG 20	N COLUMN TOP	53	SG 53	S COLUMN TOP
21	SG 21	N COLUMN TOP	54	SG 54	S COLUMN TOP
22	SG 22	N COLUMN TOP	55	SG 55	S COLUMN TOP
23	SG 23	N COLUMN TOP	56	SG 56	S COLUMN TOP
24	SG 24	N COLUMN TOP	57	SG 57	S COLUMN TOP
25	SG 25	N COLUMN BOT WEB 0°	58	SG 58	S COLUMN BOT WEB 0°
26	SG 26	N COLUMN BOT WEB 45°	59	SG 59	S COLUMN BOT WEB 45°
27	SG 27	N COLUMN BOT WEB 90°	60	SG 60	S COLUMN BOT WEB 90°
28	SG 28	N COLUMN MID WEB 0°	61	SG 61	S COLUMN MID WEB 0°
29	SG 29	N COLUMN MID WEB 45°	62	SG 62	S COLUMN MID WEB 45°
30	SG 30	N COLUMN MID WEB 90°	63	SG 63	S COLUMN MID WEB 90°
31	SG 31	N COLUMN TOP WEB 0°	64	SG 64	S COLUMN TOP WEB 0°
32	SG 32	N COLUMN TOP WEB 45°	65	SG 65	S COLUMN TOP WEB 45°
33	SG 33	N COLUMN TOP WEB 90°	66	SG 66	S COLUMN TOP WEB 90°
67	SG 67	N 1F BEAM	97	SG 97	N 2F BEAM
68	SG 68	N 1F BEAM	98	SG 98	N 2F BEAM
69	SG 69	N 1F BEAM*	99	SG 99	N 2F BEAM*
70	SG 70	N 1F BEAM*	100	SG 100	N 2F BEAM*
71	SG 71	N 1F BEAM	101	SG 101	N 2F BEAM
72	SG 72	N 1F BEAM	102	SG 102	N 2F BEAM
73	SG 73	N 1F BEAM*	103	SG 103	N 2F BEAM*
74	SG 74	N 1F BEAM*	104	SG 104	N 2F BEAM*
75	SG 75	N 1F BEAM	105	SG 105	N 2F BEAM
76	SG 76	N 1F BEAM	106	SG 106	N 2F BEAM
77	SG 77	N 1F BEAM*	107	SG 107	N 2F BEAM*
78	SG 78	N 1F BEAM*	108	SG 108	N 2F BEAM*
79	SG 79	S 1F BEAM	109	SG 109	N 2F BEAM
80	SG 80	S 1F BEAM	110	SG 110	N 2F BEAM
81	SG 81	S 1F BEAM*	111	SG 111	N 2F BEAM*
82	SG 82	S 1F BEAM*	112	SG 112	N 2F BEAM*
83	SG 83	S 1F BEAM	113	SG 113	N 2F BEAM
84	SG 84	S 1F BEAM	114	SG 114	N 2F BEAM
85	SG 85	S 1F BEAM*	115	SG 115	N 2F BEAM*
86	SG 86	S 1F BEAM*	116	SG 116	N 2F BEAM*
87	SG 87	S 1F BEAM	117	SG 117	N 2F BEAM
88	SG 88	S 1F BEAM	118	SG 118	N 2F BEAM
89	SG 89	S 1F BEAM*	119	SG 119	N 2F BEAM*
90	SG 90	S 1F BEAM*	120	SG 120	N 2F BEAM*
91	SG 91	N SIDE 1F BEAM WEB 0°	121	SG 121	N SIDE 2F BEAM WEB 0°
92	SG 92	N SIDE 1F BEAM WEB 45°	122	SG 122	N SIDE 2F BEAM WEB 45°
93	SG 93	N SIDE 1F BEAM WEB 90°	123	SG 123	N SIDE 2F BEAM WEB 90°
94	SG 94	S SIDE 1F BEAM WEB 0°	124	SG 124	S SIDE 2F BEAM WEB 0°
95	SG 95	S SIDE 1F BEAM WEB 45°	125	SG 125	S SIDE 2F BEAM WEB 45°
96	SG 96	S SIDE 1F BEAM WEB 90°	126	SG 126	S SIDE 2F BEAM WEB 90°

* LOCATE STRAIN GAUGE AT UNDERSIDE OF BEAM FLANGE

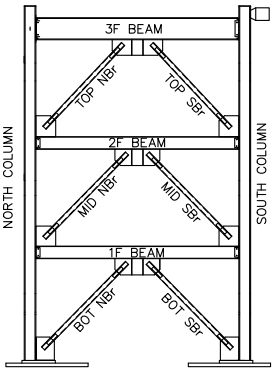

STRAIN GAUGE DETAILS

MULTI STORY SCBF WITH YIELDING BEAMS

DRAWN BY: SMI
DESIGNED BY: SMI
DATE: 1/30/2018
CONTACT: SMIBARRA@UW.EDU

DWG: IN-5

	LABEL	LOCATION		LABEL	LOCATION
127	SG 127	N 3F BEAM	135	SG 135	S 3F BEAM
128	SG 128	N 3F BEAM	136	SG 136	S 3F BEAM
129	SG 129	N 3F BEAM*	137	SG 137	S 3F BEAM*
130	SG 130	N 3F BEAM*	138	SG 138	S 3F BEAM*
131	SG 131	N 3F BEAM	139	SG 139	S 3F BEAM
132	SG 132	N 3F BEAM	140	SG 140	S 3F BEAM
133	SG 133	N 3F BEAM*	141	SG 141	S 3F BEAM*
134	SG 134	N 3F BEAM*	142	SG 142	S 3F BEAM*
143	SG 143	BOT NBr	167	SG 167	MID SBr
144	SG 144	BOT NBr	168	SG 168	MID SBr
145	SG 145	BOT NBr	169	SG 169	MID SBr
146	SG 146	BOT NBr	170	SG 170	MID SBr
147	SG 147	BOT NBr	171	SG 171	MID SBr
148	SG 148	BOT NBr	172	SG 172	MID SBr
149	SG 149	BOT NBr	173	SG 173	MID SBr
150	SG 150	BOT NBr	174	SG 174	MID SBr
151	SG 151	BOT SBr	175	SG 175	TOP NBr
152	SG 152	BOT SBr	176	SG 176	TOP NBr
153	SG 153	BOT SBr	177	SG 177	TOP NBr
154	SG 154	BOT SBr	178	SG 178	TOP NBr
155	SG 155	BOT SBr	179	SG 179	TOP NBr
156	SG 156	BOT SBr	180	SG 180	TOP NBr
157	SG 157	BOT SBr	181	SG 181	TOP NBr
158	SG 158	BOT SBr	182	SG 182	TOP NBr
159	SG 159	MID NBr	183	SG 183	TOP SBr
160	SG 160	MID NBr	184	SG 184	TOP SBr
161	SG 161	MID NBr	185	SG 185	TOP SBr
162	SG 162	MID NBr	186	SG 186	TOP SBr
163	SG 163	MID NBr	187	SG 187	TOP SBr
164	SG 164	MID NBr	188	SG 188	TOP SBr
165	SG 165	MID NBr	189	SG 189	TOP SBr
166	SG 166	MID NBr	190	SG 190	TOP SBr
191	SG 191	1F FN SLAB SURFACE	211	SG 211	2F FN SLAB SURFACE
192	SG 192	1F FN SLAB SURFACE	212	SG 212	2F FN SLAB SURFACE
193	SG 193	1F FN SLAB SURFACE	213	SG 213	2F FN SLAB SURFACE
194	SG 194	1F FN SLAB SURFACE	214	SG 214	2F FN SLAB SURFACE
195	SG 195	1F FN SLAB SURFACE	215	SG 215	2F FN SLAB SURFACE
196	SG 196	1F MN SLAB SURFACE	216	SG 216	2F MN SLAB SURFACE
197	SG 197	1F MN SLAB SURFACE	217	SG 217	2F MN SLAB SURFACE
198	SG 198	1F MN SLAB SURFACE	218	SG 218	2F MN SLAB SURFACE
199	SG 199	1F MN SLAB SURFACE	219	SG 219	2F MN SLAB SURFACE
200	SG 200	1F MN SLAB SURFACE	220	SG 220	2F MN SLAB SURFACE
201	SG 201	1F MS SLAB SURFACE	221	SG 221	2F MS SLAB SURFACE
202	SG 202	1F MS SLAB SURFACE	222	SG 222	2F MS SLAB SURFACE
203	SG 203	1F MS SLAB SURFACE	223	SG 223	2F MS SLAB SURFACE
204	SG 204	1F MS SLAB SURFACE	224	SG 224	2F MS SLAB SURFACE
205	SG 205	1F MS SLAB SURFACE	225	SG 225	2F MS SLAB SURFACE
206	SG 206	1F FS SLAB SURFACE	226	SG 226	2F FS SLAB SURFACE
207	SG 207	1F FS SLAB SURFACE	227	SG 227	2F FS SLAB SURFACE
208	SG 208	1F FS SLAB SURFACE	228	SG 228	2F FS SLAB SURFACE
209	SG 209	1F FS SLAB SURFACE	229	SG 229	2F FS SLAB SURFACE
210	SG 210	1F FS SLAB SURFACE	230	SG 230	2F FS SLAB SURFACE

* LOCATE STRAIN GAUGE AT UNDERSIDE OF BEAM FLANGE

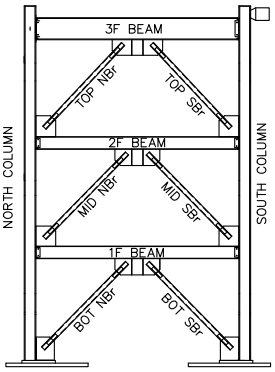

STRAIN GAUGE DETAILS

MULTI STORY SCBF WITH YIELDING BEAMS

DRAWN BY: SMI
DESIGNED BY: SMI
DATE: 1/30/2018
CONTACT: SMIBARRA@UW.EDU

DWG: IN-6

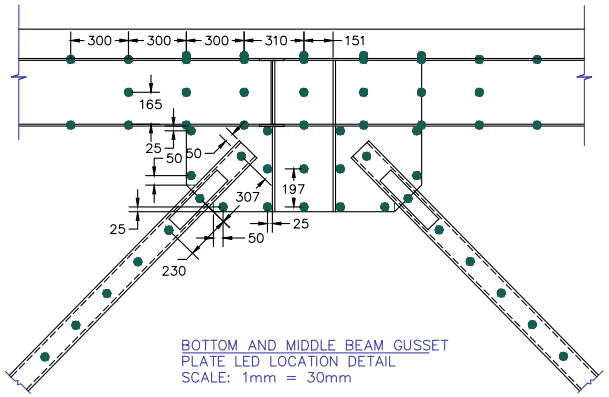

BOTTOM AND MIDDLE BEAM GUSSET
PLATE LED LOCATION DETAIL
SCALE: 1mm = 30mm

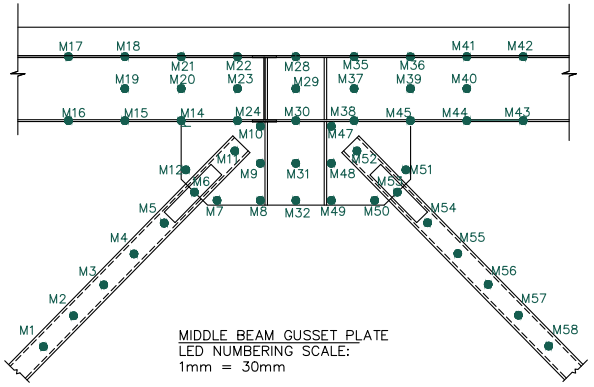

MIDDLE BEAM GUSSET PLATE
LED NUMBERING SCALE:
1mm = 30mm

NOTE: OPTITRACK WIRELESS MARKERS

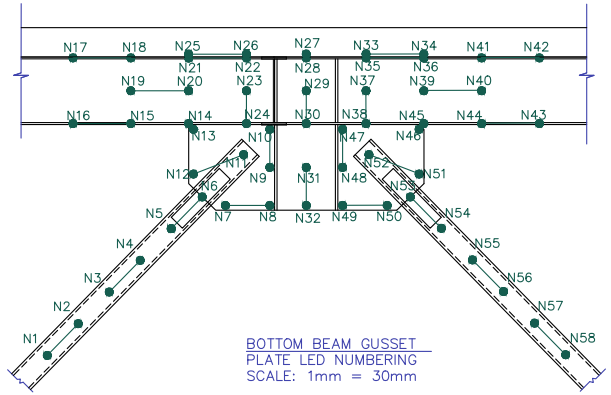

BOTTOM BEAM GUSSET
PLATE LED NUMBERING
SCALE: 1mm = 30mm

NOTE: NDI OPTOTRAK LED TARGETS

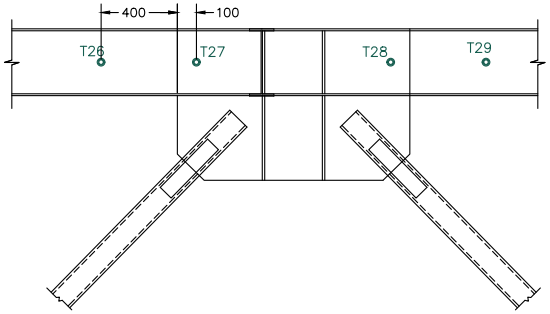

MIDDLE BEAM
INSTURUMENTATION DETAIL
SCALE: 1mm = 30mm

MID BEAM INSTRUMENTATION DETAILS	
MULTI STORY SCBF WITH YIELDING BEAMS	DWG: IN-7
DRAWN BY: SMI DESIGNED BY: SMI DATE: 1/30/2018 CONTACT: SMIBARRA@UW.EDU	

●	DESCRIPTION	●	DESCRIPTION
N1	BOT NBr MID	N30	F1 BEAM BOT FLANGE GRID
N2	BOT NBr OOP	N31	F1 BEAM MID GP GRID
N3	BOT NBr OOP	N32	F1 BEAM MID GP GRID
N4	BOT NBr OOP	N33	F1 BEAM SLAB GRID
N5	BOT NBr OOP	N34	F1 BEAM SLAB GRID
N6	BOT NBr OOP	N35	F1 BEAM TOP FLANGE GRID
N7	F1 BEAM MID GP GRID	N36	F1 BEAM TOP FLANGE GRID
N8	F1 BEAM MID GP GRID	N37	F1 BEAM WEB GRID
N9	F1 BEAM MID GP GRID	N38	F1 BEAM BOT FLANGE GRID
N10	F1 BEAM MID GP GRID	N39	F1 BEAM WEB GRID
N11	BOT NBr OOP	N40	F1 BEAM WEB GRID
N12	F1 BEAM MID GP GRID	N41	F1 BEAM TOP FLANGE GRID
N13	F1 BEAM MID GP GRID	N42	F1 BEAM TOP FLANGE GRID
N14	F1 BEAM BOT FLANGE GRID	N43	F1 BEAM BOT FLANGE GRID
N15	F1 BEAM BOT FLANGE GRID	N44	F1 BEAM BOT FLANGE GRID
N16	F1 BEAM BOT FLANGE GRID	N45	F1 BEAM BOT FLANGE GRID
N17	F1 BEAM TOP FLANGE GRID	N46	F1 BEAM MID GP GRID
N18	F1 BEAM TOP FLANGE GRID	N47	F1 BEAM MID GP GRID
N19	F1 BEAM WEB GRID	N48	F1 BEAM MID GP GRID
N20	F1 BEAM WEB GRID	N49	F1 BEAM MID GP GRID
N21	F1 BEAM TOP FLANGE GRID	N50	F1 BEAM MID GP GRID
N22	F1 BEAM TOP FLANGE GRID	N51	F1 BEAM MID GP GRID
N23	F1 BEAM WEB GRID	N52	BOT SBr OOP
N24	F1 BEAM BOT FLANGE GRID	N53	BOT SBr OOP
N25	F1 BEAM SLAB GRID	N54	BOT SBr OOP
N26	F1 BEAM SLAB GRID	N55	BOT SBr OOP
N27	F1 BEAM SLAB GRID	N56	BOT SBr OOP
N28	F1 BEAM TOP FLANGE GRID	N57	BOT SBr OOP
N29	F1 BEAM WEB GRID (CENTER)	N58	BOT SBr OOP
●	DESCRIPTION	●	DESCRIPTION
M1	MID NBr MID	M30	F2 BEAM BOT FLANGE GRID
M2	MID NBr OOP	M31	F2 BEAM MID GP GRID
M3	MID NBr OOP	M32	F2 BEAM MID GP GRID
M4	MID NBr OOP		
M5	MID NBr OOP		
M6	MID NBr OOP	M35	F2 BEAM TOP FLANGE GRID
M7	F2 BEAM MID GP GRID	M36	F2 BEAM TOP FLANGE GRID
M8	F2 BEAM MID GP GRID	M37	F2 BEAM WEB GRID
M9	F2 BEAM MID GP GRID	M38	F2 BEAM BOT FLANGE GRID
M10	F2 BEAM MID GP GRID	M39	F2 BEAM WEB GRID
M11	MID NBr OOP	M40	F2 BEAM WEB GRID
M12	F2 BEAM MID GP GRID	M41	F2 BEAM TOP FLANGE GRID
		M42	F2 BEAM TOP FLANGE GRID
M14	F2 BEAM BOT FLANGE GRID	M43	F2 BEAM BOT FLANGE GRID
M15	F2 BEAM BOT FLANGE GRID	M44	F2 BEAM BOT FLANGE GRID
M16	F2 BEAM BOT FLANGE GRID	M45	F2 BEAM BOT FLANGE GRID
M17	F2 BEAM TOP FLANGE GRID		
M18	F2 BEAM TOP FLANGE GRID	M47	F2 BEAM MID GP GRID
M19	F2 BEAM WEB GRID	M48	F2 BEAM MID GP GRID
M20	F2 BEAM WEB GRID	M49	F2 BEAM MID GP GRID
M21	F2 BEAM TOP FLANGE GRID	M50	F2 BEAM MID GP GRID
M22	F2 BEAM TOP FLANGE GRID	M51	F2 BEAM MID GP GRID
M23	F2 BEAM WEB GRID	M52	MID SBr OOP
M24	F2 BEAM BOT FLANGE GRID	M53	MID SBr OOP
		M54	MID SBr OOP
		M55	MID SBr OOP
		M56	MID SBr OOP
M28	F2 BEAM TOP FLANGE GRID	M57	MID SBr OOP
M29	F2 BEAM WEB GRID(CENTER)	M58	MID SBr OOP

OPTICAL SYSTEM MARKER DESIGNATION

MULTI STORY SCBF WITH YIELDING BEAMS

DWG: IN-8

DRAWN BY: SMI
DESIGNED BY: SMI
DATE: 1/30/2018
CONTACT: SMIBARRA@UW.EDU

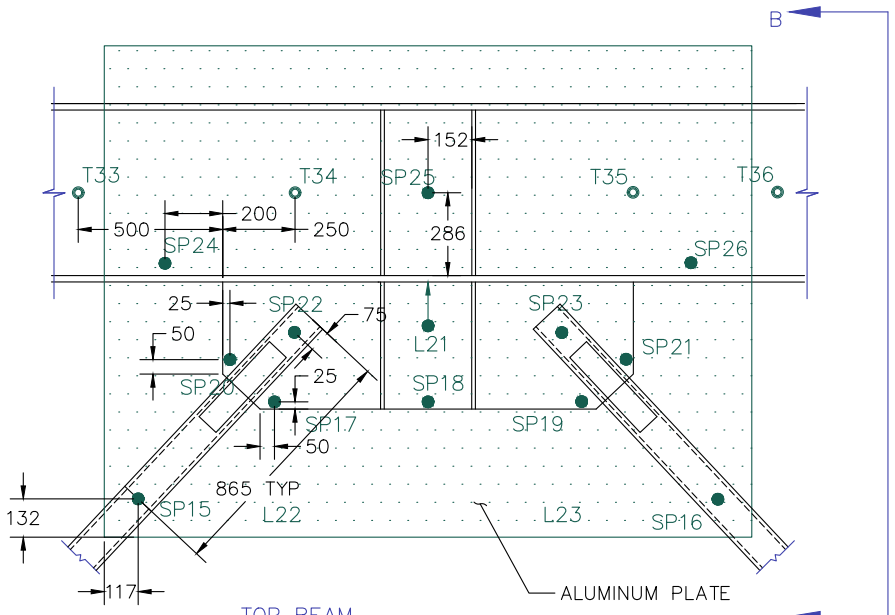

TOP BEAM
INSTURUMENTATION DETAIL
SCALE: 1mm = 20mm

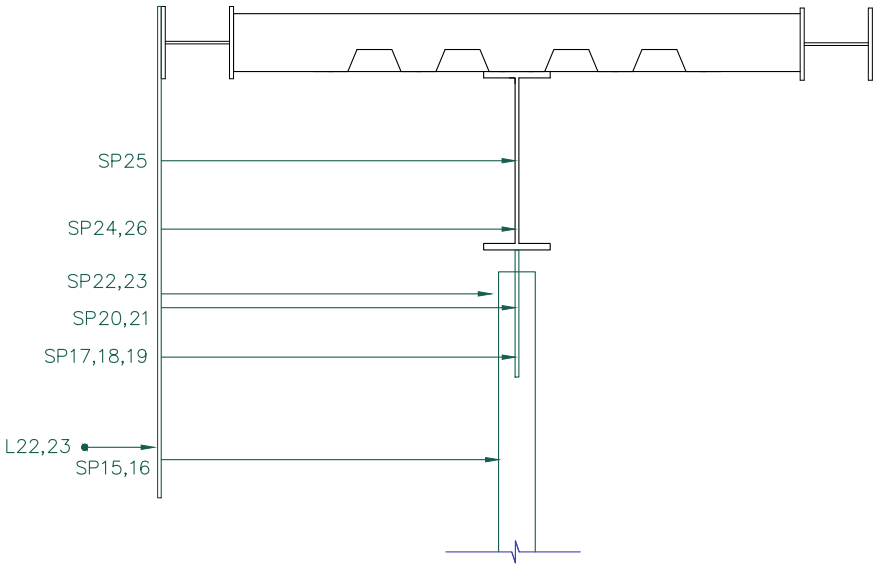

SECTION B–B
TOP FLOOR SLAB

TOP BEAM INSTRUMENTATION	
MULTI STORY SCBF WITH YIELDING BEAMS	DWG: IN-9
DRAWN BY: SMI DESIGNED BY: SMI DATE: 1/30/2018 CONTACT: SMIBARRA@UW.EDU	

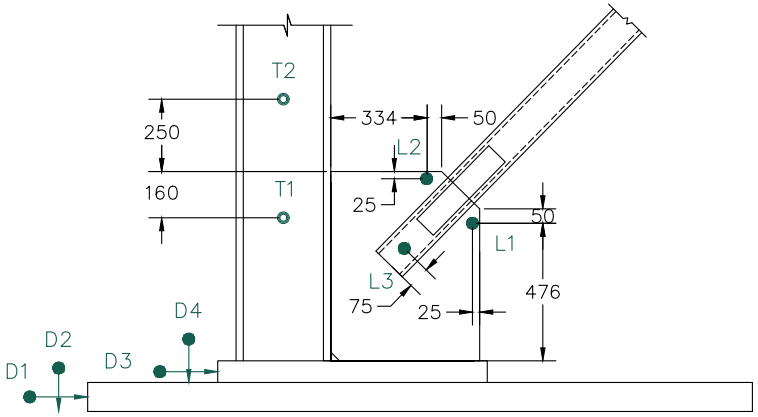

TYPICAL BASE GUSSET PLATE
INSTRUMENTATION DETAIL

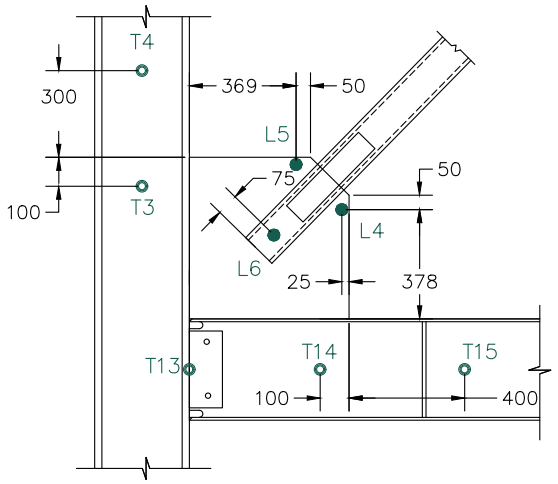

TYPICAL BEAM/COLUMN
INSTRUMENTATION DETAIL

CORNER GUSSET PLATE INSTRUMENTATION DETAILS	
MULTI STORY SCBF WITH YIELDING BEAMS	DWG: IN-10
DRAWN BY: SMI DESIGNED BY: SMI DATE: 1/30/2018 CONTACT: SMIBARRA@UW.EDU	

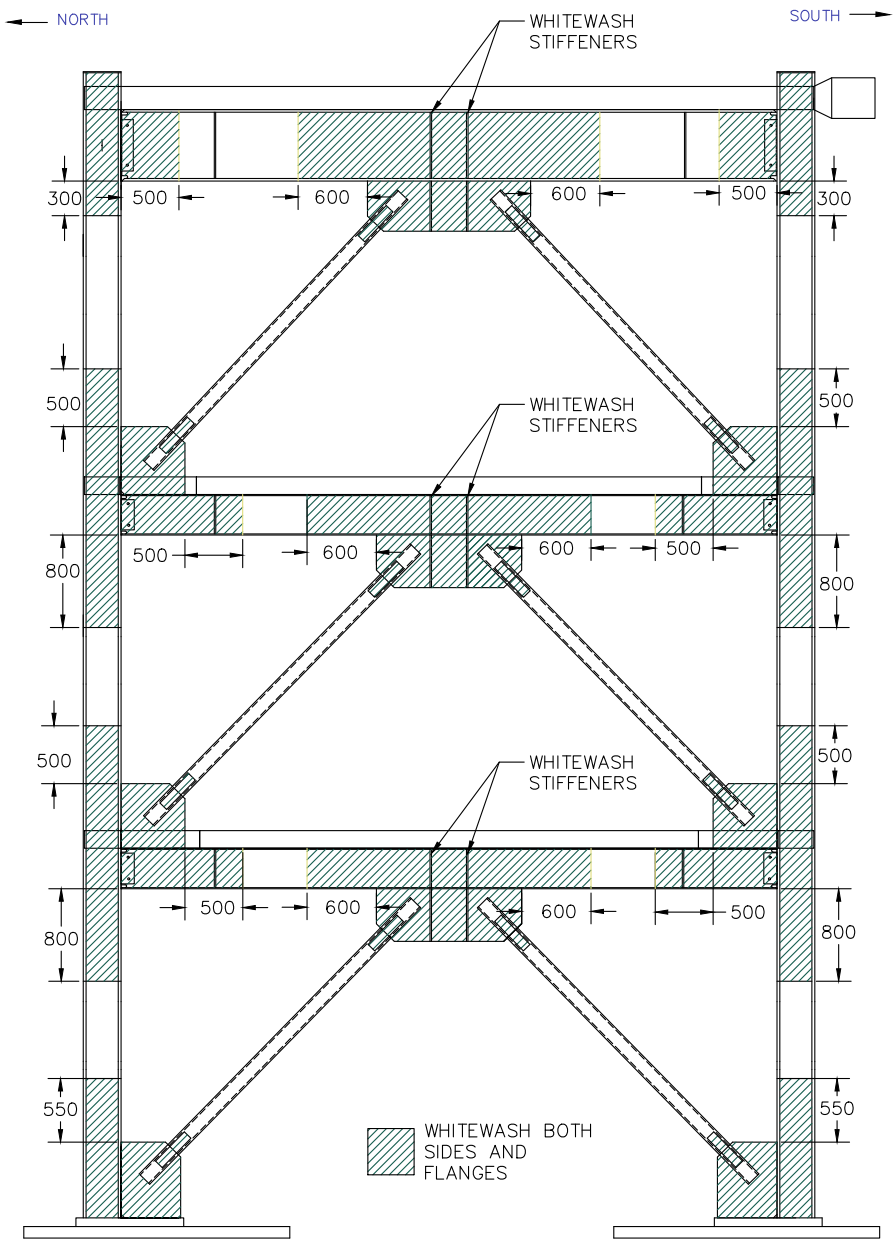

WHITEWASH PLAN

MULTI STORY SCBF WITH YIELDING BEAMS

DWG: IN-11

DRAWN BY: SMI
DESIGNED BY: SMI
DATE:1/30/2018
CONTACT: SMIBARRA@UW.EDU

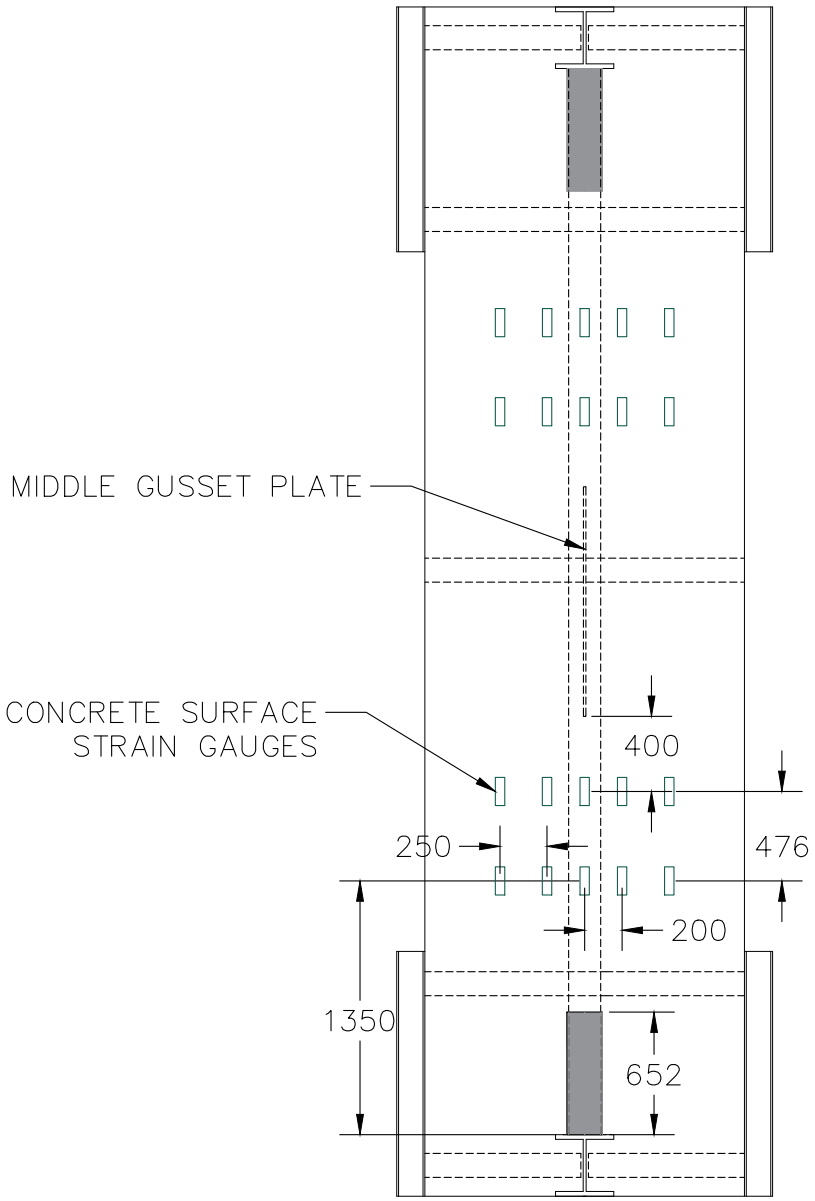

FIRST/SECOND LEVEL SLAB	
MULTI STORY SCBF WITH YIELDING BEAMS	DWG: IN-12
DRAWN BY: SMI DESIGNED BY: SMI DATE: 1/30/2018 CONTACT: SMIBARRA@UW.EDU	

B.2.2 General Test Setup

The general test setup was designed by An-Chien Wu and Te-Hung Lin at the National Center for research on Earthquake Engineering (NCREE). These drawings include the design and setup of the out-of-plane reaction frame.

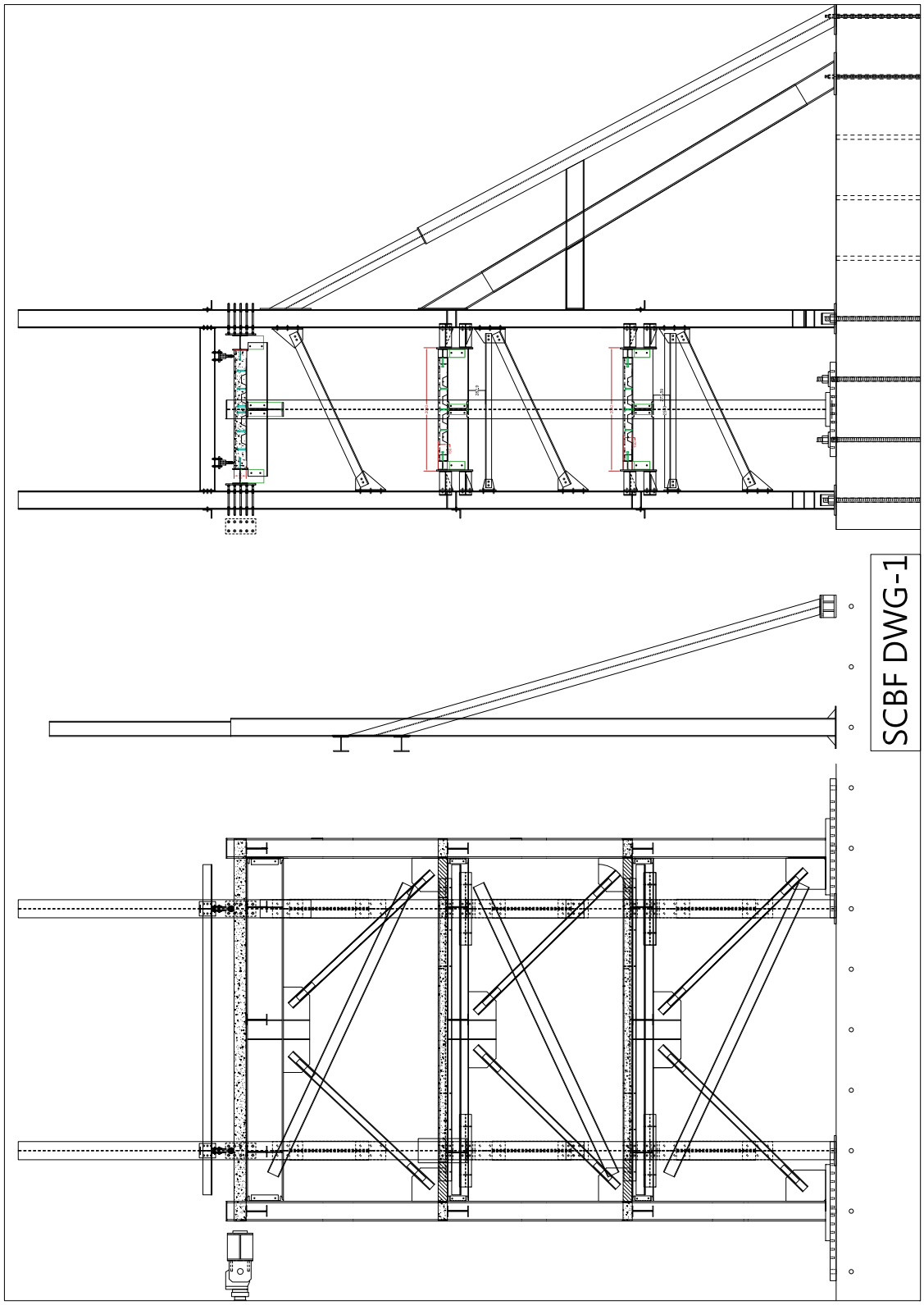
SCBF DWG-1

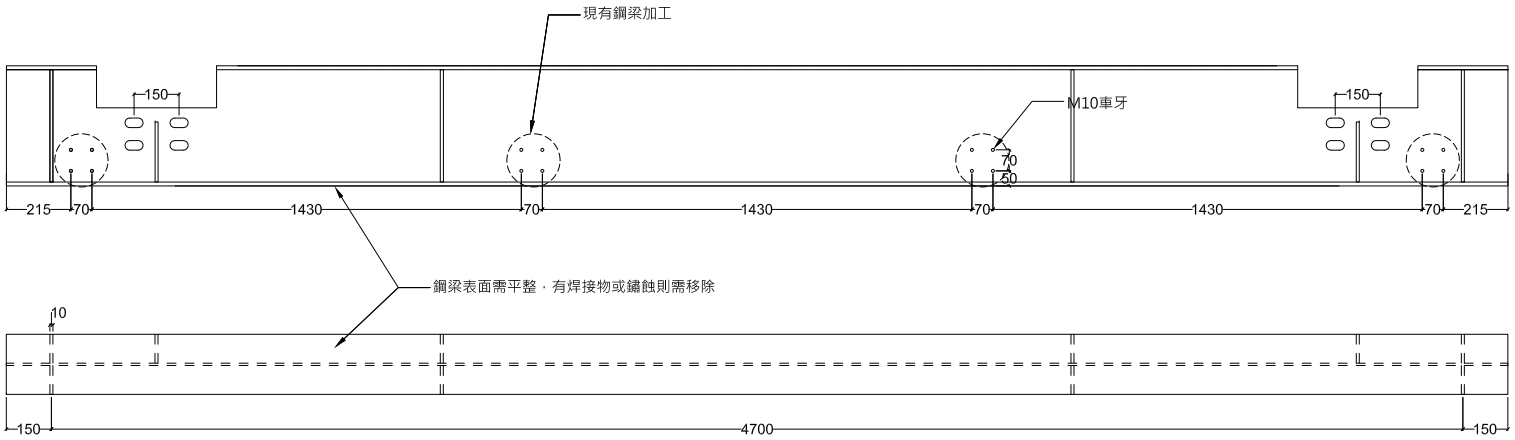

修改2F3F上層檔梁共4組

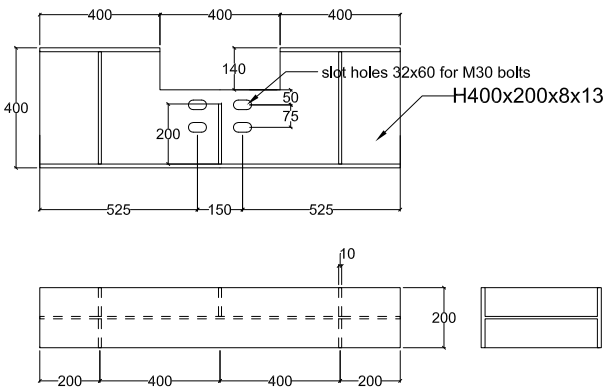

新製2F3F下層檔梁共8組

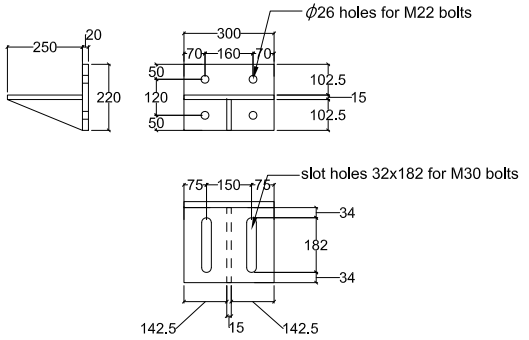

新製檔梁托架共9組

SCBF DWG-2

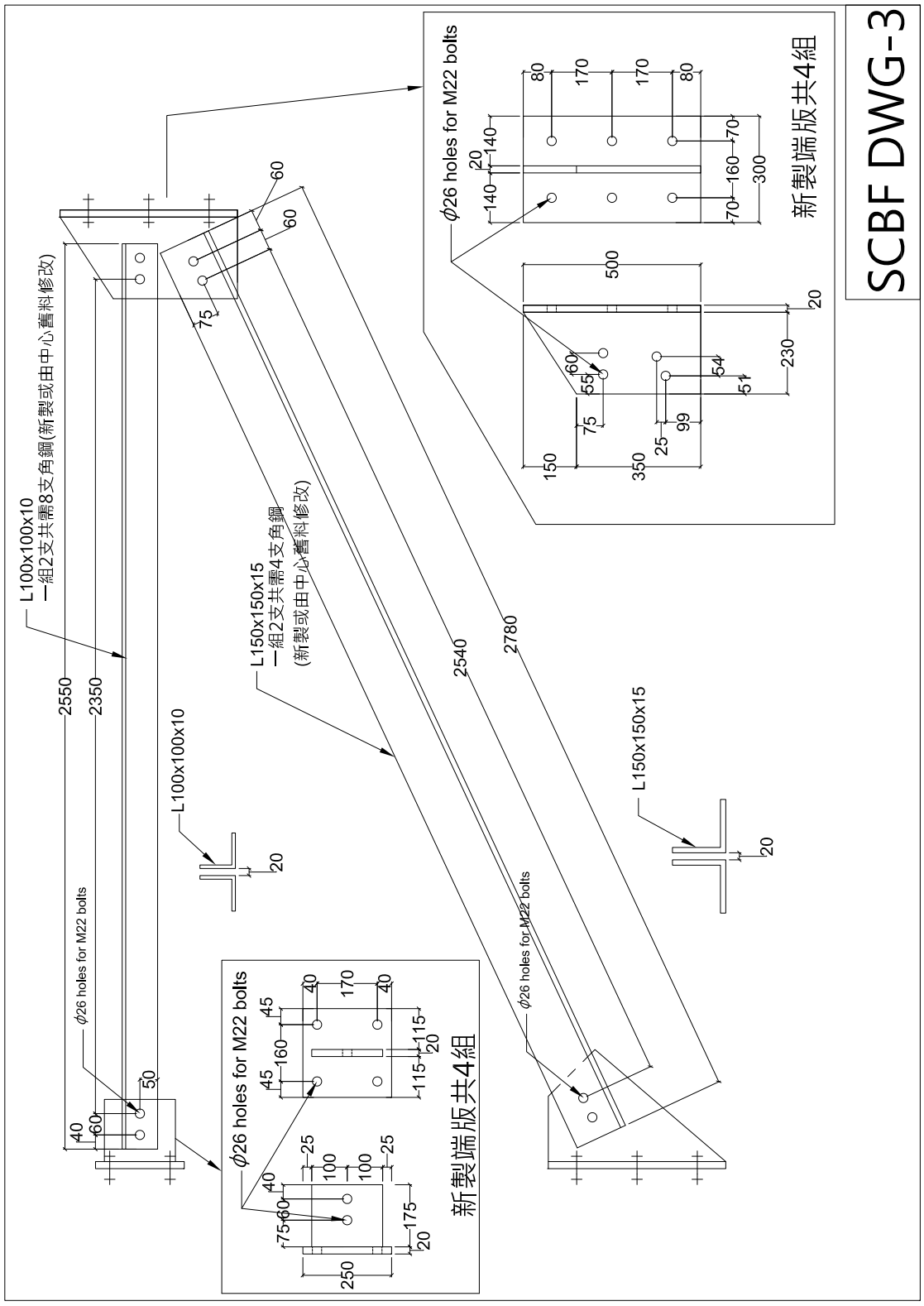
SCBF DWG-3
L100x100x10
一組2支共需8支角鋼(新製或由中心舊料修改)
L150x150x15
一組2支共需4支角鋼
(新製或由中心舊料修改)
L100x100x10
L150x150x15
2550
2350
2540
2780
ϕ26 holes for M22 bolts
新製端版共4組
ϕ26 holes for M22 bolts
新製端版共4組

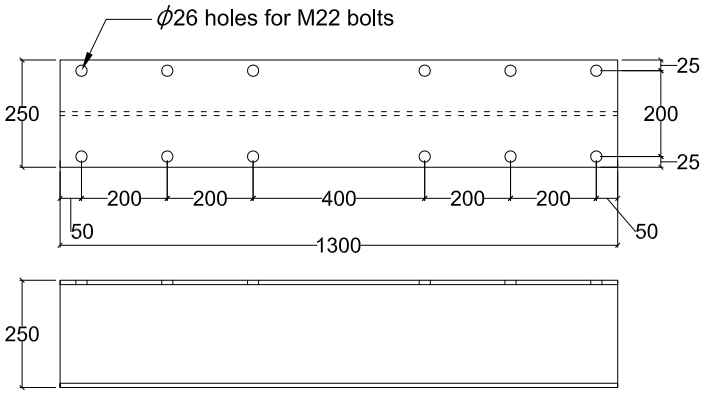

現有鋼梁切割修改(單面鑽孔) 2組

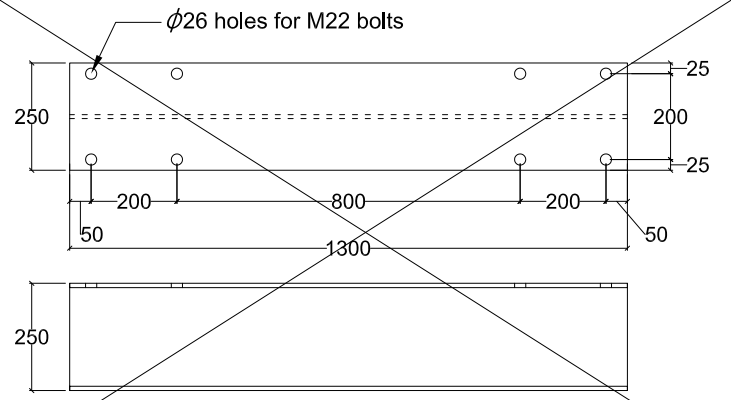

現有鋼梁切割修改(單面鑽孔) 2組

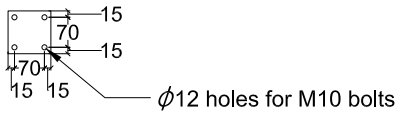

厚度8mm之圍欄底板共38片
轉接環共50組
鋼管長度詳圖SCBF DWG-5

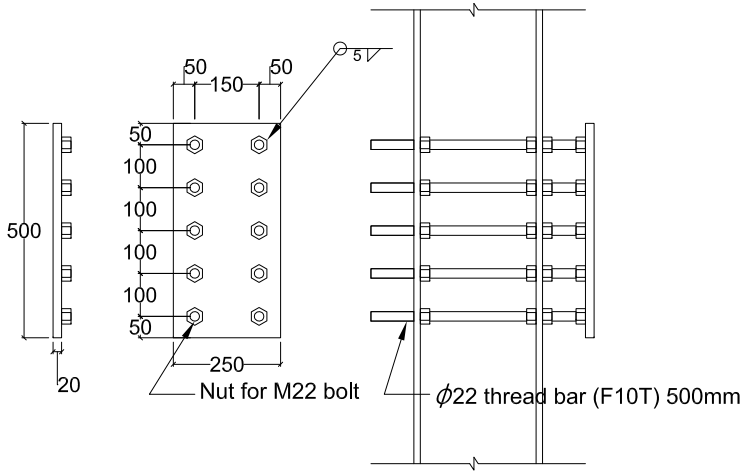

新製RF側撐擋板共4組

SCBF DWG-4

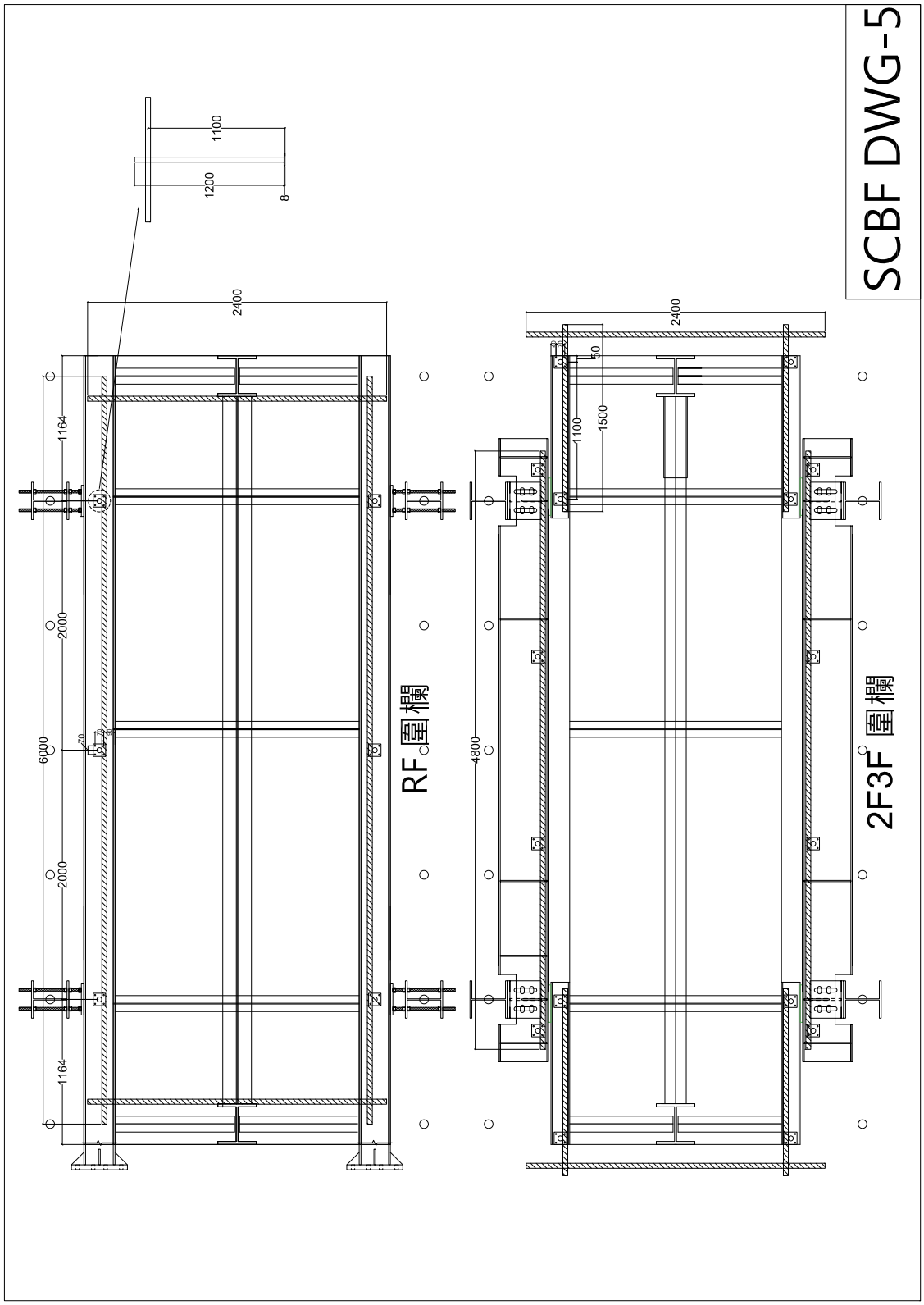
SCBF DWG-5
RF 圍欄
2F3F 圍欄
2400
1164
2000
6000
1100
1200
8
1500
4800
50

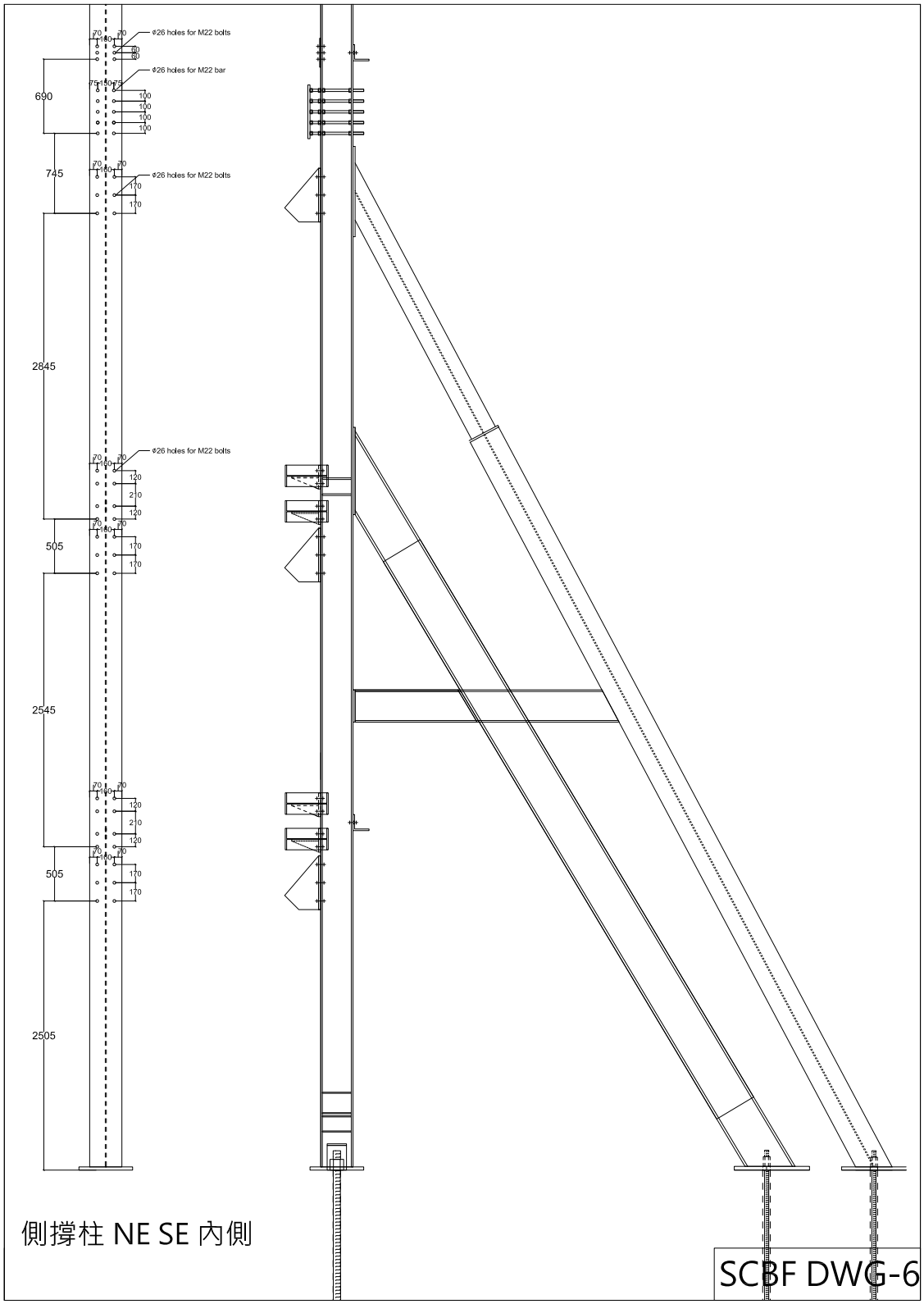
ø26 holes for M22 bolts
ø26 holes for M22 bar
ø26 holes for M22 bolts
ø26 holes for M22 bolts
690
745
2845
505
2545
505
2505
側撐柱 NE SE 內側
SCBF DWG-6

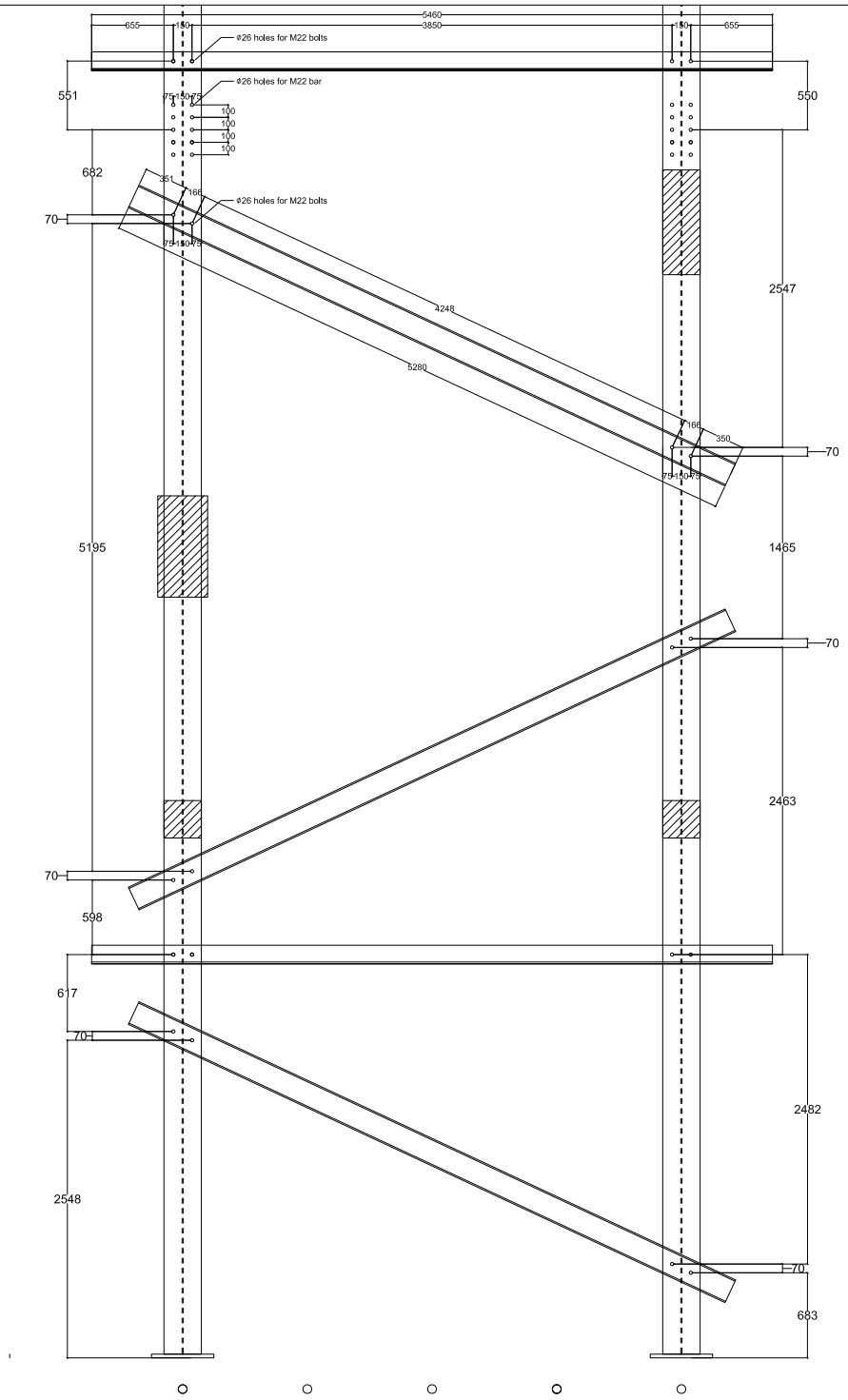

側撐柱 SE外側　　側撐柱 NE外側

SCBF DWG-7

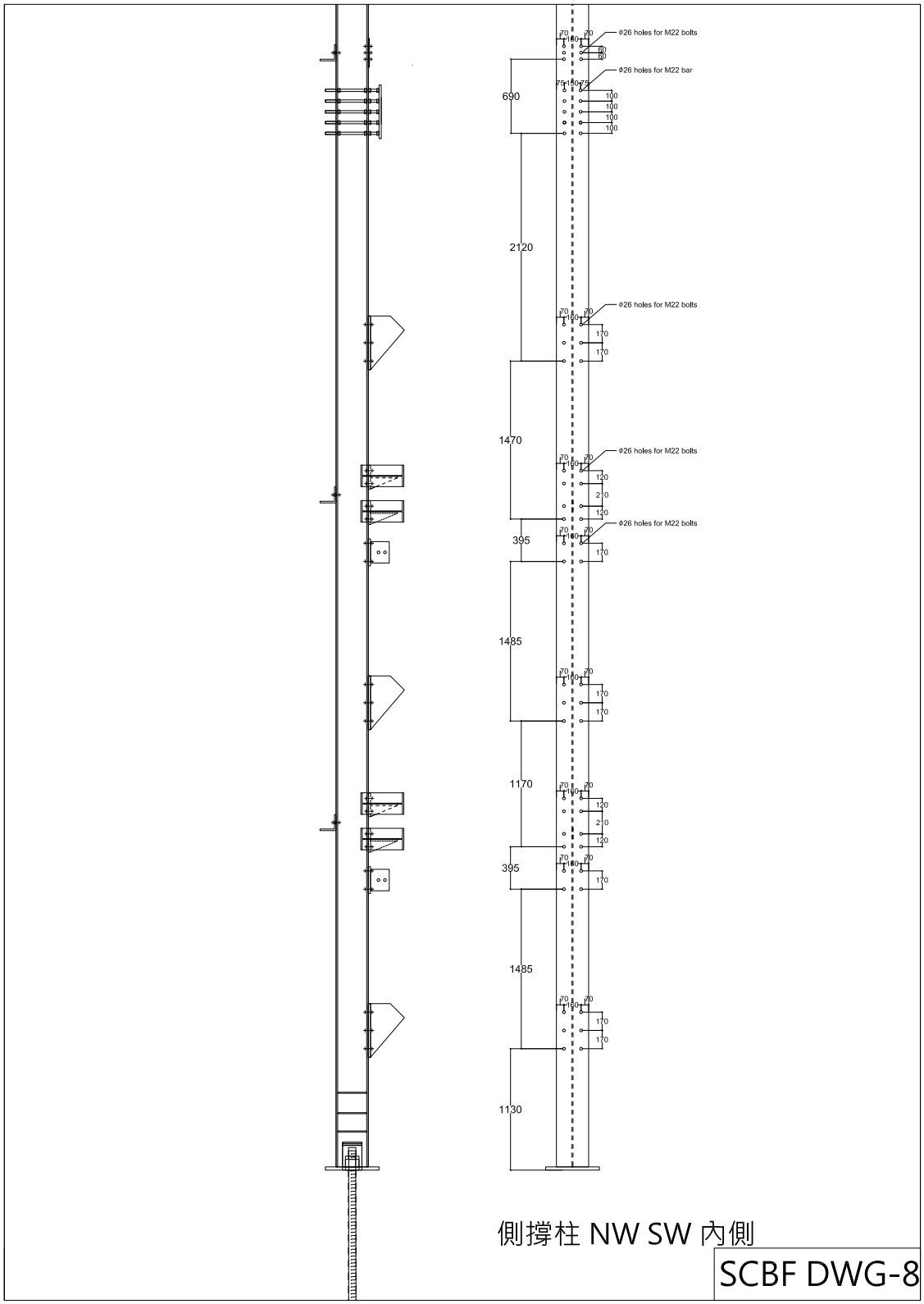

側撐柱 NW SW 內側

SCBF DWG-8

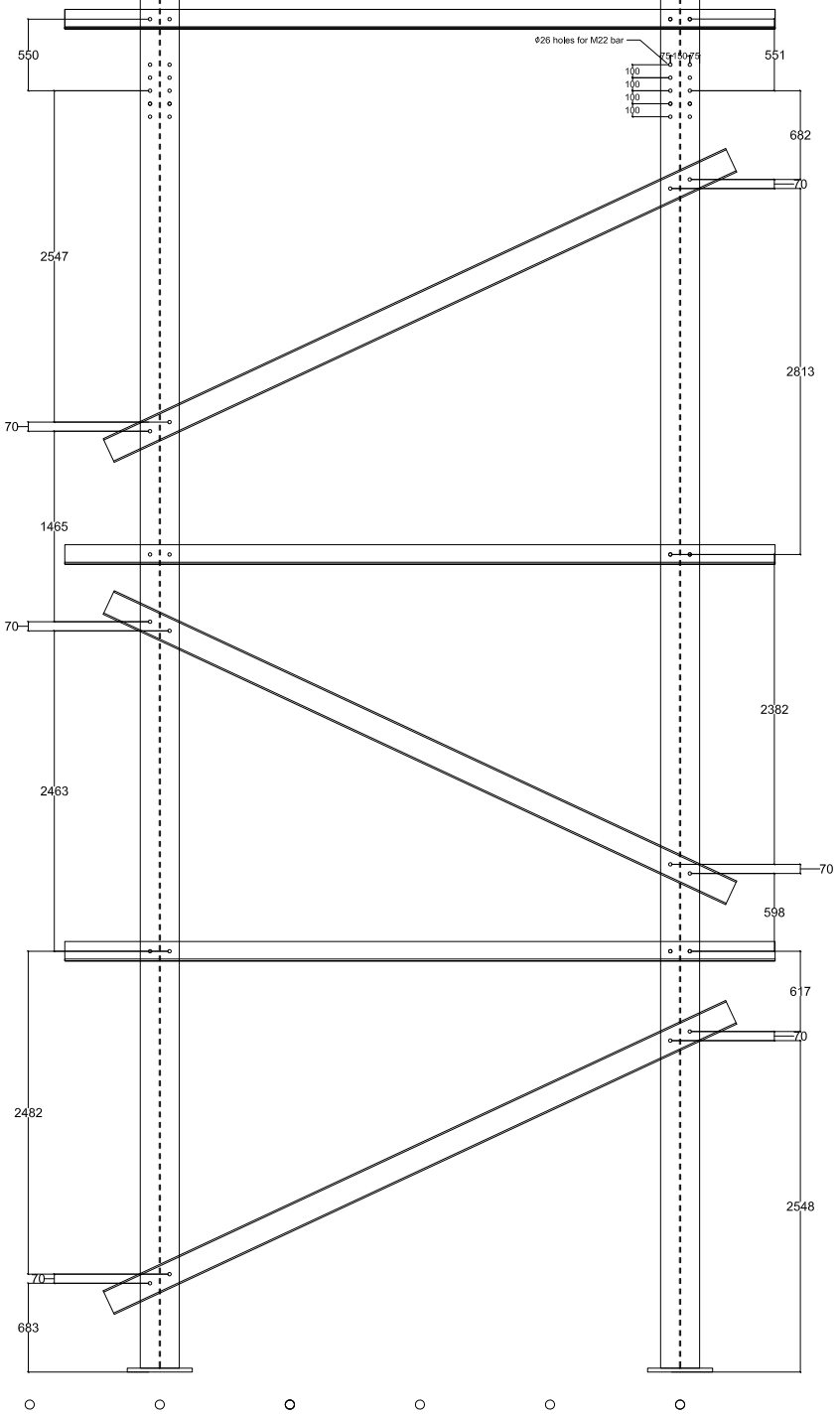

側撐柱 NW外側

側撐柱 SW外側

SCBF DWG-9

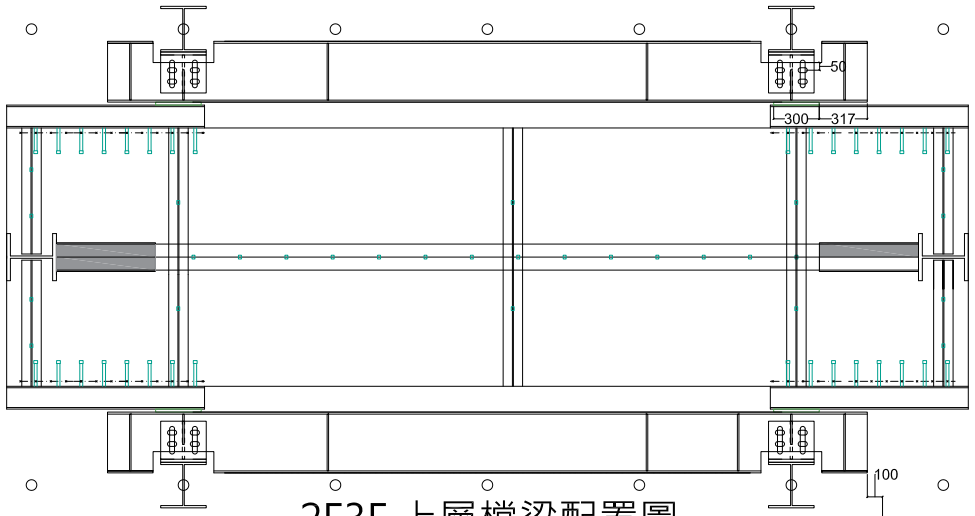

2F3F 上層檔梁配置圖

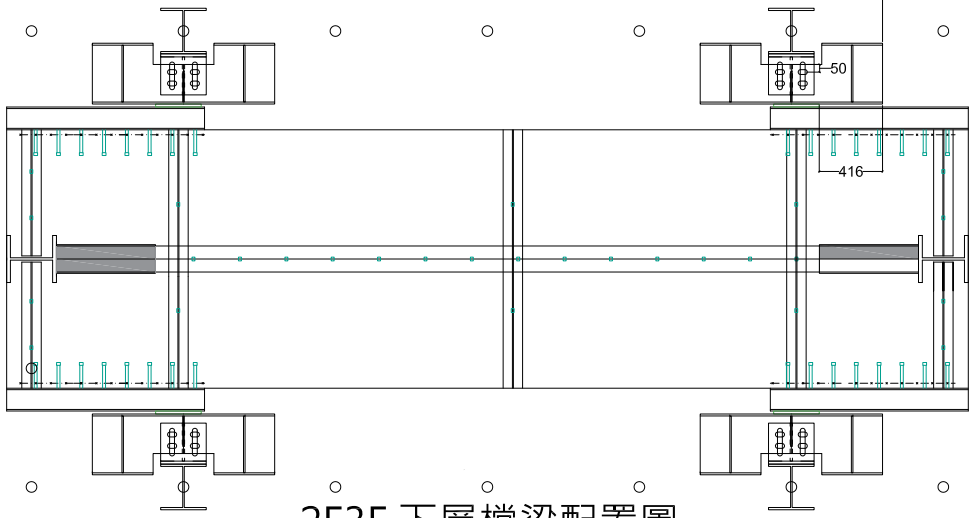

2F3F 下層檔梁配置圖

SCBF DWG-10

APPENDIX C

Data Processing

C.1 Single-Story test data

Verification of forces calculated from strain gauge data was achieved through equilibrium checks and comparison of forces derived from different sets of strain gauges. Unless noted otherwise, the force responses for each member were derived from strain gauges at that particular member.

Generally, the lateral resistance of the beams, braces, and columns agree with the applied actuator forces. Figure C.1 compares the beam total axial force and the braces' lateral resistance vs. the actuator force with column shear forces removed. The vertical unbalanced loads in the braces and in the beam do not agree as well as the horizontal forces. The vertical unbalanced force for the braces is the vertical component of the resultant of the braces' axial loads, where one brace is in tension and one brace is in compression. The vertical unbalanced force for the beam is represented by the total shear load on both sides of the beam. Force in the beam was found to differ from the total vertical brace unbalanced force by up to 40% as shown in Figure C.2. There are several factors that could be contributing to the difference in shear measurements.

- The strain gauges record measurements throughout the cyclic test, but there are various measurement offsets resulting from brace buckling, which could be partly due to the energy released upon brace buckling.
- Where there was any yielding of the material (only occurred in the braces) the stress histories were assumed to follow an elastic perfectly plastic constitutive model. Any material strain hardening not considered in the model could contribute to error in stress histories.

- The beam strain gauge readings do not reflect yielding at any of the gauged locations, however, the nearby yielding at the gusset plates could have affected stress distributions on the cross section.
- the brace axial force was not corrected for the deflection of the brace. The large out of plane deflection of the braces results in an out of plane brace force component in addition to the vertical and horizontal, in plane, force components.
- The large beam deflected of specimens with a yielding beam caused the angle of the braces changed as the beam deflected, but the angle used to calculate the horizontal and vertical brace force components was the original design angle.

Using the beam strain gauges to determine the axial force distribution showed that the axial force closer to the beam midspan was not equal, as would be expected, to the axial force near the beam-to-column connections. This appeared to be caused by various unsystematic measurement offsets throughout testing. Thus, only strain gauges in the ends of the beam were used for beam axial load calculations. However, all the gauges were necessary, and used for moment calculation and consequently shear force derivations.

Although both calculated vertical forces are suspected to have some error, the moment in the beam and associated vertical load at the midspan calculated from the beam gauges has fewer unresolved correction and thus will be used in this chapter for comparison and interpretation unless noted otherwise.

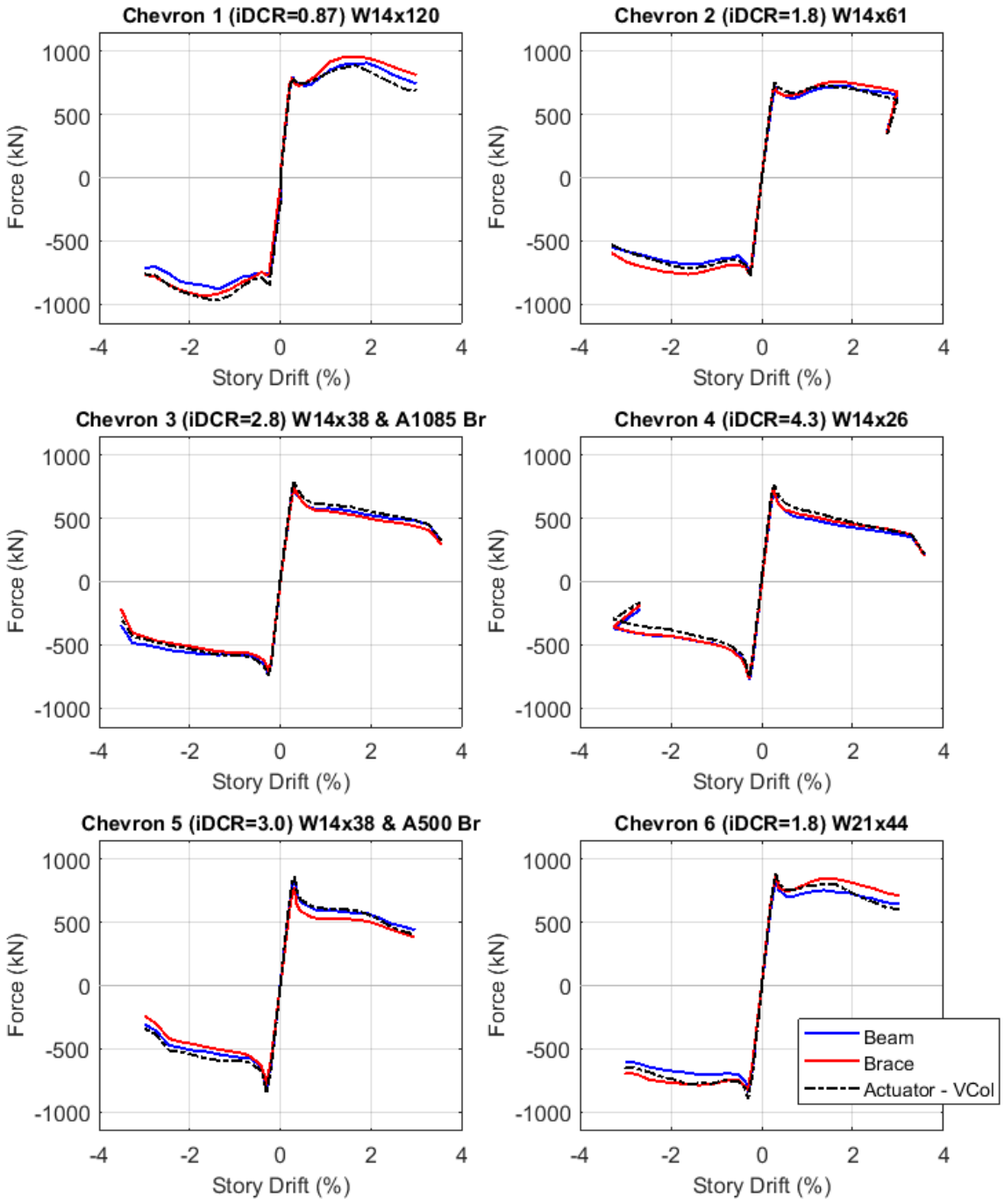

Figure C.1 Beam and Brace lateral resistance compared with actuator without the column shear forces

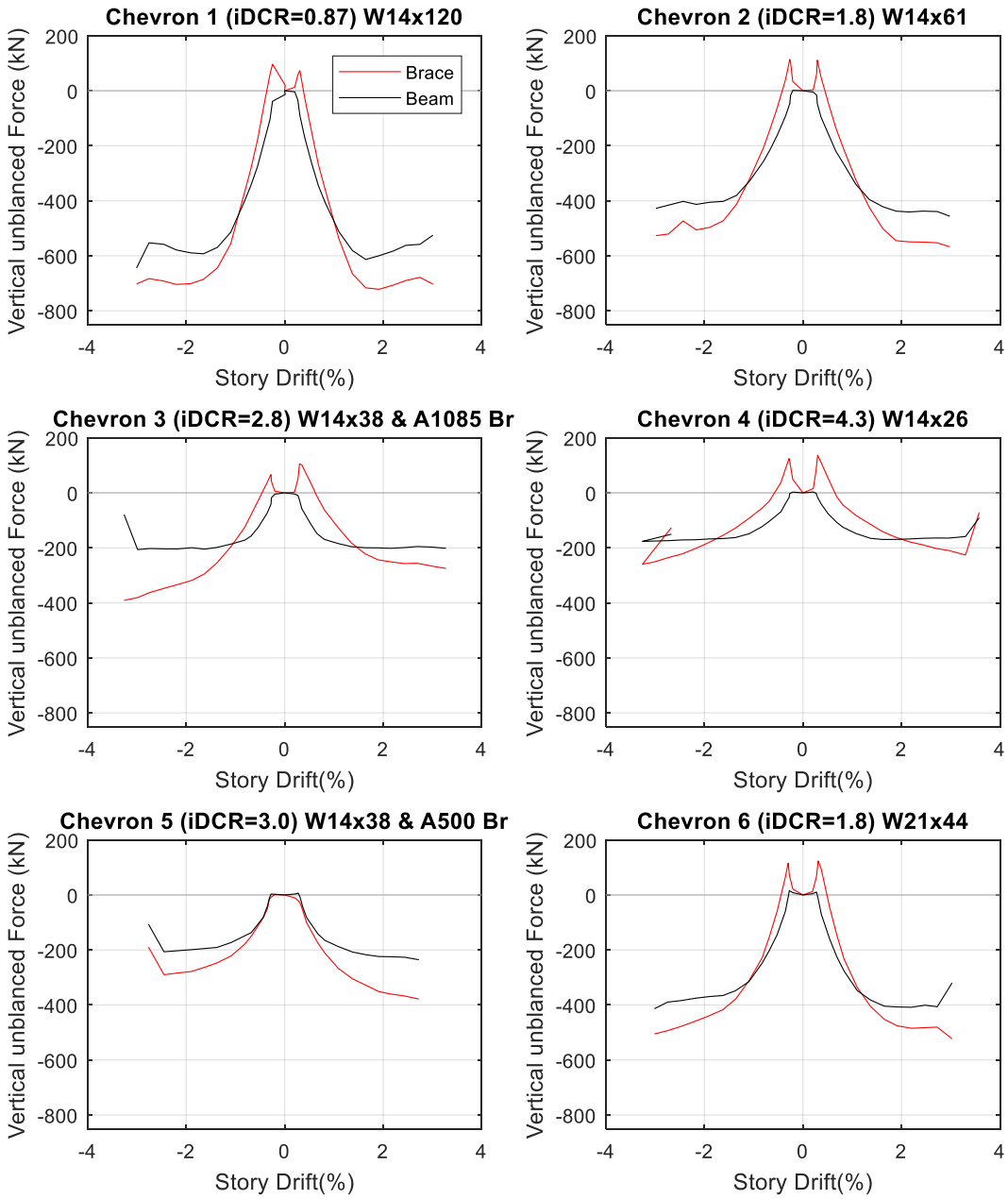

Figure C.2 Beam and brace total vertical force component comparison

C.2 Multi-Story test data

C.2.1 Data Processing

String potentiometer, LVDT, inclinometer, and strain gauge data was recorded using a data acquisition system programmed to collect instrument readings at predetermined step sizes, that varied as cycle size increased. NDI Optotrak data was collected at a rate of 300 frames per second and decimated to one frame per second for easier data processing. The OptiTrack data was collected at 30 frames per second and also decimated to one frame per second. In post processing, he Optotrak data was synched to DAQ collected data using a collection timestamp. The OptiTrack data was not fully processed before the completion of this thesis, thus limited quantitative results about the beam and brace behavior at the second story will be reported here.

C.2.2 Data Verification

As explained in Chapter 3 the column shears were directly calculated using data from rosette strain gauges on the column webs and derived from moments calculated from uniaxial strain gauges on the column flanges at the top and bottom of the column. The plots in Figure C.3 show that the two methods to calculate the column shear give the same hysteresis shape and force magnitudes for the three stories of the frame. For consistency, all succeeding results use column shears derived from moments in the columns.

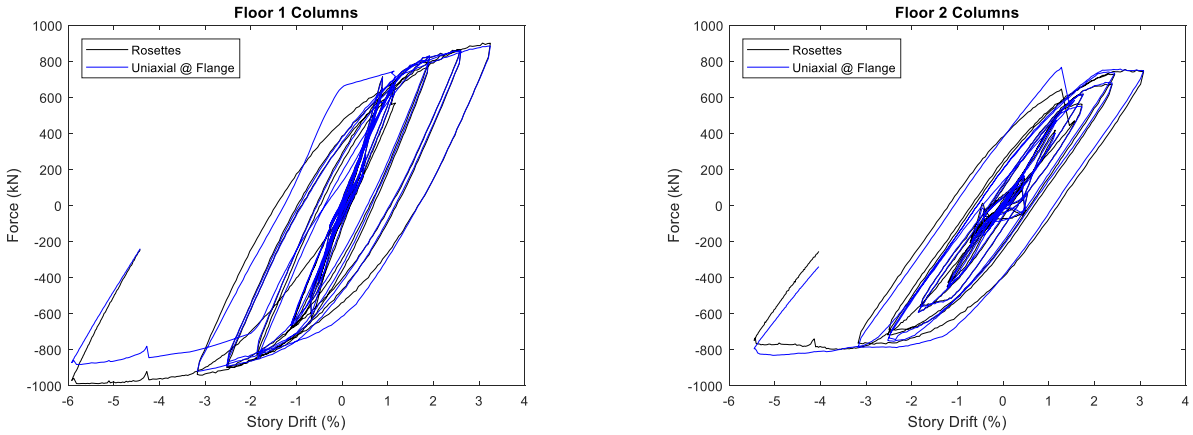

(a) First story (b) Second story

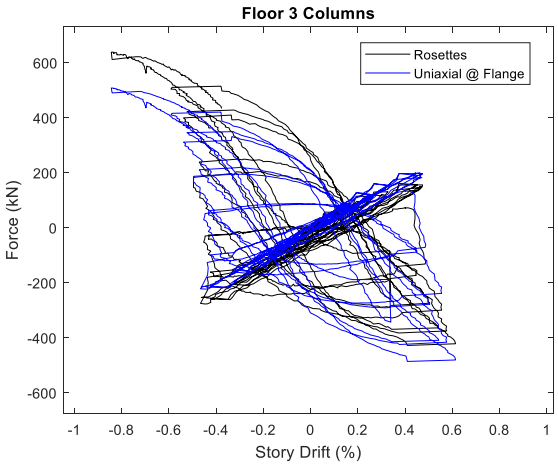

(c) Third story

Figure C.3 Total column shear results from rosettes and uniaxial strain gauges

The hysteretic plots of lateral frame resistance minus column resistance and brace lateral resistance in Figure C.4 were used to verify forces derived from strain gauge measurements. These show that the lateral resistance from the braces has very similar magnitude and hysteretic behavior as the actuator load, measured from the load cells, minus the column shear forces derived from moments calculated using strain gauges on the column flanges.

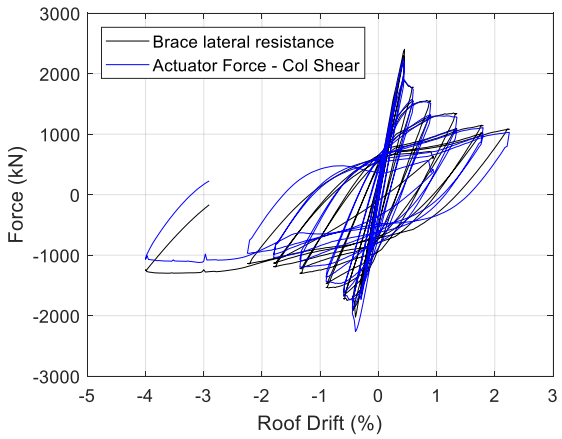

(a) First Story

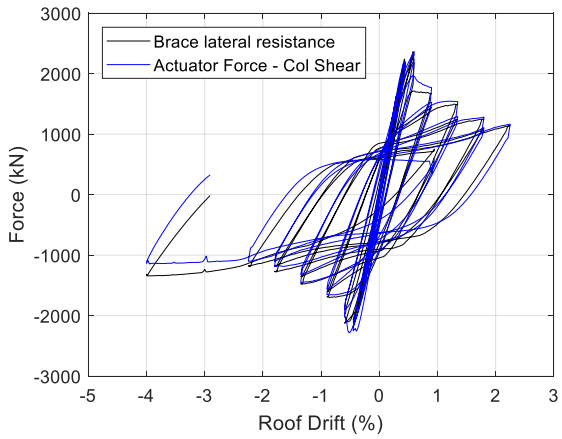

(b) Second story

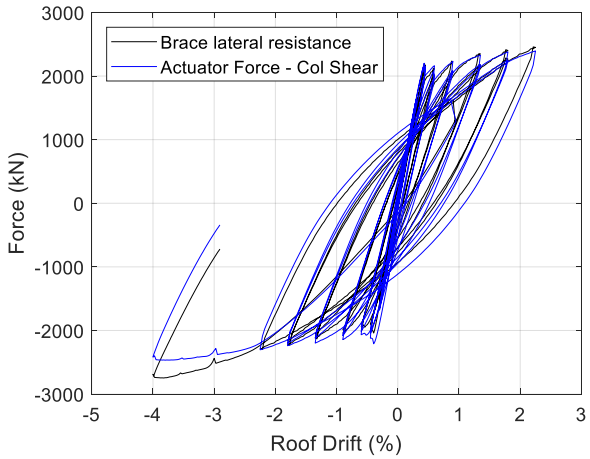

(c) Third story

Figure C.4 Brace lateral resistance compared with actuator without the column shear forces

APPENDIX D

Additional Experimental Results

D.1 Reduced Moment Capacities

Table D.1 Provides the axial loads used to calculate reduced plastic and yield moments of the beams and columns of Chevrons 1 through 6 as described in Chapter 5.

Table D.1 Reduced Moment capacities

Chevron	1	2	3	4	5	6
iDCR	0.87	1.81	2.83	4.32	3.02	1.77
			Beams			
max axial load on one side of the beam (kips)	110	104	100	83	90	90
My reduction factor	0.95	0.90	0.83	0.80	0.85	0.88
Mp reduction factor	0.97	0.95	0.90	0.88	0.91	0.92
Mp* (reduced)	973	470	245	159	248	434
My* (reduced)	848	404	201	127	205	354
			Columns			
max axial load on columns (kips)	219	156	203	163	202	228
Mp reduction factor	0.61	0.69	0.63	0.68	0.63	0.60
Mp* (reduced)	192	217	198	214	198	188

D.2 Chevron Response Comparisons

The brace axial force, beam midspan deflection, and column shear load were normalized and the response envelopes are provided below for Chevrons 1 through 4 and the first and second floor of Chevron 7. Brace forces were normalized by the brace expected buckling load. Beam deflections were normalized by half the full beam span in the chevron frame. Column shear was normalized by the total actuator load.

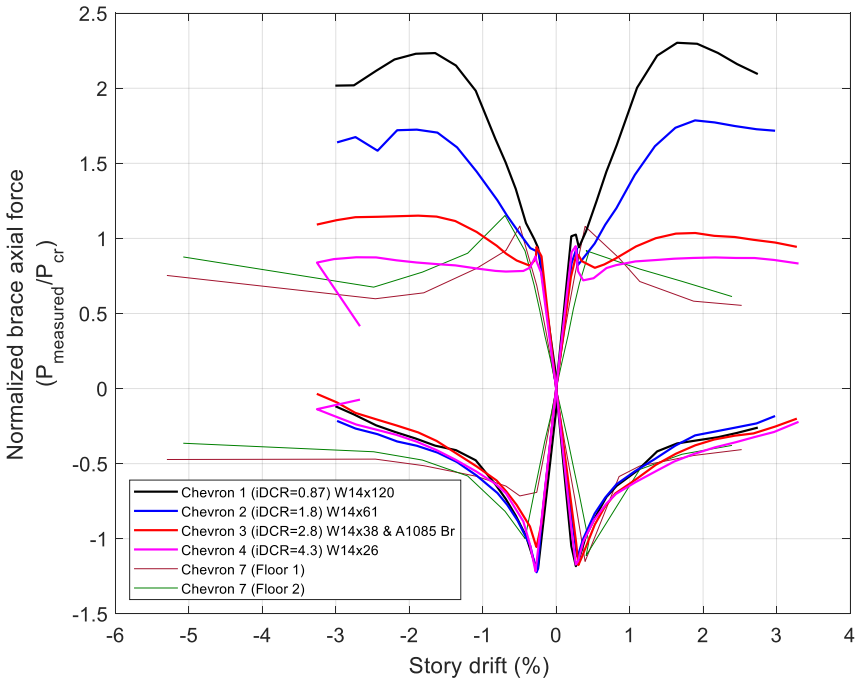

Figure D.1 Normalized brace axial force (Chevrons 1-4 and 7)

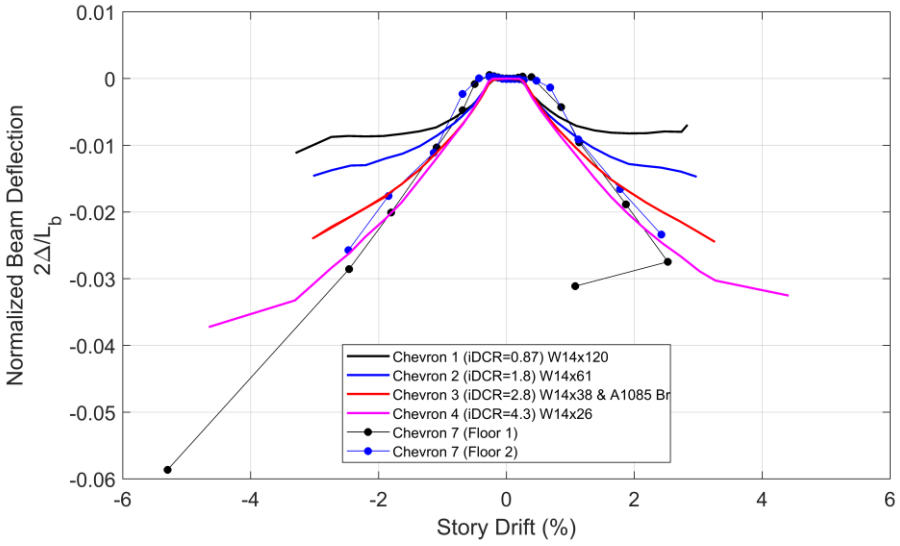

Figure D.2 Normalized beam deflection (Chevrons 1-4 and 7)

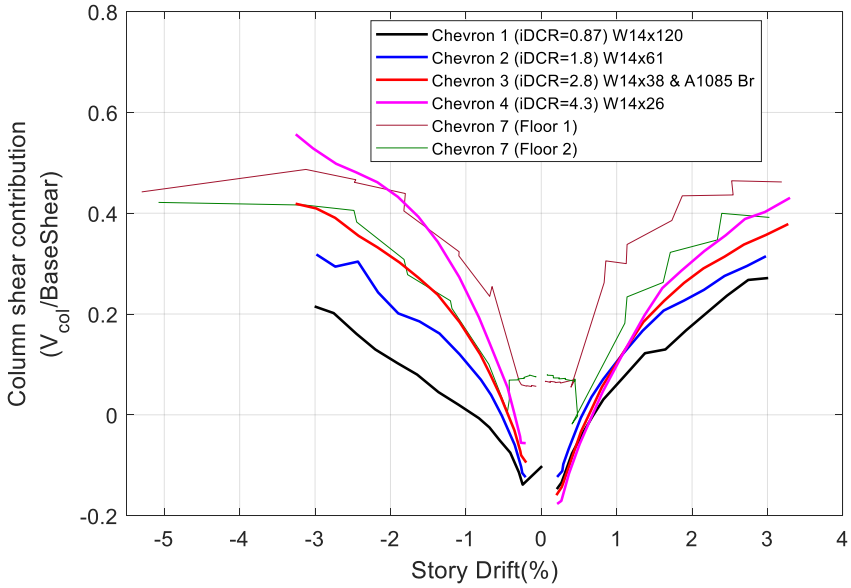

Figure D.3 Column shear contribution (Chevrons 1-4 and 7)